Tailored metal complexes for imaging applications

Clive Edwin Foster

Tailored Metal Complexes for Imaging Applications

by

Clive Edwin Foster

Department of Chemistry
University of Durham

A thesis submitted for the degree of Doctor of Philosophy

1996

Abstract

Tailored Metal Complexes for Imaging Applications

The short-lived PET radionuclide ^{134}La ($t_{1/2}$=6.7 minutes) is well suited to the repeated evaluation of blood perfusion, thus providing a method of following changes in tumour behaviour, in response to therapy. Ligands, both acyclic and macrocyclic, have been synthesised, and the complexes formed with $^{134}La^{3+}$ evaluated in vitro and in vivo. Other lanthanide complexes have also been evaluated for potential use in magnetic resonance imaging and photoimmunoassay studies. A preliminary crystal structure determination of a lanthanum tetrabenzylphosphinate complex reveals the presence of one water molecule in the inner co-ordination sphere.

The development of monoclonal antibodies with a specificity for the surface features of tumour cells presents a method for the localisation of a radionuclide at the tumour. Copper-64 ($t_{1/2}$=12.7 hours) uniquely combines the decay properties required for imaging and therapy. Ligands have been developed for derivatising antibody molecules with radioactive copper, whilst retaining specificity for the target antigen. Three modified proteins have been evaluated in vivo, and show a high tumour uptake compared with blood, but modest uptake compared with the liver, suggestive of some degree of protein denaturation during labelling.

A more subtle approach has been developed, exploiting the affinity of biotin for avidin. Higher selectivity at much shorter post-administration time is potentially attainable by the use of a multi-step procedure. A copper binding ligand incorporating biotin has been synthesised. The ^{64}Cu complex of the conjugate shows specificity for the protein avidin both in vitro and in vivo.

The prognosis of patients with hepatoma or liver metastases is poor. A lipophilic copper complex has been synthesised and retention in the liver demonstrated in vivo. Measurements with three cell lines in vitro suggest that the complex is more readily taken up by tumour cells (and cells from metastases) compared to normal cells.

Clive Edwin Foster, 1996

Declaration

The work described herein was carried out in the Department of Chemistry at the University of Durham and the Joint Department of Physics at the Institute of Cancer Ressearch, Royal Marsden Hospital Trust, Sutton, between October 1993 and September 1996. All of the work is my own, unless stated to the contrary, and it has not been submitted for a degree at this or any other university.

Statement of Copyright

Acknowledgements

I would like to thank my supervisor, Professor David Parker, for his help, advice and guidance during the course of my work. The members, past and present, of the research group are thanked for their help, friendship, and in some cases, gorgeousness beyond belief, as are the boys and girl, from my year in 29. The efforts of Janet and her fellow crystallographers, to refine the diffraction data are greatly appreciated. The technical staff of the department are thanked for all of their repairing, teaching, purchasing, spectra, coffee.....

I would like to express my gratitude to Dr Jamal Zweit for his optimistic supervision whilst at Sutton. I would like also to acknowledge the immunologists Dr Suzanne Eccles, Dr Christopher Dean and Dr Helmout Modjtahedi for guiding a myopic chemist towards enlightenment. Mr Mike Davies, Dr Ian Rowland, Dr Paul Carnochan and Dr Suzanne Eccles are all thanked for their anaesthetism skills. Many thanks to Tom and Jane for their help in the lab but not for the Northern gibes. Love to the Fiends!

Jamal, Steve, and David are thanked for their rapid and helpful proof reading of the thesis.

Financial assistance from the EPSRC and The North of England Cancer Research Campaign is gratefully acknowledged.

Most of all I would like to thank my parents for their love and support. This thesis is for them.

Mum and Dad

Science is built up of facts, as a house is built of stones, but an accumulation of facts is no more a science than a heap of stones is a house.

Henri Poincaré

Contents

β^-	beta particle
β^+	positron
BOC	t-butoxycarbonyl
br	broad
CI	chemical ionisation
COSY	correlation spectroscopy
cyclam	1,4,8,11-tetraazacyclotetradecane
cyclen	1,4,7,10-tetraazacyclododecane
Da	Dalton (1 molecular mass unit)
DCC	dicyclohexylcarbodiimide
DCI	desorption chemical ionisation
DCU	dicyclohexylurea
DMAP	N,N-dimethylaminopyridine
DMF	N,N-dimethylformamide
DMSO	dimethylsulfoxide
DNA	deoxyribose nucleic acid
DOTA	1,4,7,10-tetraazacyclododecane-1,4,7,10-tetraacetic acid
DTPA	diethylenetriamine-N,N,N',N'',N''-pentaacetic acid
EDTA	ethylenediamine-N,N,N',N'-tetraacetic acid
ES+/-	electrospray ionisation with detection in positive/negative ion mode
FAB	fast atom bombardment
$14N_4$	1,4,8,11-tetraazacyclotetradecane
HPLC	high performance liquid chromatography
ICR-12	Institute of Cancer Research antibody
IR	infra-red
Ln	Generic symbol for lanthanide element
m	metastable
M	molecular ion
m.p.	melting point
M_r	molecular mass
MRI	magnetic resonance imaging
MS	mass spectrometry
$9N_3$	1,4,7-triazacyclononane
NMR	nuclear magnetic resonance
NOBA	3-nitrobenzylalcohol
NOTA	1,4,7-triazacyclononane-1,4,7-triacetic acid
PBS	phosphate buffered saline

PEG	polyethyleneglycol
PET	positron emission tomography
PIPES	piperazine-1,4-bis(ethanesulfonic acid)
R_t	retention time
SPET	single photon emission tomography
$t_{1/2}$	physical half-life
TETA	1,4,8,11-tetraazacyclotetradecane-1,4,8,11-tetraacetic acid
TFA	trifluoroacetic acid
THF	tetrahydrofuran
$13N_4$	1,4,7,10-tetraazacyclotridecane
TLC	thin layer chromatography
TRITA	1,4,7,10-tetraazacyclotridecane-1,4,7,10-tetraacetic acid
uv	ultra-violet
v	very
VT	variable temperature
X-ray CT	X-ray computed tomography

Chapter One

Introduction

1. Introduction

After a brief introduction to the disease of cancer, (1.1.) a survey of the types of modalities, used in tumour diagnosis, is presented (1.2.) with emphasis on radionuclide methods. The array of potentially useful imaging radionuclides is introduced (1.3.) and nuclides selected for application to perfusion studies (1.4.) and radioimmuno-scintagraphy. (1.5.) The possibility of extending protocols for imaging, towards radioimmunotherapy is considered. (1.6.) The machinery required to present the chosen radionuclides in an effective way to patients is reviewed. (1.7.) Finally, the material of subsequent chapters is introduced. (1.8.)

1.1. Cancer

Cancer is a common disease in man. One person in three will be diagnosed with the disease[1] and cancer is responsible for the deaths of one in five in the developed world. Although cancer is not the primary cause of death, the disease is becoming more prevalent as life expectancy increases. Cancer has been known since antiquity, but it is only in the last forty years or so that effective means of controlling, and in some cases curing, the disease have arisen. The early diagnosis of cancer has a significant effect on the chance of survival and has a marked effect on the patient's quality of life.

The incidence of the many different types of cancer varies between the sexes, racial groups and the country of residence. This suggests that behavioural, dietary or environmental factors may have a profound effect on incidence rates, and offers the prospect of cancer prevention by a change in lifestyle.

The group of diseases, collectively known as cancer, arise from a loss of control of cell division. In normal tissues, cells have a finite lifetime and as cells expire, they are replaced with new ones, hence maintaining a constant number. If this regulation breaks down, and new cells are produced at a faster rate than old ones die, a tumour[2] results. Tumours are often classified into two groups, benign and malignant. Benign tumours are those which do not spread, and in this respect are not "dangerous," however, the presence of a growing mass in a sensitive organ or near a major blood vessel does pose a potential threat to the patient's life. Surgery is often used to remove the tumour. Malignant tumours are aggressive tumours that have the ability to break up and invade the bloodstream or lymphatic system and, hence, spread to distant sites in the body, as depicted in the schematic (figure 1.1) below. Often these tumour fragments are trapped in either the lymph nodes, the liver, bones or lungs. These secondary tumours (called metastases) can be numerous and difficult to detect and treat.

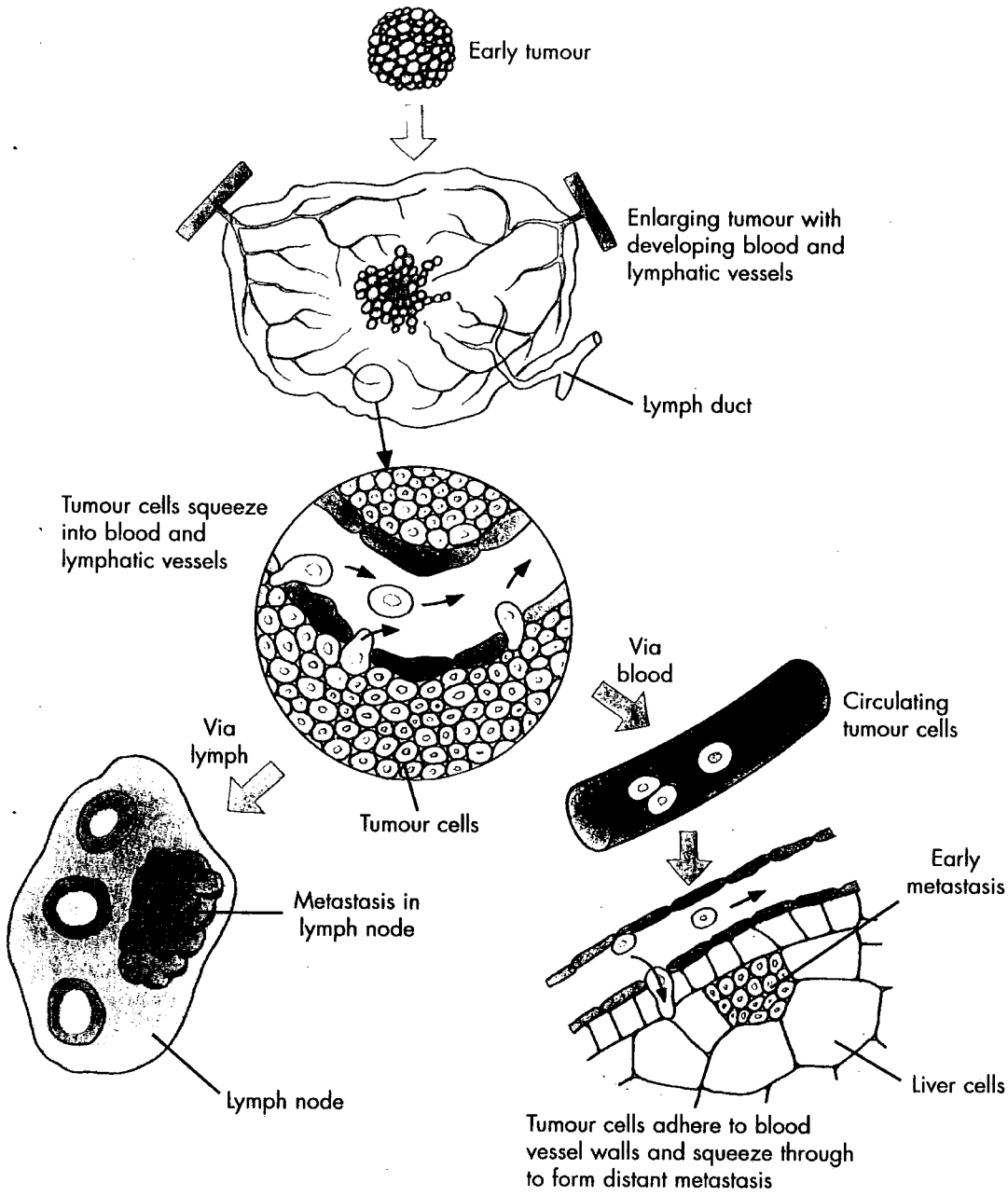

Figure 1.1. Diagram illustrating the spread of tumour cells to sites remote from the primary tumour. Reproduced from reference 1.

Despite the large number of deaths attributed to cancer, about four cases in ten can be cured. Whilst this is encouraging, further improvement is, without doubt, desirable. One way of improving cancer treatment and management is by early diagnosis of the disease. The graph below (figure 1.2.) illustrates the difference in likelihood of survival with early diagnosis.

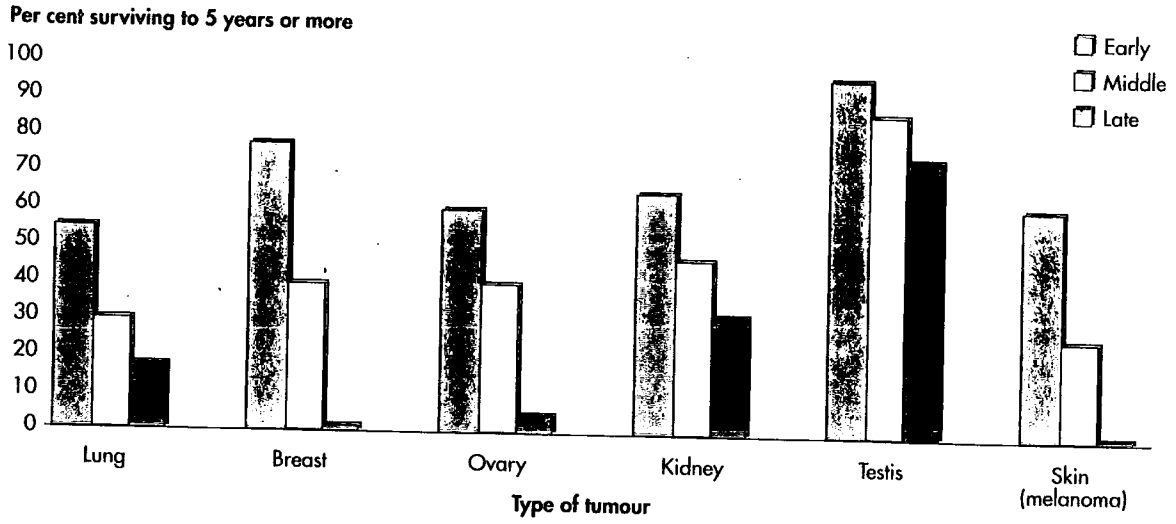

Figure 1.2. Graph showing the percentage of patients surviving five or more years, when diagnosed at an early, middle or late stage of development. Reproduced from reference 1.

1.2. Diagnosis of Cancer[3]

Some cancers, for example tumours of the skin and breast, can be detected by inspection and palpitation. Others can be accessed for diagnostic purposes fairly easily with the use of an endoscope. These include tumours of the upper and lower ends of the alimentary canal. For more deep seated tumours, diagnostic information is usually acquired by histochemical techniques which detect changes in cellular chemistry. Invasive biopsy is used to assess the extent (staging) of the disease. This type of information may also be obtained by the use of various imaging modalities.

Imaging Techniques

There are several imaging techniques available to the clinician, all of which have their merits, but in the current climate of declining healthcare expenditure, a choice often has to be made, which is based on financial constraints as well as the therapeutic benefit, set against any adverse health cost to the patient. Many of the techniques are complementary i.e. different techniques yield answers to different questions. The most obvious difference is that, whilst some provide anatomical detail, others provide information on physiological and biochemical processes, as they occur *in vivo*.

The basic requirements of an imaging procedure are (i) an energy source, which interacts in a usefully non-uniform manner with the media in the field of view (ii) a method of detection, which reflects the contrasts attained in the aforementioned interaction and (iii) a means to present the information.

The energy source may be external, in which case the difference in energy focused on the subject compared to that transmitted through the subject is measured. The differing ability of various tissues to absorb or transmit the energy is manifested in the image obtained. The mode in which the radiation is applied determines whether a simple photographic plate or a computed reconstruction is required for presenting the result. Alternatively, the energy source may be internal, as is the case with internally administered radiopharmaceuticals. Here, it is the position of the energy source which is determined, hence information is gained on the relative affinity each region of the subject has for the energy source.

Radiography

The use of X-rays may be useful for the detection of tumours in the lungs or bones, but is of limited use in the rest of the body, as the density of tumours is not significantly different from normal tissues. An increased definition may be obtained by the introduction of a contrast agent, but often this has to be done *via* cannula intra-arterially, with the associated risk of haemorrhage.

Ultrasound

Ultrasound is useful for detecting some tumours and has the advantage of avoiding radiation dose to the patient. Lesions as small as 5mm diameter can be detected, and the technique can easily distinguish between fluid filled and solid masses.

Magnetic Resonance Imaging

The action of radiofrequency pulses on samples containing hydrogen nuclei (protons) in the presence of a magnetic field, causes some nuclei to achieve a state of higher energy. Over time, the nuclei return to their original state, a process termed relaxation. The technique of magnetic resonance imaging (MRI) provides useful diagnostic information by the use of a gradient magnetic field. This causes water protons to absorb energy at a frequency dependent upon the position of the water molecule. A series of measurements allows a 3-dimensional anatomical picture to be built up.

The presence of paramagnetic ions shortens the water proton relaxation times, providing an increased contrast between areas of different paramagnetic ion concentration. The large number of unpaired electrons present in iron(III), manganese(II) and particularly gadolinium(III) has resulted in a great deal of work to target these ions to specific tissues. The degree of relaxation depends on the proximity of the water protons to the paramagnetic centre. Hence, rapidly exchanging ligated water molecules on a paramagnetic ion may be envisaged as the ideal contrast agent. Such ions would show little tissue specificity, however, being rapidly cleared by the kidney. It is, thus, essential that the metal be administered as a complex,[4] tailored to distribute the ion in a specific manner. Since the gadolinium(III) ion is toxic, accumulating in the bones, the complex must be stable and excreted intact.

The need for stability provides the chemist with an interesting challenge - to synthesise stable complexes, but, preferably, leaving the metal co-ordinately unsaturated, to permit the exchange of water molecules. Much effort has been centred around the need for stable complexes of gadolinium,[5] and this provides a useful starting point for the design of ligands for other lanthanides, as the co-ordination chemistry is similar across the series. Minor differences arise as a result of the contraction in ionic radius as the series is traversed, and the occasional occurrence of the lanthanide(II) oxidation state.

Radionuclide Imaging

There are several imaging techniques utilising the characteristic emissions produced by unstable nuclides. The different decay pathways exhibited by radionuclides provide potential, not only for highly sensitive imaging procedures, but also offer scope for use in targeted therapy.

The combination of protons and neutrons affect the energy, and, hence, stability of a nucleus. If the nucleus has too great an energy, arising from an excess of protons or neutrons, it will undergo transformations which result in a net lowering of energy. There are a number of different pathways for a nucleus to dissipate energy, either in the form of particles or as electromagnetic radiation. It is these emissions which provide the energy source for the imaging protocols.

The unstable (i.e. radioactive) nucleus is called the parent nucleus, and the more stable product is called the daughter. The daughter may itself be radioactive and decay further - this forms the basis of generator systems (see below).

Radionuclides possess a set of characteristic properties such as the mode of decay, the type and energy of emissions and the half-life. The combination of these properties determines the suitability of the radionuclide for a certain application.

Single Photon Planar Imaging and Single Photon Emission Tomography

The technique of single photon imaging is in routine clinical use in a great number of hospitals around the world, whereas the tomographic mode of this technique (SPET)[6] is becoming more widely available. The technique utilises a gamma camera to obtain an image of the distribution of the radionuclide. The radionuclides used in SPET decay principally *via* isomeric transition, electron capture and internal conversion. Other radionuclides which decay by other pathways can often be used in SPET, as γ-emission often accompanies β-decay.

Isomeric Transition - The metastable nuclide achieves a greater stability by the release of a gamma ray.

Electron Capture - The excess of protons in the nucleus can be reduced by the capture of an orbital electron. In this process, a proton and the captured electron combine to form a neutron, resulting in a reduction of one in the atomic number.

$$p + e^- \longrightarrow n$$

$$^{A}_{Z}X + {}^{0}_{-1}e \longrightarrow {}^{A}_{Z-1}Y$$

The removal of an inner electron from the atom results in an outer electron falling into the vacant inner shell. For conservation of energy, an X-ray, characteristic of the daughter nuclide, is emitted which can be detected externally. The energies of emitted X-rays increase with mass number and it is only the X-rays of heavier elements which have sufficient energy to be clinically useful. The process of electron capture followed by X-ray emission is depicted in the scheme (figure 1.3.) below using the Bohr model.

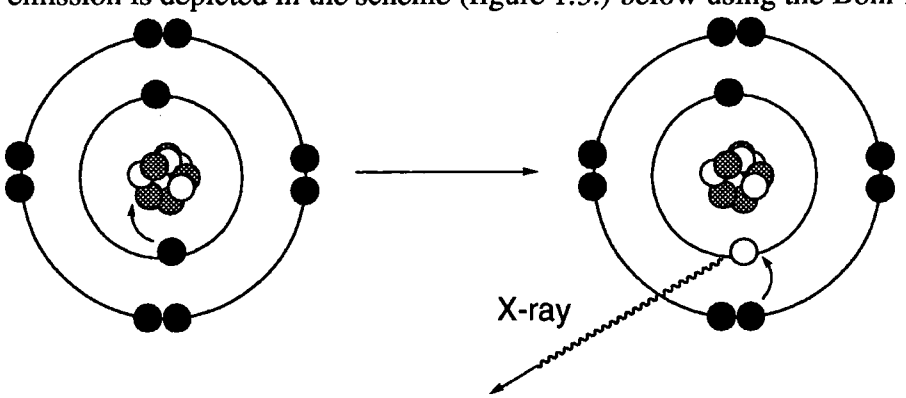

Figure 1.3. Electron capture is followed by the emission of an X-ray.

Internal Conversion - If a radionuclide transfers energy to an electron rather than emitting it as a γ-ray, then the electron is ejected from the atom. This results in an excited electronic configuration. The energy is dissipated by the emission of either an X-ray or another secondary (Auger) electron. Auger electrons are potentially useful therapeutically as a short range ionising radiation. These processes are illustrated in figure 1.4.

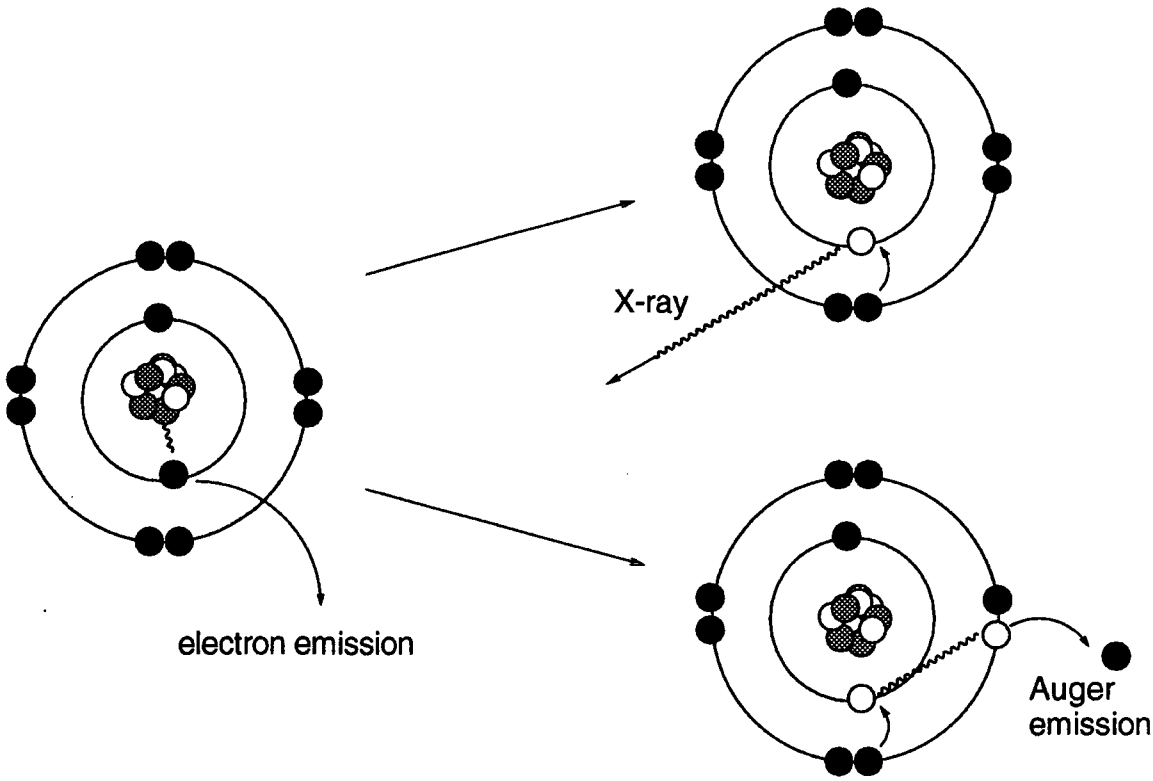

Figure 1.4. The process of internal conversion can lead to both X-ray emission and Auger emission.

Most frequently technetium-99m is chosen as the radionuclide because of the convenient availability from a generator system, at low cost, and the favourable decay characteristics, exhibited by the radionuclide. The isomeric transition has an emission (140keV) well suited to the thallium doped, sodium iodide scintillant employed to detect it.

Positron Emission Tomography

The decay of a neutron deficient nucleus may result in positron emission, β^+. Positrons are anti-electrons, possessing identical mass, but opposite charge to electrons. Anti-neutrinos accompany positron emission, but are not considered here as they have no impact in imaging.

$$\text{For } \beta^+: \quad p \longrightarrow n + e^+$$

$$^{A}_{Z}X \longrightarrow {}^{A}_{Z-1}Y + {}^{0}_{+1}e$$

β^+ particles themselves are not suitable for imaging. Positrons only exist until combining with an electron. The two annihilate, with their mass being converted to energy, in the form of two 511keV γ-rays, 180° apart. This sequence of events is depicted in figure 1.5., below. The positron and electron form a short-lived positronium which annihilates producing the two γ-rays.

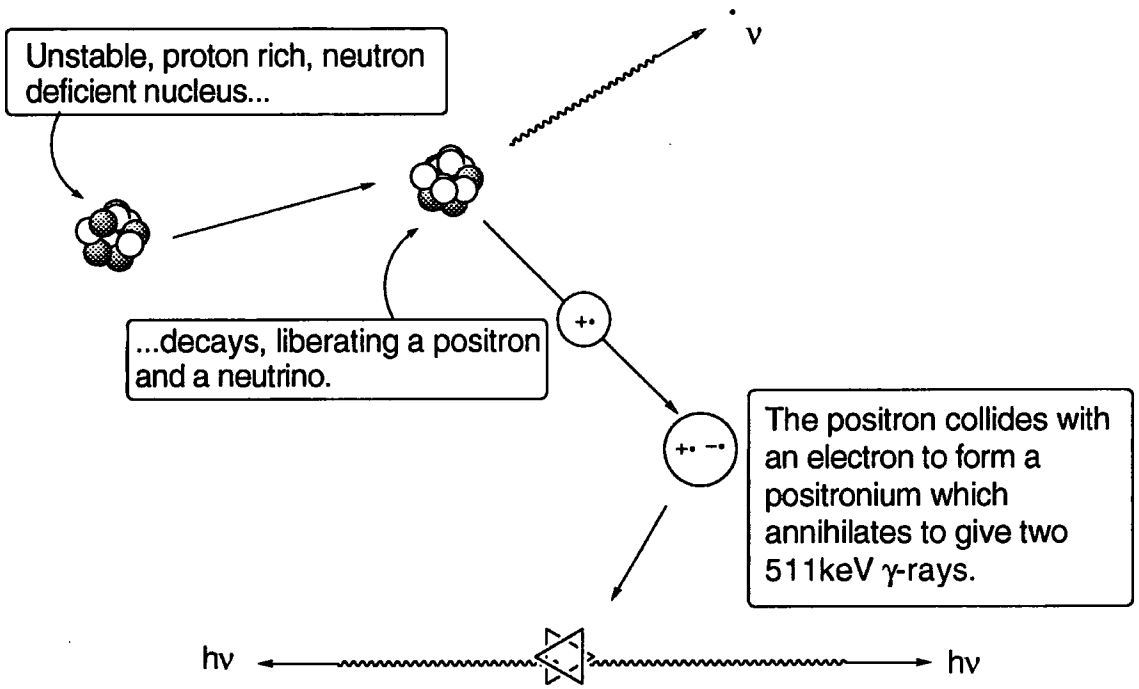

Figure 1.5. A radionuclide decays by positron emission. Kinetic energy is lost by molecular collisions, before the positron annihilates with an electron. This produces two almost collinear γ-rays.

The advent of cameras, to detect both γ-rays coincidentally, made positron emission tomography (PET) a feasible diagnostic technique in nuclear medicine. The bulk of this thesis concerns the development of radiometal complexes for use in PET imaging.

The detection of both these photons, using a coincident circuit, defines the line in which the annihilation event took place (figure 1.6., below).

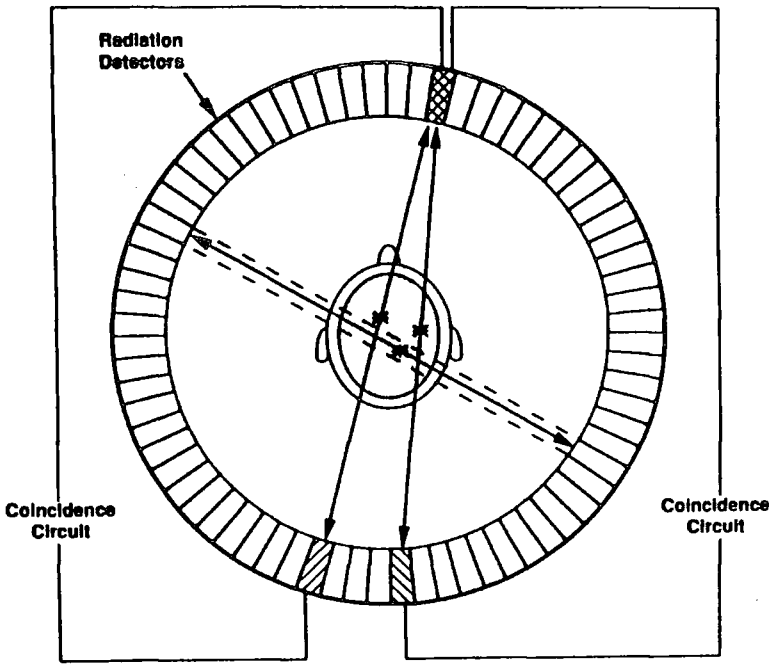

Figure 1.6. The coincident detection of both photons defines the line along which the annihilation occurred. Reproduced from reference 11.

Sets of such lines intersect at the locations of high concentrations of annihilations. As the positron only travels a short distance (1-8mm), depending on the kinetic energy of the positron, the location of the radionuclides which emitted the positrons are effectively located also. The simultaneous detection results in an increase in sensitivity, as more of the random background disintegrations can be discounted. PET cameras are not infallible, however. Scattering and background disintegations do still create signals which are incorrectly interpreted.

The technique of PET allows *in vivo* study of biochemical processes, by providing cross-sectional images of the body that quantitatively map the distribution of positron emitting radionuclides. The development of the technique has been based primarily on the "organic" radionuclides carbon-11, oxygen-15, nitrogen-13 and fluorine-18, all of which decay by positron emission. By incorporation of these radionuclides into known metabolites, for example, sugars or amino acids, it is possible to follow the path taken by the compound when administered to the body. Therefore, information about the location of various receptors in the body can be gleaned from such a technique, and, indeed, this is possible to a range of a few millimetres. Although the greatest clinical impact of PET has been in metabolism studies of the brain and heart, there is a continued interest in studies of other organs and in applications such as tumour biology.

Summary of Imaging Techniques

The sensitivity and specificity of the different imaging modalities are illustrated in figure 1.7. below.[7] The range of sensitivity spans from millimolar concentrations for MRI to sub-nanomolar concentrations, for tomographic techniques employing radionuclides. An indication of the information obtained from the techniques demonstrates the complementarity of the various modes used for imaging

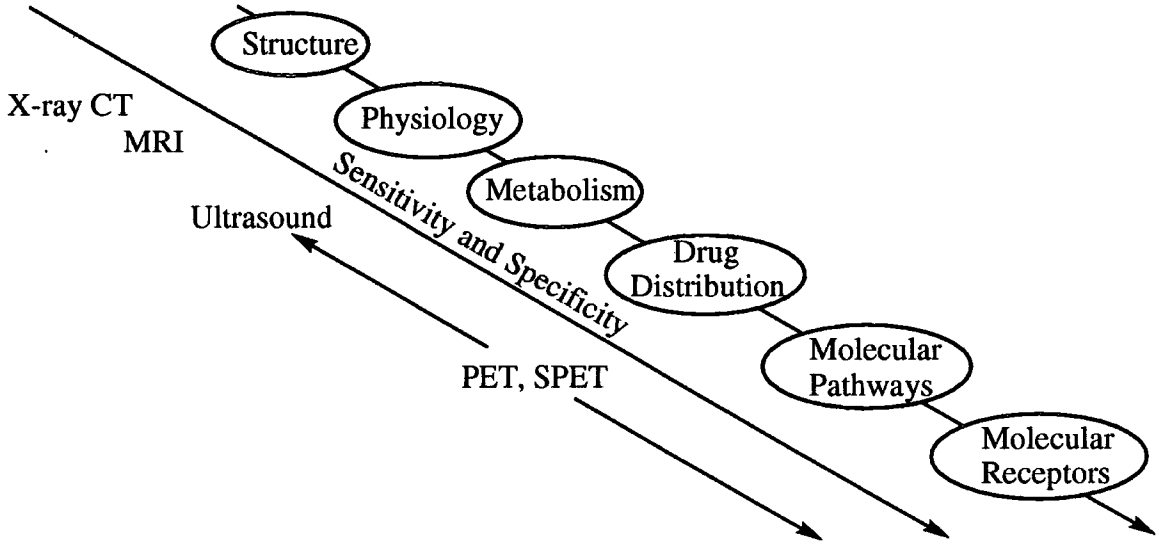

Figure 1.7. The spectrum of medical imaging, illustrating the level of information attained from various imaging modalities. Reproduced from ref. 7.

The technique of MRI has the advantage of avoiding both the handling of radionuclides and any radiation dose to the patient. However, the sensitivity of techniques utilising radionuclides renders them useful for quantitative studies, and provides biochemical information which is not as easily accessible by MRI. An additional advantage of radionuclides is the occurrence of several nuclei of the same element (isotopes) being available, which emit different radiations. This opens the possibility of therapy with ionising radiations, following initial dosimetry measurements performed with low dose γ-emitting isotopes.

The advantages of PET over SPET are greater precision in measuring the amount of activity, and the increased resolution obtained by coincident detection. Also, the sensitivity of PET is much greater, as the collimation required for a SPET system results in a large reduction in the number of counts being detected. The availability of the radionuclides of carbon, nitrogen and oxygen also add to the attraction of PET - no such analogues are available for SPET. The detection equipment for commercially available SPET systems is optimised for the emissions of technetium-99m, and, thus, the transfer to another nuclide may not be trivial. Positron emitting nuclides all give rise to 511keV

γ-rays, and so the same detector and software are applicable for all PET studies. The major disadvantage of PET is the cost of the facility. The camera itself may be ten times more expensive than a gamma camera for SPET, but the major cost incurred is the maintenance of the cyclotron. The use of a cyclotron centre, providing a service to a collection of consumers, is quite feasible, and allows the burden of cost to be shared. As PET technology becomes more available, different nuclides will play a greater rôle in diagnostic nuclear medicine.

Some nuclides used in SPET imaging have a sister isotope which decays by positron emission, such as technetium-99m/94m, which should facilitate a smooth transition from one imaging modality to the other.

1.3. Radionuclides Used for Imaging

The characteristic qualities of a suitable candidate radionuclide for imaging applications are the possession of an emission (or range of emissions) which give a detectable signal outside of the body, and a half-life appropriate to the time frame of the study. These criteria arise from the desire to minimise the radiation dose to the patient, whilst giving a respectable signal to noise quotient. Low energy γ-emitters[8] (100-200keV) and tracer amounts of β^+ emitters are suitable candidates. Fortunately, a range of radionuclides, of differing half-lives, is available offering a choice to suit each application.

Short lived radionuclides are used for studying properties such as blood flow, where the short half-life results in a smaller dose to the patient. Also, a clinical advantage is gained, as the study can be repeated after a short time period, to monitor a change with time, or under different physiological conditions. Longer lived radionuclides are useful for prolonged tracer kinetics, for example, studies using antibodies, which often localise much more slowly.

Radionuclides for Imaging - γ-Emitters

The most commonly used nuclides for SPET applications are listed in table 1.1., below.[9,10]

Radionuclide	Half life/hr	Principle γ Emissions/keV
^{67}Ga	78	93, 184
^{99m}Tc	6	141
^{111}In	68	171, 247
^{123}I	13	159
^{131}I	193	364, 367

Table 1.1. Radionuclides used for SPET.

Of these radionuclides ^{99m}Tc and ^{123}I are most suitable due to their mono-energetic emissions, which lead to a lower radiation dose to the patient, and provide an enhanced image quality, due to the reduced amount of background and scatter.

Radionuclides for Imaging - β^+ Emitters

A representative, but not exhaustive, list of positron emitting radionuclides is given in table 1.2., below.[11,12] As can be seen, a range of half-lives up to 100 hours is available. This variation of decay characteristics and chemical properties allows a choice based not only on physical half-life, but also permits some consideration to be given to the ease and flexibility with which a particular radionuclide can be tailored to fit specific applications.

Radionuclide	Half-life	Positron Yield/%	Radionuclide	Half-life	Positron Yield/%
^{11}C	20 min	>99	^{66}Ga	9.5 hr	57
^{13}N	10 min	>99	^{72}As	26 hr	88
^{15}O	2 min	>99	^{75}Br	1.6 hr	76
^{18}F	110 min	97	^{76}Br	16 hr	57
^{52}Fe	8 hr	57	^{83}Sr	33 hr	24
^{55}Co	18 hr	77	^{89}Zr	78 hr	23
^{57}Ni	36 hr	40	^{94g}Tc	5 hr	11
^{60}Cu	23 min	92	^{94m}Tc	54 min	72
^{61}Cu	3.5 hr	61	^{120}I	1.4 hr	46
^{64}Cu	13 hr	18	^{124}I	101 hr	22

Table 1.2. Positron emitting radionuclides.

An important practical consideration, when choosing a radionuclide, is the speed at which the radionuclide, or compound derived from it, can be delivered from the source to the patient. Applications involving radionuclides with half-lives of the order of minutes cannot be considered, unless a cyclotron is available at the hospital where the study is to take place.

An alternative strategy, which *does* permit the use of short lived nuclides at centres removed from a cyclotron, is to use generator produced nuclides.

Generators

A generator is a method of producing a shorter lived radionuclide from one of longer half-life. The parent radionuclide can be produced at a remote site and transported to the clinic. The parent decays to the shorter lived daughter, which is withdrawn from the generator by a physical or chromatographic separation and administered to the patient. The parent radionuclide continues to decay and so the process may be repeated until the generator becomes inefficient, due to the eventual decay of the parent.

Table 1.3., below lists some radionuclides which can be produced from generators. The half-life of the parent is clearly important. A reasonably short half-life is sought for large scale production of the daughter, but too short a half-life results in a poor "shelf-life" and the inconvenience of having to repeatedly replenish the parent activity.

Parent	Half life	Daughter	Half-life	Positron yield/%
^{52}Fe	8 hr	^{52}Mn	21 min	97
^{62}Zn	9 hr	^{62}Cu	10 min	97
^{68}Ge	271d	^{68}Ga	68 min	89
^{82}Sr	25 d	^{82}Rb	1 min	95
^{86}Zr	16 hr	^{86}Y	15 hr	34
^{110}Sn	4 d	^{110}In	69 min	62
^{122}Xe	20 hr	^{122}I	4 min	77
^{134}Ce	3 d	^{134}La	7 min	62

Table 1.3. Generator produced positron emitting radionuclides.

1.4. Perfusion Studies

The behaviour of a tumour is significantly affected by the supply of blood.[13] The nutrients and oxygen provided by the blood are necessary for the tumour cells to survive and divide. Similarly, the delivery of agents to destroy the tumour benefits from an increase in the local blood flow. In addition, the efficacy of conventional radiotherapy is compromised by hypoxia, a result of poor oxygen delivery. The *manipulation* of tumour blood supply clearly has potential as a means to affect the management and treatment of the disease, even though it may seem, intuitively, that an increase in perfusion would provide the tumour with better conditions in which to flourish.

Manipulation can be achieved by the use of various pharmacological agents, which constrict or dilate blood vessels.

Two therapeutic scenarios can be envisaged. Increasing the blood flow results in more effective radiotherapy, and potentially, increases intra-tumoral uptake of chemical agents. Alternatively, a decrease in blood flow, which promotes hypoxia, may enable tumour targeting with compounds that possess bioreductive cytotoxicity. In both these situations, it is necessary to measure tumour blood flow, to gauge the success of efforts to affect blood flow, and also to monitor any physiological change adopted by the tumour to counter the alteration.

The use of radionuclide techniques is clearly appropriate for perfusion studies. The sensitivity achievable with SPET or PET allows a tracer amount of a radionuclide to act as a marker of blood flow without perturbing the system under scrutiny. Several nuclides have been used to provide quantitative information in this way. Technetium-99m is the most commonly used radionuclide for diagnostic purposes, accounting for well over 90% of studies, and dominating the £700M per annum market.[14] Several factors have combined to enhance the popularity of the radionuclide. The physical characteristics of single photon emission (140keV) and a half life just over 6 hours, make the radionuclide amenable to SPET imaging, without exposing the patient to an excessively high radiation dose. The pertechnetate ion is readily produced in a generator, making it commercially attractive.

Several complexes have found use in the clinic for measuring blood flow. The ligands are chosen to provide the necessary tailoring to suit the application in mind. Some commercially available Technetium imaging agents[15] include Tc-MIBI **1** (Cardiolite) for imaging myocardial perfusion, Tc-HMPAO **2** (Ceretec) for cerebal perfusion and Tc-MAG_3 **3** (TechneScan) for kidney function. The ligands are supplied in sealed vials containing the lyophilised ligand together with the necessary reducing agent, usually tin(II) chloride. The radioactive pertechnetate solution is added and, after an assessment of quality, the complex is administered to the patient.

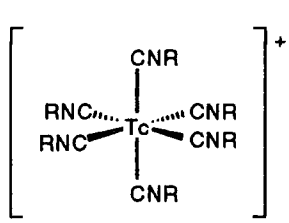

1

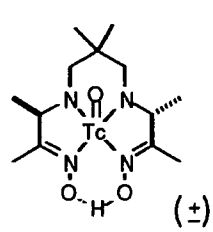

2

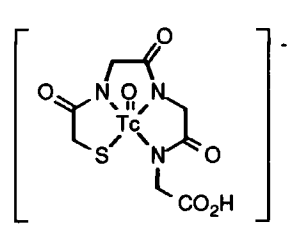

3

In PET studies, use is made of the positron emitting nuclides of oxygen and nitrogen. ^{15}O-water, ^{15}O-butanol and ^{13}N-ammonia are used as blood flow imaging agents. The use of these short lived nuclides is attractive, as the study can be repeated at brief time intervals, to give information about the effect of modifying the blood flow, at several time points during the study. However, the use of these nuclides necessitates the provision of an on-site cyclotron, and, hence, most hospitals are unable to benefit from the increased sensitivity and resolution offered by PET. Attempts to overcome this shortcoming have centred around the need for generator produced positron emitting nuclides. One much studied example is the use of copper-62 ($t_{1/2}$=9.7 mins), product of the ^{62}Zn/^{62}Cu generator.[16]

There is a great deal of investigation into ligands which bind copper. Much work is centred around the PTSM **4** complex, a very lipophilic charge neutral copper complex, which is being closely examined in the clinic, to assess suitability for studies of blood perfusion.[16]

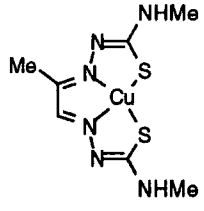

[Cu(**4**)]

The fate of copper PTSM is believed to be cellular reduction of the copper(II) ion to copper(I), with concomitant loss of complex stability, and trapping of the free reduced ion.[17] Because the extraction of the complex from the blood is essentially complete in the first pass, quantitative information is gained relating the regional uptake of activity with perfusion. A problem encountered in the use of copper-62 is the short shelf-life of the generator, resulting from the relatively short half-life of the zinc-62 parent.

An attractive alternative generator is the ^{134}Ce/^{134}La generator, which has highly desirable decay characteristics for both the parent and daughter nuclides. Lanthanum-134 has a 6.7minute half-life with high positron emission. The parent cerium-134 has a half-life of 3.2 days. This gives the generator a shelf-life of around two weeks, comparable to the ^{99}Mo/^{99m}Tc generator, familiar to all radiopharmacies.

Although the lanthanides exhibit similar co-ordination chemistry, little has been reported on the tailoring of lanthanum complexes for use in diagnostic medicine. The development of ligands to bind lanthanum for use in perfusion imaging forms the subject matter for chapter 2, below.

1.5. Imaging Receptor Sites on Tumours

Tumour cells often display an increase (overexpression) or decrease (underexpression) of surface proteins, compared with normal healthy cells. Alternatively, a slight modification in the number, type or position of prosthetic groups, e.g. carbohydrates, may be observed. These subtle differences affect the way in which the cell interacts with the environment and, in particular, affects the ionic and molecular species the cell attracts and binds to - processes essential to the survival of the cell. The surface differences are also detected by the host's immune system and trigger a response, with the body's own defence mechanism releasing antibodies to try and expel the unwanted cell.

Antibodies are high molecular weight proteins (M_r ~150 000 Da) which possess the ability to recognise surface features (antigens), differentiating between healthy and unhealthy cells. On binding to the tumour cell surface, a sequence of biochemical changes are invoked which result in cell death.

Artificial antibodies can be raised against a known antigen, and produced in a large amount by the use of the hybridoma technology, developed by Köhler and Milstein.[18] The antibodies produced do not complete the process of destroying the cell, as they are not the host's own. By the incorporation of radionuclides into the antibodies, the cell surface and, hence, tumour, can be imaged. Detailed information on the location of the tumour and metastases can be gained by such an approach. The sensitivity of radionuclide imaging permits the detection of small secondary tumours.

Choice of Radionuclide

Several radionuclides warrant investigation for their applicability in targeted imaging of receptor sites. The choice is primarily limited by the half-life, which should ideally be comparable to the time frame of the study. For antibody based imaging protocols, the time taken for localisation is 24-48 hours for whole antibodies. However, the time may be considerably less for fragments of antibodies, or other low molecular weight targeting vectors. Inspection of the abbreviated list of nuclides (under paragraph 1.3.) suggests several suitable medium lived radionuclides. It was decided for this study to use copper-64. This radionuclide was chosen primarily because it has a half-life (12.8 hours) suitable both for use with antibodies and, also, smaller targeting vehicles. Many stable complexing agents have been defined for copper, which may be elaborated for attachment to targeting modalities. In addition, copper-64 has a range of emissions, including potentially useful ionising radiations of various energies. The availability of

copper-67 as a therapeutic isotope may result in a smooth transition from imaging to targeted therapy, with the same antibodies.

Conjugation to Low Molecular Weight Targeting Vehicles

The use of radioactively labelled small molecules, which exhibit selectivity for tumour cells over healthy cells, has the significant advantage that localisation is much quicker than with antibodies. The result of this is a reduced dose to the non-target tissues. However, the specificity of these smaller molecules may not be as high as for the antibody approach. (The use of the term "small" is somewhat arbitrary. Attempts have been made to use fragments of antibodies (M_r = 50 000 Da) where only the portion of the antibody required for antigen recognition is used. For the purpose of this section, molecules of mass < 1000 Da are considered "small.")

As mentioned previously, tumours express proteins which bind with some selectivity to various molecules *in vivo*. The molecules sought include hormones and small peptides. The realisation that tumours show an increased uptake of molecules such as these has inspired the synthesis, and testing, of labelled variants, including the examples below. The ^{18}F-fluorinated steroid **5** is finding clinical application for imaging breast tumours using PET. The work has been extended to develop metal complexing agents, mimicking the structure of steroids, for both imaging and therapy of steroid positive tumours. For example, the progestin derivative **6**, functionalised at the 11β position,[19] and the rather unusual dihydrotestosterone **7** mimic **8**.[20]

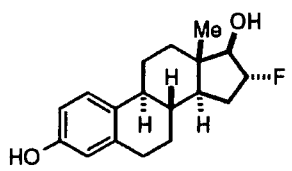

5

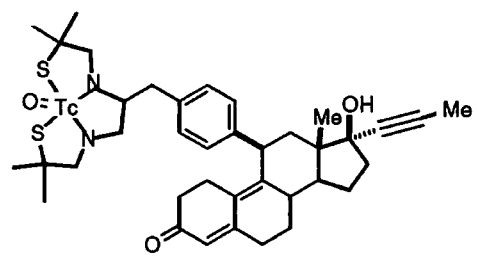

6

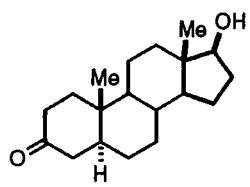

7

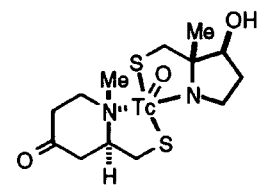

8

Octreotide, an octapeptide which binds selectively to the somatostatin receptor, has been labelled with indium *via* terminally conjugated DTPA. The conjugate **9** retained a very high affinity for the receptor.[21]

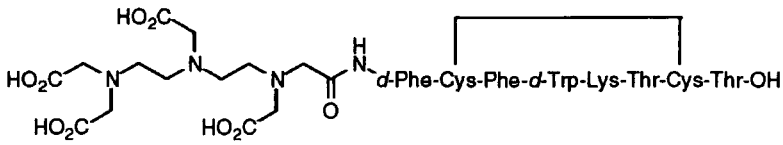

9

It seems likely that the incorporation of an unnatural prosthetic group to these small molecules will cause a large change in the three dimensional electron distribution that is recognised by the cell. This may account for the loss of specificity found with some low molecular weight targeting vehicles. With antibodies, such changes may be more tolerable, as only a fraction of the molecule is required for recognition.

The prospect of pretargeting using an unlabelled antibody followed (after localisation at the tumour) by a low molecular weight tracer, which shows a specificity for the antibody, is an attractive idea. The method offers the prospect of excellent specificity, without the radiation dose being borne by the whole body. The tools to test the validity of this approach exist with the avidin biotin system.[22]

Biotin **10** (vitamin H) is a low molecular weight enzyme cofactor whose role *in vivo* is to activate acetate groups by addition of carbon dioxide to form malonyl derivatives. Biotin shows a remarkable affinity for the tetrameric protein avidin, extracted from egg white, and the similar protein streptavidin, extracted from *Streptomyces* bacteria. The value of the dissociation constant ($K_d = 10^{-15}$ dm^3 mol^{-1}) is more akin to those of metal complexes than the non-covalent interactions between hosts and their guests, where the bonding involves principally hydrogen bonding and hydrophobic interactions. The driving force that keeps biotin and avidin bound, effectively non-reversibly, is both entropic and enthalpic in origin, with several poorly bonded water molecules being displaced from the binding site of avidin, on complexation with biotin.

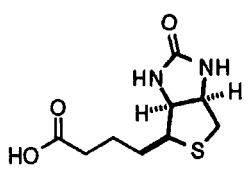

10

If a monoclonal antibody is conjugated with biotin, it may be coupled to avidin *via* one of the binding sites on the avidin. As avidin is tetrameric in nature, three binding sites are left vacant. A radiolabelled biotin conjugate, introduced after antibody localisation, would be expected to bind to the "avidinated" antibody at the site of the tumour. This hypothesis is presented schematically below (figure 1.8.)

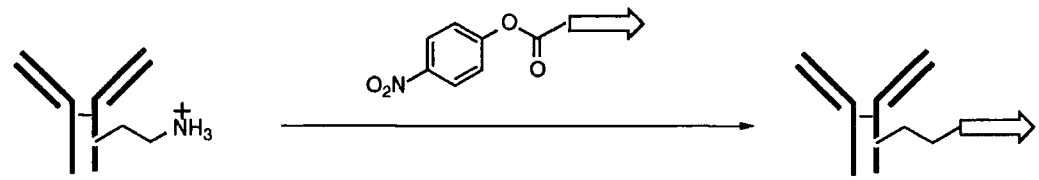

Step 1.The antibody is derivatised at lysine by reaction with biotin active ester

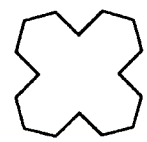

Step 2. The "biotinylated" antibody is conjugated to the tetrameric protein avidin

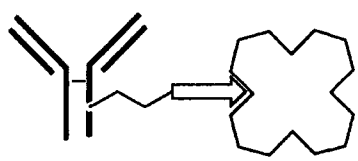

Step 3. The hybrid protein is administered to the patient, and left for 24-48 hours to achieve a high degree of localisation

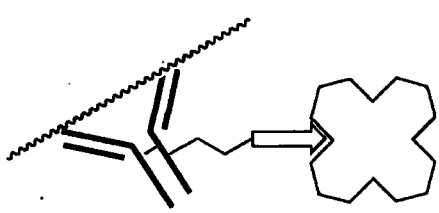

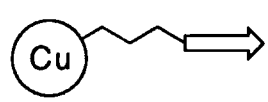

Step 4. The copper-64 conjugate, incorporating the biotin motif is administered, and rapidly forms a stable, non-covalent link with avidin anchored to a tumour cell *via* the antibody

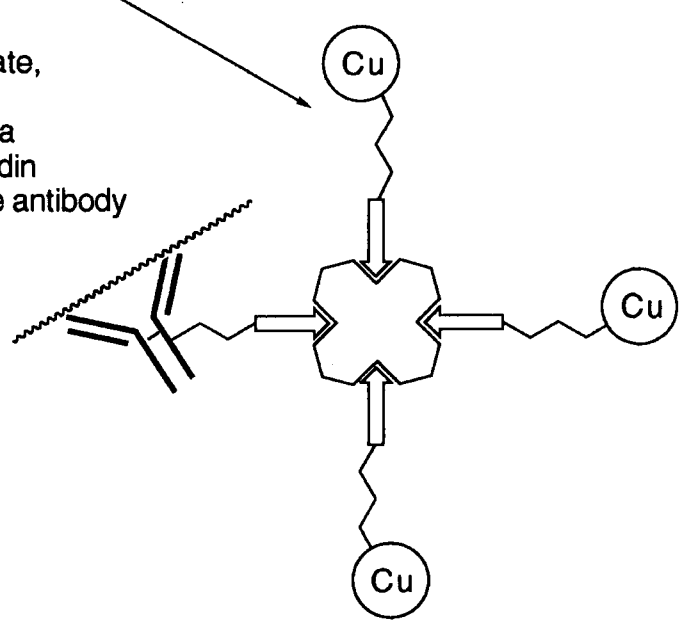

Legend:

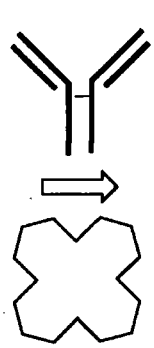

= Antibody

= Biotin

= Avidin

Figure 1.8. A schematic diagram of the envisaged multi-step approach to tumour targeting.

This approach to tumour targeting is not particularly novel. Several conjugates have been defined, incorporating radionuclides suitable for SPET imaging. The DTPA derived ligand **11** has been reported for use with indium,[23] however, the anionic complex might be expected to demetallate *in vivo*. A similar approach to targeting, using the technetium complex **12**, has also been investigated.[24] The half-life of copper-64 is suitable for consideration for PET studies using this pretargeted approach. The synthesis and characterisation of copper complexes, incorporating the biotin moiety, for potential use in PET imaging are discussed in chapter 3 below.

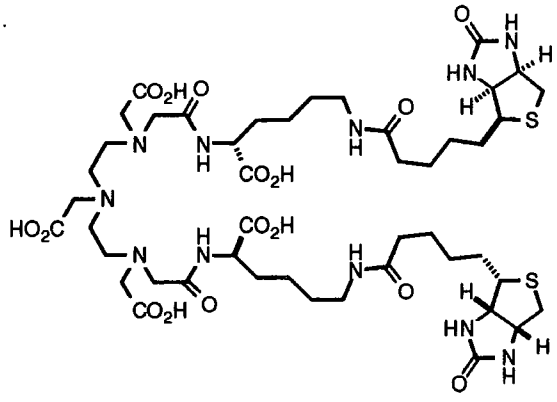

11

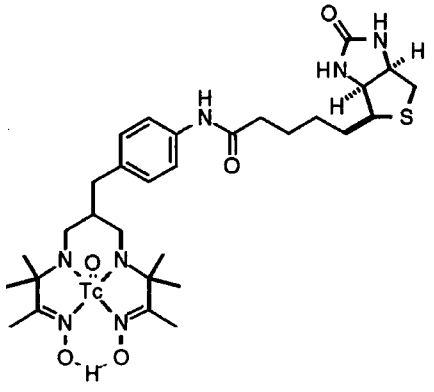

12

Conjugation to Antibodies

There are several criteria that a complexing agent must fulfil, to serve as a means of attaching a metal ion to a protein.[25] The complexing agent has to be attached in a manner which does not compromise the immunoreactivity of the antibody, i.e. the point of attachment must be somewhat removed from the binding portion of the antibody. The linkage must be covalent and stable *in vivo*, as well as not provoking an immune response from the host.

Points of Attachment

Several amino acid residues provide a convenient point for attachment of the complex. The most reactive is the thiol group of cysteine, which reacts at physiological pH. However, most of the thiols are oxidised to form disulfide bridges, which play an important structural rôle, in the conformation of proteins. Additional thiol groups may be introduced, using the method developed by Traut[26] and modified by Meares,[27] where 2-iminothiolane **13** is reacted with the ε-amino group of the lysine residue. The free thiol may then be reacted quite selectively, with either α-halo carbonyl compounds or with Michael acceptors such as maleimides, as depicted in figure 1.9., below.

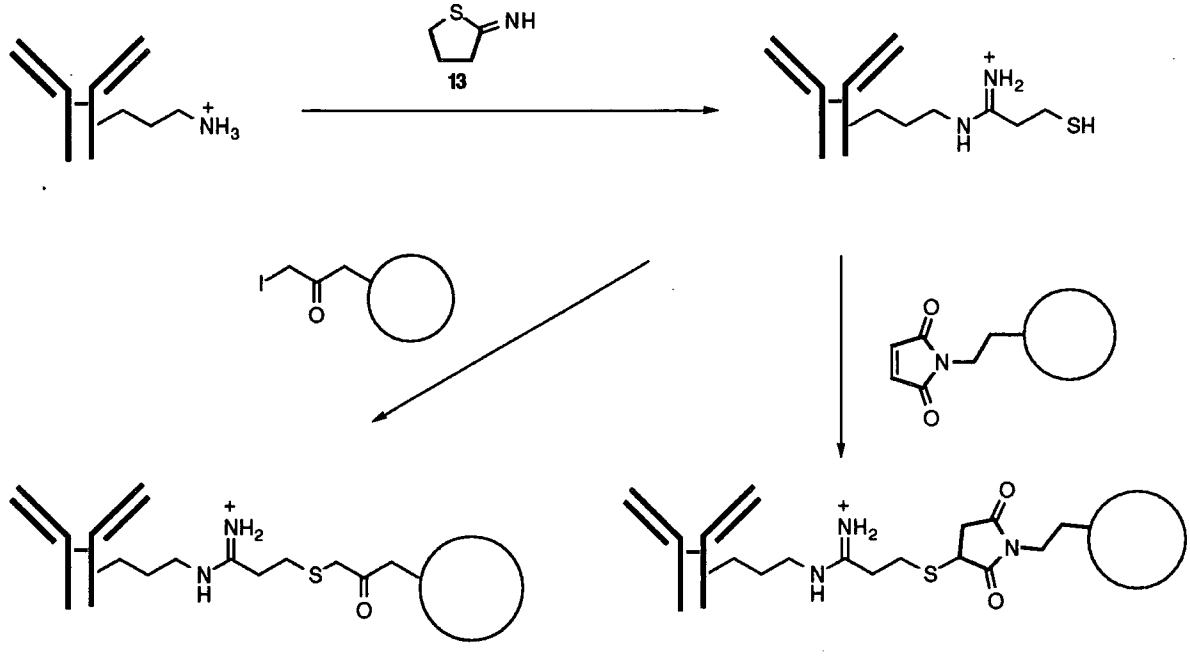

Figure 1.9. The conjugation of complexing agents with proteins, using 2-iminothiolane.

The terminal amine group on lysine residues reacts with activated esters of, for example, N-hydroxy succinimide or *p*-nitrophenol. A slightly elevated pH is required to render the amine a little more nucleophilic. The terminal amine can also react with the isothiocyanate group to form a stable thiourea linkage. These more direct conjugation reactions are shown below (figure 1.10.)

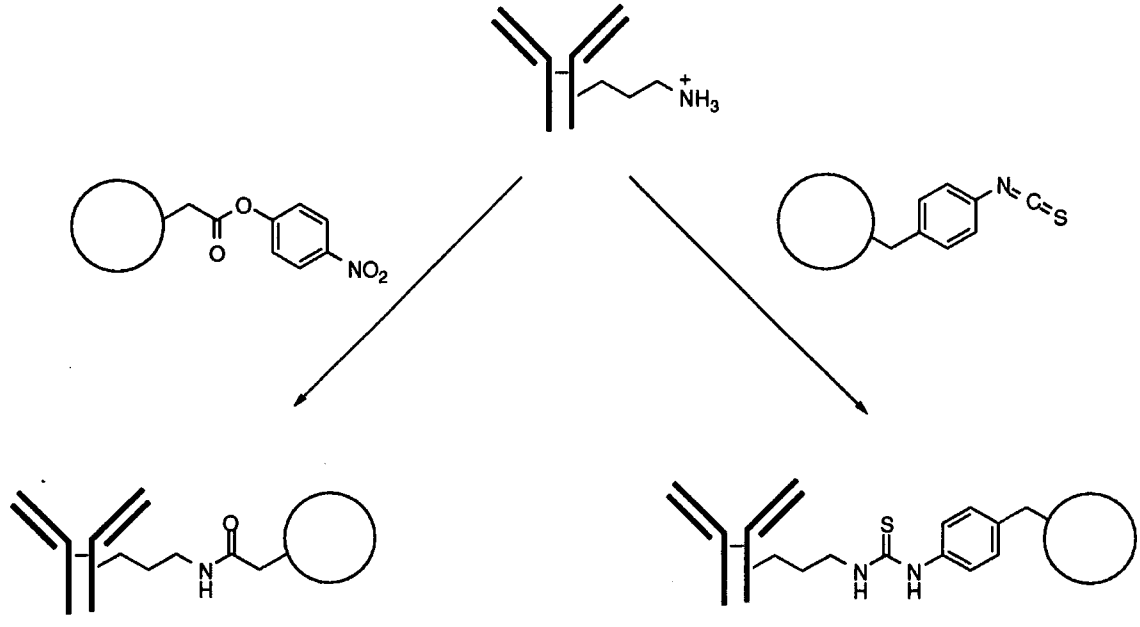

Figure 1.10. Direct conjugation at lysine.

Carboxylic acid groups on some residues have also been used, usually *via* a carbodiimide coupling reaction. The activated, aromatic group of tyrosine has seen use for conjugation, particularly with diazonium compounds. This is also the point where oxidised iodine species attack, in the direct halogenation of proteins.

In this study the point of attachment is the lysine residue, either by direct reaction with active esters or through the free sulfurs introduced by the Traut method. The number of lysines does, of course, vary between proteins, but there is a tendency for hydrophilic residues to be disposed at the more accessible sites (i.e. the surface) of the protein. Therefore, it can be expected that the modification of the lysine residue can be accomplished without a change in protein conformation. This is clearly desirable, as the specificity of the antibody is totally dependent on the complementarity of shape between the antibody and the receptor site on the tumour surface.

1.6. Towards Targeted Therapy with Radionuclides

There is considerable potential for ionising emissions from decaying nuclides to be used therapeutically. The radionuclides most likely to find use are α, β and Auger emitters.

Alpha emission - Heavy nuclides are able to lose energy by the emission of an α-particle, two neutrons and two protons. These relatively massive particles have a very short range in tissues (μm) and fail to escape the body. The strong ionising ability of α-particles renders such nuclides suitable for therapeutic applications.

$$ {}^{A}_{Z}X \longrightarrow {}^{A-4}_{Z-2}Y + {}^{4}_{2}\alpha $$

Beta emission - The decay of a proton deficient nucleus resulting in the release of an electron is termed beta decay β^-. The ionising radiations are potentially useful in therapy.

$$ \text{For } \beta^-: \quad n \longrightarrow p + e^- $$

$$ {}^{A}_{Z}X \longrightarrow {}^{A}_{Z+1}Y + {}^{0}_{-1}e $$

Auger electrons, mentioned above, are also worthy of consideration. The short path length of Auger emissions (nm) effectively limits their dose to a single cell. This is in contrast to β^- particles which may exhibit mean path lengths, in tissue, of up to 4mm.

Positron emitting nuclides could be used to provide the ionising radiation required for therapeutic applications, with simultaneous imaging. However, the number of high energy (511keV) γ-rays which accompany positron emission could result in a prohibitively high radiation dose to the patient. The criteria a positron emitting radionuclide must satisfy to be considered for therapy are (i) a β^+ energy suited to the morphology of the tumour, (ii) a low positron emission. Sufficient annihilations must take place for imaging, but ideally, not too many, otherwise the whole body dose could become too high. Finally, (iii) the rest of the decay (usually by electron capture) should not lead to other γ-rays, hence further enhancing the dose. Copper-64 is a quite unique radionuclide, combining β^+, β^- and Auger emission, and is the positron emitting nuclide most suited to therapy.

There are a number of elements possessing both a positron and a β^- emitting isotope. Such radionuclide pairs include copper-64/67, yttrium-86/90, strontium-83/89, iodine-124/131. The prospect of therapy using a cocktail of mixed isotopes of the same element appears quite attractive, and would permit the application of therapy with simultaneous imaging.

For radiotherapy, it is essential to deliver as much ionising radiation to the tumour as possible, whilst the dose to healthy tissue is minimised. Conventional radiotherapy employs an externally located source which is focused on the tumour. For a deep seated tumour, the path of radiation is obscured by the presence of healthy tissue, which subsequently receives a high dose. Targeted radiotherapy offers the prospect of delivering the dose solely to the tumour. Monoclonal antibodies offer a means to deliver the radionuclide to the site of the tumour. However, the time taken for localisation results in a high radiation dose to the whole body. For lower energy, imaging protocols, this may not give rise to much concern, but the more harmful ionising radiations used in therapy may prohibit the use of full antibodies. The use of antibody fragments may improve matters, as may low molecular weight targeting vectors, introduced above.

An alternative strategy may be to "implant" the source directly into the tumour. The poor vascularity of many tumours might be expected to result in a poor washout, effectively keeping the activity in the tumour. Some precedence for this type of therapy has been reported in the use of lipiodol **14**,[28] an iodinated ester of unsaturated fatty acids derived from poppy seed oil. Radioiodinated analogues show a remarkable uptake and retention in liver hepatoma. Conjugation to a complexing agent **15** has been achieved, which has enabled the use of nuclides more suited to therapy to be investigated.[29]

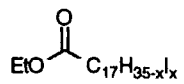

14

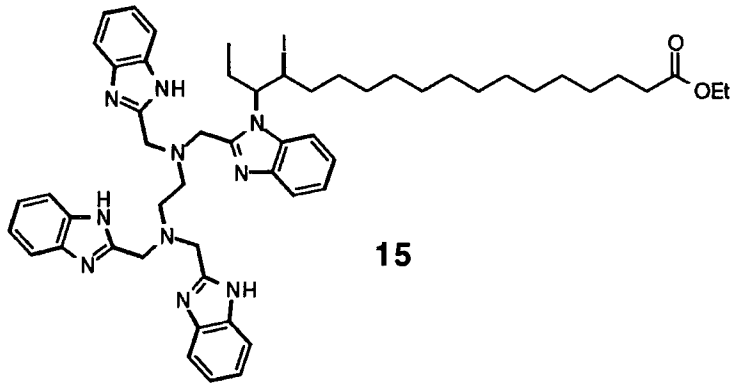

15

1.7. Ligands for Forming Metal Complexes

It is well known that the stability of complexes formed between metal ions and electron donors, arranged in a macrocyclic array, far exceeds those complexes formed by several discrete ligands.[30] When designing macrocyclic ligands, several parameters can be varied to affect stability. The primary factors to be considered are:

1) donor groups
2) ring size and conformation

The choice of donor group is important to the thermodynamic stability of the complex, the rate of formation of the complex and, also, has an effect on the charge of the complex. The main atoms which are used as donors are

nitrogen as either an amine or an imine (neither affect the charge of the complex),
oxygen as an ether or carbonyl (no effect on charge) or an "ate" (derived from deprotonation of an acid or alcohol/phenol, resulting in a lowering of the complex charge.)
sulfur. Analogous to oxygen, but, potentially, with further complications arising from the various oxidation states exhibited by sulfur.
Some other atoms are also used e.g. phosphorus analogously to nitrogen

The optimum ring size for forming stable complexes varies considerably, not only with the size of the relevant metal ion, but also depends on whether the metal sits in the plane or caps the faces described by the donor atoms. Generally, five membered chelate rings give the optimum stability, but it has been shown[31] that more stable complexes are formed with some smaller ions, if six membered chelating groups, with a smaller bite angle, are used. The combination of 5 and 6 membered chelate rings can serve to provide complexes of optimal stability for the ion in question.

For use with radionuclides *in vivo* several criteria have to be satisfied by ligands. The complexing agent must bind the metal ion quickly, preferably with some selectivity. (Although radionuclides are isolated in a radiopure form, some cold metal ions are often present as chemical impurities. Some ligands, used to bind metal radionuclides, indiscriminately bind the first ion encountered, rather than the desired one, resulting in a drop in labelling yield.) The complex formed must be stable to metal loss *in vivo*. The physiological pH of 7.39 applies to serum, and does not nearly represent the range of pH the complex may be expected to encounter in the body, where the pH drops to below 2 in the stomach and, most importantly as far as catabolism is concerned, the liver. The instability of some metal complexes at low pH has resulted in some compromised biological evaluation of conjugates, even though the known formation constants are deemed sufficiently high.

Ligands to Bind Lanthanides

There is considerable interest and synthetic effort in designing ligands to utilise the special effects that many lanthanide ions exhibit. For example, ligands to form stable complexes have been synthesised to bind toxic ions for use *in vivo*.[32] Ligands incorporating chromophore antennae have been devised, which may find use as luminescent probes, on complexation with ions possessing long lived excited states.[33]

The most commonly used ligands for binding lanthanides are polyaminocarboxylates, in particular DTPA **16** and DOTA **17**. Both form complexes of high thermodynamic stability, but are not appropriate for all applications. An array of alternatives is under continual development to tune complexes for specific uses.[34]

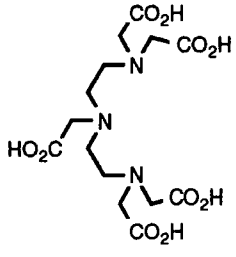

16

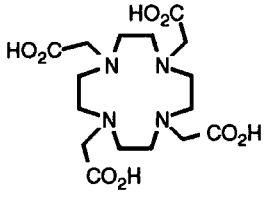

17

For use in perfusion studies, it is desirable that the nuclide be rapidly cleared from the blood, preferably on the first pass of the circulation. This necessitates the uptake and retention of the radionuclide by cells for the duration of the study. The short half-life of lanthanum-134 reduces the need for the complex to be excreted intact, as the radio tracer rapidly decays to present no long term risk. This concession to stability allows more flexibility in the design of ligands to bind lanthanum. An increased effort can be

invested towards producing complexes which are trapped quickly, rather than ensuring that the complex integrity is preserved.

The primary factors which affect the cellular uptake of complexes are the charge, molecular weight and lipophilicity. These observations point towards membrane permeability as the major factor determining whether a complex is taken up or not. All cells have a phospholipid bilayer, hence, it might be expected that lipophilic species are more adept at entering cells.

The ligands DTPA and DOTA form anionic hydrophilic complexes which are not suitable for use as perfusion agents. The basic geometry of these ligands does provide complexes sufficiently stable for *in vivo* use, and provides a framework to be built upon. A modification to these ligands is sought, which will increase the lipophilicity of complexes formed with lanthanides.

The use of complexing agents incorporating amides as ligating groups in the place of the carboxylates results in the formation of complexes with an increased positive charge. By substitution of the appropiate number of carboxylates, illustrated by the generalised structures, of figure 1.11., ligands can be produced which will form charge neutral complexes, on incorporation of a cation. Such complexes might be expected to enter cells more easily than charged ones.

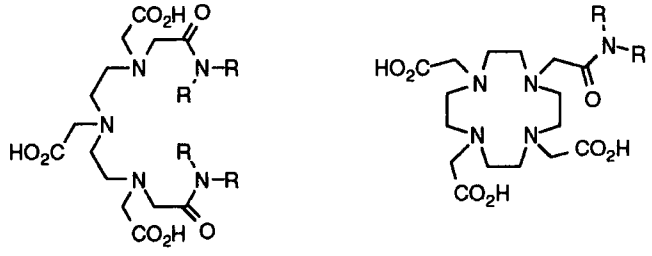

Figure 1.11. Generalised structures of ligands capable of forming charge neutral complexes on binding to lanthanide ions.

In addition to reducing the charge on the complex, incorporation of the amide provides a handle for convenient control of the complex's properties, and for conjugation to targeting vehicles, such as monoclonal antibodies.[35]

An alternative donor group to the carboxylate is the phosphinate. The change of acid moiety introduces the possibility of elaboration at the phosphorus atom, and, indeed, this has been realised[36] with, for example, the ligand **18**. Some control of lipophilicity is gained by the designer, which has an effect on the biodistribution and clearance rate of the complex. Also, the change to a more acidic group results in complexes more able to

resist protonation. This may be important in applications where stability under acidic conditions is paramount. The increase in lengths of bonds to phosphorus over carbon manifests itself as a larger bite angle being displayed to the complexed metal ion. Possibly, this may result in increased stability of complexes of larger ions, and a tolerance of geometry prohibited by carboxylate analogues.

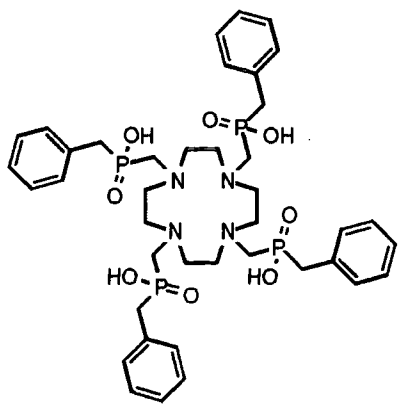

18

A comparison of complexes of DOTA with those of the analogous phosphinic acid reveal a difference in the co-ordination number of the metal. The crystal structures of the yttrium complexes have been determined.[37,38] It is quite clear that, whilst an approximately square anti-prismatic structure is adopted by both, the $[Y(DOTA)]^-$ complex exhibits 9 co-ordination of the metal centre with one face capped with a water molecule. This water molecule is absent from the phosphinic acid derived complex.

The structural curiosity demonstrated by the yttrium complexes clearly has implications for the prospects of gadolinium complexes of these ligands. The relaxivity of a paramagnetic complex is primarily a function of the number of bound water molecules and the correlation time. As the ionic radius of yttrium and gadolinium are quite similar, it may be expected that gadolinium complexes will be isostructural with the corresponding yttrium complexes. The potential for use of both complexes as contrast agents has been investigated.[39] The $[Gd(DOTA)]^-$ complex behaves as an inner sphere contrast agent, whereas the phosphinic acid derived complex behaves as an outer sphere contrast agent, consistent with the absence of metal bound water.

Ligands to Bind Copper

There are two common oxidation states of copper. The preferred co-ordination geometry changes with oxidation state. Copper(I) forms tetrahedral complexes, whereas copper(II) opts for distorted octahedral geometry. This distortion (Jahn-Teller effect) is a result of the degeneracy of the t_{2g} and e_g energy levels, present in true octahedral complexes, arising from the d^9 configuration of the ion. The distortion is

manifested to such an extent, that the complexes formed are more accurately described as square planar.

This change of geometry with oxidation state necessitates the need for ligands to be designed for the specific *ion* to be used, if complexes of high stability are sought. The change in complex stability on reduction has been exploited, however, with the copper PTSM complex [Cu(**4**)]. Bifunctional complexing agents based on the PTSM framework **19** for protein conjugation have been defined.[40]

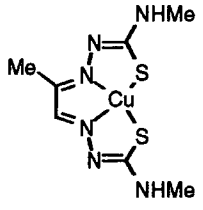

[Cu(**4**)]

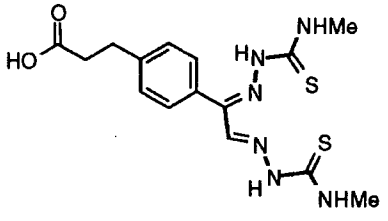

19

However, the applications to be developed herein, require copper complexes of high stability *in vivo*. Several potential complexing moieties have been defined and their stability constants, determined at 298K, are listed in table 1.4.,below.[9]

It is, however, important to remember that the body is not at equilibrium, and, although serum pH may be very mild, many metabolically important organs offer highly acidic environments to vulnerable metal complexes. Hence, it is necessary to consider the stability of the complex (and any conjugate derived from it) at a range of acidity. The charge of a complex may provide useful clues to the stability of the complexes listed in the table below. It may be expected that cationic complexes will electrostatically repel advancing protons which could lead to the extradition of the metal. The acid catalysed dissociation has been investigated,[41] and it was found that protonation, rather than donor group displacment, was the factor most important in the dissociation pathway. On the contrary, anionic complexes will attract protons, and other cations, which may lead to an increased susceptibility to metal loss. For example, the stability constants of the respective monoprotonated complexes of TETA, DOTA and NOTA (log K_{MHL}) are 14.6, 14.4 and 12.7, representing a drop of ten orders of magnitude over the unprotonated complexes. The complexes have pKa values[42] between 2.7 and 4.3, which indicates that the complexes should be *fairly* stable with respect to acid catalysed dissociation, and much work has been done on the carboxylates. An advantage of the negatively charged polyaminocarboxylates is that they would be expected to form complexes more rapidly than the dicationic (under labelling conditions) tetraamines.

Ligand	log K_{ML}	Charge
$14N_4$ **20**	27.2	+2
$13N_4$ **21**	29.1	+2
TETA **22**	21.6	-2
DOTA **17**	22.2	-2
NOTA **23**	21.6	-1
DTPA **15**	21.4	-3
EDTA **23**	18.9	-2

Table 1.4. The stability constants of some representative copper complexes.

20

21

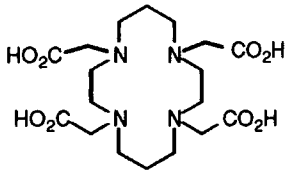

22

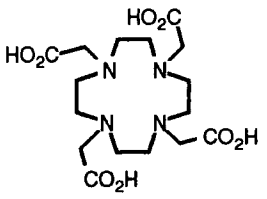

17

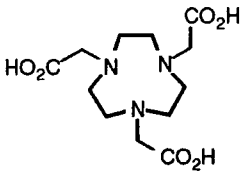

23

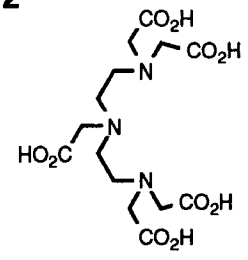

15

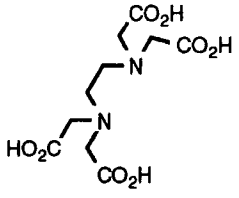

24

All of the ligands above have been investigated, to an extent, for use in antibody based imaging. The ease of incorporating DTPA and EDTA on to proteins by the use of their respective anhydrides e.g. **25** makes rapid conjugation feasible (figure 1.12). However, the conjugates produced showed a propensity to demetallate *in vivo*.[43]

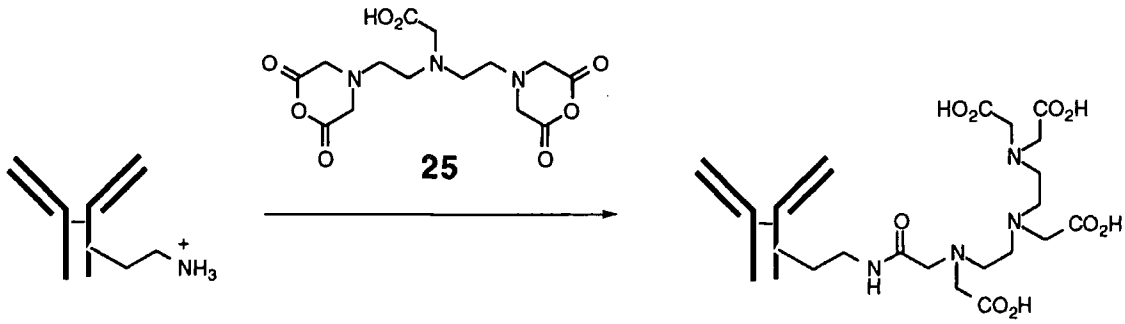

Figure 1.12. The reaction of an antibody lysine residue with DTPAA **25** allows rapid metal conjugation, albeit at the sacrifice of stability.

The macrocyclic complexes offer greater stability and many conjugates have been defined and tested with a variety of radionuclides. Much work with copper has centred around the use of the TETA ligand, coupling to thiolated antibodies by α-halo amides **26**. The tetraamine ligands have also been used, with Michael type acceptors **27**, **28** being employed in the conjugation step.[44]

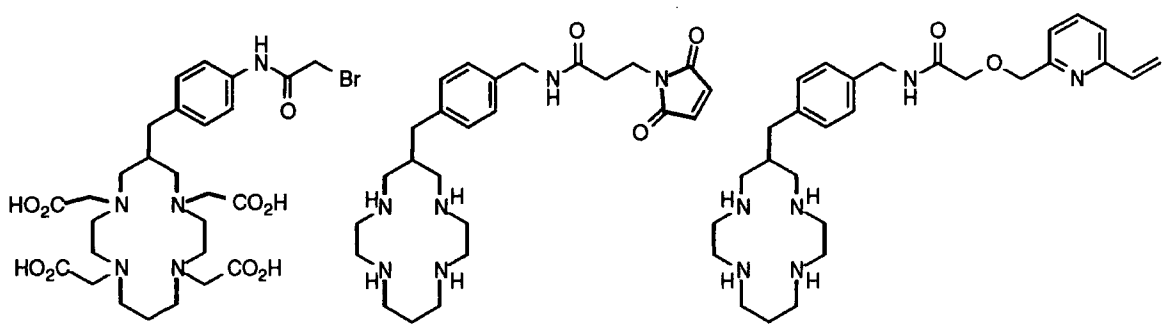

26 **27** **28**

A synthetically simpler method for conjugation of cyclam, by N-alkylation rather than C-alkylation, has also been used. An example of this approach[45] gave conjugates which were slow to label, and resulted in some, potentially problematic, non specific binding.

Ligands based on the NOTA framework, including **29** and **30**, have been synthesised[46] and evaluated for use with small trivalent metal ions such as gallium and indium. These ligands should be suitable for use with copper. Copper NOTA complexes would, of course, be anionic, hence susceptible to acid promoted metal loss. The replacement of one of the carboxylic acid groups with an amide to counter such dissociation is investigated in chapter 3.

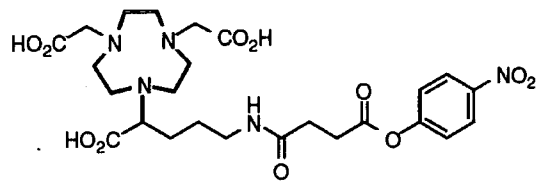

29

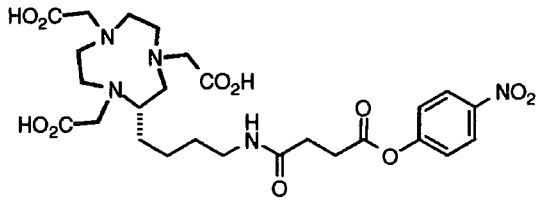

30

1.8. Scope of the Work

This thesis is concerned with methods for the detection of tumours, monitoring the behaviour and treatment of tumours, and the therapy of tumours.

Chapter 2 considers the development of complexes for use as blood flow imaging agents, with the short lived lanthanum-134 nuclide. Such complexes would permit investigation of factors affecting tumour blood supply, by repeated measurements made under different physiological conditions. The generator used to produce the radionuclide has a convenient shelf-life for use at centres not possessing a cyclotron. Discourse is introduced, illustrating the suitability of gadolinium, terbium and europium complexes of the ligands, developed for lanthanum, in other imaging applications.

Chapter 3 looks towards the use of the avidin-biotin system as a method for achieving high tumour to background ratios of activity, at time intervals shorter than those accessible with conventional antibody based approaches. The potential therapeutic use of low molecular weight lipophilic complexes to target hepatoma is also outlined.

Chapter 4 concerns the use of radiolabelled antibodies for tumour targeting, and further elaboration by the incorporation of intercalators to target the nuclear DNA of the tumour cell. Antibodies developed by the Department of Immunology at the Institute of Cancer Research are labelled with ^{64}Cu macrocycles, and investigated for their use in imaging and, potentially, therapy of solid tumours.

1.9. References and Notes

1. M. Hall, *Target Cancer*, The Association of the British Pharmaceutical Industry, 1996, London
2. Strictly a tumour is a solid mass of cells. Some cancers, such as leukaemia, which arise as a loss of control of cell division in the bone marrow, do not manifest themselves as solid masses, but as isolated cells distributed throughout the body.

3. I.S. Fentiman in *Introduction to the Cellular and Molecular Biology of Cancer,* eds. L.M. Franks and N. Teich, OUP, Oxford, 1986
4. S. Jurisson, D. Berning, W. Jia and D. Ma, *Chem. Rev.,* 1993, **93**, 1137
5. K.P. Pulukkody, T.J. Norman, D. Parker, L. Royle, and C.J. Broan, *J. Chem. Soc., Perkin Trans. 2.*, 1993, 605
6. Formerly SPET was known by the acronym SPECT. The "computed" aspect of the technique is assumed.
7 T. Jones, *Eur. J. Nucl. Med.*, 1996, **23**, 207
8. G.P. Saha, *Fundamentals of Nuclear Pharmacy,* 2nd ed., 1984, Springer-Verlag, New York
9. D.M. Goldenberg and S.M. Larson, *J. Nucl. Med.,* 1992, **33**, 803
10. K.J. Jankowski and D. Parker in *Advances in Metals in Medicine,* eds. M.J. Abrams and B.A. Murrer, JAI Press, New York, 1993, 29
11. M.A. Green in *Advances in Metals in Medicine,* eds. M.J. Abrams and B.A. Murrer, JAI Press, New York, 1993, 75
12. J. Zweit in *Current Directions in Radiopharmaceutical Research and Development,* ed. S.J. Mather, Klewer Academic Publishers, in press
13. S.M. Sagar, G.A. Klassen, K.D. Barklay and J.E. Aldrich, *Cancer Treatment Reviews,* 1993, **19**, 299
14. P. Knox in *Current Directions in Radiopharmaceutical Research and Development,* ed. S.J. Mather, Klewer Academic Publishers, in press
15. M.J. Abrams and B.J. Murrer, *Science,* 1993, **261**, 725
16. M.A. Green in *Advances in Metals in Medicine,* eds. M.J. Abrams and B.A. Murrer, JAI Press, New York, 1993, 75
17. D.H. Petering in *Metal Ions in Biological Systems*, ed. H. Sigel, Dekker, New York, 1980, 197
18. G. Köhler and C. Milstein, *Nature,* 1976, **256**, 495
19. J.P. Dizio, C.J. Anderson, A. Davison, A.G. Jones and J.A. Katzenellenbogen, *J. Nucl. Med.*, 1992, **33**, 558
20. D.Y. Chi, J.P. O'Neil, C.J. Anderson, M.J. Welch and J.A. Katzenellenbogen, J. *Med. Chem.,* 1994, **37**, 928
21. W.H. Bakker, R. Albert, C. Bruns, W.A.P. Breeman, L.J. Hofland, P. Marbach, J. Pless, D. Pralet, B. Stolz, J.W. Koper, S.W.J. Lamberts, T.J. Visser and E.P. Krenning, *Life Sci.*, 1991, **49**, 1583
22. M. Wilchek and E.A. Bayer, *Immunology Today*, 1984, **5**, 39
23. F. Virzi, B. Fritz, M. Ruscowski, M. Gionet, H. Misra and D.J. Hnatowich, *Nucl. Med. Biol.*, 1991, **18**, 719

24. G. Paganelli, P. Magnani, F. Zito, G. Lucignani, F. Sudati, G. Truci, E. Motti, M. Terreni, B. Pollo, M. Giovanelli, N. Canal, G. Scotti, G. Comi, P. Koch, H.R. Maecke and F. Fazio, *Eur. J. Nucl. Med.*, 1994, **21**, 314
25. D. Parker, *Chem. Soc. Rev.*, 1990, **19**, 271
26. R.R. Traut, A. Bollen, T-T. Sun, J.W.B. Hershey, J. Sundberg and L.R. Pierce, *Biochemistry*, 1973, **12**, 3266
27. M.J. McCall, H. Diril and C.F. Meares, *Bioconjugate Chem.*, 1990, **1**, 222
28. F.I. Chou, K.C. Fang, C. Chung, W.Y. Lui, C.W. Chi, R.S. Liu and W.K. Chan, *Nucl. Med. Biol.*, 1995, **22**, 379
29. S-J. Wang, W-Y. Lin, M-N. Chen, L-H. Shen, Z-T. Tsai and G. Ting, *Eur. J. Nucl. Med.*, 1995, **22**, 233
30. D.K. Cabiness and D.W. Margerum, *J. Am. Chem. Soc.*, 1969, 6540
31. R.D Hancock and A.E. Martell, *Chem. Rev.*, 1989, **89**, 1875
32. D. Parker in *Comprehensive Supramolecular Chemistry* ed. D.N. Reinhoudt 1996, vol. 10, 487
33. J.C.G. Bunzli in *Lanthanide Probes in Life, Chemical and Earth Sciences*, eds. J.C.G. Bunzli and G.R. Choppin, Elsevier, Amsterdam, 1989
34. V. Alexander, *Chem. Rev.*, 1995, **95**, 273
35. K. Pulukkody, T.J. Norman, D. Parker, L. Royle and C.J. Broan, *J. Chem. Soc., Perkin Trans. 2*, 1993, 605
36. C.J. Broan, E. Cole, K.J. Jankowski, D. Parker, K. Pulukkody, B.A. Boyce, N.R.A. Beeley, K. Millar and A.T. Millican, *Synthesis*, 1992, 63
37. D. Parker, K. Pulukkody, F.C. Smith, A. Batsanov and J.A.K. Howard, *J. Chem. Soc., Dalton Trans.*, 1994, 689
38. S. Aime, A.S. Batsanov, M. Botta, J.A.K. Howard, D. Parker, K. Senanayake and J.A.G. Williams, *Inorg. Chem.*, 1994, **33**, 4696
39. A. Harrison, C.A. Walker, K.A. Pereira, D. Parker, L. Royle, K. Pulukkody and T.J. Norman, *Magn. Reson. Imaging*, 1993, **11**, 761
40. Y. Fujibayashi, K. Matsumoto, Y. Arano, Y. Yonekura, J. Konishi and A. Yokoyama, *Chem. Pharm. Bull.*, 1990, **38**, 1946
41. W-J. Lan and C-S. Chung, *J. Chem. Soc., Dalton Trans.*, 1994, 191
42. The pKa of a complex is equivalent to the pH at which 50% of the species are protonated. Thus, at pH 2.77 the copper NOTA complex exists in equal quantity as the ML complex and MHL complex.
43 S.V. Deshpande, R. Subramanian, M.J. McCall, S.J. DeNardo, G.L. DeNardo and C.F. Meares, *J. Nucl. Med.*, 1990, **31**, 218
44. J.R. Morphy, D. Parker, R. Kataky, M.A.W. Eaton, A.T. Millican, R. Alexander, A. Harrison and C. Walker, *J. Chem. Soc., Perkin Trans. 2*, 1990, 573

45. J. Franz, G.M. Freeman, E.K. Barefield, W.A. Volkert, G.J. Ehrhardt and R.A. Holmes, *Nucl. Med. Biol.*, 1987, **14**, 479
46. J.P.L. Cox, A.S. Craig, I.M. Helps, K.J. Jankowski, D. Parker, M.A.W. Eaton, A.T. Millican, K. Millar, N.R.A. Beeley and B.A. Boyce, *J. Chem. Soc., Perkin Trans. 1*, 1990, 2567

Chapter Two

Lanthanide Complexes for Perfusion Imaging

2. Lanthanide Complexes for Perfusion Imaging

An overview of lanthanide co-ordination chemistry, (2.1.) defining the requirements of ligands to bind lanthanides, is followed by ligand synthesis, (2.2) and the characterisation of lanthanide complexes. (2.3.) The potential for lanthanum-134 to be used for perfusion studies is introduced.(2.4) The radiolabelling of the ligands is investigated, (2.5.) followed by an evaluation of the complexes synthesised, for potential use as imaging agents. (2.6.)

2.1. Co-ordination Chemistry of the Lanthanides

The lanthanides usually display similar physical properties and possess a preference for the +3 oxidation state. These similarities proved problematic historically in the isolation of the metals in pure form, a feat which was not realised until the 1950's following the advent of ion exchange methods of chromatography.[1] The similarity in size and bonding mode of the ions permits the usage of ligands common to all lanthanides.

A slight decrease in ionic radius is observed as the series is traversed from lanthanum to ytterbium, termed the lanthanide contraction. A high co-ordination number is characteristic of lanthanide compounds, with the lighter, larger ions exhibiting co-ordination numbers up to 12. A co-ordination number of 8-9 is commonplace. Complexes tend to adopt a square anti-prismatic geometry, with faces capped to complete the ligand field. This geometry is enforced more by the steric constraints of the ligands rather than the position of metal orbitals. This is a consequence of the non-participation of 4*f* electrons in bonding - the lanthanide(III) ions possess an almost spherical electronic distribution. This indifference to directional bonding is being exploited in the use of lanthanides as calcium mimics, to probe cellular biochemistry.[2] Lanthanide(III) ions have a similar size to Ca^{2+} and so can be accommodated at active sites of metalloproteins, without perturbing the geometry. Europium(III) and terbium(III) are finding use as luminescent probes[3] whereas gadolinium(III) has found use as an EPR probe.[4]

The lanthanides are "hard" acids and hence prefer to bind with "hard" bases, i.e. electronegative donor ligands such as oxygen and fluorine.

Macrocyclic vs Acyclic Ligands

The additional stability imparted by arranging donor atoms in a macrocycle is highly desirable for *in vivo* use of radionuclides, which emit ionising radiations. However, for

perfusion studies using minute amounts of lanthanum with a short half-life, the need for stability is not quite as acute. Indeed, copper PTSM [Cu(**4**)], an acyclic copper(II) complex, has attracted considerable attention because the complex *is* rather unstable. Decomplexation is initiated by intracellular reduction by a tripeptide (glutathione) to give a copper(I) complex of moderate stability which then dissociates, trapping the copper, and allowing quantitative measurements to be made.

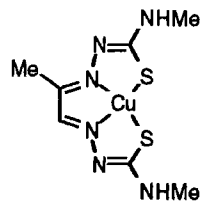

[Cu(**4**)]

It was decided to synthesise both acyclic and macrocyclic ligands for use as lanthanide complexing agents, and investigate the properties of selected lanthanide complexes, both *in vitro* and *in vivo*.

Metal Ions of Interest

Complexes of lanthanum are of particular interest because of the potential diagnostic use of the lanthanum-134 isotope, which decays by positron emission. Also of interest are the related terbium and europium complexes because of their interesting luminescence properties, and the corresponding gadolinium complexes because of the potential application as contrast agents in MRI. The common co-ordination chemistry of these ions necessitates no modification of the ligands for use with different metals of the lanthanide series.

2.2. Ligand Syntheses

Acyclic Ligands

Acyclic ligands based on the DTPA backbone, in which two of the acid groups have been replaced by amide functionality, were chosen as synthetic targets. The commercially available ligand DTPA **16** forms thermodynamically stable complexes (log K_{ML} ~20-23) with lanthanides,[5] but is not sufficiently lipophilic to be of use for perfusion studies. Also, as lanthanide complexes are dianionic, such complexes electrostatically attract cations. This renders the complex too unstable *in vivo* for many applications as the principle dissociation pathway is likely to be either proton or cation mediated.[6]

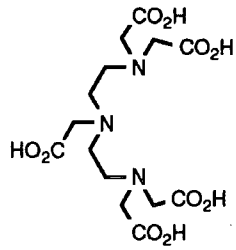

16

The amide groups co-ordinate to the metal *via* the harder oxygen, but do not affect the overall charge of the complex, on co-ordination to the metal ion. (Some charge delocalisation may occur however, as depicted in the scheme below (figure 2.1.) Thus, the acyclic complexes with two amides are charge neutral overall. In addition, the incorporation of the amides allows structural variation, through modification of the amide N-substituent. This in turn influences the lipophilicity of the complexes, which in turn is a prime consideration in the biodistribution of the complex. A low molecular weight is preferable, as smaller compounds may passively diffuse through biological membranes more easily, which should increase the amount of radiotracer extracted by cells on the first pass (i.e. the complex is removed from the circulation on the first encounter with tissues.)

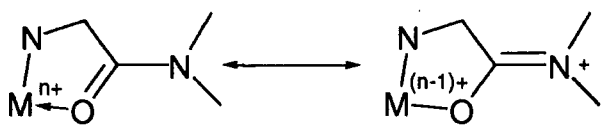

Figure 2.1. The charge on the metal ion may delocalise on co-ordination.

The acyclic diamide ligands **31-34** were easily synthesised (figure 2.2.) by addition of slightly over two equivalents of the appropriate primary amine, to a stirred solution of diethylenetriamine pentaacetic acid dianhydride **25** in pyridine. The three amines employed were chosen to give a range of lipophilicities. N,N-Dimethylaminopyridine (DMAP) was used as an acyl transfer catalyst. The groups of Geraldes[7] and Bligh[8] have simultaneously synthesised several similar ligands with a view to examining the charge neutral gadolinium complexes as MRI contrast agents.

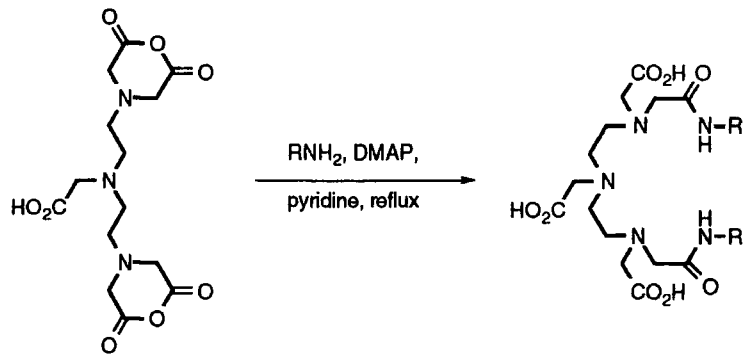

25

Figure 2.2. The reaction of an amine with the dianhydride **25** afforded the acyclic ligands **31-34**

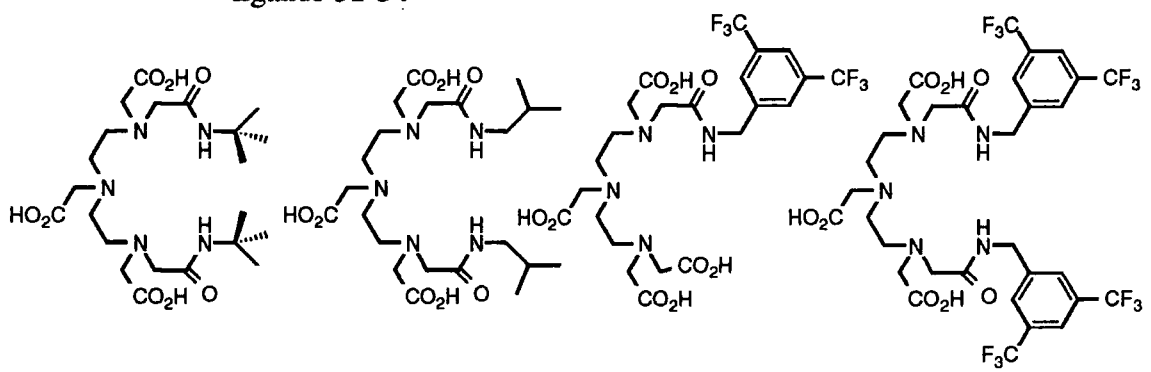

31 **32** **33** **34**

A larger excess of 3,5-bis(trifluoromethyl)benzylamine was required to make the tetratrifluoromethyl ligand **34**. The use of 2.2 equivalents of amine resulted in the formation of the monoamide **33**. This would be expected to form monoanionic complexes with trivalent lanthanide ions.

Macrocyclic Ligands

The ligand, DOTA **17**, is known to form stable complexes (log K_{ML}~ 23-29)with lanthanide ions.[9] As with DTPA, the derived complexes are very hydrophilic, anionic and are rapidly excreted by the kidneys. The replacement of the carboxylic acid donors with the isosteric phosphinic acid moiety, allows the lipophilicity of the complex to be controlled. An alternative modification to the DOTA skeleton is the replacement of one carboxylic acid group with an amide. Complexes produced from these ligands would be charge neutral. The replacement of all four acid groups with amides affords tripositive complexes on incorporation of lanthanide ions.

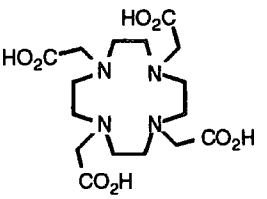

17

The ligands **18**, **35-40**, based on the tetraazacyclododecane macrocycle **41** (cyclen), were synthesised using synthetic procedures[10] established within the group.

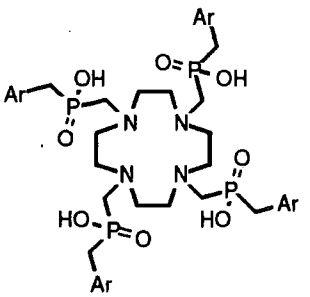

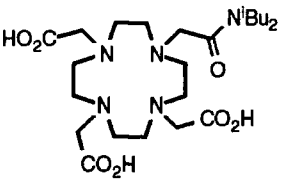

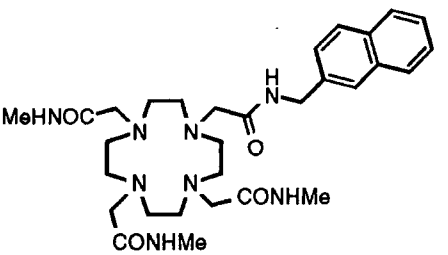

Ar= Ph **18**
= 2-MeOPh **35**
= 3-MeOPh **36**
= 4-MeOPh **37**
= 3,5-bis(F_3C)Ph **38**

39

40

The tetrabenzylphosphinate ligand **18** was synthesised by Miss Emma Smart, following the published procedure.[10] The substituted tetraarylphosphinate ligands **35-38** were synthesised using a modification of the route, depicted in the scheme below for ligand **36** (figure 2.3.) The Grignard reagent was made from the commercially available chloroaryl compound, except for the ortho derivative, for which only the benzyl alcohol compound is available. Functional group inter-conversion was achieved with thionyl chloride. The ligands **35** and **37** were synthesised by Dr Timothy Norman and Dr Stephen Faulkner respectively. The synthesis of the Grignard reagents for the ortho and para methoxy substituted benzyl phosphinates, had to be performed in tetrahydofuran, and the magnesium salts removed, by precipitation from benzene, before the Mannich reaction was attempted.

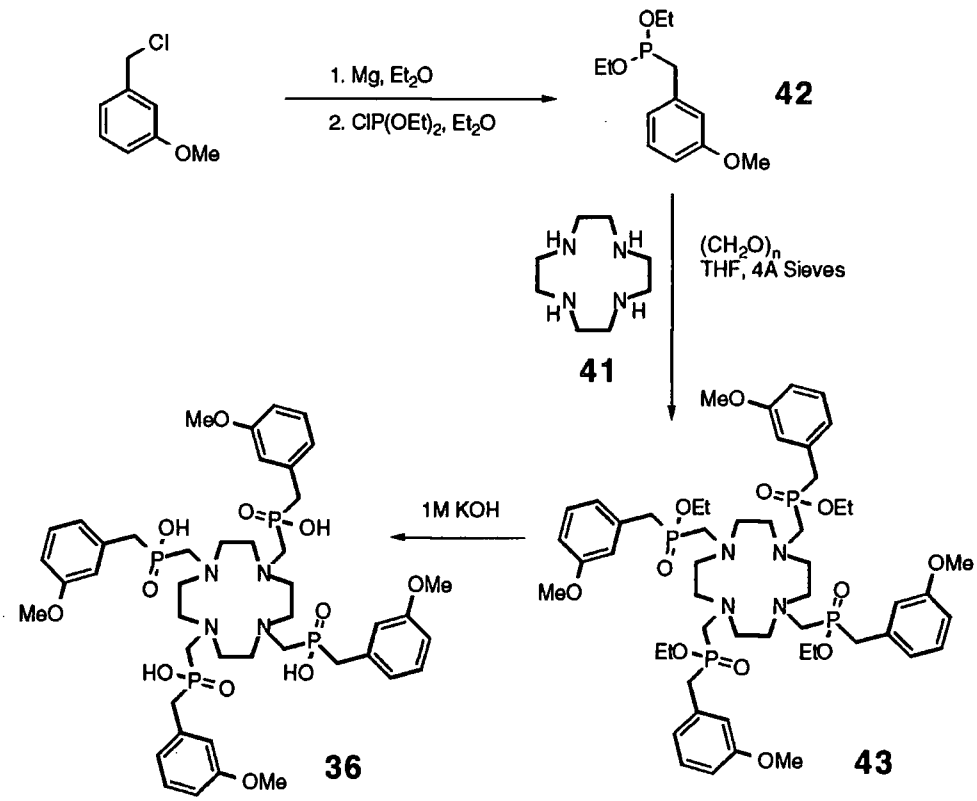

Figure 2.3. The synthetic scheme followed to produce ligand **36**.

The ligands comprising amides **39** and **40**, were synthesised by Gareth Williams and Dr Timothy Norman. The monoalkylation of cyclen **41** is realised by the use of molybdenum hexacarbonyl. Three of the four nitrogens co-ordinate to the metal centre, permitting a nucleophilic reaction by the one left vacant (figure 2.4.) The synthesis is completed by alkylation of the remaining nitrogens.

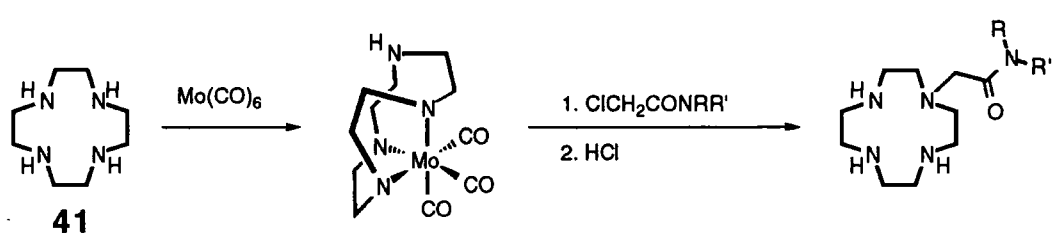

Figure 2.4. The protection of three of the nitrogens of **41** leads to mono-alkylation.

The 13 membered cycle tetraazacyclotridecane (TRITA, **44**), the homologue of DOTA was synthesised as a model cycle for developing C-functionalised complexing agents, which may be accessible more quickly than the C-functionalised DOTA ligands.[11] However, subsequent work within the group[12] has resulted in a much abbreviated synthesis to bifunctional complexing agents, based on the tetraazacyclododecane skeleton. Lanthanide complexes based upon the DOTA framework possess greater

stability than the TRITA analogues, and so would be chosen in preference for *in vivo* targeting.

The carboxymethylation of 1,4,7,10-tetraazacyclotridecane **21** was effected (figure 2.5.) by the addition of chloroacetic acid, in aqueous lithium hydroxide solution, whilst controlling the pH of the reaction.

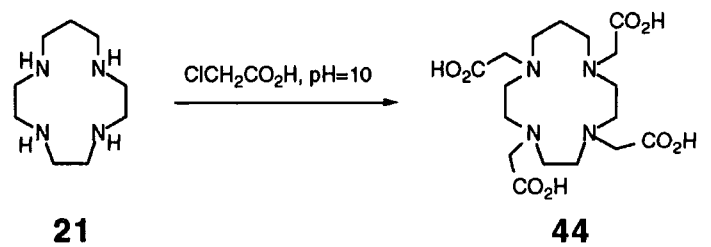

21 **44**

Figure 2.5. The synthesis of TRITA **44**.

2.3. Solution and Solid State Characterisation of Macrocyclic Complexes

Complexes were formed by reaction of the ligand in aqueous solution with one equivalent of lanthanide salt, except for complexes made with the oxide (Ln_2O_3), where 0.5 equivalents were added.

The complexation gives rise to racemic chiral complexes, with all of the ligands. For the acyclic complexes the loss of symmetry results in the non-equivalance of the resonances of geminal protons, observed in NMR spectra. In principle, the macrocyclic complexes, derived from the tetraphosphinic acid ligands, could adopt any one of a large selection of stereoisomers. On binding a metal ion, a new stereogenic centre at phosphorus is created. Eight distinct combinations of phosphorus configuration are possible (i.e. RRRR, RRRS, RRSS, RSRS and their corresponding enantiomers). Also, the macrocyclic ring may adopt one of two conformations and the array of pendent arms may define a left or right handed helix. There are thus 32 possible stereoisomers. Of course, not all isomers will have the same conformational energy, and so certain diastereomers may be expected to dominate.

The "cold" lanthanum complexes formed with the tetrabenzylphosphinic acid **18** and meta methoxy substituted ligand **36** gave two resonances in the proton decoupled phosphorus NMR spectrum, as shown in figure 2.6., below. This indicates the presence of phosphorus in two environments, in the ratio of approximately 8:1.

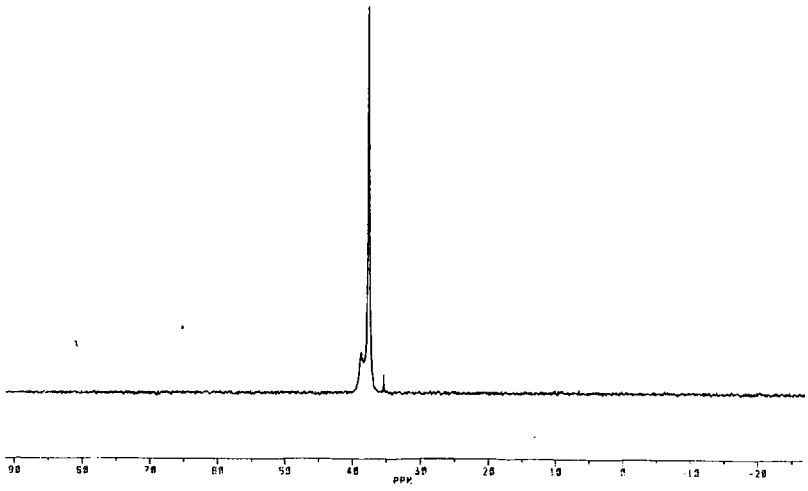

Figure 2.6. The $^{31}P\{1H\}$ NMR spectrum of [La(**18**)]$^{-}$, acquired at 25°C.

On first inspection, it appeared as though further recrystallisation was required. The nature of isomerism in DOTA and related complexes of lanthanides has been investigated.[13] As figure 2.7., below illustrates, two co-ordination modes are possible.

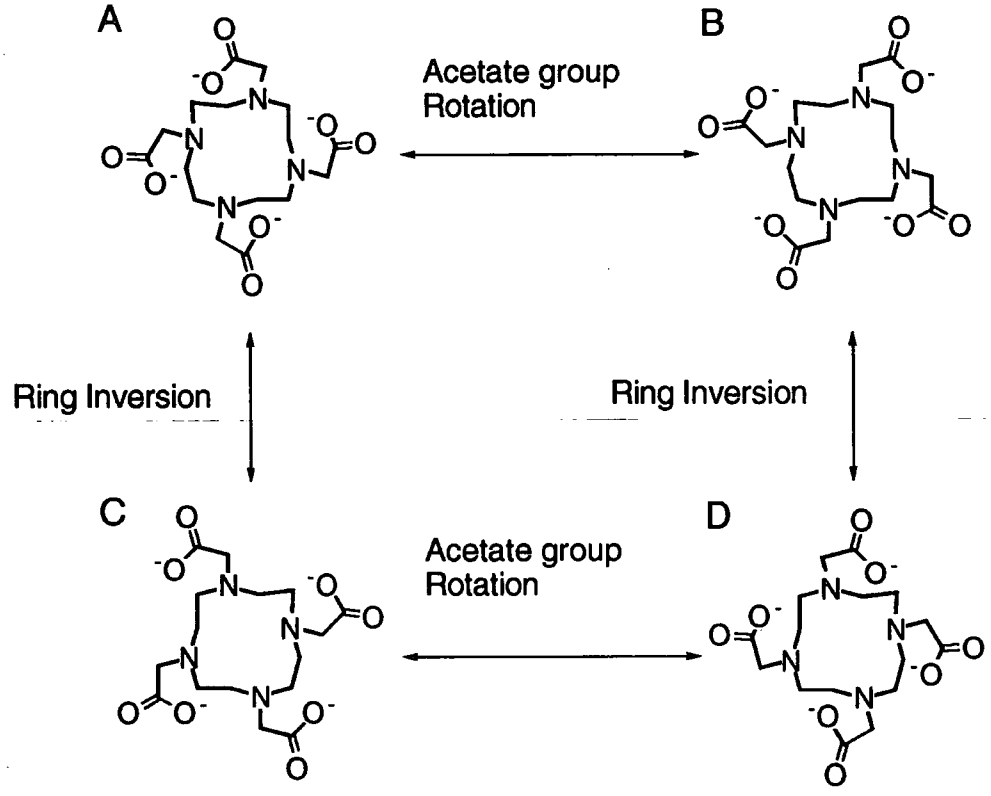

Figure 2.7. The diastereomeric relationships of DOTA complexes.

Structures A and D are enantiomers, as are B and C. Enantiomers are indistinguishable by solution state NMR in achiral media, but it is possible to observe different spectra for diastereomers. As the topology of the chelating portions of the phosphinates is

identical to that of the carboxylates, it would seem reasonable to suggest that the two resonances observed by ^{31}P NMR have arisen from the presence of both diastereomers in the sample, rather than as a result of an impurity.

The solid state structure of the corresponding yttrium phosphinate complex has been determined[14] (figure 2.8.) and demonstrates the distorted inverted square anti-prismatic structure, illustrated by B and C in the scheme above. This is in contrast to the known structures of DOTA complexes (figure 2.8.), which all display the distorted square anti-prismatic geometry, as in A and D above. Also, the complexes of DOTA are known to be nine co-ordinate, with a water molecule capping the face of the O_4 donor set. The metal sits almost in the plane of the four hard acetate oxygens. The yttrium phosphinate complex has no metal bound water. This change in geometry between phosphinates

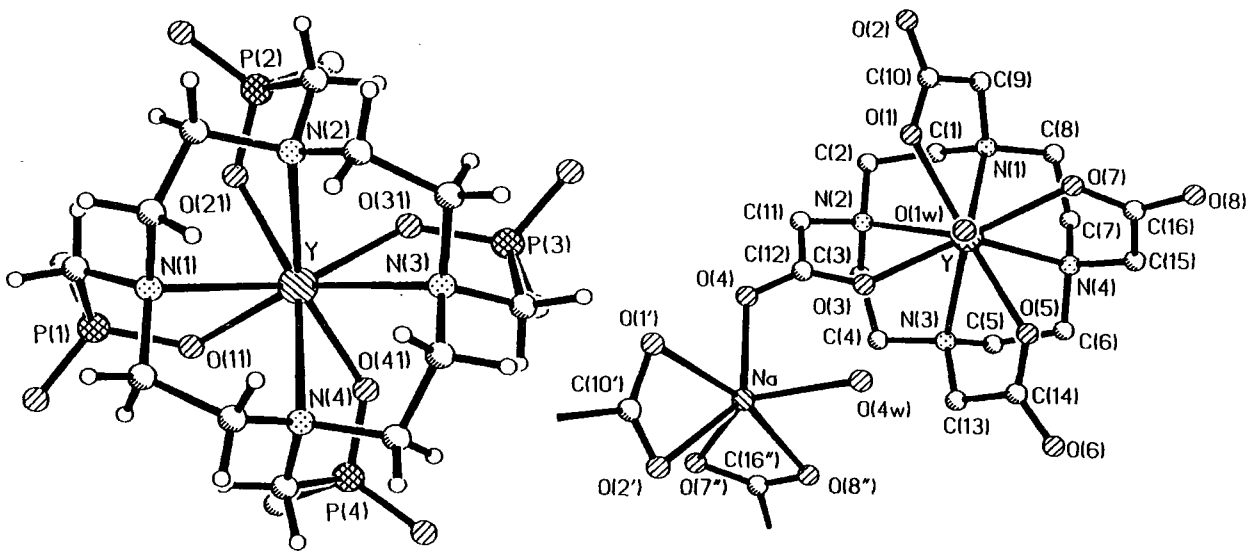

Figure 2.8. The structures of $[Y(\mathbf{18})]^-H_3O^+$ and $[Y(\mathbf{17})]^-Na^+.2H_2O$ obtained in the crystal.

and carboxylates may be a result of the increased "bite size" (illustrated in figure 2.9., below) of the phosphinate chelates, enabling the pendent arms to bisect the corners of the square described by the twelve membered ring, rather than the sides. The exclusion of the water molecule from the inner co-ordination sphere of the metal for the phosphinate class of ligands is a result of steric crowding around the phosphorus atom, rather than the presence of the aromatic groups. This is inferred by comparison with the P-methyl complexes, which also display a marked decrease in metal hydration.

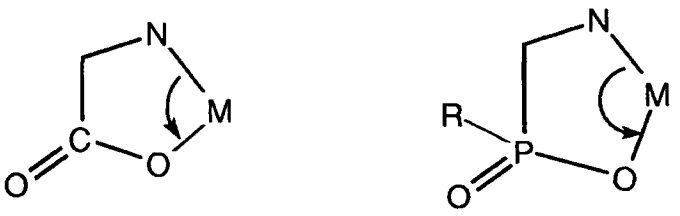

Figure 2.9. The phosphinic acid ligands offer a large "bite angle" to the metal ion.

An X-ray analysis of crystals of the lanthanum tetrabenzylphosphinic acid complex [La(**18**)]$^-$ was performed by Miss Janet Maloney. The diffraction data obtained proved difficult to refine, but the metal geometry was determined with a high degree of confidence. A water molecule is clearly seen (figure 2.10.) occupying a ninth co-ordination site on the lanthanum ion. The distorted inverted square anti-prism characteristic of the yttrium complex is retained, however.

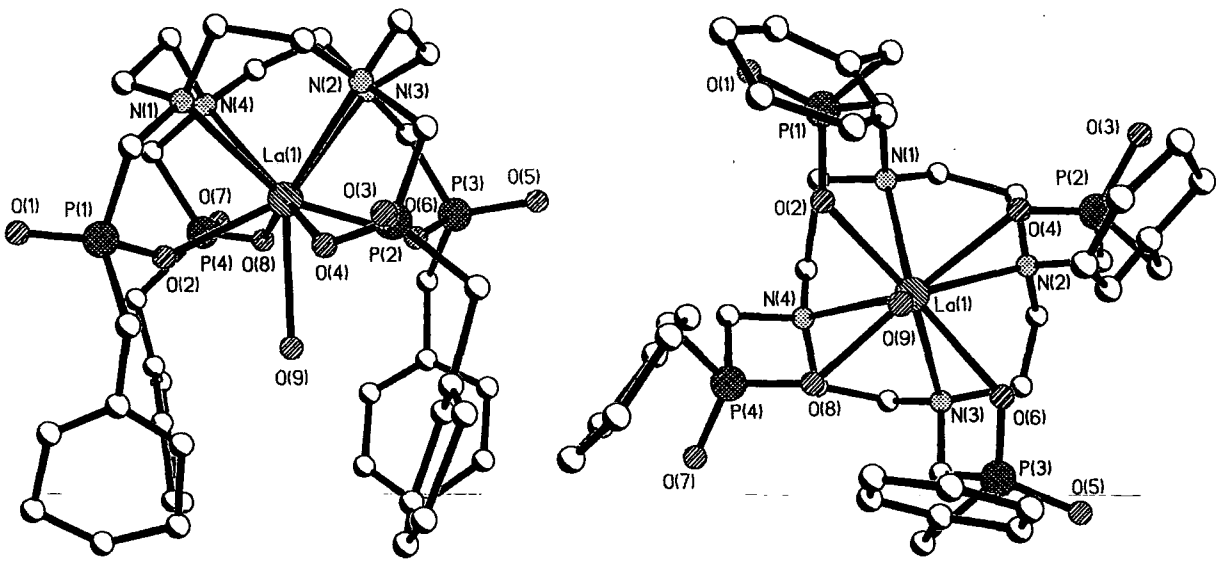

Figure 2.10. The structure, in the crystal, of [La(**18**)]$^-$

The occurrence of the two resonances in the phosphorus NMR spectrum is not explained by the crystal structure result alone. It seems quite plausible that the complex may convert between the two geometries. At elevated temperature, one sharp resonance is observed by NMR, consistent with higher C_4 symmetry. On cooling, the same sample shows the original spectrum. This clearly indicates a reversible process. Two possible changes in structure can be envisaged i) the water molecule is in slow exchange with the metal centre or ii) the complex is twisting, converting from square anti-prismatic to the inverted square anti-prismatic geometry. This second explanation is much more likely. Oxygen-17 NMR experiments with macrocyclic gadolinium

complexes have demonstrated,[15] by measuring relaxivities of nuclei, that the exchange of water molecules is far too fast ($>10^7 s^{-1}$) to be observed by NMR. Additional support for the idea of a reversible change in geometry is presented by the proton NMR spectra acquired at 25° and 80°C, which show (figure 2.11.) that the diastereotopic NCH_2P methylene protons coalesce at high temperature.

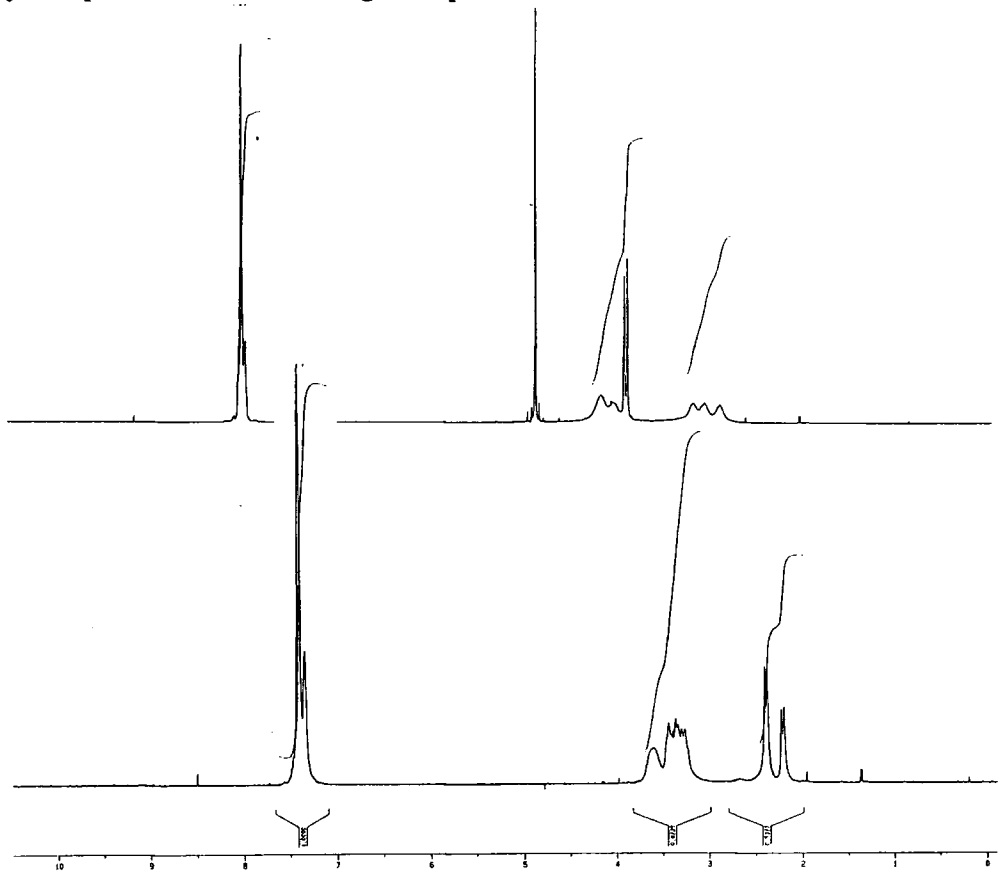

Figure 2.11. ^1H NMR spectra of [La(**18**)]$^-$ acquired at 25°C (bottom) and 80°C (top).

A variable temperature experiment was performed on the complex La[**18**]$^-$, to probe the kinetics of the change in co-ordination geometry of the metal centre. A Phosphorus-31 spectrum was acquired at 10° intervals between 0 and 80°C.

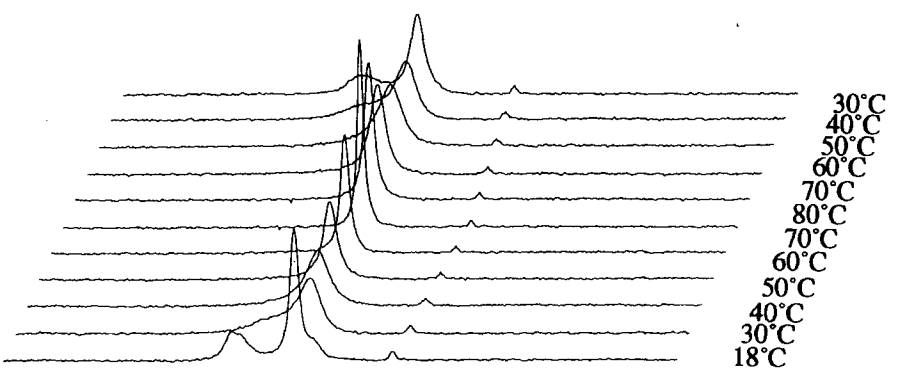

Figure 2.12. Overlaid $^{31}P\{^1H\}$ spectra of [La(**18**)]$^-$, acquired at 10° intevals.

From the spectra (figure 2.12.), an approximate coalescence temperature (T_c) of 333K (60°C) was determined. The rate constant, k_r, can be calculated from the full width, at half height ($\Delta\nu$), of the converged peaks, thus:

$$k_r = \pi\Delta\nu/\sqrt{2} = 179.9\text{Hz} \qquad 2.1.$$

This value was entered into the Eyring equation (2.2) after rearranging (2.3) to give the activation energy $\Delta G^{\ddagger}$.

$$k_c = (k_B T/h).\exp(-\Delta G^{\ddagger}/RT) \qquad 2.2.$$

$$\Delta G^{\ddagger} = RT_c(\ln k_B/h + \ln T_c/k_r) = 67.5\ \text{kJ mol}^{-1} \qquad 2.3.$$

(where k_B = Boltzmann Constant, R = molar gas constant, h = Plancks constant)

Of course, this represents only an estimate, as the analysis is based upon the assumption that the two interconverting forms are of the same energy. One isomer is clearly present in an 8:1 excess at room temperature. However, the value obtained is reasonable and shows the barrier to the twisting motion is comparable to the hindered rotation of the DOTA complex, [Nd(**17**)]$^-$. The published ^{13}C variable temperature spectra[16] exhibit a lower coalescence temperature of 45°C, and by the above calculation, $\Delta G^{\ddagger}$ is found to be ~60 kJ mol^{-1}.

A more rigorous analysis is difficult to achieve with this system, due to the poor separation of the resonances. The rate constant can be calculated from equation 2.4.,[16] where $\delta\nu$ is the difference in frequency between the resonances of A and B, the interchanging structures, k_A is the rate constant of the conversion of A to B and k_B is the rate constant of the reverse process. The fractional populations of the two structures are represented by p_A and p_B.

$$\Delta\nu = \frac{4\pi p_A p_B(\delta\nu)^2}{k_A + k_B} \qquad 2.4.$$

The determination of the average rate constant at several temperatures permits the graphical determination of the activation energy. To achieve a reasonable value with this complex would require the aquisition of several lower temperature spectra, to give the enhanced separation necessary for an accurate determination of the population of each structure.

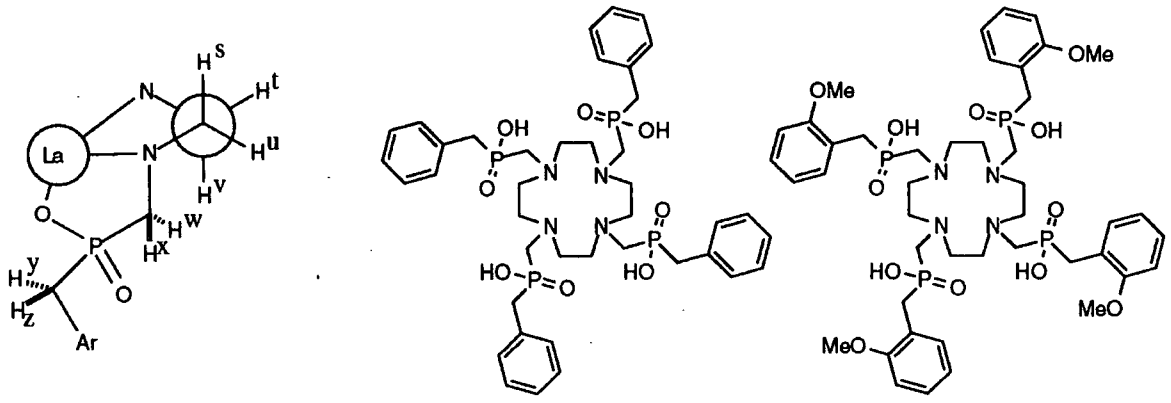

18 **36**

Figure 2.13. The atom labelling scheme used for [La(**18**)]$^-$ and [La(**36**)]$^-$

A detailed assignment of the proton spectra for the [La(**18**)]$^-$ and [La(**36**)]$^-$ complexes has been made. The ^{1}H NMR spectra of the two lanthanum complexes display a marked similarity (Figure 2.14.). This behaviour can be contrasted with that observed for the related yttrium complex,[10] [Y(**18**)]$^-$. A doublet of doublets (appears to be a triplet) at δ_H = 2.72ppm in the ^{1}H spectrum of the yttrium complex, has no

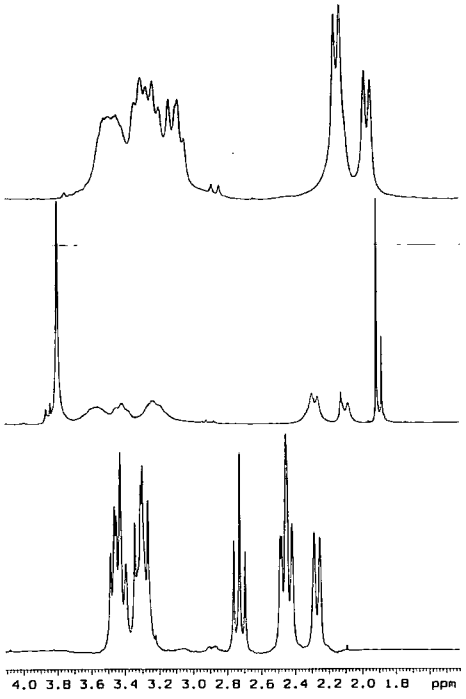

Figure 2.14. Partial ^{1}H NMR spectra of macrocylic phosphinate complexes. [La(**18**)]$^-$, top, [La(**36**)]$^-$ and [Y(**18**)]$^-$, bottom.

corresponding peak of similar shift in the spectra of the lanthanum complexes. This peak is attributed to one of the diastereotopic NCH_2P protons *w* and *x* (letters correspond to the labelling scheme of figure 2.13.), the other resonating at ~2.4ppm in complexes of both cations. The corresponding methylene proton can be identified in the lanthanum complex by acquiring a proton spectrum, whilst irradiating the sample at the frequency corresponding to the phosphorus signal. This phosphorus decoupled spectrum, ($^1H\{^{31}P\}$, below) has lost all coupling information to phosphorus. The hydrogens nearest to the phosphorus atoms are noted by inspection of the two spectra. The NCH_2P protons, *w* and *x*, are found at 2.5 and 3.6ppm. This represents a change

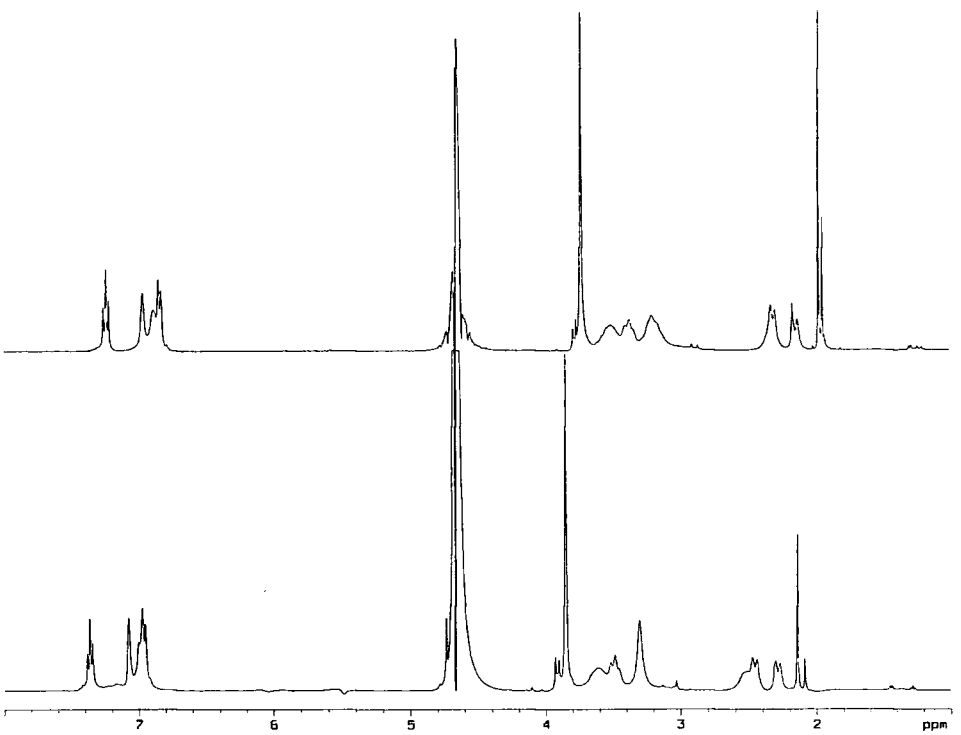

Figure 2.15. Proton spectrum of [La(**36**)]$^-$, top, and the spectrum acquired with phosphorus decoupling. (The difference in chemical shift, is an effect of the different concentration of ammonium acetate in the samples.)

in chemical shift of 0.9ppm for one of the protons, as a result of changing the metal ion. The benzylic protons, *y* and *z*, are isochronous, resonating at 3.3ppm. The four remaining resonances, of the ethylene bridges, in the cycle can be assigned partially. The lower frequency doublets at 2.1 and 2.3ppm are the resonances of the pseudoequatorial protons, *t* and *u*. The 2.1 resonance is coupled, as determined by a ^1H-^1H correlation experiment, to the multiplet at 3.5ppm. Similarly, the resonance at 2.3ppm is coupled to the resonance at 3.6ppm.

Clearly, the presence of the water molecule, observed in the crystal, is having a substantial effect on the rest of the complex, as illustrated by the contrasting spectra for the lanthanum and yttrium complexes.

Solution Structure of the [La(TRITA)]⁻ Complex

The structure of the lanthanum DOTA complex, determined by solution state NMR has been reported.[17] The incorporation of the methylene bridge into the 13 membered cycle destroys the fourfold symmetry of the complex, and hence renders all 26 protons non-equivalent. The assignment of the peaks in the proton NMR spectrum is, thus, a much more difficult task. For the DOTA complex only 6 resonances are observed, as depicted in the projection, figure 2.16. below. The chemical shifts of the protons are given in parts per million, relative to tertiary butanol, δ_H (D_2O) = 0.90.

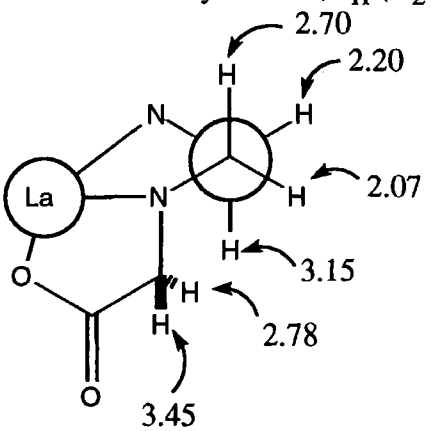

Figure 2.16. Assignment of the proton resonances in [La(DOTA)]⁻

To simplify the problem of assigning the peaks for the [La(TRITA)]⁻ complex, it was assumed that the three five membered chelate rings adopt similar conformations to the four five membered chelates of the DOTA complex. The six membered chelate must adopt a twisted boat conformation, rather than the symmetric chair, otherwise the five membered rings would be forced to adopt high energy conformations, with eclipsing interactions. The atom labelling scheme used is defined in figure 2.17.

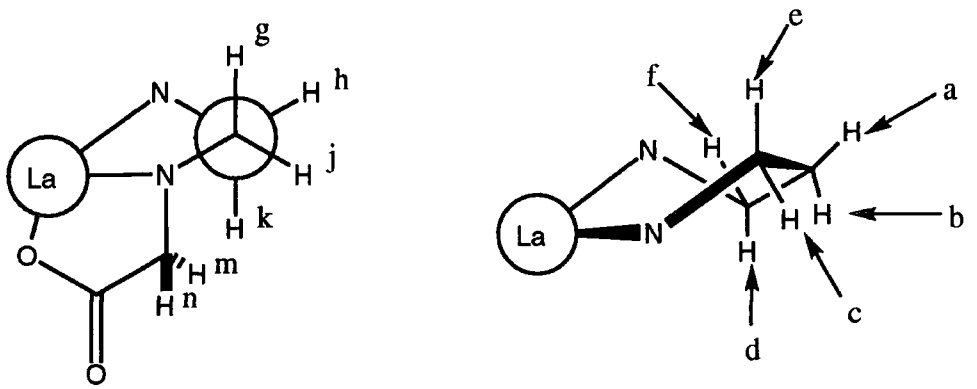

Figure 2.17. The atomic labelling scheme used for [La(TRITA)]⁻

The COSY spectrum (^{1}H-^{1}H correlation) is shown in figure 2.18. The methylene protons resonate at 1.73 and 1.80ppm. It is difficult to attribute the peaks to either *a* or *b* as both are in a somewhat intermediate position between axial and equatorial. A crosspeak is observed between the methylene 1.73 and the two pseudoequatorial protons, *c* and *f*, at 2.5ppm. Geminal couplings are detected to resonances at 3.0 and 3.2ppm - thus identifying the pseudoaxial *d* and *e*.

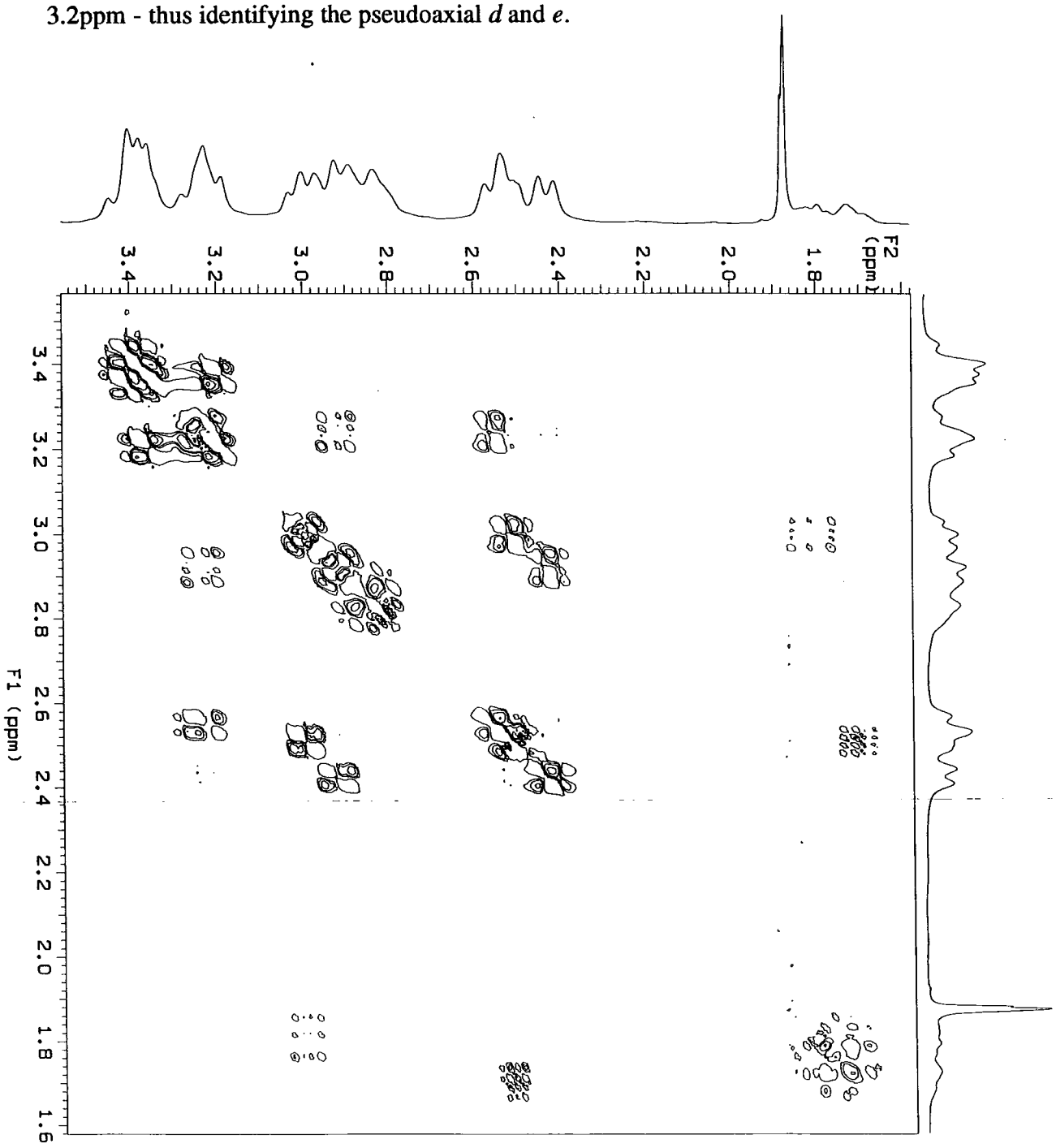

Figure 2.18. ^{1}H-^{1}H correlation spectrum of [La(TRITA)]$^-$

The study by Aime *et al* reported a 16.6Hz coupling between the acetate protons, resonating at 2.78 and 3.45 ppm.[17] However, no coupling is seen between the two

resonances at 2.8 and 3.4ppm, which are attributed here for the TRITA complex to the resonances of the corresponding acetate protons. The temperatures of acquisition of the two spectra were different. The DOTA complex was analysed at -3°C, whereas the TRITA complex was acquired at room temperature. The acetate arms of DOTA are known to concertedly slide over the surface of the metal ion in a reversible process, a conversion which is facilitated at elevated temperatures. Such an exchange process removes the non-equivalence of the acetate protons, hence the signals coalesce, but does not affect the ring conformation. Thus, the lack of geminal coupling is consistent with the presence of a fast exchange process on the NMR timescale. The resonances at 2.8 and 3.4ppm can thus be assigned to the two sets of acetate protons.

The remaining resonances of the three sets of four ethylenic protons can be found at 2.4-2.6, 2.9, 3.2 and 3.4ppm, corresponding to *g*, *h*, *j* and *k*. It was not possible to assign each of these resonances from the COSY spectrum, although, by analogy to the DOTA assignments of figure 2.16., it might be expected that the higher frequency signals arise from the pseudoaxial protons.

NMR Dispersion Studies of Gadolinium Complexes

As mentioned in the introductory chapter (paragraph 1.2., page 6.), stable gadolinium complexes are clinically useful as contrast agents in MRI imaging. On co-ordination to gadolinium, a decrease in the water proton longitudinal relaxation time of the order 10^6 is observed.[15] The change in relaxation rate affects the intensity of the signal. Most often, a T_1 weighted image is obtained (T_1 is the longitudinal relaxation time, as opposed to T_2, the transverse relaxation time.) The longitudinal relaxivity of the complex is the difference between T_1^{-1}, when measured both in the presence and in the absence of the complex. There are two components to the longitudinal relaxivity, R_1, namely the inner and outer sphere mechanisms (is and os respectively). Ligands in contact with the paramagnetic centre are said to be in the inner sphere. Longer range interactions fall into the outer sphere category. The total relaxivity is the sum of both components.

$$R_1 = R_{1is} + R_{1os} \qquad 2.5.$$

The inner sphere contribution, R_{1is}, is proportional to the number of water bound molecules, q. Hence, for the gadolinium tetraarylphosphinate complexes, this term approaches zero. The outer sphere contribution can be described by Freed's equation:[18]

$$R_{1os} = k \,.\, (C / aD) \,.\, f(\tau_S, \tau_D, \omega_H, \omega_S) \qquad 2.6.$$

Where k is a collection of constants, C is the molar concentration of complex, a is the distance of closest approach between the water molecules and the paramagnetic gadolinium centre. The constant D is a measure of the relative translational diffusion of solvent and solute, and ω_H and ω_S are, respectively, the proton and electron Larmor frequencies. The remaining parameters τ_D and τ_S are defined by:

$$\tau_D = a^2 / D \qquad 2.7.$$ and

$$\tau_S^{-1} = \frac{1}{5\tau_{SO}} \left[\frac{1}{1 + \omega_S^2 \tau_V^2} + \frac{4}{1 + 4\omega_S \tau_V^2} \right] \qquad 2.8.$$

where τ_{SO} is the electronic relaxation time at zero field and τ_v is the correlation time of the interaction.

A plot of relaxivity against the proton Larmor frequency (which is field dependent) is called a nuclear magnetic resonance dispersion profile (NMRD). Analysis of such plots facilitates the determination of the parameters τ_{SO} and τ_v, above.

A representative profile, obtained by the group of Professor Silvio Aime in Turin, for the complex [Gd(**36**)]$^-$ is shown below in figure 2.19. The profile is similar to that obtained for the tetrabenzylphosphinate [Gd(**18**)]$^-$ complex, also shown. An imaging study with the [Gd(**18**)]$^-$ has been performed showing promise as a contrast agent for imaging the gastrointestinal tract. Biliary clearance of the intact complex has been demonstated in the rat.[19]

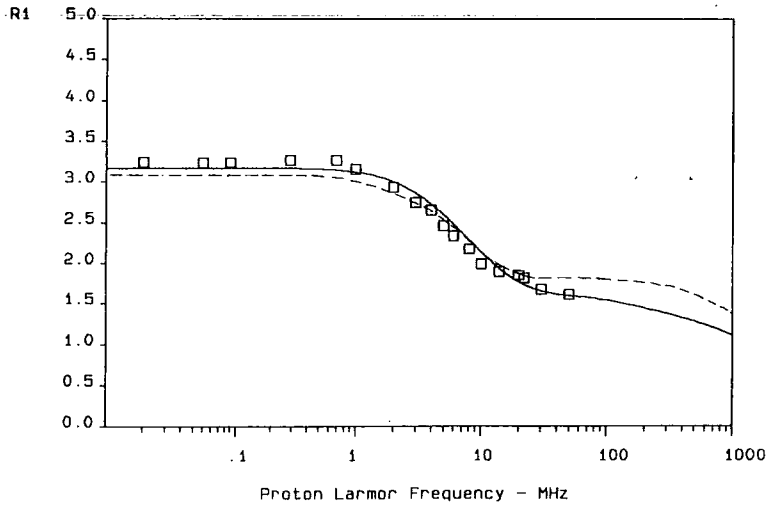

Figure 2.19. The NMR dispersion profile of [Gd(**36**)]$^-$, solid line and [Gd(**18**)]$^-$ dashed line.

The parameters derived from such plots for [Gd(**18**)]$^-$,[14] [Gd(**35-36**)]$^-$, acquired by the Turin group, are reproduced in table 2.1., below. The data show that the complexes have quite similar properties, with respect to application as MRI agents. The presence of the methoxy groups has no influence on the distance of closest approach between water molecules and the metal centre.

Complex	τ_{so} /ps	τ_v /ps	a /Å	Dx10^5 /cm^{2}s^{-1}
[Gd(**18**)]$^-$	71.0	11.5	4.25	2.0
[Gd(**35**)]$^-$	102	16.4	4.25	2.4
[Gd(**36**)]$^-$	115	10.3	4.25	2.4
[Gd(**37**)]$^-$	146	13.3	4.25	2.4

Table 2.1. Parameters obtained from NMRD measurements to give the best fit to Freed's equation (2.5.)

Luminescence Studies of Terbium Complexes

In principle, the use of luminescent markers appended to biological molecules enables the monitoring, in real time, of cellular events by fluorescence microscopy. Luminescence, the absorption of light followed by emission at a lower energy, may be divided into two main processes, illustrated on the diagram, figure 2.20. below.

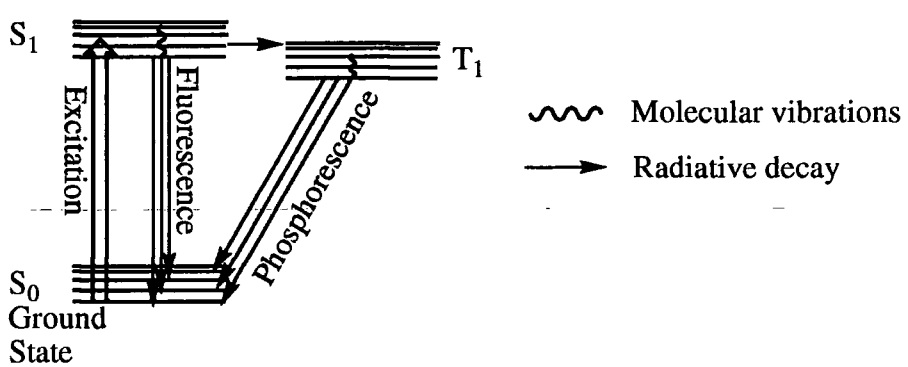

Figure 2.20. Energy level diagram showing some luminescent decay pathways

Fluorescence - Energy is absorbed by the sample, which populates an excited state, S_1. Energy is rapidly lost, by molecular vibrations, until the lowest energy level of the S_1 manifold is reached. The radiative decay from this level, is termed fluorescence and is "allowed" by the selection rules governing transitions.

Phosphorescence - If a molecule has a triplet state energy level, similar in energy to that of the excited singlet state, intersystem crossing can occur. Energy is then lost until the lowest level of the triplet state, T_1, manifold is achieved. The radiative loss of energy from a triplet state, to the ground (singlet) state is a "forbidden" process, and, hence,

occurs slowly. This process is termed phosphorescence. The lifetime of an excited state which decays by phosphorescence may be several orders of magnitude longer than one decaying by fluorescence.

Other radiationless decay pathways exist, such as molecular collisions and energy transfer to proximate energy matched OH, NH and CH oscillators.[20] These processes are not illustrated on the above diagram. The parameters which characterise the luminescent behaviour of molecules are the lifetime, τ, wavelengths of excitation, λ_{ex}, and emission, λ_{em}, and the quantum yields, ϕ, of each process.

For use in immunoassay procedures, it is essential that the light emitted by the marker molecule is distinguishable from the emissions of other chromophores in the system under study. In particular, proteins exhibit fluorescent behaviour. Therefore, the use of phosphorescent marker molecules, possessing extended lifetimes, allows a time-gated approach to be used. For example, excitation of a sample, containing both fluorescent and phosphorescent molecules, with light of 254nm wavelength, causes chromophores to achieve a state of higher energy. Those decaying by fluorescence emit energy rapidly (10^{-9}-10^{-6}s) whereas excited states, decaying by phosphorescence, emit light over a longer period (10^{-6}-10^{-3}s). Thus, if measurement of emitted light is not commenced until a few microseconds after excitation, only phosphorescent decay is observed, free from all contaminating fluorescence decay.

Many lanthanides, in particular, europium and terbium, feature the overlap of energy levels of different spins. This enables efficient intersystem crossing, and phosphorescence is commonly observed for lanthanide ions. However, the presence of water molecules provides a non-radiative decay pathway for quenching the excited state. Incorporation of the lanthanide ion in a complex offers a means to exclude water molecules, and, hence, reduce the radiationless decay. In addition, the presence of chromophore antennae has been shown[21] to increase the luminescence observed by the efficient transfer of energy from the chromophore to the metal ion. As detailed above, the yttrium complex of the tetrabenzylphosphinic acid ligand, possesses no metal bound water. The ionic radius of the yttrium(III) ion is similar to that of europium(III) and terbium(III) and so these complexes too might be expected to have no metal bound water, and, hence, long lifetimes.

The rate constant of luminescence decay has additive components from all of the relaxation modes. By comparing the lifetimes of complexes in both water and deuterium oxide, the effect of relaxation by the solvent can be estimated and the number of inner sphere water molecules inferred. The stretching vibration of the O-H bond provides a quenching mechanism for the non-radiative decay of the excited ion because

of the similarity in energy of the two processes. This process is reduced on isotopic substitution of water, as the O-D stretch is of a different energy. Simply substitution into the expression, equation 2.9., provides the estimate.

$$q = A_{Ln} \cdot (\tau_{H_2O}^{-1} - \tau_{D_2O}^{-1}) \qquad 2.9.$$

Where A_{Ln} is a proportionality constant, derived empirically for each lanthanide (A_{Tb}=4.2ms, A_{Eu}=1.05ms) and τ is the lifetime determined in the particular solvent.

The luminescence properties of the terbium complexes formed by the methoxy substituted ligands, Tb[**35-37**]$^-$ were measured, in both protiated and deuterated water, by Gareth Williams, and the results tabulated below. The data, acquired at 298K, are similar in nature with those obtained with the tetrabenzyl complex Tb[**18**]$^-$, and are

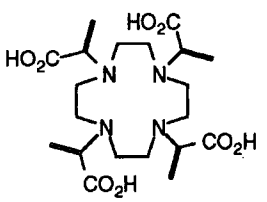

45

consistent with the absence of a water molecule in the inner co-ordination sphere. In comparison, the [Tb(**45**)]$^-$ complex has approximately one metal bound water molecule. The data for the five complexes are tabulated in table 2.2., below

Complex	$\tau(D_2O)$/ms	$\tau(H_2O)$/ms	$\phi(D_2O)$	$\phi(H_2O)$	q
[Tb(**45**)]$^-$	2.03	1.4			0.9
[Tb(**18**)]$^-$	4.44	4.13	0.49	0.44	0.07
[Tb(**35**)]$^-$	4.33	4.08	0.52	0.44	0.09
[Tb(**36**)]$^-$	4.42	4.08	0.46	0.40	0.08
[Tb(**37**)]$^-$	4.32	4.00	0.08	0.07	0.07

Table 2.2. Luminescence properties of terbium complexes. T = 298K, λ_{ex} = 250nm for [Tb(**45**)]$^-$ and [Tb(**18**)]$^-$. λ_{ex} = 278nm for methoxy substituted complexes [Tb(**35-37**)]$^-$, λ_{em} = 545nm.

The phosphinate complexes, except [Tb(**37**)]$^-$, have very high quantum yields - for every five photons absorbed by the aromatic groups of the complex, two lower energy photons are returned. Indeed, [Tb(**35**)]$^-$ has the highest quantum yield reported to date. The lifetimes of over four milliseconds are also very high, and should permit their application to time resolved photoimmunoassay studies. The poor solubility of the

complexes (and of the corresponding europium complexes) may, however, limit their application.

2.4. Lanthanum-134 for PET Studies

The characteristics of lanthanum-134 fulfil the requirements necessary for use in perfusion studies. The mean circulation time in man is approximately two minutes. The half-life, of 6.7 minutes, is thus appropriate to the time frame of the study proposed, and is also short enough for repeated measurements to be taken, at brief time intervals. Lanthanum-134 has a high positron yield (62%), and can be produced in a no-carrier added form, loosely termed "carrier-free," from a generator. The electron capture decay of ^{134}La does not lead to additional γ-rays and so the image quality and quantitation is not compromised.

Synthesis and Isolation of Lanthanum Radioisotopes ^{134}La and ^{140}La.

For use as a blood flow tracer, it is important that as little complex is administered to the patient as possible. This is to eradicate any influence the complex may have on the system under scrutiny. It is, therefore, essential that the radionuclide to be used is available in high specific activity (i.e. a large amount of activity per unit mass.) A radionuclide, which is found in the absence of any other atoms of the same element is described as "carrier free" and has a very high specific activity. This is the optimum purity achievable for a radionuclide, and can be attained, only if the nuclide is produced from another element. This then allows a chemical separation to remove the radionuclide from the sample it was produced from. (A process of enrichment can be used, whereby isotopes may be separated by a physical process such as diffusion, but this is a slow process, and only applicable to long lived or stable isotopes.) The preferred method for separating metal ions is by the use of chromatography.

Lanthanum-134 is produced from the unstable parent cerium-134 by an electron capture decay process. Cerium-134 ($t_{1/2}$=3.2 days, E.C., X-ray=33-38keV) decays, to produce the desired lanthanum-134 ($t_{1/2}$=6.7 minutes, β^+, γ=511keV, 62%). This generator is convenient because the generator has a shelf-life of around two weeks, which is acceptable to the clinic. The low energy emissions of the parent cerium reduce the amount of shielding necessary and lower the radiation dose to personnel. This is important as the short half-life may necessitate portability of the generator, for bedside delivery of the radionuclide.

Cerium-134 can be produced by several methods. Two methods involve bombardment of enriched barium targets with α-particles, *viz.* ^{132}Ba (α, 2n) ^{134}Ce and ^{134}Ba (α, 4n) ^{134}Ce. These reactions require expensive, enriched targets and rare, high energy α-particle beams. An alternative approach is the ^{139}La (p, 6n) ^{134}Ce reaction. The target, lanthanum oxide in natural isotopic abundance, is much cheaper, avoiding the inconvenience and expense of recycling precious enriched targets. A slight disadvantage of this production route is the necessity of a high energy (>60MeV) proton source. However, the sufficiently long half-life of ^{134}Ce allows production and delivery from a remote site. The cerium-134 is isolated by chromatography, after dissolving the target in nitric acid. The cerium decays as depicted in the scheme below.

$$\underset{A_1}{^{134}Ce} \xrightarrow{\lambda_1} \underset{A_2}{^{134}La} \xrightarrow{\lambda_2} {^{134}Ba}$$

The lanthanum-134 is removed from the generator, as required, by chomatography on manganese dioxide, eluting with a 0.9 mol dm^{-3} sodium chloride solution. The cerium(IV) is retained on the column and continues to decay to the daughter lanthanum, whilst the lanthanum(III) ion is eluted. The delivery of the radionuclide in salted water is attractive for potential kit formulation.

The amount of lanthanum-134 activity, A_2, can be calculated from the initial cerium activity, A_1, and the decay constants $\lambda_{1,2}$ of the two decay steps, at time, t, using the equation (2.10.) below.

$$A_2 = \frac{\lambda_1}{\lambda_2 - \lambda_1} A_1\{\exp(-\lambda_1 t) - \exp(-\lambda_2 t)\} \qquad 2.10.$$

The short half-life of lanthanum-134 makes it difficult to do development work. For this reason lanthanum-140 ($t_{1/2}$=40 hours) was chosen for experiments to evaluate the potential of the lanthanum complexes synthesised. Lanthanum-140 is produced by irradiating natural lanthanum-139 oxide with a neutron beam. The excess energy is liberated as γ-radiation. The reaction may be described therefore as ^{139}La (n, γ) ^{140}La. The lanthanum produced is described as "carrier added" as there are atoms of ^{139}La as well as ^{140}La in the sample. The ratio of isotopes found varies with the parameters used for the irradiation, but typically there will be a 10^6-10^9 fold excess of cold lanthanum-139.

2.5. Radiolabelling Studies

The labelling efficacy of the ligands was determined using carrier added lanthanum-140. Radiolabelling was attempted for twelve ligands, by adding a ligand solution (0.01mol dm^{-3}) to an equimolar lanthanum-140 chloride solution. The pH was modified by addition of sodium hydroxide. The solutions were mixed with a vortex shaker, and then analysed by HPLC with radiometric detection. The results of the radiolabelling are summarised in table 2.3., below.

Ligand	pH	temp /°C	time /min	yield /%
17	7.0	25	10	70
18	8.0	25	30	100
31	6.6	25	60	<10
32	7.6	25	10	90
33	5.6	25	10	100
34*	6.0	25	10	100
35	6.6	25	30	60
36	9.4	25	60	60
37				0
38				0
40	9.1	25	30	70

Table 2.3. Radiolabelling yields obtained for the acyclic ligands **31-34** (page 40) and macrocyclic ligands **17, 18, 35-38** and **40** (page 41). Ligand concentration = 0.01 mol dm^{-3}. pH was controlled by addition of 0.1 mol dm^{-3} sodium hydroxide solution. The optimum yields are reported.
*The solution of ligand **34** was prepared using a 50% aqueous ethanol solution, as the ligand was insoluble in water.

The insolubility of ligands **37** and **38** may explain the poor labelling yields obtained. The macrocyclic ligands **17, 18, 35, 36** and **40** labelled well. Ideally, quantitative labelling, within one half-life, would be sought for ligands to bind lanthanum-134. Some of the ligands above take a good deal longer than this, but it should be remembered that when carrier-free quantities of activity are used (10^{-9}-10^{-12} mol dm^{-3}) a great excess of ligand (10^{-6}mol dm^{-3}) is used and a faster rate of labelling might be expected.

The acyclic diamide ligands labelled very well except for the tertiary butyl amide **31**. This poor labelling is difficult to explain from a steric point of view, as the bulky groups are able to move out of the path of the incoming metal ion. An assumption was

made that this particular ligand crystallised as a triammonium salt, but a satisfactory microanalysis has not been obtained.

2.6. Evaluation of Lanthanum Complexes as Perfusion Tracers Using PET

The need for determining blood flow in patients for therapeutic gain, was outlined in paragraph 1.4. above. There are a number of methods which are used to measure perfusion.[22] A brief outline of the methods follows:

Laser Doppler Flowmetry (LDF) - This method is an invasive technique, which provides a direct measure of blood flow. Coherent light from a helium-neon laser (λ=633nm) is delivered to tissues, *via* an optical fibre, introduced through a plastic cannula. LDF measures the mean velocity of erythrocytes, by measuring the Doppler shift. This is used to calculate perfusion, by comparison with measurements under different physiological conditions, within a specific tissue type.

Thermodynamic Methods - Heat flux to a constant temperature heat sink, provides a means to determine perfusion. The flow of heat is measured and related to the oral and surface temperature of the patient. The method is subject to large errors, and although not invasive, the technique can influence the blood flow, as the tissue under investigation is either heated or cooled, depending on the temperature of the heat sink.

Magnetic Resonance Imaging (MRI) - The high spatial resolution, attainable with MRI, allows a detailed study of the heterogeneity of tumour blood flow. To achieve good images, a fairly large dose (0.2 mmol kg^{-1}) of a contrast agent, such as $[Gd(DTPA)]^{2-}$, is administered to the patient. The presence of the complex, however, may affect the flow.

Radionuclide Techniques - The washout of xenon-133, injected interstitially into tumours, can be followed by a scintillation detector, and correlated with perfusion. However, the resolution obtained is poor, and the trauma of injection may deem the assumption of a steady state redundant. The use of ^{99m}Tc-HMPAO and radiolabelled microspheres have been used to evaluate tumour perfusion with SPET. The use of ^{15}O-water has allowed the use of PET to study blood flow. It is hoped that the lanthanum-134 complexes studied herein may be useful for providing similar information, for sites remote from a cyclotron.

It would be clinically desirable to be able to determine the relative blood flow, in any region of the body, directly from the computer, processing the information, from the PET scanner. In principle this is almost possible, if we assume the complex is extracted

into tissues on the first pass through the circulation. The model below[23] describes an estimate of blood flow, in tissues of low to moderate flow, by a single measurement of tissue uptake and an arterial blood sample.

The model assumes that the tracer becomes trapped after tissue extraction, i.e. does not re-enter the circulation.

The uptake of tracer, Q, over a period of time is given by:

$$Q_{tissue} = F_{tissue} \cdot E_{tissue} \cdot \int C_{arterial}(t)\, dt \qquad 2.11.$$

where Q_{tissue} is the tissue uptake, in cpm g^{-1}, F_{tissue} is the flow through the tissue, in ml min^{-1} g^{-1}, E_{tissue} is the tissue extraction, and $C_{arterial}$ is the blood concentration of the tracer, in cpm ml^{-1}. Similarly, for the whole body, wb:

$$Q_{wb} = F_{wb} \cdot E_{wb} \cdot \int C_{arterial}(t)\, dt \qquad 2.12.$$

F_{wb}, the whole body flow, is, of course, equivalent to the cardiac output. The whole body uptake of tracer, Q_{wb}, can be expressed in terms of the activity administered, Q_{inj}:

$$Q_{wb} = Q_{inj} \cdot (1 - B) \qquad 2.13.$$

where B is the activity which is retained in the circulation. By combining the above equations, an expression relating tissue blood flow, F_{tissue} to cardiac output, F_{wb}, can be derived:

$$F_{wb} = F_{tissue} \cdot E_{tissue} \cdot Q_{inj} \cdot (1 - B) / Q_{tissue} \cdot E_{wb} \qquad 2.14.$$

A reference organ is provided by an arterial blood sample, for which the extraction, E_{ref}, is unity. Substitution gives:

$$F_{wb} = F_{ref} \cdot Q_{inj} \cdot (1 - B) / Q_{ref} \cdot E_{wb} \qquad 2.15.$$

Combining 2.11. and 2.12.:

$$F_{tissue} = Q_{tissue} \cdot F_{wb} \cdot E_{wb} / Q_{wb} \cdot E_{tissue} \qquad 2.16.$$

and substituting equation 2.15. gives:

$$F_{tissue} = F_{ref} \cdot Q_{tissue} / Q_{ref} \cdot E_{tissue} \qquad 2.17.$$

If we apply the assumption that the tracer is extracted on the first pass, then the term E_{tissue} is unity, leaving the desired relation:

$$F_{tissue} = F_{ref} \cdot Q_{tissue} / Q_{ref} \qquad 2.18.$$

The reference arterial flow, F_{ref}, and the uptake by the reference, Q_{ref}, are given by the arterial blood sample. (The radiotracer must be extracted from the blood sample, prior to counting, otherwise protein bound and free radioactivity from dissociation of the complex will be counted, as well as the intact complex. This would give an overestimate of the amount of complex left in the blood. As lipophilic complexes are to be used, a simple extraction into n-octanol permits easy counting of the complex activity.) The tissue uptake, Q_{tissue}, is determined by the PET study, to give the required tissue blood flow, F_{tissue}. The assumption that the extraction is first pass, is not applicable to high flow organs, and so the simplification of equation 2.17 cannot be justified. However, there is evidence that the relationship models perfusion in moderate to low flow organs, as determined by comparison with other perfusion methods.

To produce an accurate representation of blood flow, for the whole body, it is required that the complex shows little specificity for one tissue over another. This is a very difficult ideal to achieve. The charge, molecular weight and lipophilicity affect the biodistribution profile exhibited by agents introduced to the body. For example, lipophilic cationic complexes show a propensity to localise in the heart, whereas hydrophilic anionic complexes are rapidly excreted by extraction into the kidneys. The best (most promising) perfusion imaging agents are small, lipophilic charge neutral or cationic complexes, as exemplified by **1** and [Cu(**4**)].

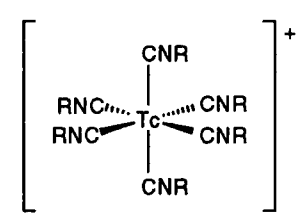

1

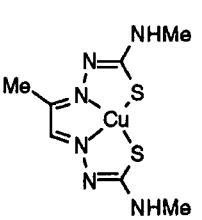

[Cu(**4**)]

The ligands used to form lanthanum complexes allow a systematic study of the effect of variation of lipophilicity, mass, and charge. The variation in the number of amide and acid donor groups permits control over the charge. The pendent arms confer differing lipophilicities upon the complexes. However, the incorporation of hydrophobic groups, results in an increase in the molecular mass of the complex. A compromise has to be

made, between the low mass required for efficient uptake into some organs, in particular the brain,[24] and a high lipophilicity for extraction into cells.

Partition Coefficient Measurements of Lanthanum Complexes

The lipophilicities of the radiolabelled complexes were determined by partitioning the complex between an aqueous phase (0.15mol dm^{-3} sodium chloride) and an organic phase (n-octanol). The amount of radioactivity associated with each phase is counted and the lipophilicity is quoted as a log P value, where:

P = (activity in organic phase) / (activity in aqueous phase) 2.17.

The lipophilicities of the complexes are tabulated below (table 2.4.)

La Complex	log P	La Complex	log P
31	-4.13	**32**	-1.51
39	-3.28	**33**	-1.06
17	-2.51	**18**	0.08
40	-2.35	**36**	0.08
$LaCl_3$	-1.72	**35**	0.49
		34	1.62

Table 2.4. The partition coefficients of lanthanum complexes.

As expected, the phosphinate and fluorine containing complexes show a higher propenisty to accumulate in the organic phase. The difference between the tertiarybutyl **31** and isobutyl amide **32** ligands was unexpected - as was their different labelling abilities. A crystal structure of the yttrium complex of a DTPA bis amide has been determined[25] showing that the amides co-ordinte *datively* to the metal, rather than ionically. An argument that the amides may cleave could be constructed, based on a potential relief of steric strain, but no evidence of this was detected by mass spectrometry of the "cold" complexes.

In Vitro Studies of Lanthanum Complexes

The behaviour of the acyclic lanthanum complexes with human sarcoma cells was investigated *in vitro*, to determine the level of cellular uptake compared with lanthanum chloride. The time points of 5 and 30 minutes were chosen as they are most appropriate to the time frame of the perfusion experiment. The complexes were incubated with the cells in the cell growth medium at 37°C. The suspension was then centrifuged to

separate the cells from the supernatant, the cells were then washed twice. The amount of radioactivity associated with the cells was compared to that measured in the combined supernatant (table 2.5.). No attempt was made to determine whether the complex had entered the cell, or was attached to the cell surface.

La Complex	%in pellet 5mins	%in pellet 30mins
$LaCl_3$	98	98
31	4	20
32	1	12
33	52	58
34	16	72

Table 2.5. Cell uptake measurements for the acyclic [^{140}La(**31-34**)] complexes, compared with $^{140}LaCl_3$

The results show that the most lipophilic complexes are indeed taken up by the cells more quickly than their hydrophilic counterparts. The increase in uptake with time suggests that a more subtle mechanism than merely an electrostatic interaction, may be involved. A purely electrostatic interaction would be diffusion controlled, and certainly complete by the first time point. The uptake value for the [La(**34**)] complex is very encouraging. The complex becomes associated with the cells fairly quickly and continues to be extracted until almost all activity is bound to cells. The free lanthanum(III) aquo ion becomes bound rather quickly. Again this could be the result of an electrostatic attraction to the acidic residues found in gangliosides in the cell membrane. It is also possible that channels for the active uptake of calcium, are providing a cellular uptake pathway. This hypothesis could be tested by repeating the measurement after blocking such channels.

In Vivo Profile of Some Lanthanum Complexes

The biodistribution profile of three of the complexes was determined, in adult hooded rats. The [La(**18**)]$^-$, [La(**35**)]$^-$ and [La(**34**)] complexes were selected on the basis of their high lipophilicities, and the interesting high uptake of [La(**34**)] with the cells *in vitro*. The choice of timepoints was made as they are the most relevant to the half life of lanthanum-134, and the time frame of perfusion studies. Unfortunately, the lack of availability of suitable animals negated the evaluation of the [La(**34**)] complex at 15 minutes.

Rats weighing 160-280g were anaesthetised, by Dr P. Carnochan, with a 1% mixture of halothane and oxygen, delivered using a commercial vaporiser system. The complexes were administered by rapid *intravenous* infusion, to the surgically exposed right jugular

vein. Animals were killed, whilst under anaesthesia, by cervical dislocation. Organs were removed by dissection, weighed and then counted in an autogamma counter. The data from the tissue dissections are given in table 2.6., as percentage of injected activity (%i.a.) per gram of organ, after normalisation to a 250g rat. The results represent an average from three animals, except for the $[La(\mathbf{18})]^-$, where only two were available for the 15 minute timepoint.

			%i.a $/g^{-1}$ of tissue			
	$LaCl_3$	[La(**34**)]	$[La(\mathbf{18})]^-$		$[La(\mathbf{35})]^-$	
organ \time	5 min	5 min	5 min	15 min	5 min	15 min
Blood	0.09±0.01	0.49±0.01	0.35±0.05	0.09±0.00	0.31±0.07	0.09±0.02
Heart	0.43±0.06	0.65±0.14	0.25±0.01	0.11±0.03	0.16±0.03	0.08±0.01
Brain	0.16±0.02	0.23±0.13	0.09±0.00	0.10±0.02	0.06±0.01	0.06±0.00
Liver	2.31±0.80	8.86±2.89	2.39±0.01	0.96±0.04	3.13±0.58	1.39±0.15
Kidney	0.68±0.07	1.39±0.54	1.21±0.35	0.18±0.01	0.73±0.29	0.17±0.02
Muscle	0.04±0.03	0.16±0.06	0.10±0.02	0.03±0.00	0.10±0.02	0.03±0.01
Spleen	3.57±1.87	7.06±1.00	0.18±0.01	0.16±0.01	0.51±0.15	0.43±0.08
Skin			0.47±0.12	0.38±0.04	0.38±0.10	0.30±0.02
Intestine*	0.09±0.03	0.83±0.81	4.06±0.25	4.34±0.50	2.57±1.21	4.76±2.84
Lungs	45.8±16.1	16.0±9.07	1.33±0.34	0.73±0.15	0.66±0.11	0.31±0.05
Stomach			0.27±0.37	0.27±0.03	1.10±0.09	0.12±0.02

Table 2.6. The biodistributions of lanthanum complexes. *The contents of the intestine were removed for the macrocyclic complexes $[La(\mathbf{18})]^-$ and $[La(\mathbf{35})]^-$ but not for $LaCl_3$ and the complex [La(**34**)].

The macrocyclic complexes show a rapid clearance *via* the biliary system. This is characterised by high and increasing liver and intestine uptake at the early timepoints. This behaviour is very similar to that of the corresponding gadolinium complexes.[19] However, whereas imaging of the gastrointestinal tract is sought after in MRI, the rapid biliary clearance observed here is not suitable for application to perfusion studies, where it is hoped the complex might become trapped in a quantitatively useful manner.

The *in vivo* profile of [La(**34**)] is very interesting and appears to show behaviour very much akin to that observed with microspheres. The first capillary bed that a microsphere encounters following intravenous injection is the lungs, where the particle becomes mechanically trapped. This behaviour pattern could prove attractive particularly as there is some concern over the potentially harmful effects of occluding capillaries with particulates. The behaviour of the complex seems to mirror that of the lanthanum ion, administered as the chloride. This may be indicative of some *in vivo* instability of the complex, hence the behaviour of the lanthanum ion, released from the

ligand may have been observed rather than the complex. Further studies are needed to probe the kinetics of dissociation. The quantification of bone uptake may have been useful in this respect, as it would be expected, that even at the short timepoints taken, free La^{3+} would have been deposited.

2.7. Conclusions

The complexes defined herein have properties which may permit their application in various imaging techniques, and could provide clinically relevant information at a range of levels. Physiological data may be accrued from the use of gadolinium complexes in MRI. Cellular events can potentially be followed by the use of phosphorescent markers. The two levels can be combined with radionuclide imaging, using positron emitting complexes.

2.8. References

1. S. Cotton, *Lanthanides and Actinides*, Oxford University Press, New York, 1991.
2. R.J.P. Williams, *Quarterly Reviews*, 1970, 351
3. J-C.G. Bünzli in *Lanthanide Probes in Life, Chemical and Earth Sciences*, eds. J-C.G. Bünzli and G.R. Choppin, Elsevier, Amsterdam, 1989
4. E.M. Stephens in *Lanthanide Probes in Life, Chemical and Earth Sciences*, eds. J-C.G. Bünzli and G.R. Choppin, 1989, Elsevier, Amsterdam
5. A.E. Martell and R.M. Smith, *Critical Stability Constants*, **6**, Plenum, New York, 1989
6. K.J. Jankowski and D. Parker in *Advances in Metals in Medicine*, eds. M.J. Abrams and B.A. Murrer, JAI Press, New York, 1993
7. C.F.G.C. Geraldes, A.M. Urbano, M.C. Alpoim, A.D. Sherry, K-T. Kuan, R. Rajagopalan, F. Muton and R.N. Muller, *Magn. Reson. Imag.*, 1995, **13**, 401
8. S.W.A. Bligh, A.H.M.S. Chowdhury, M. McPartlin, I.J. Scowen and R.A. Bulman, *Polyhedron*, 1995, **14**, 567
9. V. Alexander, *Chem. Rev.*, 1995, **95**, 273
10 K.P. Pulukkody, T.J. Norman, D. Parker, L. Royle and C.J. Broan, *J. Chem. Soc., Perkin Trans. 2*, 1993, 605
11. J.P.L. Cox, A.S. Craig, I.M. Helps, K.J. Jankowski, D. Parker, M.A.W. Eaton, A.T. Millican, K. Millar, N.R.A. Beeley, and B.A. Boyce *J. Chem Soc., Perkin Trans. 1*, 1990, 2567
12. C.D. Edlin, S. Faulkner, D. Parker and M.P. Wilkinson, *Chem. Commun.* 1996, 1249
13. S. Aime, M. Botta, D. Parker and J.A.G. Williams, *J. Chem. Soc., Dalton Trans.* 1996, 17

14. S. Aime, A.S. Batsanov, M. Botta, J.A.K. Howard, D. Parker, K. Senenayake and G. Williams, *Inorg. Chem.*, 1994, **33**, 4696
15. D. Parker in *Comprehesive Supramolecular Chemistry*, ed. D.N. Reinhoudt 1996 Pergamon, Oxford, volume 10, chapter 17, pp 487-536
16. P.J. Hore, *Nuclear Magnetic Resonance*, 1995, Oxford University Press, Oxford
17. S. Aime, M. Botta and G. Ermondi, *Inorg. Chem.*, 1992, **31**, 4291
18. J.H. Freed, *J. Chem. Phys.*, 1978, **68**, 4034
19. A. Harrison, L. Royle, C. Walker, C. Pereira, D. Parker, K. Pulukkody and T.J. Norman, *Magn. Reson. Imag.*, 1993, **11**, 761
20. R.S. Dickins, D. Parker, A.S. DeSousa and J.A.G. Williams, *Chem. Commun.*, 1996, 697
21. M. Murru, D. Parker, G. Williams and A. Beeby, *Chem. Commun.*, 1993, 1116
22. S.M. Sagar, G.A. Klassen, K.D. Barclay and J.E. Aldrich, *Cancer Treatment Reviews*, 1993, **19**, 299
23. H. Young, P. Carnochan, J. Zweit, J. Babich, S. Cherry and R. Ott, *Eur. J. Nucl. Med.* 1994, **21**, 336
24. V.A. Levin, *J. Med. Chem.*, 1980, **23**, 682
25. D. Parker, K. Pulukkody, F.C. Smith, A. Batsanov and J.A.K. Howard, *J. Chem. Soc., Dalton Trans.*, 1994, 689

Chapter Three

Tumour Targeting with Low Molecular Weight Conjugates

3. Tumour Targeting with Low Molecular Weight Conjugates

The first half of this chapter (3.1.-3.6.) concerns the synthesis and evaluation of a lipophilic copper complex for potential therapeutic use. The motivation (3.1.) is drawn from the reported hepatoma retention of lipiodol. The synthetic efforts towards suitable ligands are described (3.2.), followed by the preparation of the radionuclide copper-64 (3.3.). The ability of the ligand to form complexes is evaluated (3.4.) before comparing the cell uptake of the copper complex with radioiodinated lipiodol (3.5.). The first part concludes with the in vivo evaluation of the complex (3.6.).

The second half of the chapter (3.7.-3.11.) investigates the potential for using the affinity of the low molecular weight compound biotin for the tetrameric protein avidin. After outlining the possible clinical advantages of this approach (3.7.), the synthesis of ligands incorporating biotin is reported (3.8.). An assessment of the ligands binding to both copper-64 (3.9.) and avidin (3.10.) is made before evaluating the complex in vivo, with a rat bearing a tumour model (3.11.)

3.1. Towards Therapy with Lipophilic Copper Complexes

It was mentioned in the introduction (paragraph 1.6., page 23), that the radiation dose delivered to a patient in conventional radiotherapy, may be hazardous to health and may even give rise to new tumours. A means of reducing the dose to non-target organs may be to physically place the radiation source inside the tumour.

The mode of therapy envisaged is to regionally administer radiolabelled complexes, *via* an intra-arterial cannula directly into a tumour of the liver. The method of targeting, although lacking elegance, will obviously lead to very high initial tumour uptake. As copper-64 has a half-life of 12.8 hours, it was deemed desirable for a complex to maintain a high tumour:non tumour ratio for several days, to minimise the dose given to healthy tissues.

There have been several reports of remarkable hepatoma retention by lipiodol **14**.[1] This formulation is a mixture of iodinated ethyl esters of long chain fatty acids, derived from poppy seed oil. The reports conclude that the iodine content of these molecules is essential to the retention of the molecule in the liver tumour, but no reason is offered as to why this may be so.

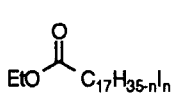

14

One might expect that all fatty molecules would remain in the liver after injection and, as the poor vascularity would lead to a poor washout from the tumour, it seems reasonable that the clearance may be quicker from healthy tissues than from the tumour. However, it may be argued that the electrophilic alkyl iodide moieties render the compound susceptible to nucleophilic attack, which may provide an "anchoring mechanism" to keep the molecule at the point of injection. It must be remembered that the method of tracing the iodinated ester *in vivo* is to use radioisotopes of iodine. Loss of iodine will almost certainly complicate the situation and any postulate offered to try and explain it. Not only must the fate of the labelled lipiodol be considered, but also the fate of any free iodide ions.

The need for increased chemical stability is obvious if a mode of therapy such as this is to be contemplated. One approach is to use a metal complexing agent. This has been attempted, albeit with the rather poor ligand **46** derived from the reaction of EDTA **24** with 1,2-diaminobenzene **47**, figure 3.1., below. The group describe the ligands application as a complexing agent for yttrium-90, which may covalently conjugated to lipiodol *via* nucleophilic substitution of iodine.[2] As might be expected, the biodistribution showed an increasing uptake into bones with time, indicative of poor complex stability.

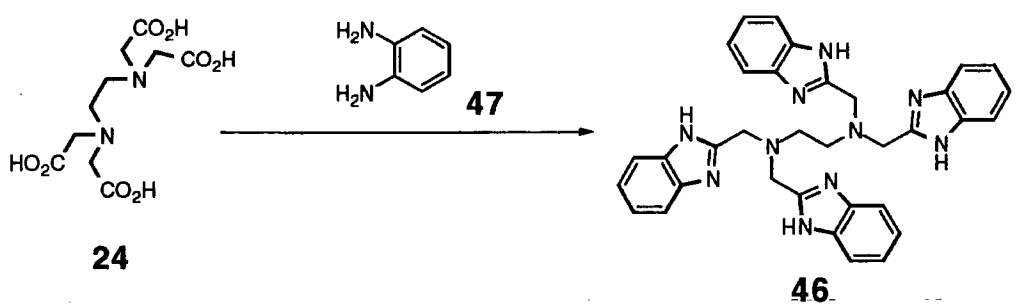

Figure 3.1. The synthesis of a complexing agent which forms both a covalent linkage to lipiodol and a complex with ^{90}Y.

One could envisage using this strategy to attach more appropriate ligating moieties to lipiodol, which offer greater stability. However, the approach is not particularly satisfying, as lipiodol is a mixture of poorly defined compounds, i.e. the number and position of iodine atoms and double bonds varies within a sample.

It was decided to prepare and evaluate well defined compounds, incorporating macrocyclic complexing agents as well as long alkyl chains to enhance the lipophilicity of the complexes. Attempts were made to synthesise iodine free molecules and iodinated analogues. However, the synthesis of the iodine containing ligands was not achieved.

3.2. Synthesis of Ligands to Bind Copper, Which Incorporate Lipophilic Moieties

Several ligands to bind copper have been defined, indeed seven are mentioned in the introduction to the thesis. It was initially anticipated that the incorporation of aliphatic chains into macrocycles designed for conjugation to other targeting vehicles, would facilitate the rapid synthesis of ligands, which would form very lipophilic complexes with copper.

The first method involved selective acylation of the known pentaamine **48** at the exocyclic nitrogen. The pentaamine was synthesised by the published route,[3] depicted in the scheme, figure 3.2., below.

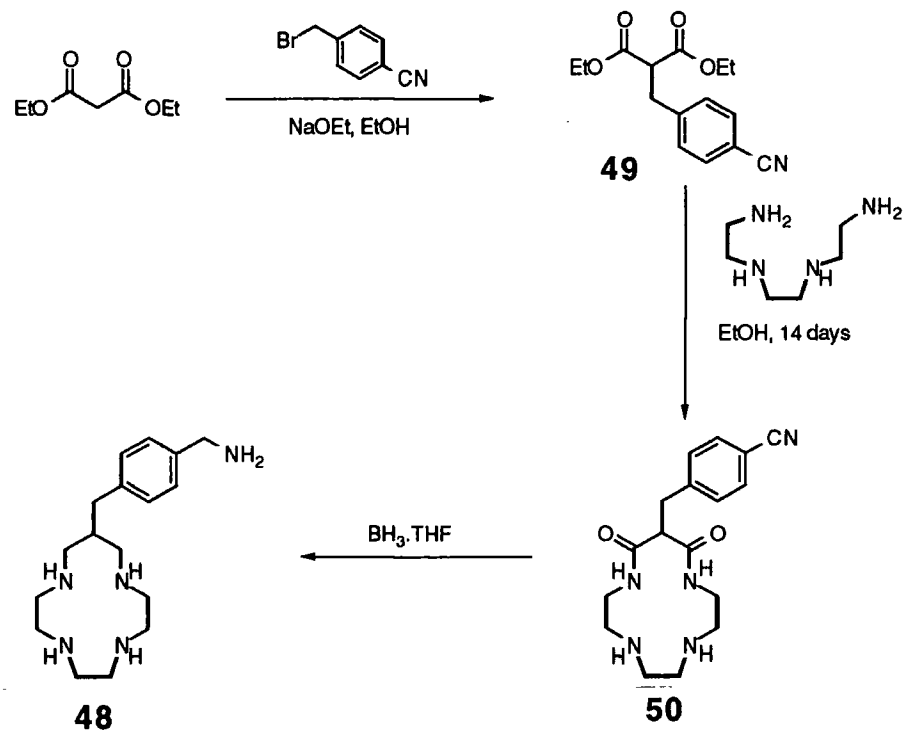

Figure 3.2. The synthesis of pentaamine **48**.

The copper binding of this cycle is compromised if the secondary ring nitrogens are acylated. The lone pair from the amide nitrogen becomes delocalised over the carbonyl system, i.e. the canonical form, shown in figure 3.3. below, makes a significant contribution to the structure of the tertiary amide. The lone pair is thus, unavailable for binding to the copper, and the resultant complexes have lower stability.

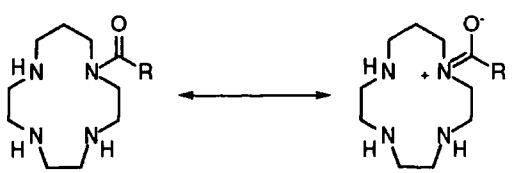

Figure 3.3. The binding of the $13N_4$ macrocycle is compromised if the nitrogens are acylated.

To effect the monoacylation at the primary amine, a pH control stategy was adopted. At a pH of 6.8, the ring is diprotonated (pK_a values are 11.5, 10.2, 1.7, 1.0[4]) and, hence, the nucleophilicity of the ring nitrogens is reduced to a greater extent than the primary amine (pK_a ~10-11). The difference in nucleophilicity is sufficient to ensure reaction selectively at the primary nitrogen. Analogous acylations have been achieved previously (and elsewhere in this work) using this pH control strategy, with 50% 1,4-dioxane in 0.5 mol dm^{-3} PIPES buffer being the preferred conditions.

In the attempted reaction of the protonated cycle **48** with an active ester **51** of stearic acid (figure 3.4.) a problem of immiscibility was encountered, which resulted in the abandonment of this approach.

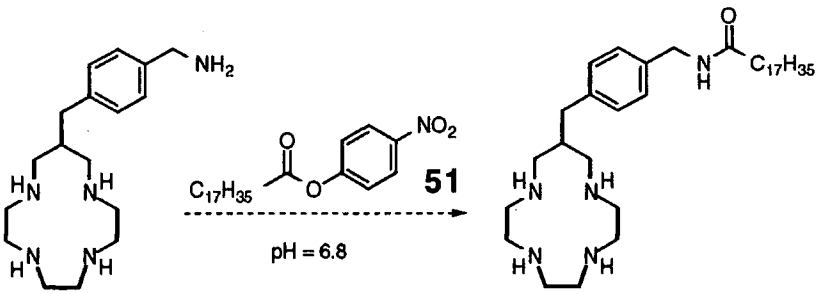

48

Figure 3.4. The acylation reaction could not be realised under the pH controlled, aqueous conditions.

Clearly, it was necessary to use wholly organic media for the reaction. The pentaamine **48** used above became unsuitable as other protection strategies for the secondary amines were based on the use of metal ions, which have been found in the past to be rather stubborn when the removal step was required.

An alternative complexing agent was sought. The ligand 1,4,7-triazacyclononane-1,4,7-triacetate (NOTA, **23**) is known to form stable complexes with copper (log K_{ML}=21.6) and, as there is an absence of any nucleophilic amines, provides an attractive parent ligating moiety for incorporating into the ligand design.

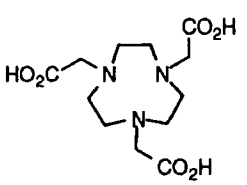

23

Several functionalised analogues of NOTA have been synthesised by our group,[5] using both N and C-alkylation approaches. The quickest route to a bifunctional complexing agent bearing a pendant amine, is achieved by N-alkylation of triazacyclononane. This compound **52** was chosen as a precursor to the target lipophilic ligands. As before, it was envisaged that the amines would react cleanly with active esters or acid chlorides to afford the desired ligands and, because organic solvents were available for use, no problems of solubility were expected. Although the compounds did go into solution, the desired acylation did not occur, figure 3.5.

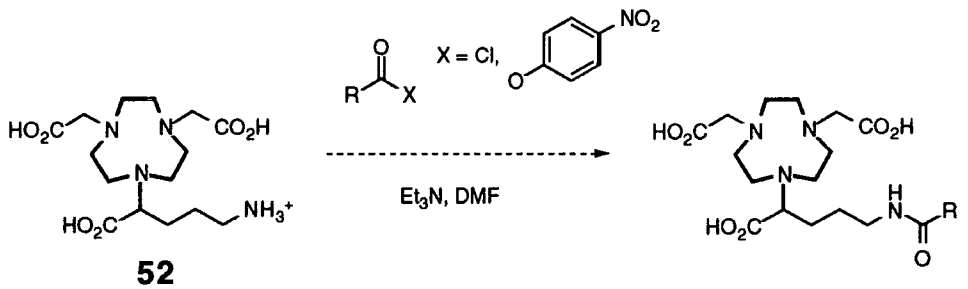

52

Figure 3.5. The acylation reaction of **52** failed with both the acid chloride and the active ester.

The reason for the failure of the reaction is uncertain, although the large difference in the polarity of the reactants may provide an explanation. It seems likely that the very polar amino acid and the relatively non-polar acylating agent, would have little affinity for each other, and hence the contact time between the reacting groups may not be sufficient.

Another ligand system, again based on the triazacyclononane macrocycle, but with two pendant carboxylic acids and one pendant amide, was investigated to ascertain whether it bound copper and whether it could be used to form conjugates, including linkage to fatty acids. This ligand system would form charge neutral complexes with copper, a feature which would reduce the electrostatic attraction of the complex to cations, including protons, and hence reasonably high stability in acidic media might be expected.

A model ligand **57** was made by the synthetic route shown in figure 3.6. 1,4,7-triazacyclononane **53** was used in excess to increase the amount of monoalkylation with the chloroacetamide **54**.

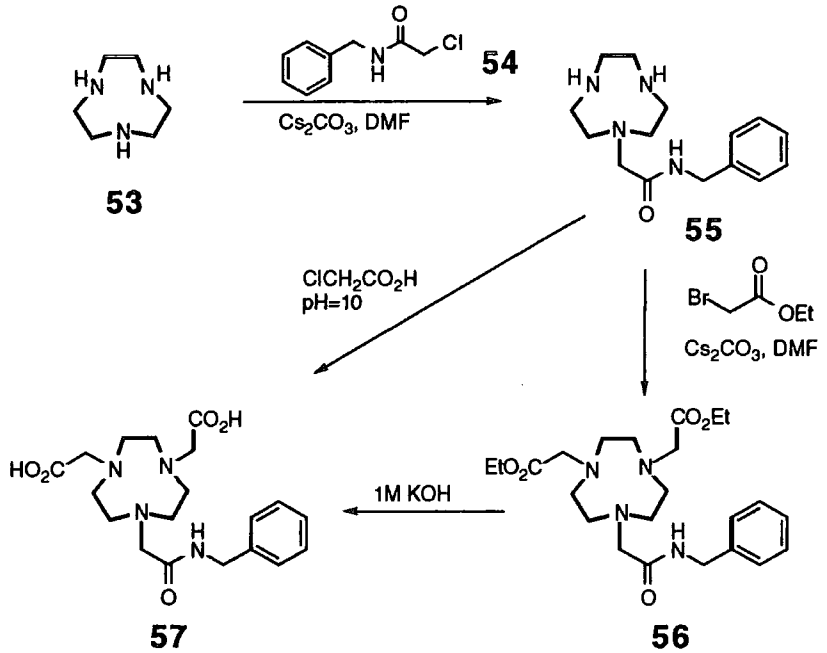

Figure 3.6. The synthetic scheme followed to give ligand **57**.

The alkylation of the two remaining nitrogens of the ring was realised by both the reaction with ethylbromoacetate followed by base hydrolysis and by reaction with chloroacetic acid under slightly basic conditions. The pH of the latter reaction was monitored during the reaction and kept to ~10 to reduce the competing hydrolysis.

A cold copper complex was made by addition of copper perchlorate to a solution of the ligand **57** under slightly acidic conditions pH~5.5, figure 3.7. An excess of copper was used and the uncomplexed copper was precipitated as the sulfide, on bubbling hydrogen sulfide through the reaction mixture.

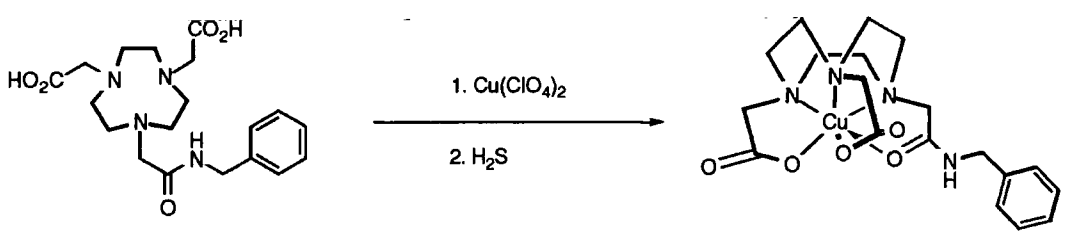

57 [Cu(**57**)]

Figure 3.7. The formation of the model complex [Cu(**57**)]

Analysis by infra red spectroscopy illustrated the participation of the amide carbonyl in binding to the metal centre, as well as the two acetates (table 3.1., below). Electrospray mass spectroscopy of a solution of the complex showed the molecular ions expected for the complex in their natural abundance. Unfortunately, attempts to obtain crystals suitable for X-ray analysis were unfruitful.

	Carbonyl Stretch /cm^{-1}	
	Ligand **57**	[Cu(**57**)]
Amide Carbonyl	1672	1633
Acetate Carbonyl	1727	1682

Table 3.1. Infra red stretching frequencies of carbonyl groups before and after complexation.

An indication of the stability of the complex under acidic conditions was obtained by monitoring the demetallation of the complex by visible spectroscopy. No change in the absorption intensity or wavelength (705nm) of a solution at pH 1.5, was detected at 3, 6, 24 or 72 hours. This suggests that the copper complex should have sufficient kinetic stability for use *in vivo*.

The ligand system defined above was elaborated to include a pendant amine **58** (the synthesis is described in the following chapter) and it was hoped that the exocyclic acylation reaction attempted for the NOTA derived systems above, might work on this slightly less polar molecule.

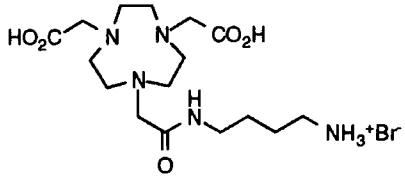

58

The coupling reaction failed, so, a decision to abandon the convergent approach to the ligands was taken, and instead a repetitive approach of synthesising the target ligands from stearic acid and linolenic acid was initialiated. The synthesis of the saturated ligand proceeded smoothly, figure 3.8., until the final step - the introduction of the carboxylic acids. The reaction with ethyl bromoacetate appeared to have gone to completion, indeed a molecular ion was visible in the mass spectrum, but the compound could not be purified by gravity chromatography on silica.

Four different fractions were collected and each hydrolysed with base. The desired compound was not identified. Ions seen in the mass spectra of the hydrolysed ester are consistent with the cleavage of one or both of the amides in the side chain. The reaction sequence was halted and the analogous synthesis, using the unsaturated linolenic acid, was not attempted.

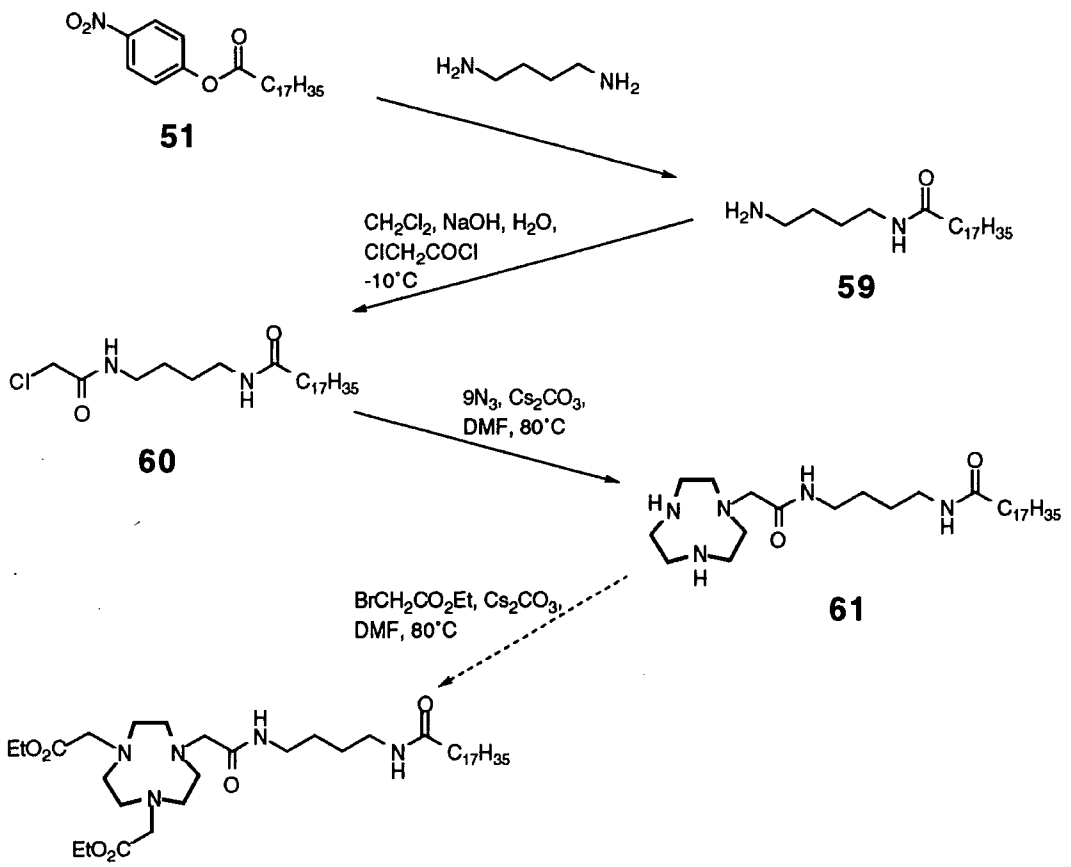

Figure 3.8. This stepwise synthesis of the ligands incorporating lipophilic chains failed to produce the desired product

The final approach towards the synthesis of lipophilic ligands was to N-alkylate the 14-membered cycle, cyclam **20**. As mentioned above, acylation of the nitrogens would result in poorer complex stability, and so the acylation step was followed with an amide reduction. The 14-membered cycle was chosen over the 13-membered homologue because the higher symmetry would result in a single compound being made, rather than the two which would result from the 13 membered cycle. Additionally, it was decided that the purification would be simplified if the triprotected cyclam **62**, prepared by Dr I. Helps,[6] was used as the starting material, as it was expected that the protected amines would behave more predictably under column chromatography conditions. The sulfonamide protecting groups were removed easily, at the end of the reaction sequence, to give the cycle **65**, which required no further purification. The sequence used is illustrated in figure 3.9.

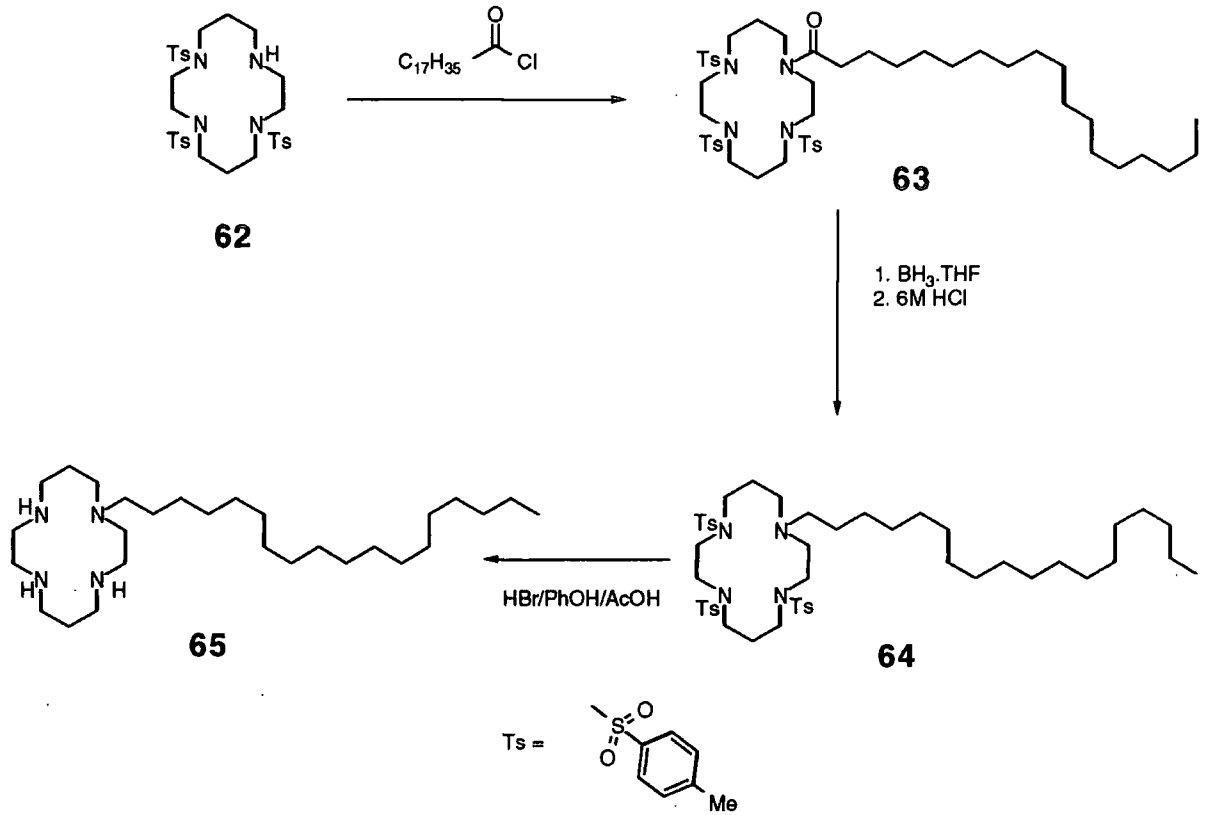

Figure 3.9. The synthesis of ligand **65**.

The synthetic route to be attempted for the unsaturated analogue necessitated modification. The presence of the double bonds prohibited the use of borane to reduce the amide. (This may, however, have offered a simple method to introduce iodine into the molecule). Also the harsh deprotection conditions employed for the saturated compound were incompatible with the alkene functionality.

In the search for alternative procedures for reduction, two potential solutions were attempted, figure 3.10. A reduction of the amide **66** using lithium aluminium hydride was tried but resulted mainly in cleavage of the amide bond to give linolenol and the starting material **62**. This reaction was attempted at both room temperature and -78°C, with little difference being seen in the ratio of products obtained, as estimated by proton NMR analysis of the crude reaction mixture. To remove the protecting groups a dissolving metal reduction was attempted, using lithium in liquid ammonia, however, the reaction did not proceed cleanly and the final product could not be isolated by chromatography. It was thought that the amide might also be reduced under the radical conditions, and indeed this did happen - again to the extent that the amide was cleaved. The tertiary amide is quite crowded and it is thought the driving force for cleavage rather than partial reduction to the amine may be the accompanying relief of crowding.

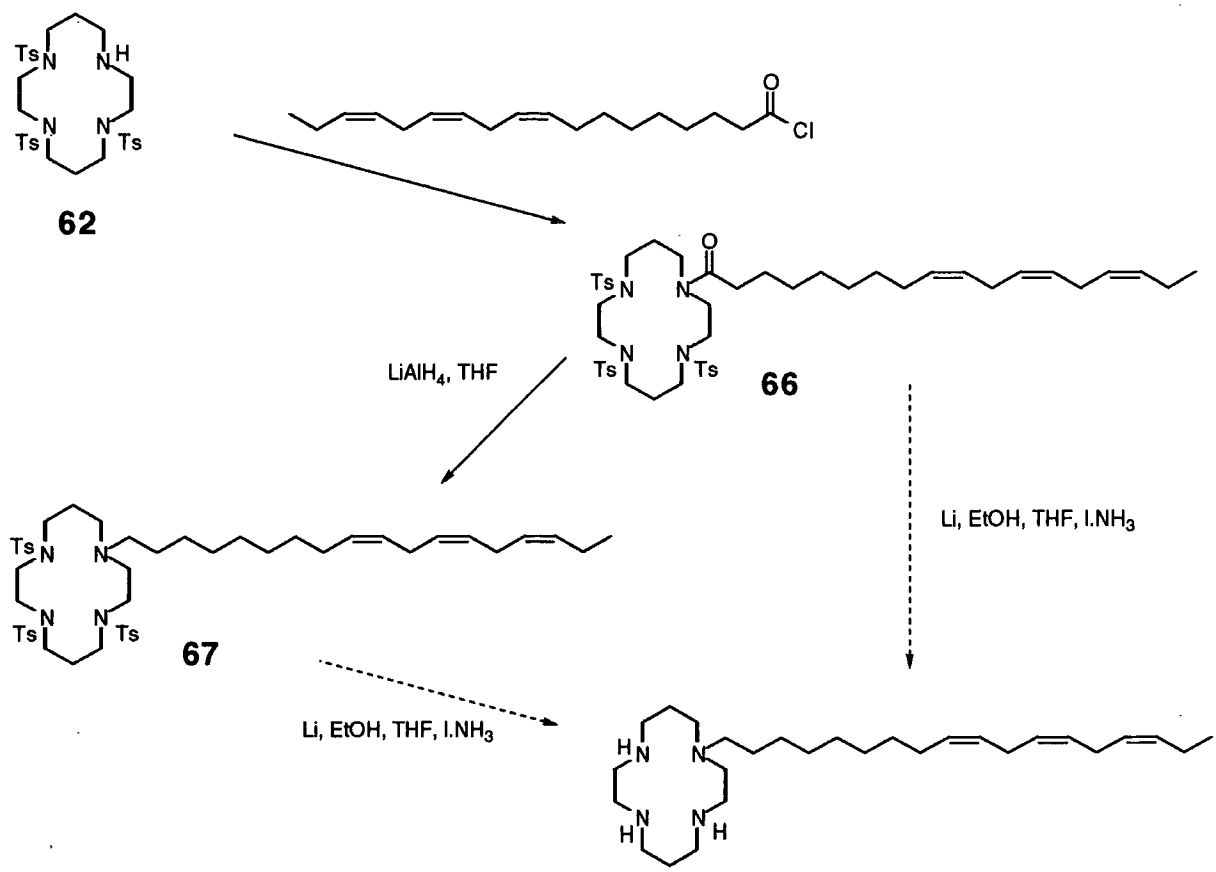

Figure 3.10. The reductive detosylation reactions failed to give the desired ligand.

The introduction of iodine into the unsaturated ligands could well present problems, in particular it might be expected that salts of the amine with iodide may be formed rather than covalent bonds formed by electrophilic addition to the double bonds. The approach intended was to utilise the surfactant properties of these ligands to perform the iodinations at the interface between water and a solution of iodine in a halogenated solvent. The reaction could be monitored by the decoloration of the organic phase.

3.3. Production of Copper-64[7]

The potential of copper-64 for use for both imaging and therapy was introduced in chapter 1. The radionuclide was obtained from irradiation of enriched nickel-64 targets. The reaction used was the bombardment of a disc of compressed powdered nickel-64 metal with a beam of deuterons $^{64}Ni(d, 2n)^{64}Cu$. The target was dissolved in a small volume of 7 mol dm^{-3} hydrochloric acid solution, with a few drops of aqueous hydrogen peroxide, to ensure complete oxidation to $^{64}Ni^{2+}$ and $^{64}Cu^{2+}$. The solvent was evaporated at ~60°C to near dryness. The caked solid was taken up with fresh 7 mol dm^{-3} HCl solution and loaded on to a AG-1X8 anion exchange column (3cm x 1.1cm diameter) which was preconditioned with 7 mol dm^{-3} acid. The nickel(II) and the trace amounts of cobalt(III), produced as a by-product of the nuclear reaction were eluted with acid, whilst the copper(II) remained on the column. The copper was then

eluted with deionised (18MΩ cm) water. The copper-64 solution was concentrated using a rotary evaporator.

The high cost (~£20 per milligram, which equates to ~£2000 per target) of the enriched nickel-64, necessitates recycling of the target material. The $^{64}NiCl_2$ solution from the column was stored, to allow the radioactivity of ^{55}Co and ^{57}Ni to decay. The eluent from the column was then concentrated and then neutralised with 5 mol dm^{-3} sodium hydroxide solution, to give a green precipitate of nickel hydroxide. The precipitate was collected by centriguation, and washed twice with deionised water. (The supernatants were retained from several "runs" to be combined and concentrated, to ensure quantitative recovery.) The wet, salt free $^{64}Ni(OH)_2$ was heated to 40°C overnight in an oven, to remove the majority of the water. The hydroxide was then reduced to metallic nickel by heating to 650°C in a furnace, under a stream of hydrogen gas, for 5 hours. The powdered metal was pressed into a pellet, which formed the recycled target.

3.4. Radiolabelling Studies

The radiolabelling efficacy of the N-octadecyl cyclam ligand **65** was assessed using copper-64. As might be expected the ligand is only sparingly soluble in water, but the addition of 20% ethanol as a cosolvent enabled a solution to be formed. On standing, however, the ligand was seen to form droplets. These were dispersed quite easily by the use of a vortex mixer, but it is quite possible that the ensuing solution was not as uniform it appeared, and may have resulted in the compounds forming smaller aggregates such as micelles. Radiolabelling yields, table 3.2., were determined at ligand to metal ion ratios over 3 orders of magnitude. The labelling reactions were performed at pH 5.5 in 0.5 mol dm^{-3} ammonium acetate buffer, at 25°C. Thin layer chromatography with radiometric detection was employed to determine the amount of complex formed, after challenging with a large excess of EDTA. The amount of copper was calculated from the specific activity, assuming that on receipt of the chromatographically purified copper, there was no cold copper and an absence of other interferring ions.

Ratio **65**:^{64}Cu	% Radiolabelling		
	30mins	120mins	18hours
10:1			0.5
100:1			9.4
1000:1	51	68	98

Table 3.2. Radiolabelling yields at various molar excesses of ligand over ^{64}Cu.

As might be expected the uptake of copper increases with time. However, the rate of binding is somewhat lower than hoped for, with over one half-life required to ensure complete complexation. The quality control of the complex is rapid and the complex requires no further purification.

3.5. Cell Uptake Studies

The extraction of the lipophilic copper complex $[^{64}Cu(\mathbf{65})]^{2+}$ was investigated, in three cell lines, and compared with the extraction of ^{125}I-lipiodol. The cell lines used were primary liver tumour cells (hepatocellular carcinoma, HepG2), liver metasteses cells from colorectal carcinoma (L_oV_o), and normal human umbilical endothelial cells (H_aV_{eo}).

Measurements were made in triplicate at three timepoints, for each type of cell, and with both compounds. The radiolabelled lipophilic compound was added to ~$2.5x10^4$ cells, suspended in 250μL of Dulbecco cell growth medium, and incubated at 37°C, with occasional stirring. Three timepoints, of 1, 5 and 24 hours were chosen, and at each, the 18 (2 compounds x 3 cell types x triplicate = 18) samples were centrifuged briefly. The supernatant was removed and the pellet was washed with 250μL of cell growth medium. The percentage of the radioactivity found in the cellular pellet is tabulated below, table 3.3.

	^{64}Cu complex			^{125}I lipiodol		
	1hr	5hr	24hr	1hr	5hr	24hr
HepG2	30.1	30.4	30.3	14.3	24.4	6.50
L_oV_o	25.4	32.9	33.9	31.9	26.8	23.6
H_aV_{eo}	20.7	18.8	21.6	17.9	13.4	11.8

Table 3.3. The amount of radioactivity taken up by cells at three timepoints.

The results for the copper complex suggest little time dependence for the primary and normal cells. The 50% greater uptake by the tumour cells compared to the normal cells could indicate quicker metabolism of these cells or may simply be a reflection of the number of cells, which was uncertain, rather than an indication of higher uptake in these cells. (All three cell lines were believed to be of similar concentration.) The increase with time for the uptake of $[^{64}Cu(\mathbf{65})]^{2+}$ complex in the secondary tumour cells is quite interesting and suggests there may be an uptake mechanism.

The collection of results for the lipiodol show less consistency. This scatter is likely to have arisen from the poor experimental procedure. The specific activity of the iodinated analogue was far lower than that of the copper complex. Consequently, a

larger amount of the compound, 30μL, was administered to the cells. The lipiodol was, of course, immiscible with the cell medium, and so formed a bolus, at the bottom of the Eppendorf tube. After centifuging, there was subsequently three phases, the supernatant, the oil and the cells. The cell pellet was not distinguishable (it was visible for the corresponding copper samples) and so separation was not easy, and a large error may have occurred. The uptake of lipiodol by human hepatoma cells (HepG2) has been investigated by others, using electron microscopy and neutron activation analysis.[1a] Both of these techniques may affect the integrity of the cells, as they are subjected to either chemical fixing agents for electron microscopy, or a beam of neutrons for the neutron activation analysis. Hence the results obtained aren't directly comparable to those presented here.

3.6. *In Vivo* Evaluation of the Copper Complex

The biodistribution of the copper complex $[^{64}Cu(\mathbf{65})]^{2+}$ was determined in adult hooded rats. The complex was administered, in 5% aqueous ethanol, by Mr M. Davies, *intravenously* to six rats (210-290g) *via* the surgically exposed right jugular vein, whilst under halothane anaesthesia. Three animals were sacrificed at each timepoint, by carbon dioxide asphyxiation. The animals were then dissected and the amount of radioactivity located in the weighed organs determined with a γ-counter. The distributions obtained at 3 and 24 hours are shown, after normalisation to a 250g rat, in table 3.4., below.

	%injected activity g^{-1}	
Tissue	3 hours	24 hours
Blood	1.30±0.09	0.57±0.10
Kidney	2.88±0.12	1.90±0.18
Spleen	4.00±0.16	1.84±0.30
Liver	3.47±0.09	3.16±0.55
Lungs	3.21±0.09	1.72±0.10
Heart	1.04±0.06	0.38±0.05
Muscle	0.47±0.13	0.16±0.02
Brain	0.11±0.01	0.07±0.01
Intestines	1.25±0.12	0.67±0.06

Table 3.4. The biodistribution profile of $[^{64}Cu(\mathbf{65})]^{2+}$ at 3 and 8 hours post-injection

The data show clearance over time from all organs except for the liver. Of course, if the complex had been infused directly into the hepatic artery, as is anticipated for the

application to hepatoma therapy, the liver uptake at both timepoints would be much greater.

The difference between the liver and intestines is interesting, and suggests that the complex is not being effectively cleared by the biliary system (as was seen, at much earlier timepoints, for the lipophilic anionic lanthanum complexes of chapter 2.) It appears as though a substantial amount of the radioactivity (~30%) is actually *trapped* in the target organ.

An experiment in a tumoured animal would be desirable, to determine whether the distribution in the liver is uniform, or whether, as the cell uptake measurements suggest, there may be a preferential uptake in the tumour cells over normal cells.

3.7. Targeting Exploiting the Affinity of Biotin for Avidin

Antibodies can show remarkable selectivities for tumour cells. However, they are very large and hence localise slowly (whole antibodies have molecular weights of 100-150 kDa.) In applications involving the use of radionuclides this represents a significant drawback, as the whole body experiences a dose of radiation. For therapeutic applications, the high background dose may limit the administered dose. The lethargic localisation is inconvenient for imaging applications, as the imaging study has to be postponed until the background radiation, from the circulating activity, has reduced to an acceptable level.

The low molecular weight (M_r=244 Da) compound biotin[8] **10** has a remarkable affinity for the tetrameric protein, avidin. The dissociation constant (K_d=10^{-15} mol^{-1} dm^3) is so small the binding, though non-covalent, can almost be considered irreversible, and is only a few orders of magnitude higher than the constants determined for some "stable" metal complexes. The use of the avidin-biotin system may enhance the quality and speed of images obtained by antibody/radionuclide methods, and may improve the efficacy of therapy with antibodies.

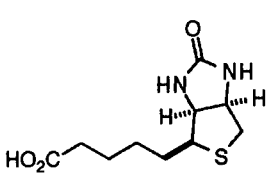

10

In conventional antibody based imaging procedures, a radiolabelled antibody is administered to a patient, which then localises by binding to an antigen on the tumour

cell, after recognising a complementary molecular surface. Of course, on each pass of the circulation, only a fraction (0.0001-0.005% injected activity per gram, depending upon the local perfusion) of the administered antibody "sees" the antigen binding site, and, so, the majority of the radiolabelled antibody remains in the circulation. If a clear image is to be obtained, with a sharp contrast between the tumour and healthy tissue the tumour:blood ratio must be sufficiently high. In time, the radiolabelled antibody will all become associated with the tumour, or be metabolised by the body. The time taken for localisation may be too long, however, for some radionuclides, due to physical decay. The use of the avidin/biotin system may be useful for improving the quality of images at shorter post-administration time intervals.

If the antibody is labelled with both a radionuclide *and* biotin, it can be administered to a patient with little change in the immunoreactivity of the antibody. After a time of a few hours, some of the activity will have localised in the tumour, whilst most would be expected to remain in the circulation. An injection of the tetrameric protein avidin will then bind to the biotinylated antibodies in the blood, causing protein aggregation. Such aggregates (M_r ~450-650 kDa), would be rapidly trapped and catabolised by the liver, hence removing the radionuclide from the circulation, and providing much enhanced tumour:blood radioactivity levels.[9] Imaging can be performed earlier, with better contrast.

A reduction in radiation dose to healthy tissue is potentially attainable, if avidin could be selectively concentrated at a tumour site, by attachment to a tumour seeking antibody. A radiolabelled biotin tracer, administered after localisation of the antibody avidin conjugate, should also concentrate at the site of the tumour, *via* "molecular recognition" of the avidin binding site. The smaller biotin conjugate, would localise much more rapidly than a whole antibody, hence, reducing the radiation dose given to the rest of the body. Strategies have been proposed for this mode of therapy.[10]

The purpose of our work in this area was to investigate the possibility of using biotin as a vehicle for transporting the positron emitting copper-64 to the tumours for imaging. The possibility of using copper-64/67 as therapeutic radionuclides, adds further impetus to the enquiry. As only the cis-fused ring system of biotin is required for recognition, the carboxylic acid group is free to provide a covalent linkage to the complexing agent, with little effect on the binding with avidin.

3.8. Synthesis of the Macrocycle-Biotin Conjugate

It was decided that it would be prudent to synthesise ligands capable of forming copper complexes of differing charges. The binding between avidin and biotin may be

compromised if the charge on the complex is incompatible with amino acid residues close to the binding site of the protein, certainly one might expect to see a kinetic difference if, for example, a positively charged complex is compared with a charge neutral one. A ligand **11** expected to form an anionic copper complex, based on DTPA, is commercially available. The ligand has been studied[11] for a similar application to that presented here, using indium-111.

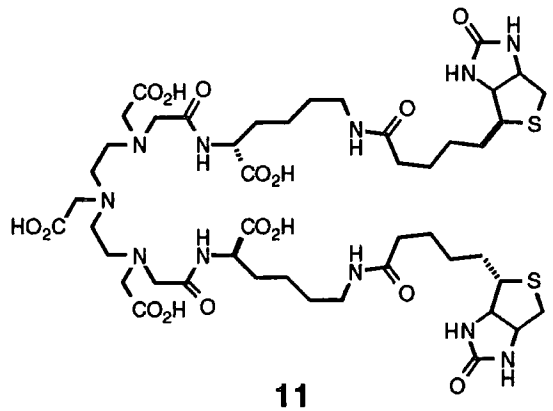

11

Complexes formed between **11** and copper would be expected to show poor kinetic stability. The copper complex also showed a very poor solubility in water, indeed a molecular ion was not obtained in an attempt to probe the speciation of the copper complex by electrospray mass spectrometry. A ligand based on the NOTA framework was designed (figure 3.11.) which would also form a negatively charged copper

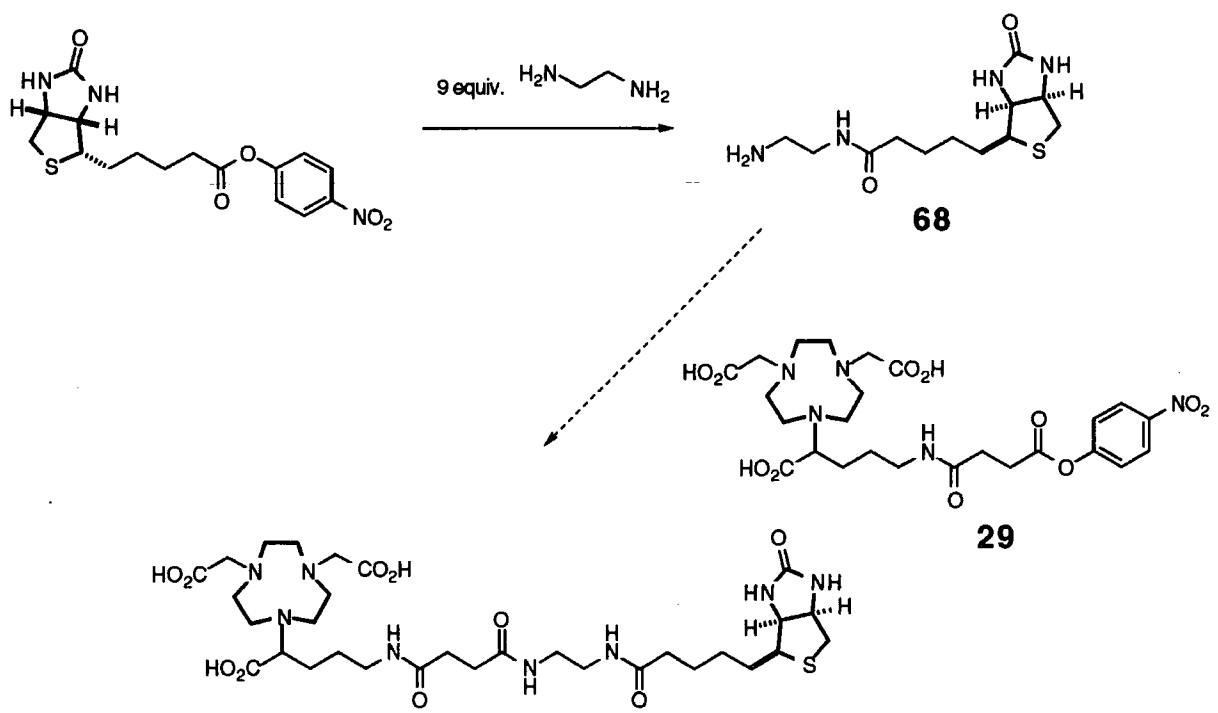

68

29

Figure 3.11. The aborted synthesis of a ligand incorporating the biotin functionality and a copper complexing moiety.

complex. The coupling reaction between the amine **68** and active ester **29** did not take place. This was somewhat surprising as analogous acylations have been achieved. It is believed the ester hydrolysed under the reaction conditions, as 4-nitrophenol was identified in the reaction mixture.

The synthesis of a ligand **69** to form a cationic copper complex proceeded cleanly, figure 3.12., below. The tetraamine macrocycle **48** was acylated at the primary nitrogen with the biotin modality, pH control being used to protect the four secondary amines.

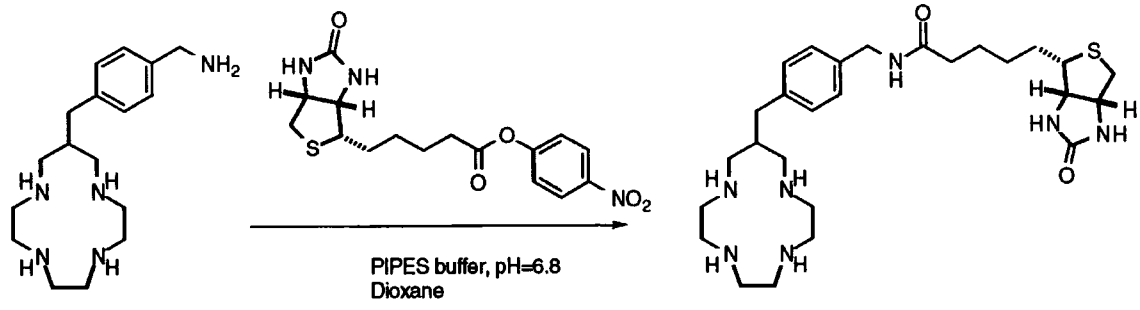

48 **69**

Figure 3.12. The synthesis of ligand **69**.

The ^{1}H NMR (figure 3.13.) and electrospray mass spectra (figure 3.14.) provide convincing evidence of the formation of the desired conjugate.

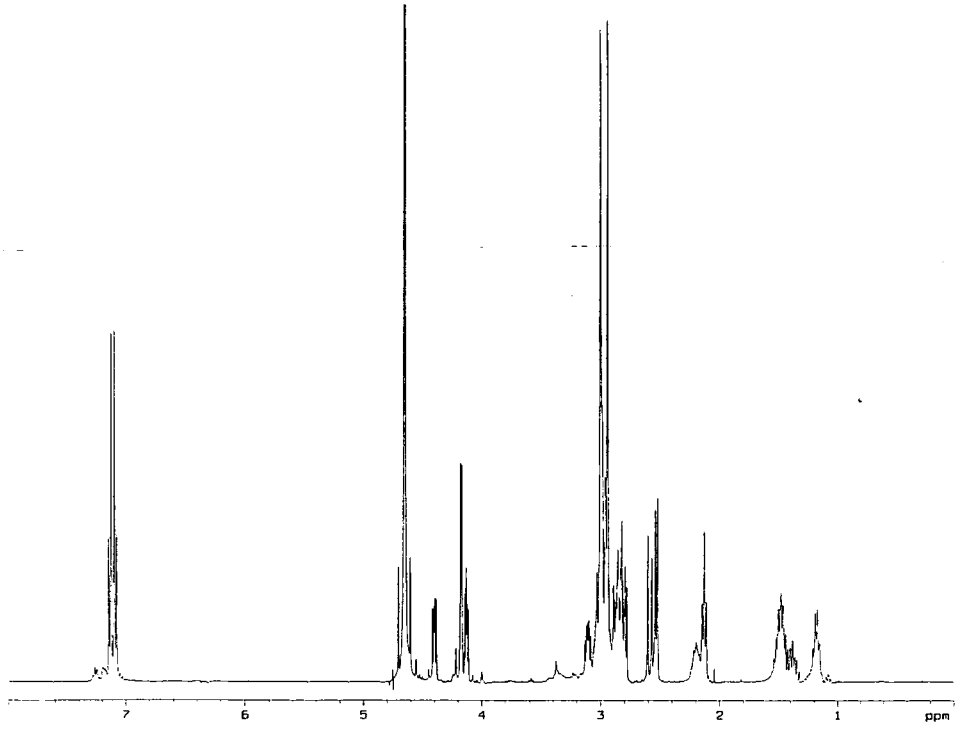

Figure 3.13. ^{1}H NMR spectrum of **69**.

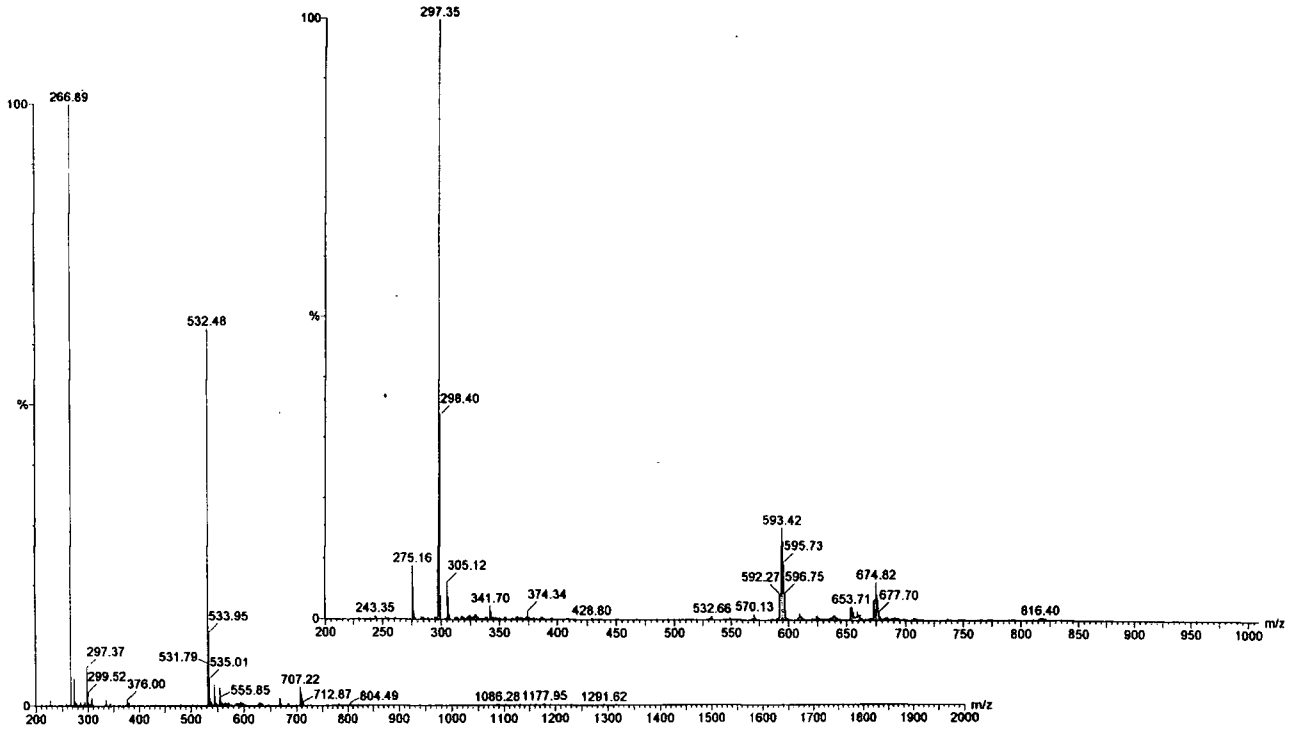

Figure 3.14. Electrospray mass spectra of **69** left and $[Cu(\mathbf{69})]^{2+}$ right.

3.9. Radiolabelling Studies

A high specific activity is desirable for radio metal complexes as there are a finite number of binding sites at the biochemical target which is being pursued. The presence of a large excess of complexing agent with no bound copper would result in competition for the available receptors. Radiolabelling was attempted at a range of ligand to macrocycle ratios, to try and maximise the specific activity obtained. The amount of copper was calculated from the measured radioactivity. Complexation reactions were performed at pH 5 in 0.5 mol dm^{-3} ammonium acetate, 30 minutes, 37°C. Radiolabelling yields were determined by thin layer chromatography, after challenging the complex with EDTA, which sequestered any free copper ions. The eluent system used for chromatography was 50% ammonium acetate (0.15 mol dm^{-3}):50% methanol. With this solvent system, the dianionic $[^{64}Cu(EDTA)]^{2-}$ complex eluted at the solvent front, whereas the dicationic $[^{64}Cu(\mathbf{69})]^{2+}$ remained at the baseline when adsorbed on to silica impregnated glass fibre sheets. The labelling yields obtained are tabulated below (table 3.5.) at various ligand ratios.

Ratio of **69**:$^{64}Cu^{2+}$	Radiolabelling yield /%
10:1	4
100:1	81
1000:1	84

Table 3.5. The radiolabelling of ligand **69** at 30 minutes.

The radiolabelling yield of 80%, obtained at a 100 fold ligand excess represents a very high specific activity. Furthermore the copper EDTA complex can be easily removed by the use of a solid phase extraction cartridge (SAX Isolute, International Sorbent Technology). Elution with 0.15 mol dm^{-3} ammonium acetate provides the pure conjugate, with no breakthrough of the anionic EDTA complex.

3.10. Binding Studies

An experiment was conducted to assess the affinity of the radiolabelled copper conjugate for avidin. A sample of the labelled complex was incubated with avidin at different stoichiometries, and for different periods of time. The binding was assessed by elution through a gel filtration column (PD10) collecting fractions. Large species elute first, enabling a comparison to be made between protein bound conjugate and the unbound conjugate. The experiment was also performed with tritiated biotin T_2(**10**), obtained commercially, and the indium complex of the DTPA-lys_2-$biotin_2$ complexing agent **11**.

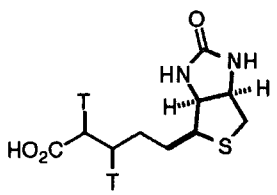

T_2(**10**)

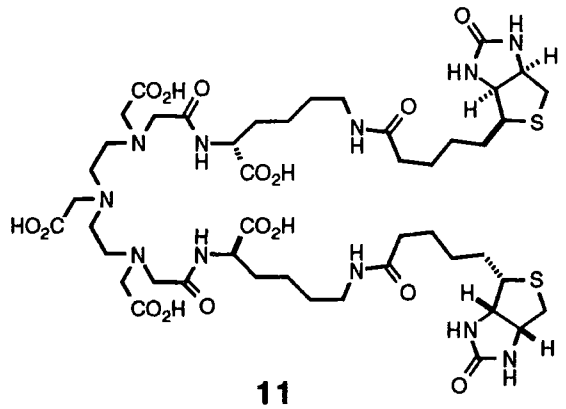

11

The experiments were conducted on both chromatographically and affinity purified avidin. The more expensive chromatographically treated protein resulted in a greater uptake of complex. It is thought that the affinity purification step may have introduced some blocking of binding sites. Table 3.6. below shows the amount of radioactivity which became bound to avidin on incubation of avidin with the two complexes and the tritiated biotin, for 30 minutes. A four fold excess of complex over avidin was used, as avidin and biotin are known to form a 4:1 complex.[12]

Complex	% Bound to protein
$[^{64}Cu(\mathbf{69})]^{2+}$	90
$[^{111}In(\mathbf{11})]^{-}$	50
T_2(**10**)	95

Table 3.6. The amount of biotinylated complex bound to avidin after 30 minutes, pH 7.4, 37°C

The results obtained suggest that the binding of the conjugate has not been significantly compromised by the incorporation of the macrocyclic copper complex, and that binding is almost instantaneous. Interestingly the indium complex, which has two biotinyl groups per complex binds only half as well. This leads one to speculate that the complex is acting as a bridge, between two binding sites, preventing access of another complex from binding. Intuitively this seems unlikely, due to the sheer bulk of the protein molecules, but spacer groups of similar size have been shown to be long enough for three antibody fragments to be attached to one complexing agent, in previous work.[13] Of course it may be possible that the complex is binding to two of the four sites on avidin, with the tethering of one half of the complex predisposing the complex in the vicinity of the other.

Competition Experiment

Although the binding experiments show that the complex binds to avidin, it offers no information on the strength of the binding. Such detail was investigated by challenging the protein-conjugate complex with biotin. No release of the conjugate was detectable, with up to 1000 fold excess of biotin, over 1 hour. It can be stated with confidence that the binding is essentially irreversible.

3.11. *In vivo* Evaluation

The biodistribution profile of the copper biotin complex $[^{64}Cu(\mathbf{69})]^{2+}$ was determined in a rat model, and compared with the profile obtained using the parent $13N_4$ complex $[^{64}Cu(\mathbf{21})]^{2+}$. Eight rats were anaesthetised by Dr I. Rowland with 2.8ml kg^{-1} Hypnorm and Hypnovel. Each then received an intramuscular injection of polymer supported streptavidin (0.1-0.2 mg on 6% beaded agarose, Pierce) into the right thigh. After 24 hours, a time chosen arbitrarily to represent the time taken for localisation of an antibody administered intravenously, each complex was administered *via* the tail vein to four animals, under anaesthetic. Two animals from each set were killed at 2 and 8 hours by cervical dislocation, whilst under anaesthesia. Selected organs were removed and the amount of radioactivity in the tissues determined with a γ-counter. The biodistribution data is tabulated below (table 3.7.), as the %injected activity per gram of tissue.

	%injected activity g^{-1}			
	$[^{64}Cu(\mathbf{21})]^{2+}$		$[^{64}Cu(\mathbf{69})]^{2+}$	
	2 Hours	8 Hours	2 Hours	8 Hours
Blood	0.38±0.21	0.17±0.02	0.24±0.08	0.33±0.06
Kidney	7.51±0.81	2.47±0.03	4.62±1.30	2.46±1.14
Liver	3.30±0.18	1.67±0.22	1.86±0.04	1.30±0.36
Spleen	0.40±0.01	0.27±0.01	1.05±0.02	0.69±0.12
Lungs	0.53±0.04	0.18±0.07	1.21±0.23	0.61±0.20
Left Thigh	0.07±0.01	0.06±0.01	0.09±0.00	0.10±0.01
Right Thigh	0.09±0.01	0.11±0.04	0.15±0.05	0.21±0.08
Intestine	0.81±0.01	0.26±0.13	1.38±0.45	0.70±0.29
Heart	0.19±0.01	0.25±0.05	0.21±0.01	0.35±0.07

Table 3.7. The biodistribution profile of $[^{64}Cu(\mathbf{69})]^{2+}$ compared with $[^{64}Cu(\mathbf{21})]^{2+}$ in rats bearing an intramuscular deposit of polymer supported streptavidin.

The data shows a similar pattern for both complexes, with a large amount of the complex rapidly excreted, as expected for hydrophilic cations such as these, primarily *via* the kidney. Analysis of a urine sample by HPLC showed a retention time characteristic of the administered complex, but little of the radioactivity in the urine bound to avidin, perhaps suggesting some modification (e.g. amide cleavage or N-carboxylation) of the pendent biotin functionality. The avidinated beads were administered to the right thigh, and so the left thigh can be used as a reference organ. The tissue counts for the left thigh show a high level of consistency, with a small error. The results from the right thigh muscle are more irregular, which suggests that the intramuscular injection of the previous day has had a negative effect on the quality of the results obtained. An approximately two-fold difference between the biotinylated complex and the parent complex can be seen from the data. However, one has to be careful in interpreting the data as the fairly large error on some measurements suggests there is little difference between the two compounds, if an assumption of the worst case scenario is made. (Throughout this work biodistribution data are presented in the format "mean ± error." The error quoted is the sample standard deviation, σ_{n-1}, rather than the population standard deviation, σ_n. The value of the error obtained is larger with the sample standard deviation than the population standard deviation, especially when small sample sizes (here n=2) are used.) If the average values are taken as "real" then the result is quite encouraging. The difference between the left and right muscles is the few milligrammes of beads, however when processing the tissue counts the weight of the whole muscle is considered and hence the difference in uptake is diluted

throughout the whole tissue. If the beads themselves were separable from the rest of the muscle and were able to be counted as an organ in their own right, as for xenografted tumours, the high activity concentrated in the low mass would give a very high %injected activity per gram of tissue.

In conclusion, a further experiment is required with tumour bearing animals. The model nature of the *in vivo* experiment doesn't tackle the potentially problematic antibody-avidin localisation, but it does suggest that the approach may be useful, to reduce the dose to non-target tissues, due to the rapid clearance from the circulation. Also the stability of the complex *in vivo* has been demonstrated.

3.12. References and Notes

1. (a) F. I. Chou, K.C. Fang, C. Chung, W.Y. Lui, C.W. Chi, R.S. Liu and W.K. Chan, *Nucl. Med. Biol.*, 1995, **22**, 379 (b) J.L. Raoul, P. Bourguet, J. F. Bretagne, R. Duvauferrier, S. Coornaert, P. Darnault, A. Ramee, J.Y. Herry and J. Gastard, *Radiology*, 1988, **168**, 541 (c) K. Ivancev, A. Lunderquist, R. McCuskey, P. McCusky and A. Wretlind, *Acta Radiol.*, 1989, **30**, 291
2. S-J. Wang, W-Y. Lin, M-N. Chen, L-H. Shen, Z-T. Tsai and G. Ting, *Eur. J. Nucl. Med.*, 1995, **22**, 233
3. J.R. Morphy, D. Parker, R. Kataky, M.A.W. Eaton, A.T. Millican, R. Alexander, A. Harrison and C. Walker, *J. Chem. Soc., Perkin Trans. 2*, 1990, 573
4. M. Kodama and E. Kimura, *J. Chem. Soc., Dalton Trans.*, 1976, 1720
5. J.P.L. Cox, A.S. Craig, I.M. Helps, K.J. Jankowski, D. Parker, M.A.W. Eaton, A.T. Millican, K. Millar, N.R.A. Beeley and B.A. Boyce, *J. Chem. Soc., Perkin Trans. 1*, 1990, 2567
6. I.M. Helps, D. Parker, J.R. Morphy and J. Chapman, *Tetrahedron*, 1989, **45**, 219
7. J. Zweit, A.M. Smith, S. Downey and H.L. Sharma, *Appl. Radiat. Isot.*, 1991, **42**, 193
8. The role of biotin *in vivo* is to effect α-carboxylations, i.e. it is an enzyme cofactor (vitamin H). In processes such as fatty acid biosynthesis, the biotin group is linked *via* the carboxylic acid to a protein, leaving the free urea functionality to fix carbon dioxide to acetate.
9. D.B. Axworthy, J.A. Sanderson, L.M. Gustavson, F-M. Su, A. Srinivasan, J.M. Reno, D.R. Woodle, P.L. Beaumier and A.R. Fritzberg, *J. Nucl. Med.*, 1992, **33**, 880 (Abstract)
10. D.A. Goodwin, C.F. Meares, M. McTigue, W. Chaovapong, C. Ransone, O, Renn, M.J. McCall and M. Studer in *Radiolabelled Blood Elements*, Ed. J. Martin-Commin, Plenum, New York, 1994

11. F. Virzi, B. Fritz, M. Ruscowski, M. Gionet, H. Misra and D.J. Hnatowich, *Nucl. Med. Biol.*, 1991, **18**, 719
12. M. Wilchek and E.A. Bayer, *Immunology Today*, 1984, **5**, 39
13. T.J. Norman, D. Parker, L. Royle, Alice Harrison, P. Antoniw and D.J. King, *Chem. Commun.*, 1995, 1877

Chapter Four

Targeting with Monoclonal Antibodies

4. Targeting with Monoclonal Antibodies

The possibility of antibody based targeted imaging and therapy with copper-64 labelled ICR-12 is introduced (4.1.). The synthesis of bifunctional complexing agents is detailed (4.2.) and the radiolabelling (4.3.) and antibody conjugation (4.4.) described. Damage caused to the antibody is assessed (4.5.) and the conjugates are evaluated in vivo (4.6.).

4.1. Introduction

The potential use of monoclonal antibodies as targeting vectors for tumour imaging and therapy was introduced in chapter 1. The high specificity of monoclonal antibodies makes their application to targeting attractive. In principle, the administration of a monoclonal antibody, radiolabelled with an appropriate nuclide, will result in the localisation of radioactivity at the site of tumours. The tumours may then be visualised by one of several radionuclide based imaging modalities, or if appropriate radiations are liberated in the physical decay, one can envisage using the radiolabelled antibodies to cause cell death.

The monoclonal antibody ICR-12, binds to the external domain of a transmembrane glycoprotein, produced by the human c-erbB2 proto-oncogene.[1] It is believed that the protein functions as an autocrine receptor in breast cancer. The gene that codes the protein is also over expressed in adenocarcinomas of the lung, endometrium, ovary and possibly the bladder. ICR-12 does not bind significantly to normal cells and, thus, the antibody represents a versatile targeting vehicle for the detection and treatment of a number of important tumours, when labelled with radionuclides.

Copper-64 is a unique radionuclide because the radioactive decay gives rise to three different, potentially useful types of emission. The γ-rays arising from the annihilation of positrons are useful for PET imaging, both diagnostically and as a mode to monitor therapy. The positron and beta emissions are useful therapeutically as ionising radiations. As the pathlengths of the emissions are greater than cellular dimensions, a degree of "crossfire" may be expected which could cause cell damage, even though the ionising radiation is delivered from a nuclide bound to a different cell. This is crucial if therapy is to be effective, as some cells are inaccessible to the antibody conjugate because of poor perfusion. It is important that the radiation pathlength is large enough to deliver a sterilising dose to these cells. The third useful decay process of copper-64 is electron capture, which leads to the emission of Auger electrons. Although Auger electrons have a short pathlength, they may be useful for causing the critical DNA double strand cleavage, required for cell death. The range of Auger electrons, from the decay of copper-64 is 1.3μm-38nm, hence the radionuclide must be bound to the DNA

double helix, if damage is to be effective. To target the DNA of tumour cells, a means of locating the target cell and then finding the DNA is required. The use of a monoclonal antibody promises an answer to localisation at the tumour cell, but if damage is to be caused to the nuclear DNA, the radiolabel must then become internalised in the cell, and localise at the nucleus. Several antibodies are known to internalise, and may be useful for nucleic acid targeting.

4.2. Synthesis

Bifunctional complexing agents for use in antibody based targeting require a set of ligating groups to bind the radionuclide, and a linking group which allows conjugation to the antibody. The nature of the complex (e.g. the charge, size and shape) may affect the ability of the antibody to bind with the receptor site on the tumour cell. The three ligand systems **21**, **23** and **57** are known to form complexes of different charges on binding copper.

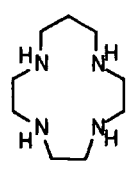

21

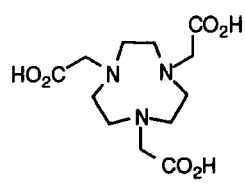

23

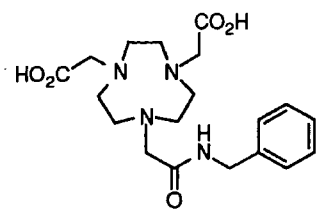

57

Kinetic stability *in vivo* has been demonstrated for the $[Cu(\mathbf{21})]^{2+}$ complex.[2] The complexes derived from **23** and **57** should also be kinetically stable *in vivo*. To facilitate the linkage to the antibody, a pendent reactive group is necessary. It is convenient to use an exocyclic amine for derivatisation, as there are several methods for forming stable amide linkages.

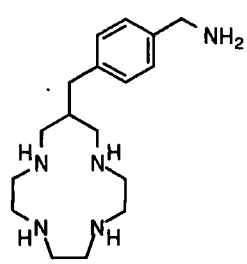

48

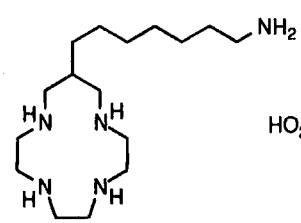

70

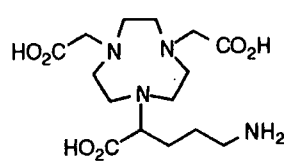

52

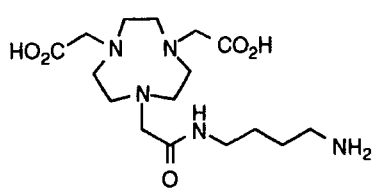

58

The four ligands **48**, **52**, **58** and **70**, bearing pendent amines were selected for synthesis. The synthesis of **48**, was described in the previous chapter. Whilst the aromatic group of **48** provides a useful chromophore for analysis of conjugates, it was thought that the

group may exhibit a degree of immunogenicity, hence the aliphatic ligand **70** was also prepared. The synthetic sequence depicted below (figure 4.1.) afforded the ligand in three steps.

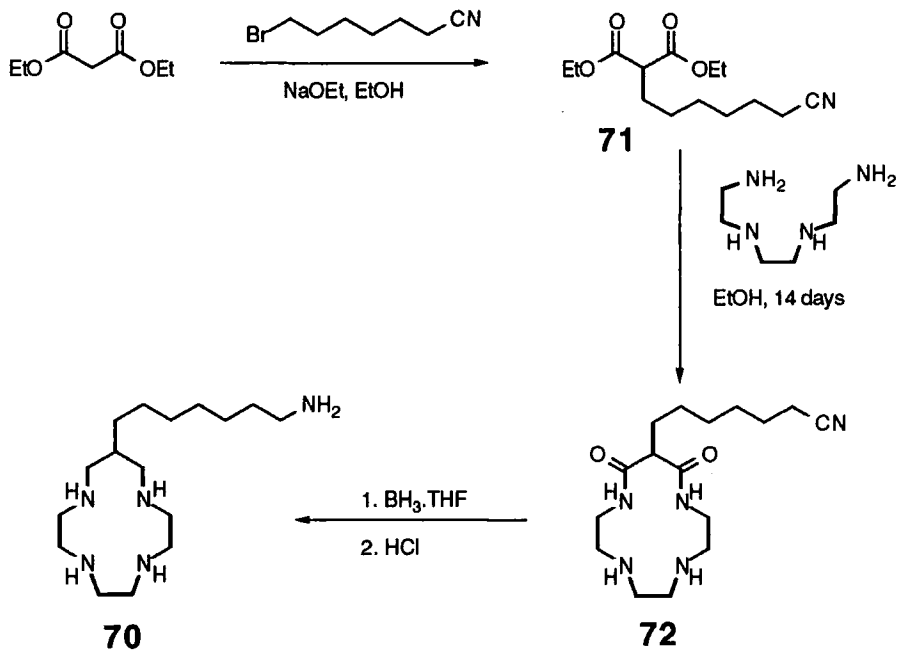

Figure 4.1. The synthesis of the aliphatic ligand **70**.

Ligand **52** was prepared by Fiona Smith following the published route.[3] NOTA **23** was prepared as a model compound (figure 4.2.) to investigate the radiolabelling efficacy of **52**, by alkylation of **53** with chloroacetic acid.

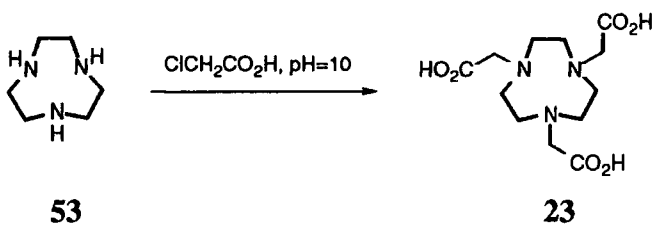

Figure 4.2. The synthesis of NOTA.

The ligand **58**, was prepared using the reaction sequence illustrated in figure 4.3., below. The alkylation of 1,4,7-triazacyclononane **53** with the N-protected amide **74** was performed with the cyclic amine present in an excess, to reduce the amount of dialkylated material produced. The alkylation of the remaining two nitrogens was achieved by two methods. The first method tried was the reaction with ethyl bromoacetate in DMF. This procedure resulted in the formation of a substantial amount of the alkylated sulfonamide product **79**. The second method used was the aqueous alkylation with chloroacetic acid, under carefully controlled pH conditions, using lithium hydroxide to maintain a slightly basic pH, and minimise glycolic acid formation. Although some alkylation of the sulfonamide was seen, preparative HPLC

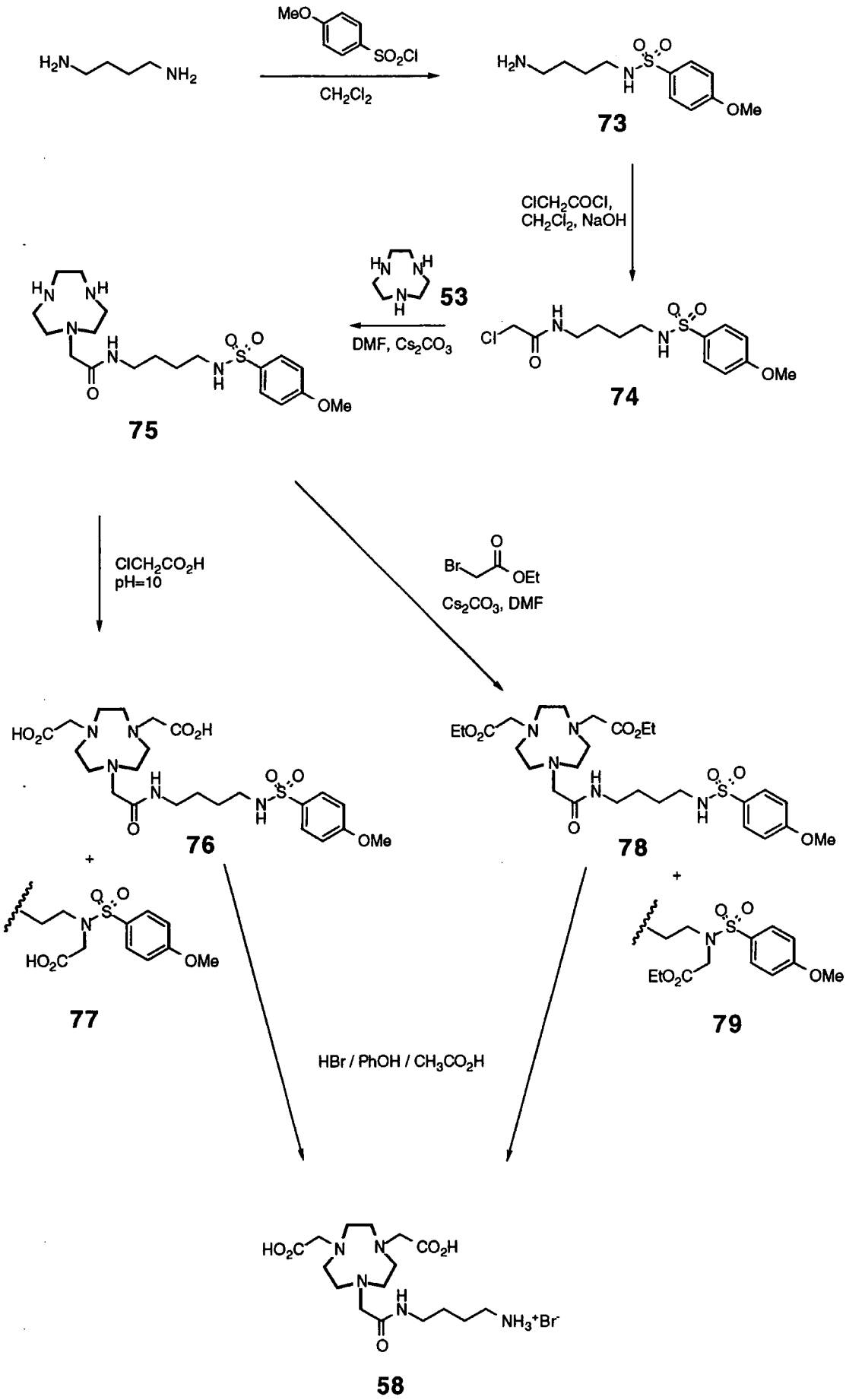

Figure 4.3. The synthesis of ligand **58**.

under anion exchange conditions provided an easier purification than the gravity chromatography used to purify the diester. Detosylation proceeded cleanly to give the desired ligand **58**.

A sample of **80** was isolated by HPLC. This compound is a potentially useful intermediate for introducing three different substituents on the nine membered cycle. The remaining secondary nitrogen was alkylated (figure 4.4.) with the α-bromo diprotected δ-aminovaleric acid **81**. The compound **82** has two protected pendent amines, which can be made available selectively by the choice of deprotection sequence. The use of a BOC protecting group for one nitrogen would be more versatile, as the difference in reactivity between the two amides of **82** may not be sufficient for an efficient deprotection.

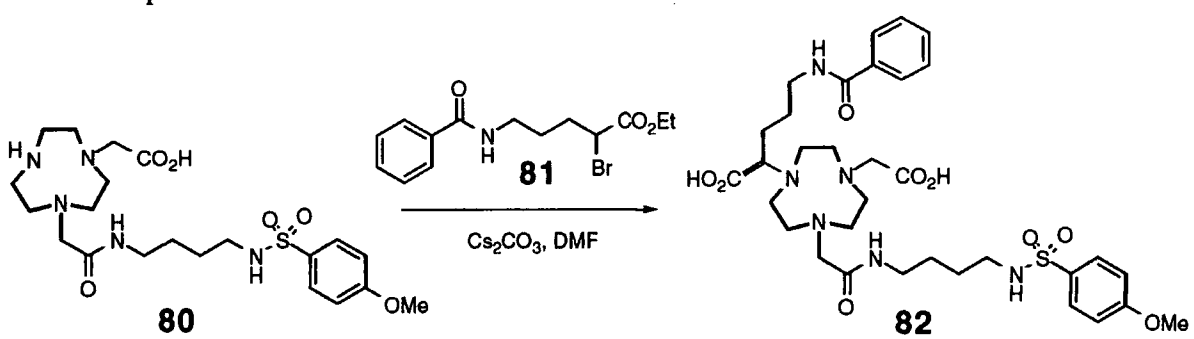

Figure 3.4. The synthesis of **82**.

It is important that the complexing agent is conjugated rapidly to the antibody, under mild conditions, to ensure minimal damage to the protein. A simple coupling is achievable by either Michael type addition to an electron deficient double bond, or by substitution of an active ester, figure 4.5. Thus, the protein behaves as a nucleophile. The most nucleophilic groups of antibodies are the thiols on the cysteine residues, and the free amines of lysine residues. The maleimide group reacts rapidly, in aqueous media (pH ~7), with thiols to form a stable linkage (the analagous reaction with amines is slower).

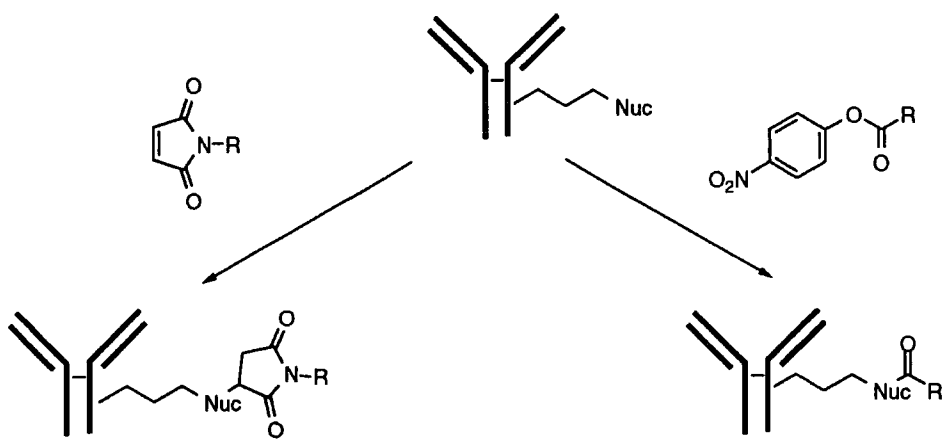

Figure 4.5. Coupling reactions for derivatising monoclonal antibodies.

Active esters such as N-hydrroxysuccinimidyl and para-nitrophenyl react rapidly in slightly basic media (pH ~7.5) with the terminal amine of lysine. The three active esters **85-87** were synthesised (figure 4.6.), as a means of introducing maleimides and active esters to the ligands **48**, **52**, **70** and **58**.

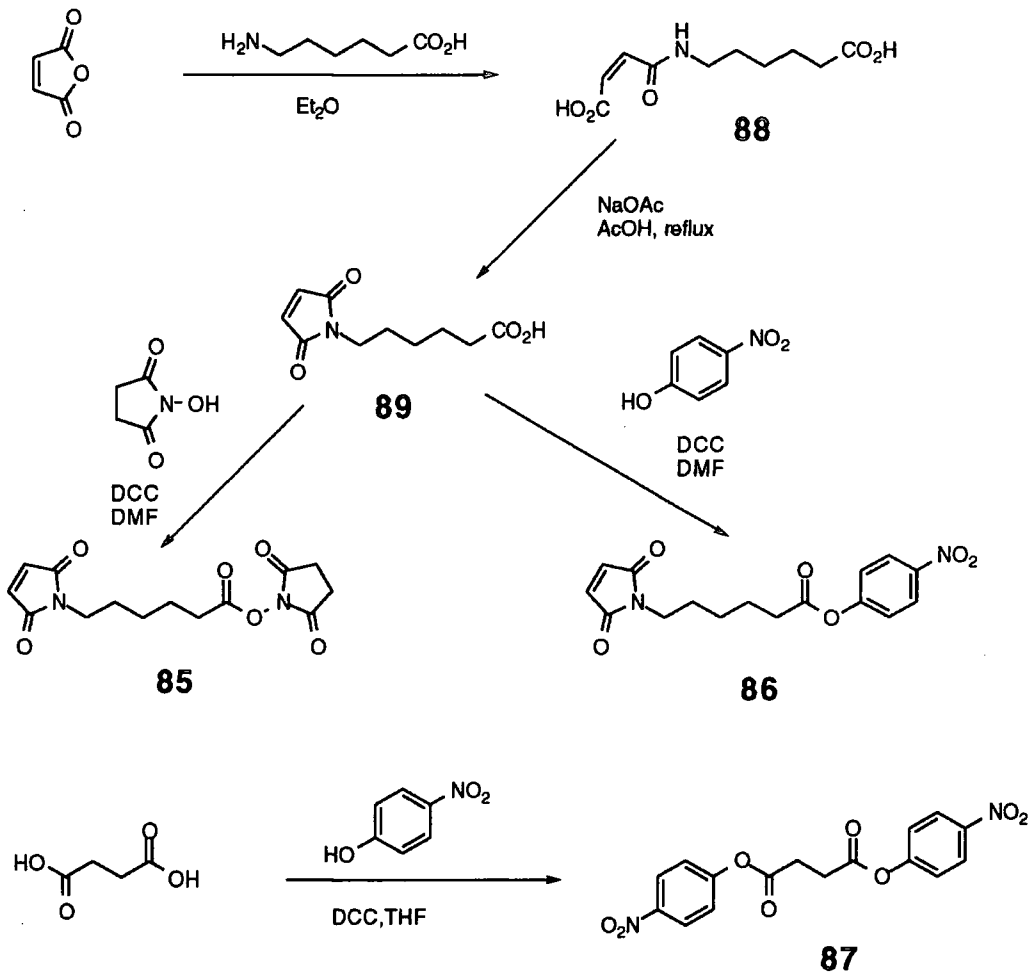

Figure 4.6. The synthesis of active esters **85-87**.

None of the desired product was identified in the coupling reaction (figure 4.7.) between the aliphatic pentaamine and the active esters **85** and **86**. The absence of a suitable UV active chromophore in the amine should not have caused a problem, as the transferred maleimide exhibits an absorption (λ_{max}=305nm). The reaction was performed using the same mixed solvent system used for the selective acylation of the primary amine in the preparation of the biotin conjugate **69**, in the previous chapter. The reaction was followed by HPLC, but no compound with the characteristic absorbance and retention time was detected. The use of the commercially available ester **90** also failed to produce the desired conjugate.

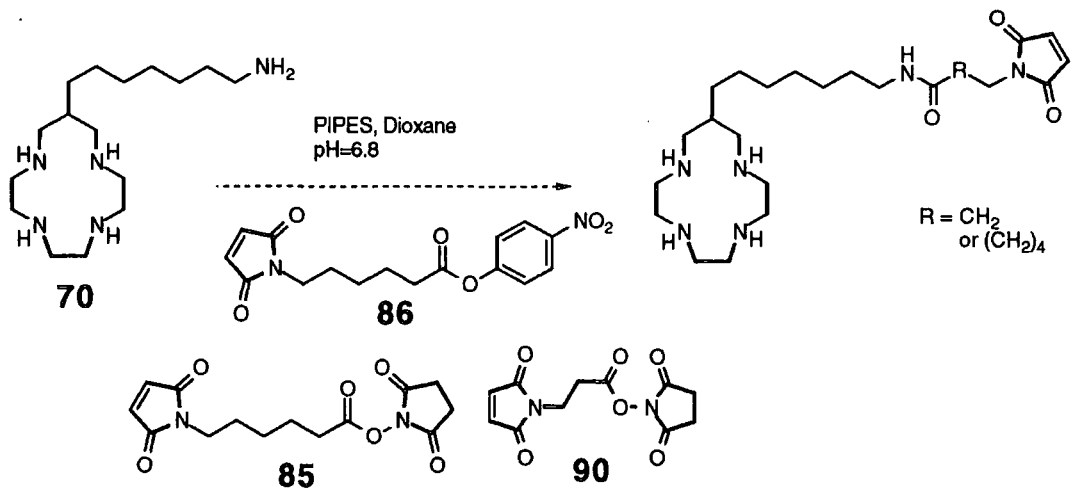

Figure 4.7. The attempted synthesis of a bifunctional complexing agent.

The synthesis of the conjugate **91** proceeded smoothly with the ester **90**, and was purified by preparative HPLC (figure 4.8.). It appears as though the subtle difference in the solubility of the two pentaamines may account for the unsuccessful synthesis of conjugates of **70**.

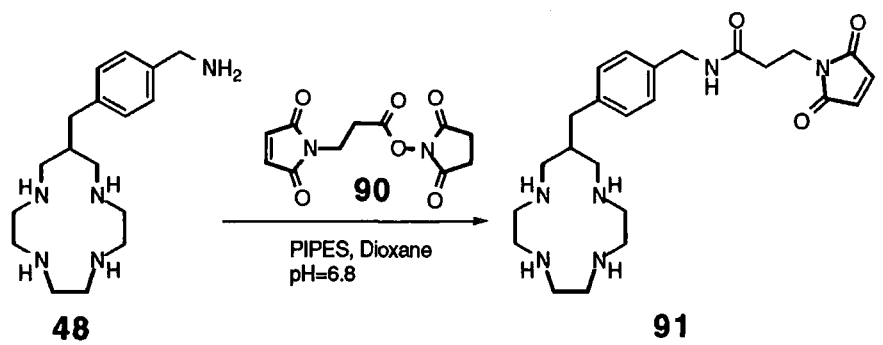

Figure 4.8. The synthesis of **91**.

Similarly, the monoamide ligand **58** was used to form the bifunctional complexing agent **92**, incorporating the maleimide group (figure 4.9.)

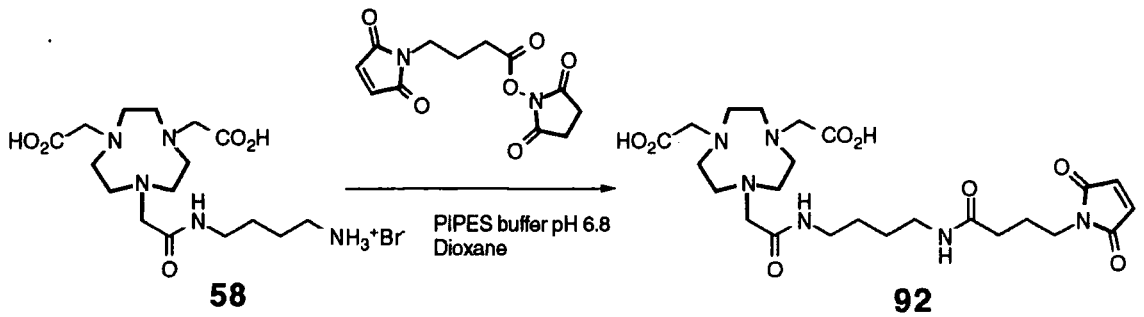

Figure 4.9. The synthesis of **92**.

The use of paranitrophenyl active esters is not compatible with the secondary amines of the pentaamine ligands **48** and **70**. However, the ligands **52** and **58**, in which all

nitrogens are tertiary are useful for preparing active esters. The reaction of the ligands with the bis-ester proceeded cleanly (figure 4.10.), and the presence of the strong chromophore facilitated HPLC purification. The reaction of the NOTA derived ligand **52** proceeded in higher yield than the with monoamide ligand, **58**.

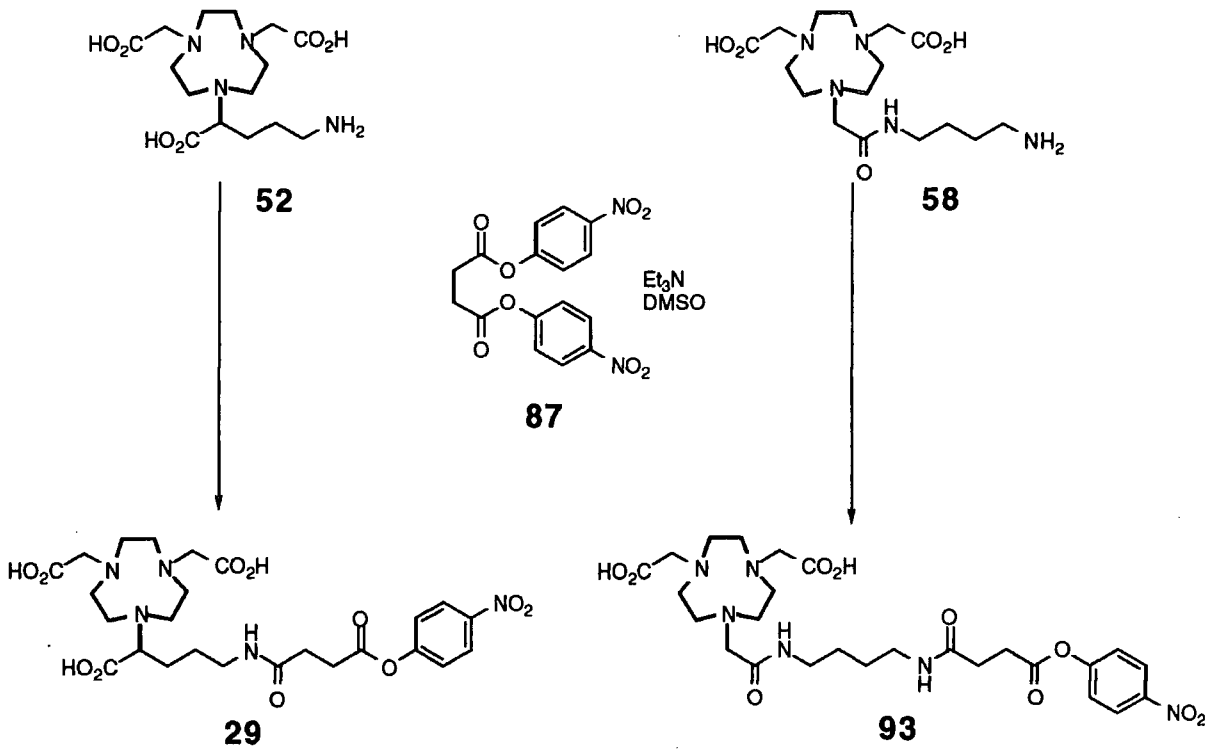

Figure 4.10. The synthesis of bifunctional complexing agents **29** and **93**.

The potential utility of the Auger emission from copper-64 warrants the synthesis of bifunctional compounds, which could both bind with the polyanionic DNA molecules, and also allow conjugation to the radionuclide or protein targeting vehicle. Two types of conjugate can be envisaged. One can modify the protein to possess both a complexing agent and an intercalating moiety. Alternatively, the protein can be conjugated to a trifunctional molecule, where both the intercalating and radionuclide complexing groups are attached *via* one linkage. These two situations are illustrated in figure 4.11., below.

Figure 4.11. Possible antibody-intercalator-radionuclide conjugates.

The simpler approach is to attach both groups individually. The intercalating acridine group has been incorporated into an agent **95** suitable for protein derivatisation.[4] The synthesis (figure 4.12.) from the triamine **96** incorporates one tertiary amine, which

should be protonated at cellular pH, thus providing an electrostatic attraction between the intercalating group and the anionic DNA. Two other compounds **98** and **99** were synthesised (figure 4.13.) which incorporate maleimide linking groups. The asymmetric amine **98** bears a free amine for attaching the complexing agent, and hence provides a potential route to the trifunctional complexing agent **100** described above. The final coupling was attempted, but the trifunctional conjugate was not identified by electrospray mass spectrometry.

The dimaleimide compound **99** could be used as a non-specific protein modification reagent, by employing 2-iminothiolane as a linking molecule. The compound could also be further elaborated to provide an alternative synthesis a of trifunctional conjugate, figure 4.14.

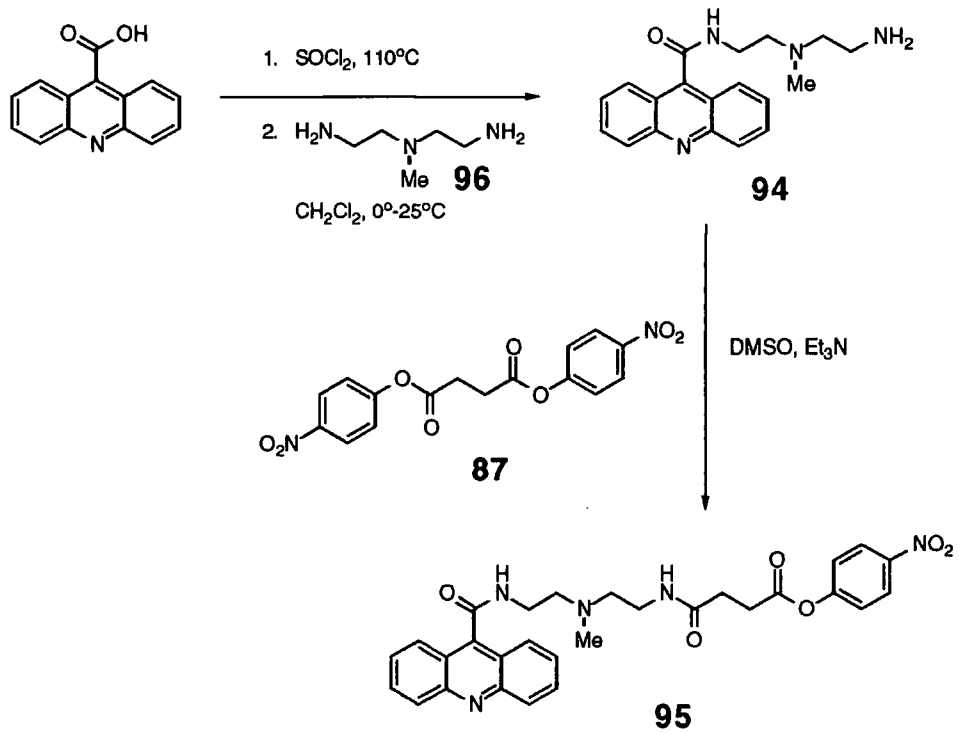

Figure 4.12. The synthesis of the bifunctional intercalating agent **95**.

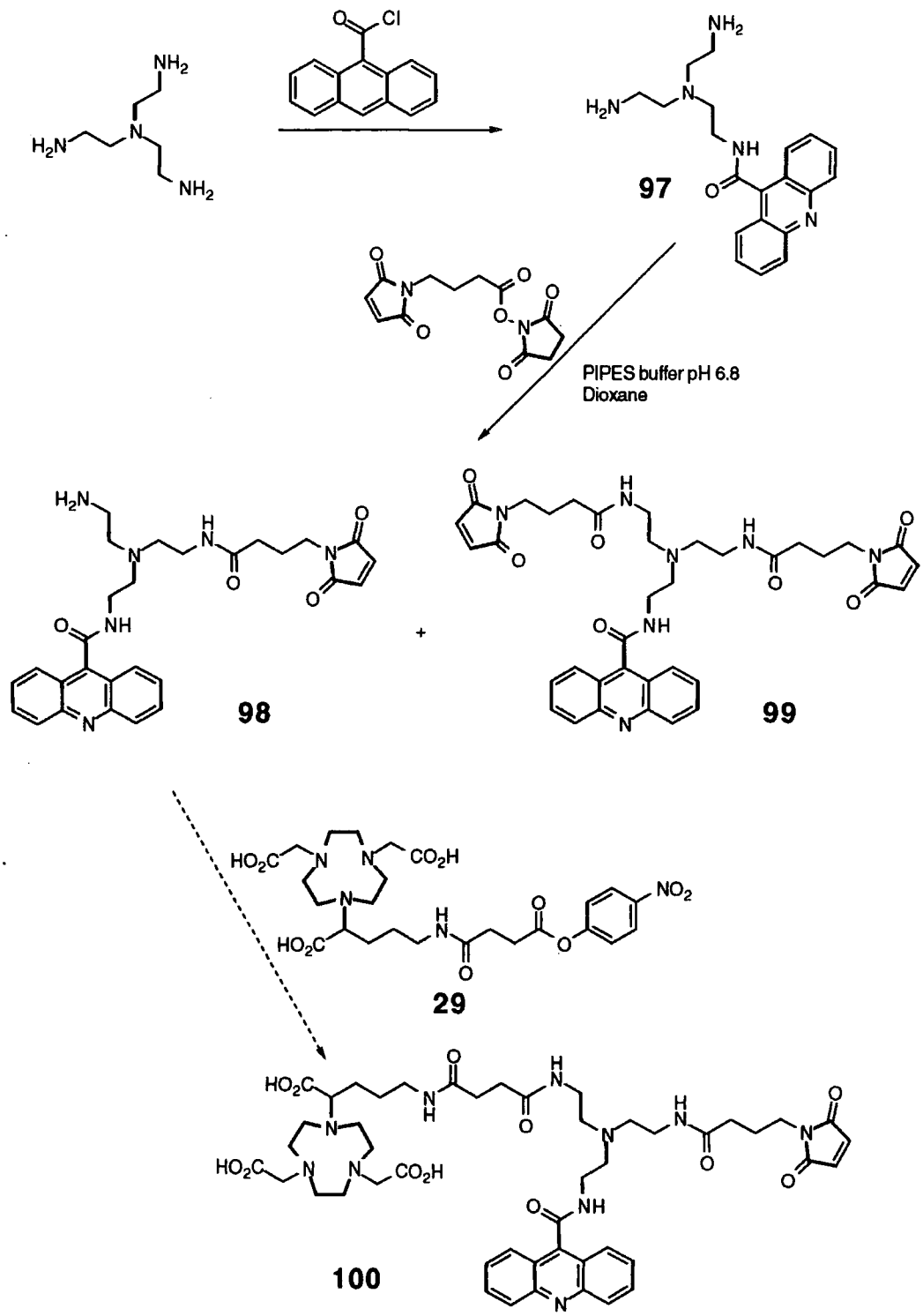

Figure 4.13. The synthesis of **98** and **99**, precursors to trifunctional complexing agents such as **100**.

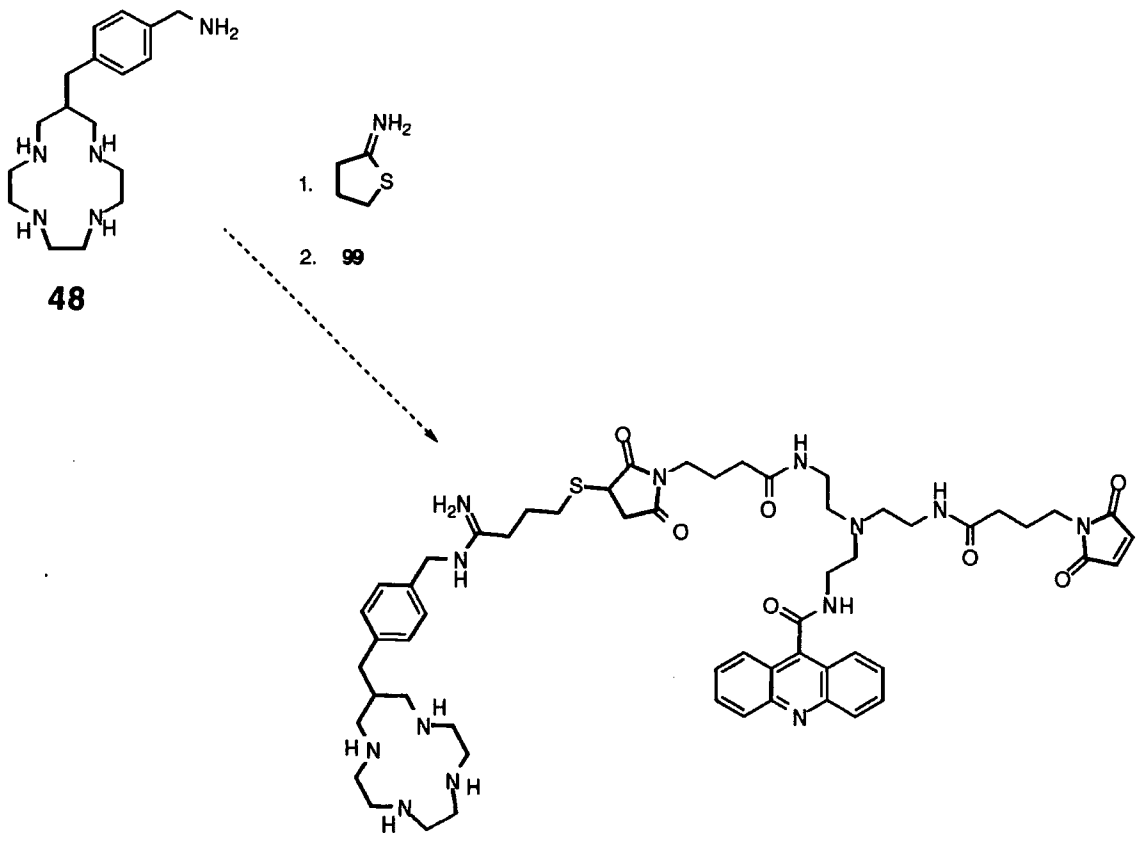

4.3. Radiolabelling

The radiolabelling of the parent ligands **21**, **23** and **57** was investigated using carrier added copper-64. This nuclide was prepared from a natural abundance copper foil, using the reaction $^{63,65}Cu$ (n, γ) $^{64,66}Cu$. The copper-66 produced decays rapidly ($t_{1/2}$= 5.1 minutes). The complexation reactions were performed in a 0.2 mol dm^{-3} ammonium acetate buffer pH=5.5, at 25°C, with equimolar amounts of copper and ligand. The reactions went to completion within 20 minutes. The optimum radiolabelling yields, determined by HPLC after challenging the complex with EDTA, are tabulated below (table 4.1.).

	Radiolabelling Yield / %	
Ligand	20 mins	60 mins
21	100	100
23	100	100
57	60	60

Table 4.1. Radiolabelling of parent ligands with ^{64}Cu.

The radiolabelling of **21** and **23** is very good. The 60% labelling shown by the monoamide ligand **57** is a little disappointing, as it would be expected that the anionic

ligand would electrostatically attract the cationic copper ions. The EDTA challenging step could result in some trans complexation, but the radiolabelling was not affected when a greater excess of EDTA was added. At the no carrier added concentration, it would be expected that a higher labelling yield would be obtained, as there would be an excess of ligand over copper.

4.4. Conjugation to Antibody

There are two distinct methods for attaching the complex to the antibody.[5] In the post-labelling approach the ligand is attached to the antibody, and then the conjugate is radiolabelled. The pre-labelled strategy involves the formation of the copper complex, followed by attachment of the complex to the antibody. The post-labelling method is clearly more efficient for short lived radionuclides, but the labelling conditions used for some metals, in particular the reductive methods used with technetium-99m, may be incompatible with the vulnerable protein. Also, the post-labelling strategy can result in a large amount of non-specific binding to certain amino acid sequences on the protein, which may dissociate *in vivo* leading to loss of the radionuclide. This is minimised for copper by labelling under mildly acidic conditions (pH 4-5.5).[2] The pre-labelling approach has the advantages that the protein is not subject to the labelling conditions, and, if the complex is purified before conjugation, does not result in non-specific binding.

The approach employed in this work depended on the particular conjugate. In all cases carrier free copper-64 was used. The maleimide ligands **91** and **92** were pre-labelled. The complexes were made by incubating the ligand with the $^{64}CuCl_2$ solution for 30 minutes at pH 6, 25°C. Any free $^{64}Cu^{2+}$ ions were then sequestered by the addition of DTPA. Analysis by TLC indicated 60-80% labelling for both conjugates. The mixture of the maleimide complex and the DTPA complex were added to a solution of ICR-12 (1 mg ml^{-1}) followed by the addition of 2-iminothiolane.[6] The reaction mixture was incubated at 37°C for 1 hour, with periodic mixing. In contrast, the NOTA derived ligand **29** was conjugated to the protein, by incubation at 37°C. The excess ligand was removed by the use of a gel filtration column (PD10). The copper solution was then added and the mixture incubated for 1 hour at 37°C, before adding EDTA. All three conjugates were then purified by chromatography on pre-packed PD10 columns.

4.5. Immunoreactivity

It is important to monitor the effect of introducing the unnatural prosthetic groups to the antibody. Ideally, the labelled antibody will show a similar affinity for the antigen binding site as the untreated antibody. In practice this is seldom achieved, but usually

most of the activity is retained. The *immunoreactivity* of the conjugate is a measure of retained binding capability. For example, if three-quarters of the modified protein still binds, the conjugate is said to have an immunoreactivity of 75%.

The measurement is made *in vitro*, and thus provides information solely on the relative ability of the modified protein to bind with the receptor. No indication is gained about the stability of the conjugate in the presence of the broad spectrum of enzymes, which will attempt to metabolise the conjugate.

The determination of the immunoreactivity is made with nanogrammes of antibody, and so a sensitive method of detection is required. Colorimetric methods are often used to determine such low concentrations of analytes, but here radionuclides were employed. Two simple protocols can be envisaged for determining the amount of protein bound. As the conjugates to be evaluated are radiolabelled, a simple measure of the amount of radioactivity bound to the antigen can be made. Alternatively, the ability of the conjugate to block the binding of another radiolabelled conjugate, which is known to have a high specificity for the antigen, can be measured. The method used for determining the immunoreactivity of the three conjugates is based on the method developed by Lindmo.[7]

The antigen was coupled to sepharose beads by Dr Christopher Dean. The absolute amount of antigen is not known, but by measuring the binding at several concentration ratios, the amount of binding at infinite antigen concentration can be determined graphically by extrapolation. Each conjugate (~2ng) was added to Eppendorf tubes containing 1, 2 and 3 units of antigen coated beads. The Eppendorf's were gently rotated at 4°C for 4 hours. The tubes were centrifuged and the supernatant removed. The pellet was washed and recentrifuged. The pellets, supernatants and washes were all counted in a γ-counter, enabling the amount of radioactivity bound to be determined.

A double inverse plot of $(\text{activity bound})^{-1}$ against $(\text{antigen units})^{-1}$ gives a straight line. Extrapolation to $(\text{antigen units})^{-1} = 0$ (i.e. the y-axis) gives the $(\text{activity bound})^{-1}$ at infinite antigen concentration. Thus, simply taking the reciprocal of the intercept on the y-axis gives the immunoreactivity. The graph below (figure 4.15.) illustrates the type of plot obtained.

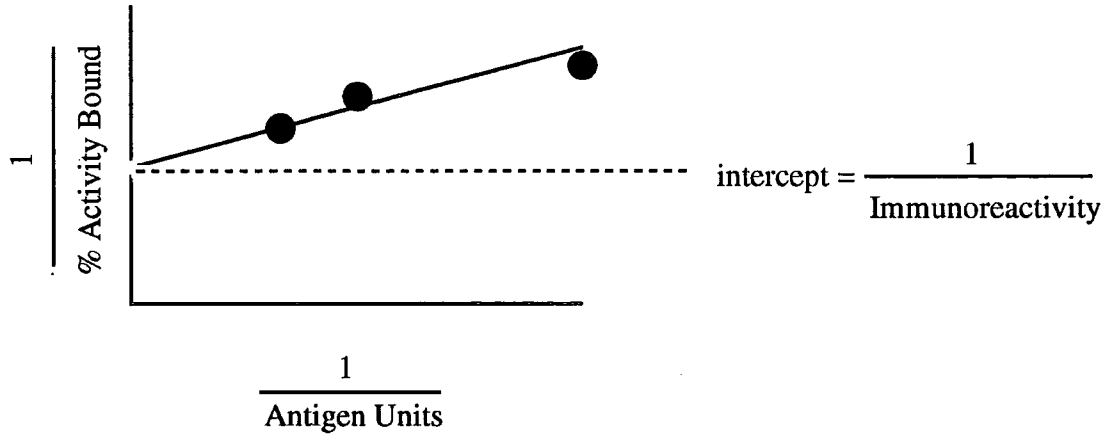

Figure 4.15. A Lindmo plot for the determination of immunoreactivity.

The immunoreactivities obtained by this method are tabulated below (table 4.2.). The data obtained showed some scatter as indicated by the rather poor correlation.

Conjugate	Immunoreactivity	Correlation
^{64}Cu-**91**-ICR12	79	0.84
^{64}Cu-**92**-ICR12	40	0.70
^{64}Cu-**29**-ICR12	15	0.83

Table 4.2. The immunoreactivities of conjugates.

The values indicate that *some* specificity has been retained by all three conjugates. The amount of antigen on the beads is very much lower than the amount of antigen present on tumour cells. It is, therefore, possible that more of the ^{64}Cu-**29**-ICR12 conjugate may become bound in the presence of a higher concentration of antigen found in a real tumour.

4.6. *In Vivo* Evaluation

The biodistribution profiles of the three conjugates were determined in nude mice, bearing bilateral MDA MB 361 tumours. The tumours were initiated by Dr Suzanne Eccles from trocar fragments. Each mouse received two fragments, located at the midpoint of each flank. The tumours were allowed to mature for three weeks. At this time all mice exhibited at least one good tumour, i.e. one with a visible increase in size and an indication of the formation of blood vessels. The conjugates were administered, by Dr Suzanne Eccles, to fifteen mice whilst under anaesthetic (halothane). Six mice received the ^{64}Cu-**91**-ICR12 conjugate, six received the ^{64}Cu-**92**-ICR12 conjugate and three received the ^{64}Cu-**29**-ICR12 conjugate. Three mice from each of the ^{64}Cu-**91**-ICR12 and ^{64}Cu-**92**-ICR12 groups were sacrificed at 5 hours, by cervical dislocation. The remaining nine were killed at 24 hours. Organs of interest were removed by

dissection, weighed and the radioactivity measured in a γ-counter. The amount of radioactivity in the tissues are tabulated below (table 4.3.), expressed as the percentage injected activity per gram of tissue.

	%injected activity g^{-1}				
	^{64}Cu-**91**-ICR12		^{64}Cu-**92**-ICR12		^{64}Cu-**29**-ICR12
	5 hours	24 hours	5 hours	24 hours	24 hours
Blood	2.07±0.94	2.18±0.56	1.22±0.06	0.98±0.21	1.40±0.21
Kidney	5.65±0.14	5.46±0.29	3.43±0.22	2.43±0.29	4.86±0.15
Heart	3.30±0.02	3.31±0.57	1.89±0.07	1.83±0.40	3.85±0.87
Spleen	6.32±0.60	4.78±1.11	2.71±0.58	2.16±0.69	4.63±1.34
Liver	11.8±1.61	9.37±1.81	5.10±0.70	3.57±0.35	7.20±0.69
Lungs	38.0±6.92	19.9±4.36	8.70±3.28	6.44±2.76	5.39±0.57
Tumour	6.08±2.85	3.45±1.31	2.68±0.79	2.58±0.37	12.9±6.02
Intestines	5.60±1.90	3.23±0.41	2.62±0.34	1.82±0.15	3.27±0.13

Table 4.3. The biodistribution profile of three radiolabelled ICR12 conjugates.

The data show a rapid clearance from the blood in the first five hours, followed by a much slower clearance phase. Whilst the low blood background level of radioactivity is desirable, it suggests that the conjugates were not as pure as believed, indicative of some low molecular weight free complex or antibody fragments. A figure of ~10%i.d. g^{-1} would be more consistent with other results. The very high uptake in the lungs with the ^{64}Cu-**91**-ICR12 group suggests that some particulates may be present in the sample, and that the conjugate is being mechanically trapped in the first capillary bed encountered. The nature of a colloidal species is not known, but the aggregation of proteins is clearly possible. The high uptake in the liver compared to the blood suggests some denaturation of the protein has occurred, consistent with the observed loss of some immunoreactivity. (Ideally the liver uptake should be about one third of the blood, as approximately 30% of the the liver's weight is blood.)

The tumour uptake is quite high, particularly when the rapid clearance of most activity is taken into consideration. The tumour to blood ratios are very encouraging. At 24 hours the ratios are 1.6:1, 2.6:1 and 9.2:1 for the three conjugates, which compare favourably with the tumour:blood ratio of 1.2:1 obtained in the biodistribution of the same antibody labelled with iodine-124.[1] However, the iodinated antibody shows little sign of protein damage, with a very low amount of activity in the liver, blood:liver ratio ~4:1. The longer half-life (100 hours) of ^{124}I permits the study over a longer time period. At five days the tumour:blood ratio had risen to 2:1

4.7. Conclusions

The high tumour to blood ratio obtained with the conjugates are promising. However, further work is required to ensure more of the conjugate stays in the circulation for longer. In particular an improved purification procedure is desirable. The use of a chromatographical separation by the use of an HPLC gel filtration column would result in a reduction of protein aggregates, and perhaps also reduce the breakthrough of any low molecular weight fragments.

4.8. References

1. M.A. Bakir, S.A. Eccles, J.W. Babich, N. Aftab, J.M. Styles, C.J. Dean and R.J. Ott, *J. Nucl. Med.* 1992, **33**, 2154
2. J. R. Morphy, D. Parker, R. Kataky, M.A.W. Eaton, A.T. Millican, R. Alexander, A. Harrison and C. Walker, *J. Chem. Soc., Perkin Trans. 2*, 1990, 573
3. J.P.L. Cox, A.S.Craig, I. M. Helps, K.J. Jankowski, D. Parker, M.A.W. Eaton, A. T. Millican, K. Millar, N.R.A. Beeley and B.A. Boyce, *J. Chem. Soc., Perkin Trans. 1*, 1990, 2567
4. T.J. Norman, D. Parker, F.C. Smith and D.J. King, *Chem. Commun.*, 1995, 1879
5. D. Parker in *Comprehensive Supramolecular Chemistry,* ed. D.N. Reinhoudt, Pergamon, Oxford, 1996, vol. 10, 487
6. M.J. McCall, H. Diril and C.F. Meares, *Bioconjugate Chem.,* 1990, **1**, 222
7. T. Lindmo, E. Boven, F. Cuttitta, J. Fedorko and P. A. Bunn, *J. Immunol. Methods*, 1984, **72**, 77

Chapter Five

Synthetic Procedures

5. Synthetic Procedures

The methods and instrumentation employed for the purification and characterisation of compounds are detailed. (5.1.) The synthetic procedure used for each compound synthesised (5.2.) is reported, in order of appearance in the text of chapters two to four.

5.1. Instrumentation and Chemicals

Chromatography

Column chromatography was carried out using either neutral alumina (Merck Art 1077), which had previously been treated with ethyl acetate, or "gravity" silica (Merck Art 7734) using the eluent specified. R_f values refer to either alumina TLC (Merck Art 5550) or silica gel TLC (Merck Art 5554.) HPLC analyses were performed on a Varian 9010 / 9065 Polychrom system using either reverse phase, anion exchange or cation exchange column with a flow rate of 1.4ml min^{-1}. Semi-preparative HPLC was achieved using either the above system or a Varian Vista 5500 / 9050 system equipped with a reverse phase or anion exchange column, operating at a flow rate of 5.0ml min^{-1}. A larger reverse phase column, operating at 10ml min^{-1}, was also employed on the Vista. "TFA" refers to 0.1% trifluoroacetic acid added to the solvent. The specific solvent system used for each purification is stated individually.

Spectroscopy

Several spectrometers were used for acquiring NMR spectra. ^{1}H NMR were recorded on either a Brüker AC250, Varian Gemini-200, XL-200, VXR-200 or VXR-400. ^{13}C NMR were obtained on the Gemini, and ^{31}P NMR on the Brüker. Variable temperature NMR spectra were obtained on a Brüker AMX500. The NMR solvent used is stated in brackets, followed by the chemical shifts, in parts per million, to high frequency of TMS for ^{1}H and ^{13}C or H_3PO_4 / H_2O for ^{31}P NMR. Peaks are referenced to known solvent peaks, except for phosphorus spectra, which are referenced externally to 85% phosphoric acid. Coupling constants are given in Hertz. For spectra acquired in deuterated water, an approximate acidity is given.

Infra-red spectra were recorded with a Perkin-Elmer 1600 FTIR spectrometer. Samples were prepared either as a KBr disc or as a thin film on NaCl plates. Frequencies are quoted in cm^{-1}.

Ultra-violet / visible spectra were obtained on either a Kontron Instruments Uvikon 930 or Unicam UV2. Absorption maxima are quoted in nanometres.

Luminescence measurements were made with a Perkin-Elmer LS50B spectrometer, in both protiated and perdeuteriated solvents. Lifetimes and quantum yields of luminescent complexes were determined by monitoring the decay in phosphorescence after excitation at 277nm. The number of bound water molecules (q) was estimated according to the method of Horrocks.[1]

Mass spectra were recorded with a VG 7070E spectrometer, operating in CI, DCI or FAB modes, with DCI samples presented as dilute methanol or dichloromethane solutions, ammonia being used as the impingent gas. A glycerol matrix was used for the FAB spectra. A VG Platform electrospray mass spectrometer was also used, both in negative and positive modes. Typically, samples were analaysed with a cone voltage of 110 volts, presented as aqueous methanol or acetonitrile solutions (~10^{-5}mol dm^{-3}).

Analysis

Elemental analyses were determined on a Carlo ERBA 1106.

Melting points were determined on a Reichert Köfler Block and are uncorrected.

Reagents and Solvents

Reagents were used as received, unless otherwise stated. Solvents were dried from an appropiate drying agent: methanol and ethanol from the corresponding magnesium alkoxide, dichloromethane and acetonitrile from calcium hydride, chloroform from phosphorus pentoxide, pyridine from potassium hydroxide, tetrahydrofuran from potassium, and ether from sodium. Benzophenone was used as an indicator when drying ethereal solvents. Dimethylformamide and dimethylsulfoxide were used directly from "sure-seal" bottles, and water was purified by the "Purite" system.

5.2 Syntheses

The characterisation of compounds is reported, after the synthetic procedure, in the order chromatography, NMR data, IR data, UV/visible spectra, luminescence data, mass spectra, elemental analysis and melting point.

N,N''-bis(tertiarybutylcarbamoylmethyl) diethylenetriamine-N,N',N''-triacetic acid **31**

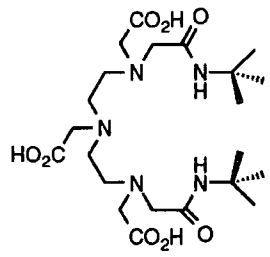

To a stirred solution of diethylenetriamine pentaacetic acid dianhydride (DTPAA, **25**) (357mg, 1mmol) in pyridine (5ml) was added tertiary butylamine (315μL, 219mg, 3mmol) and N,N-dimethylamino-pyridine (DMAP, 5mg.) The solution was heated to 50°C and stirring continued for 36 hours, under argon. The reaction mixture was then cooled and the pyridine removed under reduced pressure. Water (1ml) was added and the pH lowered to 2 (HCl). Ethanol was added and the precipitated DTPA filtered off. The remaining solution was basified (pH=13) with 1.0 mol dm^{-3} NH_4OH and washed with chloroform (10ml). Concentration afforded the triammonium salt as a white solid. (123mg, 24%)

^1H NMR(D_2O, pD ~7) 1.20(18H, s, Me), 3.06(4H, br t, $NC\underline{H}_2CH_2N$), 3.37(4H, br t, $NCH_2C\underline{H}_2N$), 3.49(2H, s, NCH_2CO), 3.91(4H, s, NCH_2CO), 3.92(4H, s, NCH_2CO) ^{13}C NMR (D_2O) 27.6(CH_3), 49.3, 53.6, 55.2, 56.5(CH_2N), 164.2 & 169.4(2C+2C, CONH+CO_2^-), 173.4(1C, CO_2^-) IR(KBr disc) 3246 (v br), 3066, 1733 (acetate), 1677 (amide), 1567, 1457, 1406, 1222 MS(ES-) 502.59 (M-1) ($C_{22}H_{41}N_5O_8$ requires 502.29) A satisfactory elemental analysis could not be obtained m.p. 163-170°C

N,N''-bis(isobutylcarbamoylmethyl) diethylenetriamine-N,N',N''-triacetic acid **32**

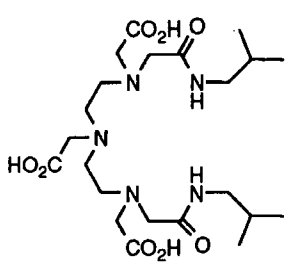

The reaction was carried out as above. DTPAA **25** (227mg, 0.636mmol) was reacted with isobutylamine (189μL, 139mg, 1.91mmol) for 24 hours, to give a white solid ammonium salt. (215mg, 61.0%)

^{1}H NMR(D_2O, pD ~7) 0.86(12H, d (J=6.6Hz), Me), 1.78(2H, m, CH_2CHMe_2), 3.04(4H, d (J=6.7Hz), NCH_2CH), 3.20(8H, s br, CH_2N (backbone)), 3.55(4H, s, NCH_2CO), 3.67(2H, NCH_2CO_2H), 3.73(4H, s, NCH_2CO) ^{13}C NMR (D_2O) 19.3(CH_3), 27.7(CH), 46.6, 51.1, 51.6, 57.3, 57.5, 57.5(CH_2N), 169.7(2C), 171.9(1C, CO_2^-), 174.4(2C) IR(KBr disc) 3154 (br), 2963, 1634, 1401 MS(ES-) 502.53 (M-1) ($C_{22}H_{41}N_5O_8$ requires 502.29) Found C=46.65 H=8.48 N=15.16 $C_{22}H_{41}N_5O_8.NH_3.2.5H_2O$ requires C=46.71 H=8.73 N=14.86 m.p. 96-98°C

N-(3,5-bistrifluoromethylbenzylcarbamoylmethyl) diethylenetriamine-N,N',N'',N''-tetraacetic acid **33**

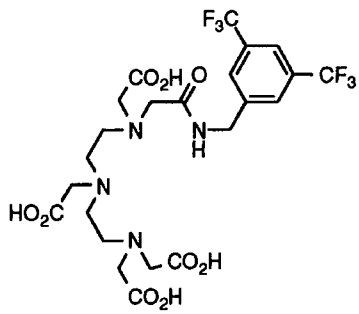

DTPAA **25** (71mg, 0.198mmol) and 3,5-bistrifluoromethylbenzylamine (106mg, 0.436mmol, 2.2 equiv.) were stirred in pyridine (5ml). DMAP (2mg) was then added, and the temperature of the solution raised to 60°C Stirring was continued for a further 18 hours. Preparative HPLC afforded the trifluoroacetate salt. (23mg, 19%).

HPLC: Dynamax 60A (10ml min^{-1}); elution A=MeCN/TFA; B=H_2O/TFA; from 10% A, 90% B, to 75% A, 25% B in 20 minutes λ=254nm R_t=15.3 minutes ^{1}H NMR(D_2O, pD ~4) 3.12(8H, m, CH_2N (backbone)), 3.41(4H, s, NCH_2CO+NCH_2CO_2H), 3.68(4H, s, NCH_2CO_2H), 3.71(2H, s, NCH_2CO_2H) 4.42(2H, s, benzylic), 7.72(2H, s, ArH), 7.85(1H, s, ArH) ^{19}F NMR(D_2O) -63.1 IR(film) 3196, 3072, 1669 (with shoulder to low frequency), 1401, 1282, 1203, 1183, 1132 MS(ES-) 617.46 (M-1) ($C_{23}H_{27}N_4O_9F_6$ requires 617.17)

N,N''-bis(3,5-bistrifluoromethylbenzylcarbamoylmethyl) diethylenetriamine-N,N',N''-triacetic acid **34**

The reaction was performed as above, using DTPAA **25** (310mg, 0.86mmol) and 3 equivalents of 3,5-bis-trifluoromethylbenzylamine (633mg, 2.61mmol). HPLC afforded a flocculent white hygroscopic solid (141mg, 19%).

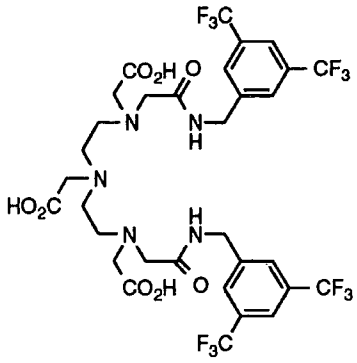

HPLC: Dynamax 60A (10ml min^{-1}); elution A=MeCN/TFA; B=H_2O/TFA; from 10% A, 90% B, to 75% A, 25% B in 20 minutes λ=254nm R_t=19.8 minutes ^1H NMR(CD_3OD) 3.23 & 3.48(4H+4H, 2xbr s, CH_2N (backbone)), 3.61 & 3.65(4H+4H, 2x s, NCH_2CO+$NC\underline{H}_2CO_2H$), 4.22(2H, s, $NC\underline{H}_2CO_2H$), 4.51(4H, s, benzylic), 7.80(2H, s, ArH), 7.84(4H, s, ArH), ^{13}C NMR (CD_3OD) 43.2, 51.0, 54.5, 56.1, 58.0(CH_2N), 122.0(2C), 124.8 (q, J_{CF}=270Hz, CF_3), 129.1(4C), 132.8 (q, J_{CCF}=33Hz, CCF_3), 143.3(quaternary carbon), 169.3(1C, CO_2^-), 173.6 & 174.2(2C+2C, CONH+CO_2^-) ^{19}F NMR(CD_3OD) -63.2 IR(film) 3292, 2936, 1668, 1552, 1390, 1286, 1178, 1136 MS(ES-) 842.35 $(M-1)^+$($C_{32}H_{32}N_5O_8F_{12}$ requires 842.21) a reliable melting point could not be determined because of the hygroscopic nature of the ligand.

3-methoxybenzylmagnesiumchloride

3-Methoxybenzylchloride (6.42g, 41mmol) was added to a stirred suspension of magnesium (2g, excess) in THF (40ml), with a crystal of iodine. After an incubation period a vigorous reaction commenced. The reaction was stirred for 1 hour, and boiled gently due to the exothermic reaction. The quality of the Grignard reagent was assessed by quenching a sample in D_2O. NMR intensities show almost quantitative conversion. The reaction was found to proceed equally well in dry ether. Integration of the two singlets to low frequency of the isotopically labelled 3-methoxy-[^2H]-toluene indicated near quantitative conversion.

^1H NMR 2.9(2H, s, CH_2D), 3.8 (3H, s, OMe), 6.7-7.4 (4H, m, ArH)

(3-methoxybenzyl)diethoxyphosphine **42**

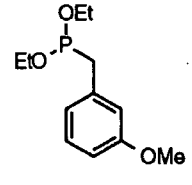

An ethereal solution of the Grignard reagent, prepared above (ca. 24mmol) was filtered, *via* a steel cannula, to remove unreacted magnesium. Diethyl chlorophosphite (3.6ml, 3.88g, 24mmol) was added at a temperature of -20°C. The product was not isolated in a pure form as the compound exhibits a propensity to decompose when distilled. A 72% conversion was estimated from NMR analysis of ^{31}P intensities, by comparison of the product's resonance, with that of the oxidised material (δ_P=26ppm).

^1H NMR ($CDCl_3$) 1.23 (6H, t, CH_3), 2.95 (2H, d (J=3.9Hz), CH_2P), 3.81 (3H, s, OMe), 3.89 (4H, qd (J=1.4Hz), OCH_2), 6.8 (3H, m, ArH), 7.2 (1H, t, ArH) ^{13}C NMR 16.9(CH_3), 42.7 (d (J_{CP} ~80Hz), Ar$\underline{C}H_2$) 54.8(OCH_3), 62.9(d (J_{COP}=21Hz), OCH_2), 111.2, 112.4 , 114.8, 121.8, 130.0(Ar), 159($\underline{C}$OMe) ^{31}P NMR ($CDCl_3$) 176.8 (s) IR (film) 2974,1600, 1490, 1198, 1163 MS (DCI) 243 (M^++1)

Tetraethyl-1,4,7,10-tetrakis(methylenetetra(3-methoxybenzylphosphinate))-1,4,7,10-tetraazacyclododecane **43**

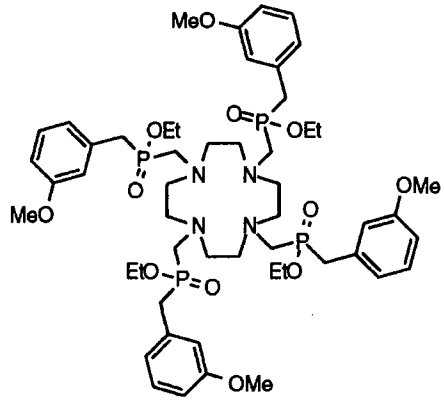

To a stirred solution of 1,4,7,10-tetraazacyclododecane **41** (475mg, 2.76mmol) and paraformaldehyde (414mg, 13.8mmol), boiling under reflux, over 4Å molecular sieves, in THF, under an argon atmosphere, was added crude (3-methoxybenzyl)diethoxyphosphine **42** (assumed to be 80% pure, 13.8mmol.) An orange precipitate was formed almost immediately, and the remaining solution became orange and turbid. The reaction mixture was allowed to cool after 6 hours, and solvent was removed under reduced pressure. Column chromatography (alumina EtOH:CH_2Cl_2 gradient elution from 0-5% ethanol) of the residue afforded the ester as a pale yellow glass. (528mg, 18%)

TLC (5% EtOH:CH_2Cl_2) R_f=0.4 HPLC: Spherisorb 5ODS2 (1.4ml min^{-1}); elution A=MeCN/TFA; B=H_2O/TFA from 5% A, 95% B to 95% A, 5% B over 30 minutes; observed λ=278nm; R_t=24.8minutes (Very broad); ^1H NMR ($CDCl_3$) 1.15(12H, t, CH_3), 2.8(24H, m, CH_2N), ~3.2(8H, m, ArCH_2P), 3.75(12H, s, OMe), 3.8-4.2(8H, m, OCH_2), 6.84(12H, m, ArH), 7.17(4H, t, ArH) ^{13}C NMR ($CDCl_3$) 16.5(CH_3), 35.8(d (J_{CP}=81Hz),

Ar$\underline{C}H_2P$), 52.6(d (J_{CP}=107Hz), PCH_2N), 53.5(CH_2N), 55.1(OCH_3), 60.8(OCH_2), 112.1, 115.5, 122.2, 129.4(Ar), 132.9(quaternary Ar), 159.5($\underline{C}$OMe) ^{31}P NMR ($CDCl_3$) 49.3 IR(film) 2980, 2835, 1663,1600, 1498, 1452, 1298, 1268, 1213, 1151 MS(CI) 1077(M^++1), 215 (100%) MS(FAB, NOBA) 1077(M^++1) 1099(M^++Na) MS(FAB, PEG) found 1077.4801 $C_{52}H_{81}N_4O_{12}P_4$ requires 1077.4801

1,4,7,10-tetrakis(methylenetetra(3-methoxybenzylphosphinic acid))-1,4,7,10-tetraazacyclododecane **36**

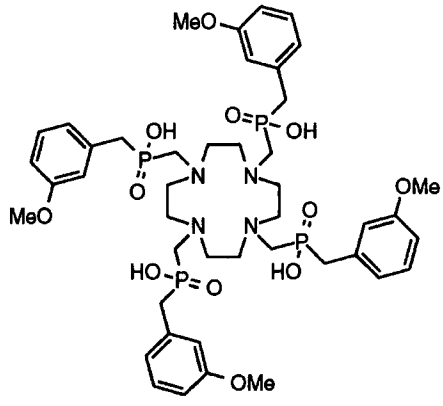

The ester **43** was hydrolysed with potassium hydroxide solution (1mol dm^{-3}), and the potassium salt was used to form lanthanide complexes without isolating the tetraphosphinic acid **36**. A small amount of the 3-methoxy substituted ligand was purified by HPLC for the purpose of characterisation.

HPLC: Synchropak AX100 (5ml min^{-1}); elution A=MeCN; B=H_2O; C=NH_4OAc pH=5.6 from 20% A, 70% B, 10% C to 20% A, 0% B, 80% C in 20 minutes R_t=13.1 minutes ^1H NMR(D_2O, pD ~6) 2.8-3.2(32H, m (maxima at 2.82, 2.91, 3.09), CH_2N+$ArCH_2$), 3.65(12H, s, OMe), 6.76(12H, br s, ArH), 7.16(4H, t, ArH) ^{13}C NMR (D_2O) 41.2 (d (J_{CP}=87Hz), Ar$\underline{C}H_2P$), 54.1 (CH_2N ring), 54.1 (d (J_{CP}=93Hz), NCH_2P), 58.1(OMe), 115.1($^4J_{CP}$=2.8Hz), 118.2($^3J_{CP}$=5.4Hz), 125.5($^3J_{CP}$=5.3Hz), 132.8($^5J_{CP}$=2.6Hz), 137.7($^2J_{CP}$=8.0Hz), 161.8($^4J_{CP}$=2.8Hz) ^{31}P NMR (D_2O) 31.9 (br) IR(film) 3326(br), 1682, 1595, 1486, 1448, 1266, 1164, 1039 MS(ES-) 1016.4(100%) (M^++52) 507.9(100%) $(M+52)^{2+}$

1,4,7,10-tetraazacyclotridecane-1,4,7,10-tetraacetic acid [2] **44**

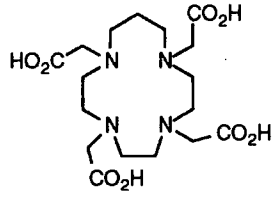

1,4,7,10-tetraazacyclotridecane **21** (183mg, 0.984mmol) prepared by J.R.Morphy was stirred in water (15ml). Chloroacetic acid (560mg, 6 equiv.) was then added and the pH modified to 10 using lithium hydroxide. The mixture was stirred at 80°C for 18 hours. The reaction was then acidified and concentrated. The product was recrystallised from ethanol to give a white solid (174mg, 42%)

^{1}H NMR(D_2O, pD ~3) 2.07(2H, p, CH_2), 3.3(16H, m, CH_2N), 3.83(8H, br s, NCH_2CO) m.p. 160-165°C (dec.) (lit.[3] 185°C)

Lanthanide Complexes

[La(**31**)]

The complex of the tertiarybutylamine derived ligand **31** was prepared in the same manner as for the isobutylamine complex [La(**32**)], but, during the reaction, the complex precipitated out, as a white solid. The ligand **31** (66mg, 131μmol) was reacted with lanthanum acetate (42mg, 131μmol). The complex (54mg, 64%) was found to be soluble in dilute hydrochloric acid (0.1mol dm^{-3}).

^{1}H NMR(D_2O, pD ~1) 1.11(18H, s, CH_3), 3.08(4H, br t, CH_2N), 3.43(4H, br t, CH_2N), 3.54(2H, s, NCH_2CO), 3.97(4H, s, NCH_2CO), 4.11(4H, s, NCH_2CO) ^{13}C NMR (D_2O) 30.2(CH_3), 51.7, 54.7, 56.0, 56.3, 58.0, 59.3(CH_2N), 166.2, 170.9, 176.2(CO) IR(KBr disc) 3100 (v br), 1740, 1636 (br), 1402, 1250 MS(ES+) 320.8 (100%) $(M+2)^{2+}$, 639.88 (55%) $(M+1)^+$ ($C_{22}H_{39}N_5O_8$ requires 640.19), 640.7 (90%) $(M+2)^+$ A satisfactory elemental analysis was not obtained m.p. >250°C

[La(**32**)]

A solution of ligand **32** (26mg, 52μmol) and lanthanum acetate (16mg, 52μmol) was stirred at 80°C for 16 hours, pH=6. The solvent was removed, and the complex purified by chromatography on alumina (25% MeOH:CH_2Cl_2) to give a white solid. (9mg, 27%)

TLC(10%MeOH:CH_2Cl_2) R_f=0.9 ^{1}H NMR(D_2O, pD ~7) 0.74(12H, d, CH_3), 1.6(2H, m, CH), 2.2-3.7(22H, br m, CH_2N) ^{13}C NMR(D_2O) 17.4(CH_3), 25.7 & 25.9(CH+CH), 45.2, 45.6, 54.0, 55.3, 58.6, 60.1, 60.5(CH_2N), 172.6, 173.3, 177.9, 178.0, 178.7(CO) IR(KBr disc) 3416, 3250, 3092, 2960, 1620 (br), 1403, 1331, 1257, 1159, 1098 MS(ES+) 640.61 $(M+1)^+$ ($C_{22}H_{39}N_5O_8La$ requires 640.19) A satisfactory analysis could not be obtained m.p. 205-210°C (dec.)

[La(**34**)]

The fluorinated ligand **34** (33mg, 38.9μmol) was taken up in methanol (0.5ml) and water (5ml). Lanthanum acetate (12.3mg, 1 equiv.) was then added, and the reaction mixture was stirred at 80°C for 16 hours. The complex (7mg, 17%) was isolated by preparative HPLC.

HPLC: Dynamax 60A (10ml min^{-1}); elution A=MeCN; B=H_2O; from 10% A, 90% B, to 75% A, 25% B in 20 minutes λ=254nm R_t=18.8 minutes ^1H NMR(CD_3OD) 2.3-3.7(18H, m (symmetry of ligand lowered by complexation), CH_2N), 4.7(4H, m, benzylic), 7.95(6H, s, ArH) ^{19}F NMR(CD_3OD) -63.3 (s) IR(film) 2932, 1624, 1394, 1282, 1178, 1132 MS(ES+) 1019.45 (M+K+1)($C_{32}H_{31}N_5O_8F_{12}KLa$ requires 1019.06) m.p. >250°C

[Eu(**34**)]

The europium complex was made by the same method as the lanthanum complex above, on a 21.9μmolar scale. The reaction was left stirring at 80°C for 36 hours. The complex was purified by HPLC, to give a white solid. (7mg, 32% yield)

HPLC: Dynamax 60A (10ml min^{-1}); elution A=MeCN; B=H_2O; from 10% A, 90% B, to 75% A, 25% B in 20 minutes λ=254nm R_t=18.8 minutes ^1H NMR(CD_3OD) -14.0, -13.7, -7.6, -6.8, -6.1, -3.9, 1.0, 2.5, 5.4, 7.0, 8.4, 9.1, 9.8, 10.2, 11.3, 11.4, 12.0, 22.6, 25.4, 30.9 ^{19}F NMR(CD_3OD) -60.3 (6F, s), -61.1 (6F, s) IR(film) 3405 (br), 2926, 1615, 1381, 1280, 1176, 1131 MS(ES+) 1014, 1015, 1016.52 (M+Na), 1018, 1019 ($C_{32}H_{30}N_5O_8F_{12}NaEu$ requires 1016.10) m.p. 210-215°C (dec.)

[La(**18**)]$^-$

The ligand **18** (210mg, 0.256mmol) was dissolved in water (25ml). To this was added lanthanum oxide (41.6mg, 0.5equiv) and the mixture stirred for 8 hours at 80°C. The pH was modified to 6-7 (KOH), and the reaction left to continue for another 3 hours. The reaction mixture was allowed to cool. The complex was recrystallised from water, after filtration, to give colourless crystals which became opaque on losing water of crystallisation *in vacuo*. (201mg, 77%)
^1H NMR(D_2O, pD ~6) 2.01 (4H, d (J=13Hz), CH_2), 2.18 (8H, d (J=13Hz), CH_2), 3.0-3.6 (20H, br m, CH_2), 7.14(4H, br m, ArH), 7.22 (16H, br m, ArH) ^{13}C NMR (D_2O) 41.4 (d (J_{CP}=92Hz), Ar$\underline{C}H_2P$), 54.5, 54.7, 56.7, 58.5 (d (J_{CP}=98Hz), NCH_2P), 129.2, 131.5(Ar), 132.8 (d ($^3J_{CP}$=5Hz), Ar), 136.7 (d ($^2J_{CP}$=8Hz), quaternary Ar) ^{31}P NMR (D_2O) 37.6, 38.8 ratio ≈8:1 IR (KBr disc) 1654, 1601, 1495, 1453, 1233, 1167, 1124, 1026 MS(ES-) 979.24 ($C_{40}H_{52}N_4O_8P_4La$) requires 979.18) An accurate analysis was not obtained for this complex mpt >250 (dec) The crystal structure analysis of this complex is nearing

completion. The preliminary data shows the complex has one water molecule in the inner co-ordination sphere.

[Pr(**18**)]$^-$

The tetrabenzylphosphinic acid ligand **18** (134mg, 0.159mmol) and praesodymium nitrate hexahydrate (69mg, 0.159mmol) were stirred for 18 hours in water (10ml, pH=5) at 80°C. The complex was collected by filtration after concentration, as an off-white solid. (51mg, 31%)

^{1}H NMR(D_2O, pD ~6) -37.1(4H), -3.8(4H), -1.1(4H), 7.8(4H), 8.9(4H), 9.1(8H), 11.1(8H), 11.8(4H), 14.1(4H), 16.9(4H), 32.6(4H) ^{13}C NMR (D_2O) 14.0 (d (J_{CP}~100Hz)), 36.0, 52.3, 53.2, 76.7 (d (J_{CP} ~80Hz), 128.8, 130.7, 132.6, 139.0 ^{31}P NMR (D_2O) 34.2 IR(film) 1656, 1552, 1500, 1456, 1158, 1032 MS(ES-) 980.91 ($C_{40}H_{52}N_4O_8P_4Pr$ requires 981.18) A satisfactory analysis was not obtained m.p. >250°C

[Yb(**18**)]$^-$ [4]

The ligand **18** (95mg, 0.113mmol) and ytterbium oxide (22.2mg, 0.056mmol) were stirred at 80°C for 18 hours. The pH was raised to 6, by addition of hydrochloric acid, and the reaction continued for a further 4 hours. The product, isolated by lyophilisation as a white solid (81mg, 69%), was found to be soluble in weakly basic solution.

^{1}H NMR(D_2O, pD ~11) -68.2 , -35.4 , -28.4, -9.4, -2.8, 2.7(t), 7.4(2H, m), 14.9(2H, m), 18.6(2H, m), 19.7, 33.0(2H) 104.0 ^{31}P NMR (D_2O) -40.7 MS(ES-) 1014.7 ($C_{40}H_{52}N_4O_8P_4Yb$ requires 1014.2) Crystals suitable for X-ray analysis were obtained of this complex. The preliminary data are consistent with the absence of an inner sphere water molecule. This is in accord with the analagous europium, gadolinium and yttrium complexes but not with the larger lanthanum complex.

[La(**36**)]$^-$

The lanthanum complex was prepared in an analagous manner to the europium complex. The ester **42** (508mg, 0.472mmol) was subjected to base hydrolysis, followed by reaction with lanthanum acetate (166mg, 0.524mmol). Preparative HPLC afforded a white solid (130mg, 25%).

HPLC R_t=9.2 minutes ^{1}H NMR(D_2O, pD ~6) 2.14 (4H, d (J=15Hz), CH_2), 2.30 (8H, d (J=12Hz), CH_2), 3.0-3.6 (20H, br m, CH_2), 3.72(12H, s, OMe), 6.8(12H, br m, ArH), 7.21 (4H, t, ArH) ^{31}P NMR (D_2O) 37.5,38.8 ratio ≈8:1 (collapsed to a singlet on heating)

IR(KBr disc) 3135, 3049, 1762, 1601, 1405, 1261, 1163 MS(ES-) 1099.34 ($C_{44}H_{60}N_4O_{12}P_4La$ requires 1099.22) A satisfactory analysis was not obtained m.p. >250°C (dec)

[Tb(**36**)]$^-$

To the crude acid **36** (42.4mg, 43.9μmol) in water (0.5ml, pH=6) was added terbium triacetate (14.8mg, 43.9μmol). Stirring at 80°C for 14 hours, followed by filtration and removal of the solvent under reduced pressure, afforded the complex. (42mg, 86%). A small sample was purified by preparative HPLC for the luminescence measurements.

Synchropak AX100 (1.4ml min-1); elution A=MeCN; B=H_2O; C=NH_4OAc pH=5.6 from 20% A, 70% B, 10% C to 20% A, 0% B, 80% C in 20 minutes R_t=9.7 minutes ^1H NMR(D_2O, pD ~6) -198 (v br), -126 (br), -117 (br), -93, -73 (br), -57, -42 (12H), 35 (v br), 51 (br), 140 (v br), 199 (v br), 290 (v br) ^{31}P NMR (D_2O) 441 (br) IR (KBr disc) 3404, 1600, 1487, 1297, 1268, 1231, 1168, 1119 uv (H_2O) λ_{max}=273, 278 ε=3.6x10^3 M^{-1} cm^{-1} $\tau(H_2O)$= 4.08ms $\tau(D_2O)$=4.42ms ϕ (H_2O) = 0.40, ϕ (D_2O) = 0.46 q=0.08 MS(ES-) 1119.3, 1120.3, 1121.3 ($C_{44}H_{60}N_4O_{12}P_4Tb$ requires 1119.24) m.p. >250°C (dec.)

[Eu(**36**)]$^-$

The europium complex was prepared from the ester **42**, without isolating the intermediate acid **36**. The ester **42** (55mg, 51μmol) was taken up in ethanol (1ml) and water (10ml). A large excess of potassium hydroxide was added (0.5g) and the reaction stirred at 60°C for 3 hours. Phosphorus NMR analysis verified the consumption of the ester **42** and the emergence of the potassium salt of the acid **36**. The pH was modified to 6.5 (HCl) and europium acetate (16.8mg, 51μmol) was added, after filtration. The complexation was stirred for 12 hours at 60°C before concentrating. Preparative anion exchange HPLC gave the complex. (16mg, 28%).

Synchropak AX100 (5ml min^{-1}); elution A=MeCN; B=H_2O; C=NH_4OAc pH=5.6 from 20% A, 70% B, 10% C to 20% A, 0% B, 80% C in 20 minutes R_t=11.9 minutes ^1H NMR(D_2O) -18.0, -11.4, -7.4, -4.8, -1.6, 0.4 (8H, d (collapses to a singlet on {^{31}P})), 5.3 (12H), 8.5 (d), 10.4, 10.6, 14.2, 34.3 ^{31}P NMR (D_2O) 87.2 IR(KBr disc) 3428, 3148, 3058, 1610, 1488, 1406, 1266, 1229, 1165, 1117, 1030 uv (H_2O) λ_{max}=273, 278 ε= 3.8x10^3 M^{-1} cm^{-1} Luminescence $\tau(H_2O)$= 1.26ms $\tau(D_2O)$=2.01ms q= 0.31 MS(ES-) 1111.3, 1113.2 (most abundant ion $C_{44}H_{60}N_4O_{12}P_4Eu$ requires 1113.24), 1114.2 m.p. >250°C (dec.)

[Gd(**36**)]$^-$

The gadolinium complex was prepared in an analagous manner to the europium complex, except that a 3 fold excess of gadolinium acetate was used. The ester **42** (370mg, 343μmol) afforded the complex (34mg, 8.9%) after HPLC purification.

HPLC R_t=13.3 minutes NMR spectra could not be obtained due to the paramagnetic line broadening induced by the gadolinium. IR(KBr disc) 3419, 1654, 1601, 1487, 1405, 1266, 1229, 1167, 1117, 1027 uv (H_2O) λ_{max}=273, 278 MS(ES-) 1115.3, 1116.3, 1117.3, 1118.39 (most abundant ion $C_{44}H_{60}N_4O_{12}P_4Gd$ requires 1118.24), 1119.6, 1120.4, 1121.4 A satisfactory analysis was not obtained m.p. >250°C

[La(TRITA)]$^-$ complex [La(**44**)]$^-$

1,4,7,10-tetraazacyclotridecane-1,4,7,10-tetrayltetraacetic acid **44** (105mg, 0.33mmol) and lanthanum acetate (104mg, 0.33mmol) were stirred in water (15ml) at 80°C for 24 hours pH=4. Concentration afforded the complex as a white solid. (152mg, 83%)

^{1}H NMR(D_2O, pD ~4) 1.7(1H, br m, CH (methylene, axial)), 2.25-2.55(5H, m, CH_2N+CH equatorial), 2.7-3.4(20H, m (maxima at 2.78, 2.88, 2.92, 3.17, 3.26, 3.32), CH_2N) ^{13}C NMR (D_2O) 24.9(CH_2), 58.9, 59.0, 59.1, 61.3, 64.7, 66.7(CH_2N), 183.3(CO) IR(film) 3200-3500 (br), 1592 (br), 1452, 1410, 1342, 1270, 1202, 1144, 1084 MS(ES-) 553.11 ([$C_{17}H_{26}N_4O_8La$]$^-$ requires 553.08) A satisfactory analysis was not obtained m.p. >250°C

5.2.2. Chapter 3

Diethylcyanobenzylmalonate [5] **49**

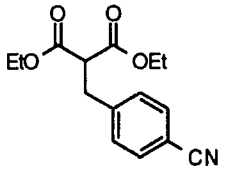

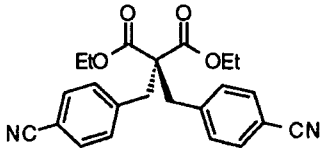

To a stirred solution of sodium ethoxide (2.20g, 28.0mmol) in ethanol (100ml) was added diethylmalonate (8.9g, 55mmol) dissolved in ethanol (50ml), and the system left to equilibriate, stirring at room temperature. Bromobenzylnitrile (5.0g, 25.2mmol) dissolved in DMF (50ml) was then added slowly. Stirring continued at 60°C overnight. The reaction was then quenched by the addition of water (150ml) and some dialkylated product (584mg, 12%) was filtered off as a white solid. The remaining solution was extracted with ether

(400ml). The dried ether extract contained a little unreacted diethylmalonate, which was removed by heating *in vacuo,* to leave a pale yellow glassy oil. (6.2g, 89%)

^{1}H NMR($CDCl_3$) 1.21(6H, t, CH_3), 3.26(2H, d (J=8Hz), benzylic), 3.63(1H, t (J=8Hz), CH) 4.16(4H, qd, CH_2O) 7.32 & 7.58(4H, dd, ArH)

The isolated (584mg, 12%) dialkylated material was also characterised by NMR.

^{1}H NMR($CDCl_3$) 1.12(6H, t, CH_3), 3.24(4H, s, benzylic), 4.07(4H, q, CH_2O) 7.27 & 7.57(4H, dd, ArH)

12-(4-cyanobenzyl)-1,4,7,10-tetraazacyclotridecane-11,13-dione[3] **50**

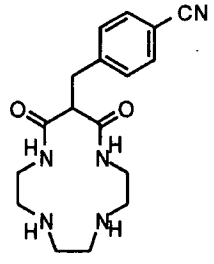

The diester **49** (6.18g, 22.3mmol) and 1,4,7,10-tetraazadecane (3.26g, 1equiv.) were boiled under reflux in dry ethanol (200ml) for 13 days. A white solid precipitated out during the reaction, which was filtered off after cooling. Recrystallisation from hot ethanol gave a white solid, (964mg, 13.1%).

^{1}H NMR (CD_3OD) 2.64(8H, m, CH_2N), 3.0(2H, m, CH_2N), 3.22(2H, d, benzylic) 3.45(1H, t, CH), 3.6(2H, m, CH_2N), 7.42(2H, d, ArH), 7.63(2H, d, ArH) m.p. 239-241°C (dec.) (lit.[3] 245-247°C)

12-(4-aminomethylbenzylamine)-1,4,7,10-tetraazacyclotridecane [3] **48**

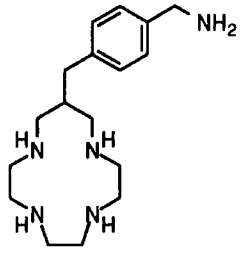

The diamide **50** (964mg, 2.93mmol) was dissolved in a solution of borane in THF (1.0mol dm^{-3}, 70ml), and the mixture boiled under reflux for 2 days. An aliquot was taken and analysed by infra red spectroscopy, which revealed the absence of a carbonyl stretch. The

reaction was then quenched by the slow addition of methanol (20ml), and concentrated under reduced pressure. Boiling in 6M HCl (30ml) for 3 hours, followed by washing with ether (50ml), basifying to pH>13 with KOH pellets and extraction into chloroform (3x50ml), afforded a yellow oil (816mg, 92%)

^{1}H NMR ($CDCl_3$) 1.65-1.8 (6H, br m, NH+NH_2); 2.2-2.75(19H, m, CH_2N + CH +benzylic), 3.60(2H, s, Ar$\underline{CH_2}NH_2$), 6.90 & 6.99(4H, dd, ArH) MS(ES+) 306.3 (M^++1)

4-Nitrophenyl octadecanoate **51**

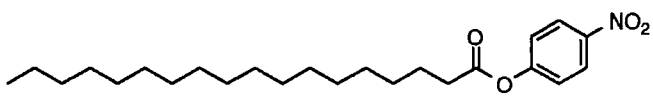

Stearic acid (542mg, 1.91mmol) and oxalyl chloride (1.2ml, large excess) were stirred in CH_2Cl_2 at room temperature. One drop of DMF was added, causing an initial effervescence, which ceased after a couple of minutes. Stirring was continued for a further two hours, followed by removal of CH_2Cl_2 and excess oxalyl chloride. DMF (20ml) was then added, and sodium 4-nitrophenoxide (307mg, 1.91mmol) dissolved in DMF (10ml) was added slowly to the stirrred solution. The reaction was terminated after 30 minutes. The solvent was removed, and the ester isolated (331mg, 43%) by column chromatography on silica, eluting with 20% ethyl acetate:hexane, as a white solid, which appeared iridescent under an optical microscope, melting to give a colourless oil.

TLC (50% EtOAc:CH_2Cl_2) R_f=0.9 ^{1}H NMR ($CDCl_3$) 0.81(3H, t, CH_3), 1.10(28H, m, CH_2), 1.68(2H, p, $C\underline{H_2}CH_2CO$), 2.52(2H, t, CH_2CO), 7.20(2H, d, ArH), 8.19(2H, d, ArH) ^{13}C NMR ($CDCl_3$) 14.6(CH_3), 23.2, 25.2, 29.5, 29.7, 29.9, 29.9, 30.1, 30.2, 32.4, 34.8(CH_2), 122.9, 125.7(Ar), 145.7(CNO_2), 156.0(quaternary Ar, CO), 171.8(CO) IR (film) 2917, 2850, 1752, 1532, 1346, 1201, 1144 MS (CI) 424 ($M+NH_3+1)^+$ Found C=71.1, H=9.69, N=3.45 $C_{24}H_{39}NO_4$ requires C=70.9, H=9.71, N=3.09 m.p. 54.5-56.0°C

1-(benzylcarbamoylmethyl)-1,4,7-triazacyclononane **55**

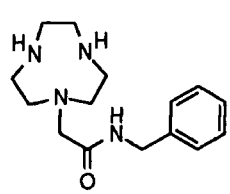

1,4,7-Triazacyclononane **53** (375mg, 2.91mmol) in dry DMF (5ml) was stirred at 60°C, with potassium carbonate (fine mesh, 220mg, 1.6mmol). N-benzylchloroacetamide **54**,

prepared by Gareth Williams, (267mg, 1.45mmol) in DMF (5ml) was added over a period of 3.5 hours, using a mechanical pump. Stirring continued at this temperature for 20 hours, before cooling to room temperature. The solid was then filtered off, and the DMF removed *in vacuo*, to afford 440mg of a crude yellow oil. A sample (80mg) was purified by HPLC, which was characterised as the trifluoroacetate salt.

HPLC Dynamax 60A (10ml min^{-1}); elution A=MeCN/TFA; B=H_2O/TFA from 10% A, 90% B to 90% A, 10% B over 20 minutes; observed λ=254nm; R_t=9.9 minutes; ^1H NMR(D_2O, pD ~4) 3.03 (4H, t (J=6Hz), $C\underline{H}_2NCH_2CO$); 3.28 (4H, t (J=6Hz), CH_2N); 3.58 (2H, s, NCH_2CO); 3.64 (4H, s, CH_2N (opp. alkylated N)); 4.39 (2H, s, benzylic); 7.3 (5H, m, ArH). ^{13}C NMR (D_2O) 45.7, 46.1, 47.0, 51.8, 59.1(CH_2N), 130.2, 130.5, 131.7(Ar), 140.5(quaternary Ar), 176.5(CO). IR (film) 3277 (NH), 1676 (CO) MS(ES+) 277.2, 100% (M^++1)

7-(benzylcarbamoylmethyl)1,4-bis(ethoxycarbonylmethyl)-1,4,7-triazacyclononane **56**

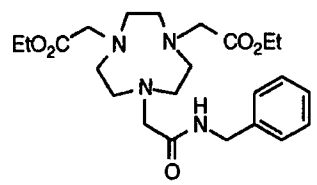

To the crude amide **55** (356mg, ~1.3mmol), in dry ethanol (20ml), was added ethyl bromoacetate (431mg, 2.58mmol), and caesium carbonate (840mg, 2.58mmol). The temperature was raised to 60°C, and the reaction left to stir overnight. Purification by alumina chromatography (CH_2Cl_2:MeOH from 0 - 5% MeOH) afforded a yellow oil (196mg, 34%).
TLC (1% MeOH:CH_2Cl_2) R_f=0.4 ^1H NMR ($CDCl_3$) 1.24 (6H, t (J=7Hz), CH_3); 2.64 & 2.79 (12H, m, CH_2N ring); 3.08 (4H, s, $NC\underline{H}_2CO_2Et$); 3.35 (2H, s, $NC\underline{H}_2CONH$); 4.10 (4H, q (J=7Hz), $OC\underline{H}_2CH_3$); 4.45 (2H, d, benzylic); 7.28 (5H, m, ArH); 9.30 (1H, br t, CONH) ^{13}C NMR ($CDCl_3$) 14.1(CH_3), 43.3($Ar\underline{C}H_2N$), 54.5, 55.6, 56.5, 57.6(CH_2N), 60.0(CH_2O), 61.1($N\underline{C}H_2CO$), 127.1, 127.8, 128.3, 138.7, 171.6, 172.5. IR (film) 3194 (NH), 2928, 1738 (ester), 1666 (amide) MS (CI) 449 (100%, M^++1)

7-(benzylcarbamoylmethyl)-1,4-bis(caboxymethyl)-1,4,7-triazacyclononane **57**

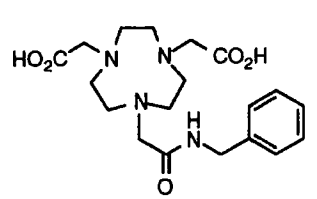

The ester **56**, prepared above (170mg, 0.38mmol), was dissolved in aqueous potassium hydroxide (1.0mol dm^{-3}, 20ml), and stirred overnight. The solvent was removed and the residues dissolved in ethanol. After filtration, a yellow oil was collected (135mg, 90%). A small amount was purified by HPLC.

HPLC: Spherisorb 5ODS2 (1.4ml min^{-1}); elution A=MeCN/TFA; B=H_2O/TFA from 5% A, 95% B to 95% A, 5% B over 20 minutes; observed λ=254nm; R_t=9.9 minutes; ^1H NMR(D_2O) of TFA salt 2.85 (4H, t, CH_2N ring), 3.0 (4H, t, CH_2N ring), 3.10 (4H, s, CH_2N ring), 3.52 (6H, s, NCH_2CO), 4.30 (2H, s, benzylic), 7.2 (5H, m, aromatic). [The presence of the amide was confirmed by acquiring a spectrum in trifluoroacetic acid. ^1H NMR (CF_3CO_2H + CH_2Cl_2 reference: 5.58ppm) 4.13 (10H, br s); 4.23 (4H, br s); 4.66 (4H, br s), 4.87 (2H, br s, benzylic); 7.63 & 7.70 (5H, 2 x br s, ArH); ~8.3 (1H, br s, CONH)] ^{13}C NMR (D_2O, pD ~3) 45.9(Ar$\underline{C}H_2N$), 52.4, 52.5, 53.4, 59.0(CH_2N), 130.2, 130.5, 131.8, 140.6(Ar), 174.1(1C, CONH), 174.8(2C, CO_2^-). IR (film) 3377 (OH), 1727 (CO acid), 1672 (CO amide) MS(ES-) 391.4 (M), 505.4 (M+TFA)

The ligand was also made using chloroacetic acid. To **55** (76mg, 0.275mmol), stirring in water (15ml), was added chloroacetic acid (65mg, 0.69mmol, 2.5 equiv.) The pH was then raised to 10 by the careful addition of LiOH, and the reaction temperature was then raised to 60°C. Stirring continued for 16 hours. Concentration followed by purification by preparative HPLC afforded the ligand (43mg, 40%).

[Cu(**57**)]

The ligand **57** (135mg, 0.344mmol) and copper perchlorate (128mg, 1 equiv.) were stirred together in water at pH=4.5 for 3 hours. The solution turned a darker blue. Hydrogen sulfide was bubbled through the solution, and the resulting suspension filtered. An attempt to crystallise the sample yielded a blue oil. The complex was then purified by HPLC to give the complex, as a blue solid (23mg, 15%).

HPLC: Dynamax 60A (10ml min^{-1}); elution A=MeCN; B=H_2O from 10% A, 90% B to 50% A, 50% B over 20 minutes; observed λ=278nm; R_t=11.3 minutes The presence of the paramagnetic Cu(II) ion broadens the NMR spectra ^1H NMR(D_2O) 5.5(2H, v br, benzylic), 7.45(4H, br m, aromatic), 7.9(1H, br, aromatic) ^{13}C NMR (D_2O, pD ~7) 47.5(Ar$\underline{C}H_2N$), 128.0, 128.4, 129.0, 137.8(Ar) IR (film) 1682, 1633 $\lambda_{max}(H_2O)$= 705nm ε= ~ 200 M^{-1} cm^{-1} MS(ES+) 227.6 (14%), 228.7 (7%) $(M+1)^{2+}$; 454.1 (100%), 455.6 (45%) $(M+1)^+$ Found C=46.25 H=5.89 N=11.08 $C_{19}H_{26}N_4O_3Cu.2H_2O$ requires C=46.63 H=6.13 N=11.45 m.p. 117.5-118.5°C

N-Octadecanoylbutane-1,4-diamine **59**

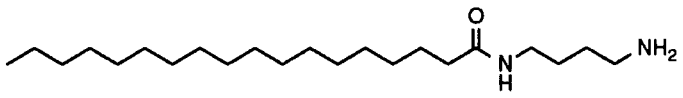

To 1,4-diaminobutane (2g, large excess) in CH_2Cl_2 (10ml) was added **51** (220mg, 0.543mmol), dissolved in CH_2Cl_2 (10ml). Analysis by TLC (SiO_2) indicated an almost instantaneous reaction. The solvent was removed and the residue treated with dilute acid to produce a white solid, which was collected by filtration. The solid was then suspended in potassium hydroxide solution (1.0mol dm^{-3}, 10ml) and extracted into $CHCl_3$ (4 x 20ml). Concentration afforded the amino amide, as a white solid (134mg, 70%).

^1H NMR ($CDCl_3$) 0.83(3H, t, CH_3), 1.21(28H, br s, CH_2), 1.46(6H, m, $NCH_2C\underline{H}_2$ + $C\underline{H}_2CH_2CO$), 2.10(2H, t, CH_2CO), 2.67(2H, t, $C\underline{H}_2NH_2$), 3.21(2H, q like m, $C\underline{H}_2NHCO$), 6.10(1H, br s, NHCO) ^{13}C NMR ($CDCl_3$) 13.9(CH_3), 17.9, 25.6, 26.8, 29.4, 30.7, 31.7, 36.5, 39.0, 41.5(CH_2), 173.0(CONH) IR (film) 3309, 2919, 2848, 1632, 1548, 1469 MS (ES+) 355.30 ($C_{22}H_{47}N_2O$ requires 355.37) An accurate analysis was not obtained for this product m.p. 98.0-98.5°C

N'-(N''-Octadecanoylbutane-1,4-diamine) chloroacetamide **60**

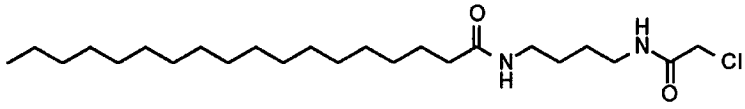

The amine **59** (120mg, 0.339mmol) was dissolved in CH_2Cl_2 (10ml), and the temperature lowered to -10°C. NaOH (13.5mg, 0.339mmol) dissolved in water (1ml) was then added, followed by the slow addition of chloroacetylchloride (38mg, 27µL, 0.339mmol) in CH_2Cl_2 (5ml). Concentration afforded an oil, which crystallised at -18°C. (103mg, 74%) The compound was deemed sufficiently pure for the next step, by inspection of ^1H and ^{13}C NMR spectra.

^1H NMR ($CDCl_3$) 0.87(3H, t, CH_3), 1.25(28H, br s, CH_2), 1.56(6H, m, $NCH_2C\underline{H}_2$ + $C\underline{H}_2CH_2CO$), 2.17(2H, t, CH_2CO), 3.3(4H, m, $C\underline{H}_2NHCO$), 4.05(2H, s, $ClCH_2CO$), 5.65 & 6.75(1H+1H, 2x br s, NHCO) ^{13}C NMR ($CDCl_3$) 14.1(CH_3), 22.7, 25.8, 26.7, 26.9, 29.3, 29.5, 29.7, 31.9, 36.8, 38.9, 39.4, 42.6(CH_2), 166.1, 173.3(CONH) IR (film) 1643 MS (CI) 431, 433 (3:1) (M+1) m.p. 93.0-94.0°C

1-(Octadecanylamido)butylcarbamoylmethyl)-1,4,7-triazacyclononane **61**

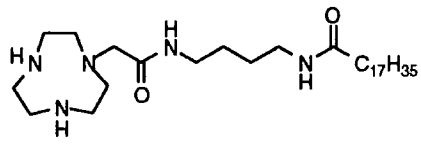

The chlorodiamide **60** prepared above (90mg, 0.219mmol), dissolved in DMF (5ml), was slowly added to a stirred suspension of caesium carbonate (71mg, 0.219mmol) and 1,4,7-triazacyclononane **53** (57mg, 0.438mmol) in DMF (20ml) at 80°C. After 18 hours, the DMF was removed under reduced pressure, to leave a brown oil (140mg). ^{1}H NMR analysis of the oil revealed the absence of a resonance at 4.05ppm, due to the CH_2Cl group. The oil was used in the next step, without further purification.

^{1}H NMR (Crude, $CDCl_3$) 0.84(3H, t, CH_3), 1.22(28H, br s, CH_2), 1.5(6H, m, $NCH_2\underline{CH_2}$ + $\underline{CH_2}CH_2CO$), 2.1(2H, t, CH_2CO), 2.5-3.5(18H, m (maxima at 2.78&3.25), CH_2N), 6.3 & 8.2(1H+1H, br s + br s, NHCO) MS(CI) 525 (M^++2) (no peak for dialkylated cycle was observed)

7-(Octadecanylamido)butylcarbamoylmethyl)-1,4,7-triazacyclononane-1,4-diyldiacetate

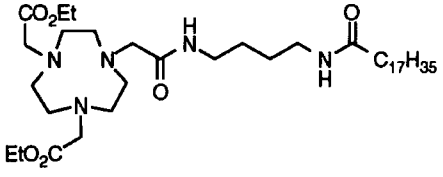

The crude alkylated triamine **61** (140mg, assumed 0.263mmol) and caesium carbonate (255mg, 0.788mmol) were suspended in DMF(15ml) at 80°C. Ethyl bromoacetate (132mg, 88μL, 0.788mmol) was slowly added and the reaction was left to stir for 24 hours. The molecular ion was clearly seen in the CI mass spectrum of the crude reaction mixture. However, no product was isolable by column chromatography.

1-octadecanoyl-4,8,11-tri(4-methylbenzenesulfonyl)-1,4,8,11-tetraazacyclotetradecane **63**

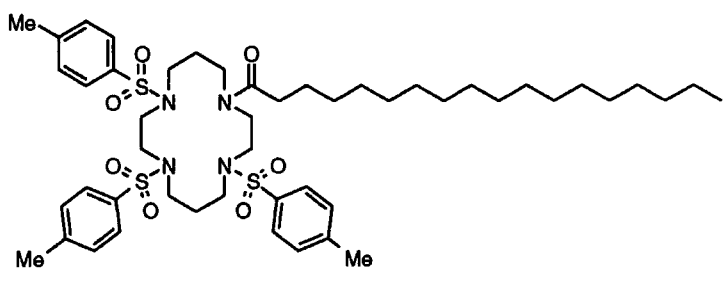

Stearoyl chloride was made by adding oxalyl chloride (1.2ml) to stearic acid (301mg, 1.06mmol) in CH_2Cl_2 (20ml), with one drop of DMF. The mixture was stirred for two hours. Excess oxalyl chloride was removed *in vacuo* after addition of CH_2Cl_2 (2ml), repeated twice. The acid chloride was taken up in CH_2Cl_2 (10ml) and added to the triprotected cyclam **62** (702mg, 1.06mmol, prepared by Dr. I. Helps), dissolved in CH_2Cl_2 (10ml). The mixture was left to stir at room temperature for two hours, followed by TLC. The reaction was stopped, and the mixture chromatographed on silica, with a gradient elution (0-0.5% MeOH:CH_2Cl_2). The title compound was isolated as a white foam. (431mg, 44%)

TLC (10% MeOH:CH_2Cl_2) R_f=0.8 ^{1}H NMR ($CDCl_3$) 0.86(3H, t, CH_3), 1.24(28H, m, CH_2), 1.64(2H, br p, $C\underline{H}_2CH_2CO$), 1.92(4H, m, $NCH_2C\underline{H}_2CH_2N$), 2.42(11H, $ArC\underline{H}_3$ + CH_2CO), 2.9-3.7(16H, br m, CH2N), 7.33(6H, m, Ar), 7.65(6H, m, Ar) ^{13}C NMR ($CDCl_3$) 16.2(CH_3), 23.6, 24.7, 31.7, 33.9, 35.0, 35.1(CH_2), 44.9, 49.3, 49.3, 49.5, 51.7, 52.3, 54.3(CH_2N), 55.5($Ar\underline{C}H_3$), 129.1. 129.5, 129.7, 130.0, 131.9, 134.7, 135.3, 137.5, 146.0, 146.1(Ar), 175.3(CO) IR (film) 2920, 2852, 1643, 1597, 1455, 1338, 1158, 1091 MS(CI) The molecular ion was not detected under the probe conditions used. Found C=62.6 H=8.05 N=5.81 $C_{49}H_{76}N_4O_7S_3.0.5(H_2O)$ requires C=62.7 H=8.27 N=5.97

1-octadecanyl-4,8,11-tri(4-methylbenzenesulfonyl)-1,4,8,11-tetraazacyclotetradecane **64**

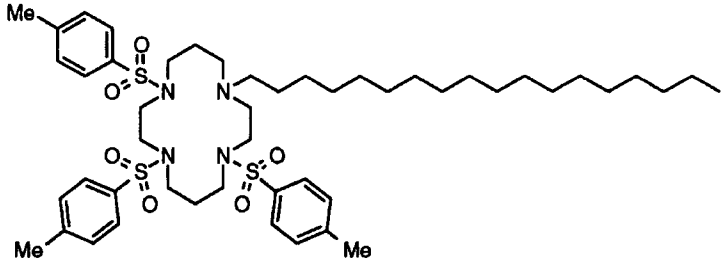

The amide **63** prepared above (412mg, 0.444mmol) was boiled under reflux with borane (1.0mol dm^{-3} solution in THF, 15ml) for 16 hours. Analysis of an aliquot by IR spectroscopy indicated the absence of the amide functionality. The reaction was worked up by cooling in ice, followed by the careful addition of MeOH. Evaporation under reduced pressure afforded a white solid, which was boiled under reflux with hydrochloric acid solution (6mol dm^{-3}, 10ml) for 6 hours. Neutralisation (KOH), followed by extraction into chloroform (3 x 20ml) and evaporation of solvent, afforded a yellow oil. (371mg, 92%)

^{1}H NMR ($CDCl_3$) 0.83(3H, t, CH_3), 1.22(28H, br s like m, CH_2), 1.6(2H, br m, $C\underline{H}_2CH_2N$ (side chain)), 1.88(4H, m, $NCH_2C\underline{H}_2CH_2N$), 2.29(2H, br t, CH_2N), 2.38(9H, m, $ArC\underline{H}_3$), 2.55(2H, br t, CH_2N), 2.9-3.4(10H, m, CH_2N), 3.51(4H, m, CH_2N), 7.30(6H, br s like m, Ar), 7.61(6H, m, Ar) ^{13}C NMR ($CDCl_3$) 14.1(CH_3), 21.4, 22.6, 25.9, 27.0, 27.5, 27.6,

29.3, 29.6, 31.8, (CH_2), 44.1, 47.5, 48.0, 48.1, 48.3, 49.4, 50.4, 53.9, 55.1(CH_2N), 127.2, 129.7, 135.1, 135.4, 143.6(Ar) IR (film) 2923, 2852, 1598, 1454, 1337, 1156 MS(CI) 915 (M^++1) A satisfactory analysis was not obtained for this compound

1-octadecanyl-1,4,8,11-tetraazacyclotetradecane **65**

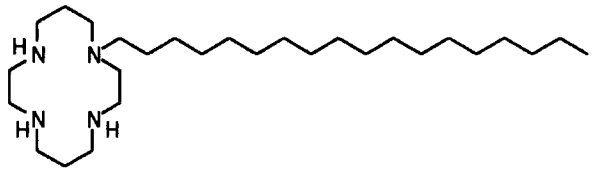

The triprotected amine **64** prepared above (344mg, 0.376mmol) was boiled under reflux with phenol (1.5g) in 45% HBr/glacial acetic acid solution (15ml) for 18 hours. More HBr/acetic acid was then added (15ml) and the reaction left for a further 24 hours. The mixture was cooled and added carefully to ether, giving a grey precipitate, which was separated by centrifugation. Basification (pH>13, KOH) was followed by extraction into chloroform to give, on concentration, a colourless oil. (150mg, 97%)

^1H NMR ($CDCl_3$) 0.86(3H, t, CH_3), 1.23(32H, m, CH_2), 1.69(4H, h like m, $NCH_2C\underline{H}_2CH_2N$), 2.3-2.8(18H, m, CH_2N) ^{13}C NMR ($CDCl_3$) 14.1(CH_3), 22.7, 25.5, 26.4, 27.6, 29.0, 29.3, 29.7, 29.7, 31.9(CH_2), 47.8, 48.1, 48.9, 49.5, 49.7, 51.2, 52.6, 53.8, 54.8(CH_2N) IR (film) 3297, 2922, 2851, 2807, 1466 MS(CI) 453 (M^++1) $C_{28}H_{61}N_4$ requires 453.489 found 453.489

linolenoyl chloride

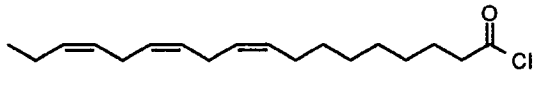

To linolenic acid (194mg, 1.40mmol) was added thionyl chloride (2ml). Immediately, a bright orange colour developed. The mixture was stirred at room temperature for a further hour. The excess thionyl chloride was removed *in vacuo*, followed by repeated cycles of adding dichloromethane (2ml) and evaporating, to give the acid chloride as an orange oil. Analysis by infra red spectroscopy indicated quantitative conversion. No high frequency NMR signal was identifiable, indicating the absence of the carboxylic acid functional group, and the retention of unsaturation was noted.

^1H NMR ($CDCl_3$) 0.97(3H, t, CH_3), 1.31(8H, br s, CH_2), 1.7(2H, p, $C\underline{H}_2CH_2CO$), 2.05(4H, m, allylic CH_2 (to one double bond)), 2.88(6H, m, CH_2CO + allylic CH_2 (to two double bonds)), 5.36(6H, m, CH) IR (film) 1799 (A drop of methanol was added to the

sample on the NaCl plate, and another spectrum obtained. The carbonyl peak moved to 1739cm^{-1}, consistent with the formation of an ester from the acid chloride)

1-linolenoyl-4,8,11-tri(4-methylbenzenesulfonyl)-1,4,8,11-tetraazacyclotetradecane **66**

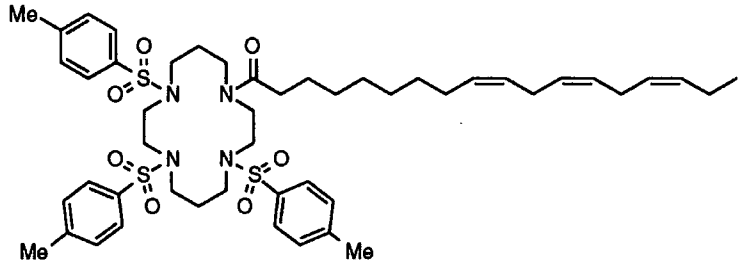

Linolenoyl chloride prepared above (1.40mmol) in CH_2Cl_2 (10ml) was added to the triprotected amine **62** (938mg, 1.42mmol) in CH_2Cl_2 (10ml). The mixture was left to stir for 18 hours, before removing the solvent under reduced pressure. The almost black glue was purified by flash chromatography on silica, using identical conditions to the saturated analogue, to give a yellow foam. (544mg, 41%)

TLC (10% MeOH:CH_2Cl_2) R_f=0.8 ^{1}H NMR ($CDCl_3$) 0.96(3H, t, CH_3), 1.33(8H, br d like m, CH_2), 1.6(2H, br m, $C\underline{H}_2CH_2CO$), 2.03(8H, m, $NCH_2C\underline{H}_2CH_2N$ + allylic CH_2 (to one double bond)), 2.33(2H, m, CH_2CO), 2.43(9H, m, $ArC\underline{H}_3$), 2.79(4H, t, allylic CH_2 (to two double bonds)), 2.9-3.6(16H, m, CH_2N), 5.35(6H, m, CH), 7.33(6H, m, Ar), 7.66(6H, m, Ar) ^{13}C NMR ($CDCl_3$) 14.2(CH_3), 21.5, 24.7, 25.1, 25.6, 26.6, 27.2, 29.2, 29.4, 32.7, 33.1, 34.0(CH_2), 42.8, 46.6, 47.2, 48.4, 48.8, 49.6, 50.3, 52.4(CH_2N), 127.1, 127.5, 127.7, 127.9, 129.2, 129.8, 130.0, 130.1, 131.9, 143.8, 144.0(Ar + vinylic), 173.4(CO) IR (film) 2929, 2857, 1726, 1622, 1598, 1792, 1453, 1339, 1159, 1091 MS(CI) molecular ion not detected, 663 (macrocycle fragment following amide cleavage +1)

1-(octadec-9,12,15-cis, cis, cis-trienoyl)-4,8,11-tri(4-methylbenzenesulfonyl)-1,4,8,11-tetraazacyclotetradecane **67**

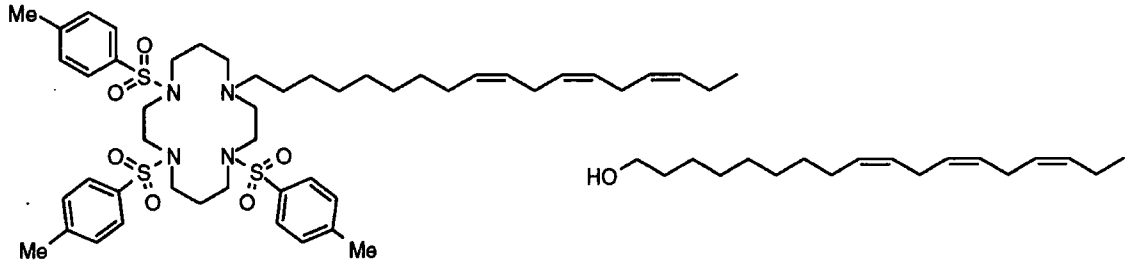

To a solution of the acylated macrocyle **66** (128mg, 0.139mmol) in CH_2Cl_2(10ml) stirring at -78°C, was added lithium aluminium hydride(27mg, 0.694mmol) as a solid. The

temperature of the mixture was allowed to rise slowly to ambient temperature over 4 hours. The reaction was quenched by adding methanol (2 drops), followed by 15% sodium hydroxide solution (1ml). The suspension was extracted with chloroform, and the residue obtained on concentration was chomatographed on silica (elution: 0-0.5%MeOH:CH_2Cl_2), to give the title compound as a colourless glass. (23mg, 18%)

TLC (10% MeOH:CH_2Cl_2) R_f=0.8 ^{1}H NMR ($CDCl_3$) 0.97(3H, t, CH_3), 1.32(10H, br m, CH_2), 1.6&1.9(2H+2H, br m, $C\underline{H}_2CH_2CO$ + homoallylic CH_2), 2.03(4H, m, $NCH_2C\underline{H}_2CH_2N$), 2.3(4H, m, allylic CH_2 (to one double bond)), 2.43(9H, m, $ArC\underline{H}_3$), 2.79(4H, t, allylic CH_2 (to two double bonds)), 2.9-3.6(18H, m, CH_2N), 5.36(6H, m, CH), 7.31(6H, m, Ar), 7.68(6H, m, Ar) ^{13}C NMR ($CDCl_3$) 14.0(CH3), 21.5, 25.6, 26.0, 27.2, 27.8, 29.2, 29.5(CH_2), 47.6, 48.0, 48.4, 49.4, 49.8, 50.5, 53.9, 55.2(CH_2N), 127.3, 127.6, 127.9, 128.2, 129.7, 130.3, 135.2, 143.4, 143.8(Ar + alkene) IR(film) 2927, 2855, 1645, 1597, 1456, 1343, 1159, 1091 MS(CI) 909 (M^++1)

ω-linolenol, formed by amide cleavage and reduction, was identified by ^{1}H NMR spectroscopy.

R_f=1.0 ^{1}H NMR ($CDCl_3$) 0.97(3H, t, CH_3), 1.34(8H, br s, CH_2), 1.58(5H, br m, $C\underline{H}_2CH_2O\underline{H}$ + homoallylic CH_2), 2.05(4H, q like m, CH_2 (allylic to one double bond)), 2.81(4H, t like m, CH_2 (allylic to two double bonds)), 3.64(2H, t, $C\underline{H}_2OH$), 5.36(6H, m, CH)

N-Biotinylethane-1,2-diamine [7] **68**

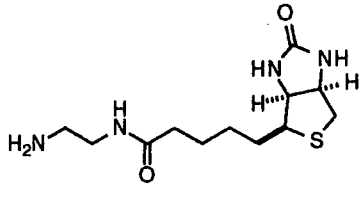

To biotin-4-nitrophenyl ester (12mg, 0.033mmol) in chloroform (1ml) was added a solution of ethylenediamine (200mg, 0.30mmol) in chloroform (3ml) with rapid mixing (Fison's "Whirlimixer"). After 15 minutes, the mixture was concentrated, and the excess ethylenediamine removed *via* Kugelrohr distillation. The title compound crystallised from acidic solution (pH=4), to give the hydrochloride salt as a white solid (6mg, 56%) , which gave data in accord with that synthesised *via* a different route.[6]

^{1}H NMR(D_2O, pD ~2) 1.4(2H, m, CH_2), 1.7(4H, m, CH_2), 2.2(2H, t, CH_2CO), 2.6(2H, t, CH_2N), 2.8(1H, d like m, CHS), 3.0(1H, dd like m, $C\underline{H}HS$), 3.2(2H, t, CH_2N), 3.3(1H, m,

CHHS), 4.1(1H, m, SCH_2CHNH), 4.3(1H, m, SCHRCHNH) MS(ES+) 287.2 (100%, M^++1)

12-(4-(N-biotinylamidomethyl) benzylamine)-1,4,7,10-tetraazacyclotridecane **69**

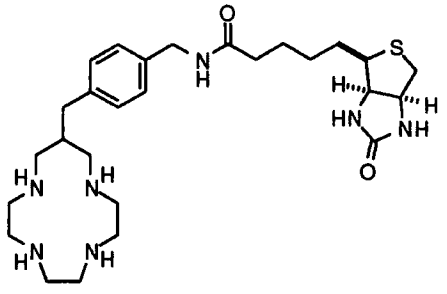

The macrocycle **48** (24mg, 0.079mmol) was dissolved in PIPES buffer (0.5M, pH=6.8, 0.7ml). The pH of the solution was restored to 6.5-7.0, by slowly adding 1mol dm^{-3} HCl dropwise. The biotin paranitrophenyl active ester (Aldrich, 25mg, 0.069mmol) was dissolved in 1,4-dioxane (0.7ml). The two solutions were mixed and the reaction held at 40°C for 12 hours with periodic whirlimixing, with the course of the reaction being monitored by cation exchange HPLC. Concentrated HCl was added to lower the pH to 1-2. Centrifugation then permitted removal of the precipitated PIPES buffer. The acidic supernatant was washed with ether to remove excess ester and paranitrophenol. The required conjugate was then isolated as a white solid, following purification by reverse phase HPLC (19mg, 55%).

HPLC Synchropak CM300 (1.4ml min^{-1}); elution A=MeCN; B=H_2O; C=NH_4OAc pH=5.6 from 20% A, 70% B, 10% C to 20% A, 0% B, 80% C in 20 minutes R_t(product)=7.3 minutes ^1H NMR(D_2O) 1.16(2H, m, CH_2), 1.44(4H, m, CH_2), 2.10(2H, t, CH_2CO), 2.2(1H, m, CH), 2.52(3H, m, CHRS & CH_2S) 2.7-3.2(22H, m, CH_2N), 4.09(1H, m, SCH_2CHNH), 4.15(2H, s, $ArCH_2NHCO$), 4.36(1H, m, CH ring fusion), 7.08(4H, q like 2xd, ArH) ^{13}C NMR(D_2O) 28.1, 30.6,30.7, 38.4, 38.8, 39.3,42.7,45.6, 46.9,47.3, 48.4, 53.8, 58.3, 63.2, 64.9(Aliphatic C), 130.6, 132.4, 139.9, 139.9(Ar), 168.3(NCON), 179.7(CON) IR(KBr disc) 3447, 1685, 1429, 1203, 1131 MS(ES+) 266.9 ($(M+2H)^{2+}$, 100%)), 532.5 ($(M+H)^+$, 65%) m.p. 91.0-92.0°C

The copper complex $[Cu(\mathbf{69})]^{2+}$was also characterised by electrospray mass spectoscopy, uv and IR. The complex was made by adding copper chloride (2mg, excess) to an aqueous solution of the KBr disc used to obtain the above infra red spectrum. Hydrogen sulfide was then bubbled through the solution, and the copper sulfide precipitate filtered off.

IR(KBr disc) 3410(water), 3212, 2924, 1648, 1458, 1204, 1152 uv λ_{max}(H_2O) 264, 558 MS(ES+) 297.4(100%) 298.4(35%) ie M^{2+} with statistical copper isotope pattern.

7.2.3. Chapter 4

Diethylheptanenitrilemalonate **71**

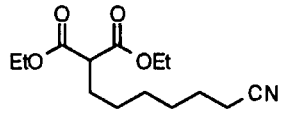

Sodium (1.3g, 56.5mmol) was dissolved in dry ethanol (125ml). Diethyl malonate (17.6g, 110mmol) dissolved in dry ethanol (50ml), was then added dropwise, and the system left to equilibriate for 1 hour. Bromoheptanenitrile (10g, 52.6mmol) was then added, dissolved in dry DMF (50ml). The reaction was left to boil under reflux for 26 hours. After cooling to room temperature, the solution was extracted into diethylether (400ml) and dried over $MgSO_4$. Concentration afforded a pale yellow oil. (12.76g, 90%)

^1H NMR ($CDCl_3$) 1.1-1.5 (6H, br m, CH_2), 1.27 (6H, t, CH_3); 1.63 (2H, p, $C\underline{H}_2CH_2CH_2CN$), 1.89 (2H, p, $C\underline{H}_2CH_2CN$), 2.34 (2H, t, CH_2CN), 3.33 (1H, t, CH), 4.20 (4H, q, OCH_2) ^{13}C NMR ($CDCl_3$) 13.8(CH_3), 16.7, 24.9, 26.7, 28.0, 28.1, 28.2, 51.6(CH_2+CH), 61.0(OCH_2), 119.5(CN), 169.2(CO) IR(film) 2937, 2246, 1731 MS (CI) 287 $(M+NH_4)^+$ $C_{14}H_{23}NO_4{}^1/_9H_2O$ requires C=62.0; H=8.6; N=5.2; found C=61.8; H=8.7; N=5.4

12-heptanenitrile-1,4,7,10-tetraazacyclotridecane-11,13-dione **72**

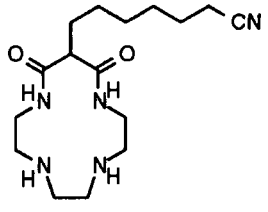

The diester **71** (12.76g, 47.4mmol) and 1,4,7,10-tetraazadecane (6.92g, 1equiv.) were refluxed in dry ethanol for 16 days. Cooling afforded a white solid, which was recrystallised from hot ethanol, (2.05g, 13.4%).

^1H NMR ($CDCl_3$) 1.34 (6H, br m, CH_2); 1.65 (2H, p, $C\underline{H}_2CH_2CH_2CN$); 1.87 (2H, p, $C\underline{H}_2CH_2CN$); 2.12 (2H, br s, NH); 2.32 (2H, t, CH_2CN); 2.67 (8H, br m, CH_2N); 3.10 (1H, t, CH); 3.39 (4H, br dm, $C\underline{H}_2NHCO$); 7.08 (2H, br t, NHCO) ^{13}C NMR ($CDCl_3$) 17.1, 25.2, 27.4, 28.3, 28.5, 29.3, 39.3(CH_2+CH), 46.8, 48.0, 55.9(CH_2N), 119.8(CN), 169.9(CONH). IR (KBr disc) 3342, 2938, 2245 (CN), 1663+1628 (sym + antisym CO) MS(EI/CI) 324 (M^++1) $C_{16}H_{29}N_5O_2$ requires C=59.4, H=9.0, N=21.7 found C=59.4, H=9.3, N=21.4 Mpt. 181-184°C (dec)

12-heptylamine-1,4,7,10-tetraazacyclotridecane **70**

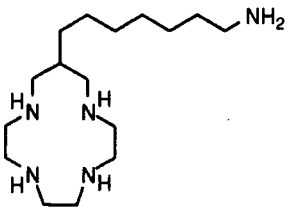

The diamide **72** (1.3g, 4.02mmol) was reacted with a large excess of a solution of borane in THF (1.0mol dm^{-3}, 20ml) under reflux overnight. An aliquot was analysed by infrared spectroscopy showing the absence of carbonyl functionality. The reaction was quenched by repeatedly adding methanol (20ml) and concentrating. The residue was stirred at 60°C overnight in HCl (6mol dm^{-3}, 20ml). The mixture was then cooled, and washed with ether (2 x 10ml). The pH raised to 13, and extraction into dichloromethane (5 x 20ml), followed by concentration, afforded a yellow gum. (875mg, 73%).

^{1}H NMR ($CDCl_3$) 1.22 (13H, br m, alkyl side chain); 1.6 (2H, br m, $C\underline{H}_2NH_2$); 2.05 (6H, br s, NH); 2.62 (16H, br m, CH_2N ring) ^{13}C NMR 27.8, 29.8, 30.3, 32.9, 34.3, 39.0(CH_2+CH), 42.7, 47.9, 48.1, 49.5, 55.9(CH_2N). IR (film) 3660 (primary NH), 3292 (secondary NH), 3046, 2929, 2854,1464 MS(ES+) 150.6 (M^{2+}), 300.3 (M^+)

1,4,7-triazacyclononane-1,4,7-triyltriacetic acid[7] **23**

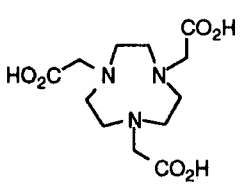

Chloroacetic acid (440mg, 4.65mmol) was added to a stirred solution of 1,4,7-triazacyclononane **53** (200mg, 1.55mmol) in water (10ml). Lithium hydroxide was added periodically over 24 hours, to keep the pH at 10. The pH was then lowered to 1.5 (conc. HCl) and the solvent removed *in vacuo*. The solid remaining was taken up in water (1ml), and ethanol (10ml) was then added to give a white gluelike precipitate. The supernatant was then removed, and the title compound was recrystallised from ethanol/water (5ml + 5ml) to give a white solid (104mg, 22%), identical to an authentic sample.

^{1}H NMR(D_2O) 3.40(12H, s, CH_2N ring), 3.85(6H, s, NCH_2CO) m.p. 210-215°C (dec.) (lit.[8] 205°C)

N-(paramethoxybenzenesulfonyl)-1,4-diaminobutane [8] **73**

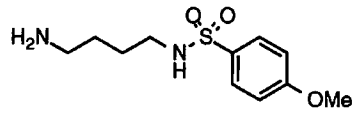

To a solution of 1,4-diaminobutane (22.05g, 0.25mol, ~7equivs.) in dichloromethane (200ml) was added paramethoxybenzenesulfonyl chloride (7.5g, 36.3mmol) in CH_2Cl_2 (100ml), over a period of 1 hour. The reaction was stirred for 16 hours at room temperature to give a turbid suspension. The solvent was removed, and then the product was extracted into chloroform, after washing with KOH solution. Removal of excess diamine afforded a white glue. (8.97g, 96%)

^{1}H NMR ($CDCl_3$) 1.5(4H, m, CH_2); 2.68 (2H, t, $C\underline{H}_2NH_2$) 2.92 (2H, t, $C\underline{H}_2NHTs'$); 3.88 (3H, s, OMe); 6.98 (2H, d, SO_2CCH); 7.79 (2H, d, $C\underline{H}COMe$); ^{13}C NMR ($(CD_3)_2SO$) 26.8, 30.7(CH_2), 41.1, 42.8(CH_2N), 55.8(OCH_3), 114.5 (2C, Ar)), 128.9 (2C, Ar)), 132.6(CSO_2), 162.2($\underline{C}OCH_3$)

N'-(2-chloroethanoyl)-N''-4-methoxybenzenesulfonyl-1,4-diaminobutane **74**

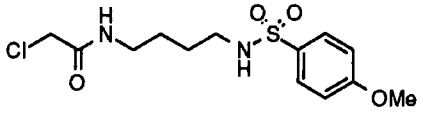

The protected amine **73** (8.95g, 34.7mmol) was stirred below -10°C in CH_2Cl_2 (100ml). To this solution was added sodium hydroxide (1 equiv.) in water (10ml), followed by chloroacetylchloride (3.92g, 2.77ml, 1 equiv.) in dichloromethane (100ml), over 30 minutes. The temperature was kept at -10°C for the following two hours, before raising to room temperature overnight. Washing with NaOH (0.1mol dm^{-3}, 50ml), HCl(0.1mol dm^{-3}, 50ml), and water (100ml), followed by drying ($MgSO_4$) and concentration, gave a yellow oil which crystallised to a white solid at -18°C. (9.64g, 83%).

^{1}H NMR ($CDCl_3$) 1.54 (4H, m, CH_2); 2.95 (2H, t, $C\underline{H}_2NHCO$); 3.29 (2H, dt, $C\underline{H}_2NHTs'$); 3.88 (3H, s, OMe); 4.04 (2H, s, $ClCH_2CO$); 4.8 (1H, br s, $N\underline{H}Ts'$); 6.65 (1H, br s, CONH); 6.99 (2H, d, ArH); 7.80 (2H, d, ArH) ^{13}C NMR ($CDCl_3$) 26.4, 26.6(CH_2), 39.2(CH_2Cl), 42.5, 42.6(CH_2N), 55.6(OCH_3), 114.2, 129.1, 131.3, 162.8(Ar), 166.1(CO). IR (film) 3281, 2944, 1662, 1597. MS (DCI) 335:337 ratio 3:1 (M^+ ^{35}Cl, ^{37}Cl); 352:354 (plus NH_3) Found C=46.4, H=5.84, N=8.63; $C_{13}H_{19}N_2O_4SCl$ requires C=46.6, H=5.68, N=8.37 m.p. 84.0-85.0°C

[1-(4-methoxybenzenesulfonamido)butylcarbamoylmethyl]-1,4,7-triazacyclononane **75**

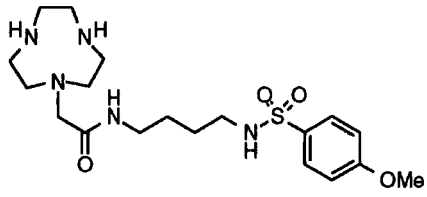

1,4,7-Triazacyclononane **53** (460mg, 3.48mmol) was stirred at 60°C in DMF (10ml), with caesium carbonate (240mg). The chloroamide **74** (582mg, 1.75mmol) in DMF (5ml) was added over 6 hours, using a mechanical pump. Stirring continued for a further 18 hours, before cooling. The solid was filtered off, and the DMF / excess triazacyclononane removed under reduced pressure. Some dialkylated material was produced, in addition to the required monoalkylated product. Conversion was estimated to be 65-80%. A portion of the product was purified by HPLC, for characterisation purposes.

HPLC: Dynamax 60A (10ml min^{-1}); elution A=MeCN/TFA; B=H_2O/TFA from 0% A, 100% B to 60% A, 40% B over 30 minutes; observed λ=275nm; R_t=17.5 minutes. ^1H NMR (D_2O, pD ~4) 1.36 (4H, m, CH_2); 2.78 (2H, t, $CONHC\underline{H}_2$); 2.95 (4H, t, CH_2N, ring α to alkylated N); 3.06 (2H, t, $C\underline{H}_2NHSO_2$); 3.22 (4H, t, CH_2N, β to alkylated N); 3.41 (2H, s, NCH_2CO); 3.59 (4H, s, NCH_2, ring δ to alkylated N); 3.80 (3H, s, OMe); 7.05 & 7.70 (2 x 2H, 2 x d, ArH) ^{13}C NMR (D_2O) 28.1, 28.9(CH_2), 41.8, 45.1, 45.7, 47.0, 51.8(CH2N), 58.6, 59.1($N\underline{C}H_2CO$+OCH_3), 117.6, 131.9, 132.7(Ar), 165.8(COMe), 176.3(CO). IR (film) 1677 (amide) MS(DCI) 428 (M^++1) Found M^++1 428.2348 $C_{19}H_{35}N_5O_4S$ requires 428.2332

7-[(4-methoxybenzenesulfonamido)butylcarbamoylmethyl]-1,4,7-triazacyclononane-1,4-diyldiacetate **78**

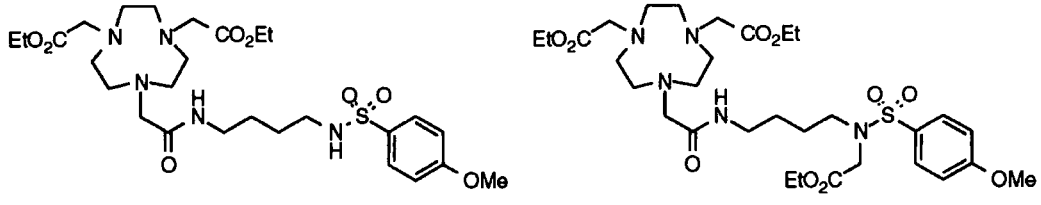

The crude amide **75** (1.49g, ~3.5mmol), caesium carbonate (2 equiv.), and ethyl bromoacetate (2 equiv.) were stirred in ethanol (30ml) at room temperature, raising to 60°C overnight. The ethanol was removed by concentrating repeatedly after addition of CH_2Cl_2, decanting the liquid from the residual solid. Repeated attempts at chromatographic purification, gradient elution EtOH:CH_2Cl_2 (0-5% EtOH) afforded a yellow oil 92mg, 4.4%.

TLC (2% EtOH:CH_2Cl_2) R_f=0.7 ^{1}H NMR ($CDCl_3$) 1.23 (6H, t, CH_3); 1.47 (4H, br m, CH_2); 2.61 (2H, br m, $C\underline{H}_2NHSO_2$); 2.80 (8H, m, CH_2); 3.20 (6H, m, CH_2); 3.35 (2H, s, $NC\underline{H}_2CONH$); 3.83 (3H, s, OMe); 4.12 (4H, q, OCH_2); 5.45 (1H, t, $NHSO_2$); 6.93 & 7.76 (2 x 2H, 2 x d, ArH); 8.9 (1H, t, NHCO) ^{13}C NMR ($CDCl_3$) 14.2(CH_3), 26.6, 27.0(CH_2), 38.3, 42.6, 55.0, 55.5, 56.0, 56.3, 58.2, 60.3, 61.3(CH_2N+OCH_3+OCH_2), 114.1, 129.0, 131.7(Ar),162.6(COMe), 171.8, 172.8(CO). IR (film) 3188, 2931, 1738 (ester), 1652 (amide) MS (DCI) 600 (M^++1) $C_{27}H_{45}N_5O_8S$ requires 599.2989 found 599.2985

The alkylated sulfonamide product **79** was characterised by ^{1}H NMR and MS.

^{1}H NMR ($CDCl_3$) 1.20 (3H, t, Ts'$NCH_2CO_2CH_2C\underline{H}_3$), 1.27 (6H, t, CH_3), 1.5 (4H, br m, CH_2, side chain), 2.6-3.4(22H, br m, CH_2N), 3.8 (3H, s, OMe), 4.08 (2H, q, Ts'$NCH_2CO_2C\underline{H}_2CH_3$), 4.16 (4H, q, $OC\underline{H}_2CH_3$), 6.9 & 7.8(4H, 2 x d, ArH) MS (DCI) 686 (M^++1)

7-[(4-methoxybenzenesulfonamido)carbamoylmethyl]-1,4,7-triazacyclononane-1,4-diyldiacetic acid **76**

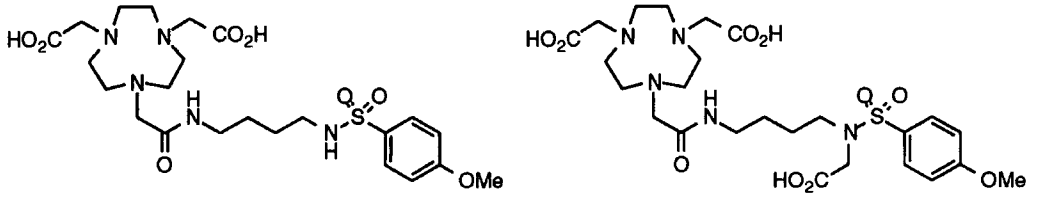

To a stirred solution of the previously prepared crude amine **75** (1.93g, ~3.6mmol) and chloroacetic acid (1.70g, 18mmol) at 60°C, was slowly added lithium hydroxide (432mg, 18mmol), to keep the pH in the range 9.5-10.5. The reaction was monitored by anion exchange HPLC. The reaction was stopped after 3 days, as the $NHSO_2$ alkylated material **77** was observed on the HPLC trace. The pH was lowered to 3 and repeated washes with diethylether removed much of the unreacted chloroacetic acid. The pH was then raised to neutral and the volume reduced to make the sample amenable to preparative HPLC. Two columns were required to give a yellow oil (675mg, 34%).

HPLC: Dynamax 60A (10ml min^{-1}); elution A=MeCN/TFA; B=H_2O/TFA from 10% A, 90% B to 25% A, 75% B over 20 minutes; observed λ=278nm; R_t=11-14 minutes. Synchropak AX100 (5ml min^{-1}); elution A=MeCN; B=H_2O; C=NH_4OAc pH=5.6 from 20% A, 70% B, 10% C to 20% A, 0% B, 80% C in 20 minutes R_t(product)=8.0 minutes ^{1}H NMR(D_2O, pD ~4) 1.24(4H,br, CH_2); 2.61(4H, br m, CH_2N); 2.77(2H, m, $C\underline{H}_2NHSO_2$); 2.91(6H, m, CH_2N); 3.03(4H, m, CH_2N); 3.23(2H, s, $NC\underline{H}_2CONH$); 3.45(4H, s, $NC\underline{H}_2CO_2H$); 3.73(3H, s, OMe); 6.97 & 7.64(2 x 2H, 2 x d (J=8.8Hz), ArH) ^{13}C NMR(D_2O) 24.6, 29.0, 41.7, 45.3, 51.4, 52.0, 53.7, 58.6, 58.6, 60.1, 62.9

(CH_2N+OCH_3), 117.5, 131.9, 133.1(Ar), 165.6, 176.3(CO) IR(film) 3376, 3272, 3098, 2948, 1725, 1672, 1597, 1498, 1321, 1261, 1199, 1153 MS(DCI) 259(100%, fragment in which the NCH_2--CONH bond has been cleaved) 544(M^++1)

The side product, R_t($NHSO_2$ alkylated side product **77**)=15.2 minutes, was characterised by proton NMR

^{1}H NMR(D_2O) 1.3(4H, br m, CH_2), 2.6(4H, br m, CH_2N), 2.96(6H, m, CH_2N), 3.08(6H, m, CH_2N), 3.28(2H, s, $NC\underline{H}_2CONH$), 3.50(4H, s, $NC\underline{H}_2CO_2H$ exo to ring), 3.68(2H, s, $NC\underline{H}_2CO_2H$ diagnostic peak), 3.76(3H, s, OMe), 7.0 & 7.7(2 x 2H, 2 x d (J=8.9Hz), ArH)

7-[(4-aminobutyl)carbamoylmethyl]-1,4,7-triazacyclononane-1,4-diyldiacetic acid **58**

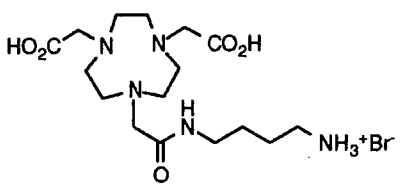

The diester **78** (74mg, 0.124mmol) and phenol (150mg, large excess) were stirred at 110°C for 24 hours in HBr solution (45% w/v in acetic acid, 8ml). Additional HBr solution (4ml) was then added, and the reaction continued for a further 24 hours. Cooling to room temperature gave a brown solid. (58mg), mixed counter ions (AcO^-, Br^-)

^{1}H NMR (D_2O) 1.4(4H, m, alkyl CH_2); 2.76(2H, t, CH_2N), 3.02(2H, t, CH_2N), 3.33(8H, br m, CH_2N (ring)), 3.4(4H, s, CH_2N (ring)), 3.76(2H, s, $NC\underline{H}_2CONH$), 3.93(4H, s, $NC\underline{H}_2CO_2H$) ^{13}C NMR 24.0, 25.1(CH_2), 38.9, 42.8, 50.1, 51.2, 56.8, 58.0(CH_2N), 168.0, 170.4(CO) IR (film) 1737 (acid), 1673 (amide) MS(ES+) 374.1 (M^++1), 187.7 $(M+1)^{2+}$

Detosylation of **76**

The above compound was also prepared by deprotection of **76**. The sulfonamide (319mg, 0.588 mmol, TFA salt) and phenol (600mg, a large excess) were dissolved in 45%HBr/AcOH (10ml) and stirred at 110°C for 2 days. The cooled solution was then added dropwise to a flask containing ether (200ml), whereupon the product precipitated as a beige solid (257mg, 96%).

4-[(4-methoxybenzenesulfonamido) carbamoylmethyl]-1,4,7-triazacyclononane-1-ylacetic acid **80**

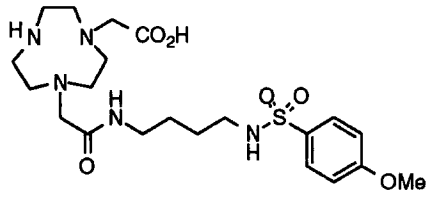

The crude diamine **75** (1.46g, 2.73mmol, assumed from previous step) was dissolved in water (25ml) with chloroacetic acid (645mg, 6.83mmol). Solid lithium hydroxide was added carefully over a period of two days, to maintain the pH=10. When the reaction was complete, the volume was reduced to 1ml. The title compound was isolated by preparative HPLC as the trifluoroacetate salt (482mg, 29%).

HPLC: Dynamax 60A (10ml min^{-1}); elution A=MeCN/TFA; B=H_2O/TFA from 10% A, 90% B to 25% A, 75% B over 20 minutes; observed λ=278nm; R_t=10-11 minutes. ^1H NMR(D_2O, pD ~4) 1.08(4H,br, CH_2); 2.47(2H, br m, $C\underline{H}_2NHSO_2$); 2.80(2H, m, $C\underline{H}_2NHCO$); 3.02(4H, s, CH_2N); 3.21(8H, m, CH_2N); 3.49(3H, s, OMe), 3.58 & 3.74(2H+2H, 2x s, $NC\underline{H}_2CONH + NC\underline{H}_2CO_2H$); 6.70 & 7.39(2 x 2H, 2 x d (J=8.8Hz), ArH) ^{13}C NMR($CDCl_3$) 28.1, 28.8(CH2), 41.8, 45.0, 45.4, 45.7,52.7, 53.6, 53.8, 54.1(CH_2N), 58.3(CH_3), 58.6, 60.4($N\underline{C}H_2CO$), 117.3, 131.7, 132.8(Ar), 165.5(COMe), 171.2, 174.9(CO) IR(film) 2500, 3500 (v br), 1680, 1596, 1496, 1446, 1318, 1266, 1202, 1148 MS(ES+) 486.46

2-[4-[(4-methoxybenzenesulfonamido) carbamoylmethyl]-1,4,7-triazacyclononane-7-ylacetic acid]-N-benzoyl-5-aminopentyl ethanoate **82**

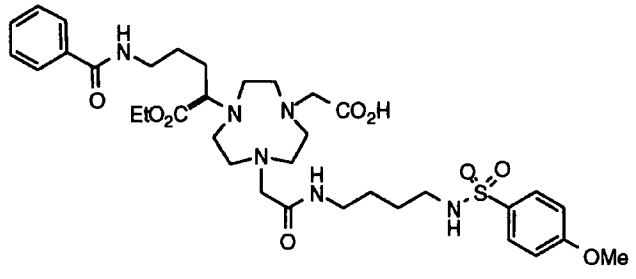

To the TFA salt of **80** (347mg, 0.579mmol) and caesium carbonate (480mg, 1.529mmol) in DMF (15ml) was added 2-bromo-N-benzoyl-5-aminopentyl ethanoate **81**, prepared by Fiona Smith (190mg, 0.579mmol), dissolved in DMF (5ml) over a period of 3 hours at 60°C. The mixture was allowed to stir for a further 18 hours. The DMF was then removed. Preparative HPLC afforded the N,N'-diprotected cycle (71mg, 14%).

HPLC: Dynamax 60A (10ml min^{-1}); elution A=MeCN/TFA; B=H_2O/TFA from 10% A, 90% B to 90% A, 10% B over 20 minutes; observed λ=254nm; R_t=16.2 minutes. ^1H NMR($CDCl_3$) 1.17(3H, t, CH3), 1.42(4H, br, CH_2); 1.57(2H, br, CH_2); 1.88(2H, br, CH_2); 2.5-3.7(23H, br m (maxima at 2.75, 3.10, 3.38, 3.56), CH_2N), 3.76(3H, s, OMe), 4.10(2H, q, $OC\underline{H}_2CH_3$), 5.01(1H, br t, $NHSO_2$), 6.85(2H, d , ArH), 7.02(1H, br t, CONH), 7.34(4H, m, ArH + CONH), 7.69(4H, t like m, ArH) ^{13}C NMR($CDCl_3$) 14.0(CH_3), 25.2, 26.3 (m), 28.3(CH_2), 39.2 (m), 42.6, 43.8(CH_2N), 55.5(OCH_3), 61.8(OCH_2), 72.7(CHN), 114.2, 127.0, 128.5, 129.0, 131.3, 131.5, 134.2, 162.7(Ar), 168.0, 169.7, 169.7, 171.4(CO) IR(film) 3400 (br), 1744, 1688, 1660, 1552, 1496, 1456, 1314, 1262, 1194, 1150 MS(CI) 733 An accurate mass could not be obtained at the Swansea Centre due to the low intensity of the molecular ion under the probe conditions.

N-(6-carboxyhexyl)maleamic acid[9] **88**

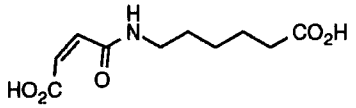

Maleic anhydride (1.13g, 11.5mmol) and 6-aminocaproic acid (1.51g, 11.5mmol) were suspended in diethyl ether (~30ml), then brought to reflux overnight. Cooling afforded a white solid, a mixture of the starting materials, and the desired product (~25:75% estimated from NMR intensities.) The product was used in the next step, without further purification.

^1H NMR (CD_3OD) 1.4 (2H, m, CH_2), 1.6 (4H, m, CH_2), 2.31 (2H, t, $C\underline{H}_2CO_2H$), 6.25 (1H, d (J=13Hz), CH vinylic, cis), 6.46 (1H, d (J=13Hz), CH vinylic, cis)

N-(6-carboxyhexyl)maleimide[9] **89**

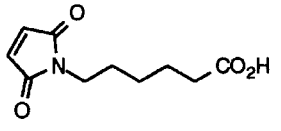

The crude maleimic acid **88** prepared above was stirred in acetic anhydride (30ml). To this was added sodium acetate (1.06g), and the reaction left to stir at 50°C overnight. Water (100ml) was then added and the mixture stirred at 60°C for 3 hours. Extraction into ethyl acetate (3 x 100ml), and concentration, afforded a brown oil. Addition of $CHCl_3$ gave a beige precipitate of trans maleimic acid. This was filtered off and the remainder recrystallised (EtOAc/ hexane) to give the product as a white solid. (712mg, 29%).

^{1}H NMR ($CDCl_3$) 1.31 (2H, m, CH_2), 1.59 (4H, m, CH_2), 2.32 (2H, t, $C\underline{H}_2CO_2H$), 3.50 (2H, t, CH_2N), 6.69 (2H, s, CH), ~11.5 (1H, br s, CO_2H) ^{13}C NMR ($CDCl_3$) 24.5, 26.6, 34.3, 38.0, 134.5, 171.4, 180.0 m.p. 81.0-82.0°C (lit.[10] 89-90°C)

N-succinimidyl-6-maleimidohexanoate[9] **85**

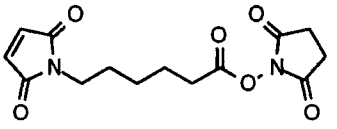

The acid **89** prepared above (130mg, 0.62mmol) and N-hydroxysuccinimide (71mg, 1equiv.) were dissolved at 0°C in DMF (10ml). To this was added dicyclohexylcarbodiimide, DCC, (155mg, 1.2equiv.) in DMF (20ml). The reaction was kept at 0°C for 2 hours, and then left to raise to room temperature overnight. The DMF was removed, and CH_2Cl_2 added. The DCU was filtered off. Column chromatography on flash silica (100% EtOAc) gave a white solid after concentration (80mg, 42%).

TLC (50%EtOAc:Hexane) R_f = 0.3 ^{1}H NMR ($CDCl_3$) 1.38 (2H, m, CH_2), 1.60 (2H, p, CH_2), 1.73 (2H, p, CH_2), 2.56 (2H, t, CH_2CO_2N), 2.80 (4H, s, CH_2CO), 3.49 (2H, t, CH_2N), 6.66 (2H, s, CH) m.p. 60-65°C (lit.[9] 62-65°C)

4-nitrophenyl-6-maleimidohexanoate **86**

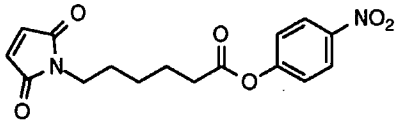

To a mixture of paranitrophenol (468mg, 3.37mmol) and N-(6-carboxyhexyl)maleimide **89** (712mg, 3.37mmol) at 0°C in DMF (20ml), was added dicyclohexylcarbodiimide (DCC, 834mg, 4.05mmol) in DMF (20ml) over a period of 10 minutes. Stirring continued, and the reaction raised to room temperature over 16 hours. The DMF was then removed under reduced pressure, and the residue taken up in dichloromethane. The precipitated dicyclohexyl urea was filtered off, and silica chromatography (flash, 20-100% EtOAc:hexane) afforded a lilac solid. (275mg, 25%)

TLC (50%EtOAc:Hexane) R_f = 0.3 ^{1}H NMR($CDCl_3$) 1.4(2H, m, CH_2), 1.65(2H, m, CH_2), 1.8(2H, m, CH_2), 2.60(2H, t, CH_2CO), 3.55(2H, t, CH_2N), 6.70(2H, s, CH vinylic), 7.27(2H, d, ArH), 8.27(2H, d, ArH) ^{13}C NMR ($CDCl_3$) 23.9, 24.6, 25.8, 27.9, 33.7(CH_2), 37.2(CH_2N), 122.2, 124.9, 133.9(Ar+maleimide), 144.9, 155.2(Ar), 170.6, 170.7(CO) IR(film) 2933, 1765 (ester), 1705 (amide), 1615, 1592, 1523 MS(DCI) 211 (acid), 350

$(M+NH4)^+$ Found C=57.6 H=4.97 N=8.34 $C_{16}H_{16}N_2O_6$ requires C=57.8 H=4.82 N=8.43 m.p. 63.0-64.0°C

Bis-4-nitrophenyl-1,4-butanoate [11] **87**

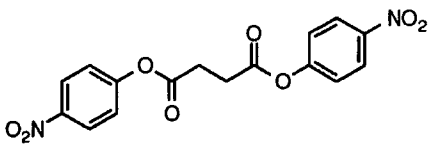

Paranitrophenol (4.72g, 33.9mmol) and succinic acid (2.0g, 16.9mmol) were stirred in THF (100ml) at 0°C. DCC (7.33g, 35.6mmol) dissolved in THF was then added slowly. Dicyclohexyl urea was precipitated during the course of the reaction, as the temperature was allowed to increase to room temperature over 24 hours. The precipitate was filtered off, and the crude ester columned on silica, using 100% CH_2Cl_2 as an eluent. The crude material was loaded on silica, due to poor solubility in dichloromethane. A white solid was collected (2.0g, 33%). Unreacted bis active ester was reclaimed from future reactions, purified by recrystallisation from 1,4-dioxane.

TLC (100% CH_2Cl_2) R_f=0.8 ^{1}H NMR($CDCl_3$, poorly soluble) 3.06(4H, s, CH_2CO), 7.31(4H, d (J=9.2Hz), ArH), 8.28(4H, d (J=9.2Hz), ArH) m.p. 178-180°C (dec.)

12-(4-(N-(3-maleimidopropyl)amidomethyl) benzylamine)-1,4,7,10-tetraazacyclotridecane **91**

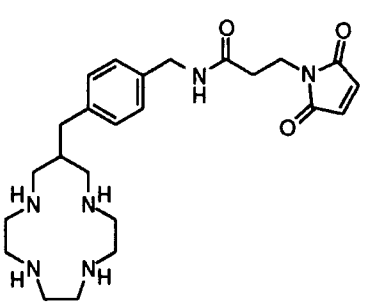

The reaction was performed similarly to the above preparation of the biotin conjugate **69**. Following with cation exchange HPLC, the macrocycle **48** (32mg, 0.106mmol) and the hydroxysuccinimidyl active ester **90** (22mg, 0.083mmol) were reacted in the equivolume PIPES/dioxane solvent. The reaction went to completion in under 30 minutes. Acidifying precipitated the PIPES, which was filtered off. Washing with ether was followed by reverse phase HPLC purification. An off white glass was obtained (20mg, 53%)

HPLC Synchropak CM300 (1.4ml min^{-1}); elution A=MeCN; B=H_2O; C=NH_4OAc pH=5.6 from 20% A, 70% B, 10% C to 20% A, 0% B, 80% C in 20 minutes R_t(product)=6.0 minutes ^1H NMR(D_2O, pD ~4) 2.13(1H, m, CH), 2.5(2H, t, $COC\underline{H}_2CH_2N$), 2.65(2H, d, $ArC\underline{H}_2CH$), 2.8-3.2(16H, m, CH_2N ring), 3.75(2H, t, CH_2N(mal)), 4.23(2H, s, $ArC\underline{H}_2N$), 6.73(2H, s, vinylic), 7.18(4H, s, ArH) ^{13}C NMR(D_2O) 34.3, 34.4, 35.9, 36.5, 42.5, 43.9, 45.6, 51.9(CH+$\underline{C}H_2CO$+CH_2Ar+CH_2N), 127.6, 129.2, 134.1, 138(Ar+Maleimide), 173, 174(CO) IR(KBr disc) 3446, 1711, 1681, 1203, 1132 MS(ES+) 229.3 ($(M+2H)^{2+}$, 85%)), 457.6 ($(M+H)^+$, 100%)

The copper complex $[Cu(\mathbf{91})]^{2+}$ was made as for the biotin complex $[Cu(\mathbf{69})]^{2+}$ above.

IR(KBr disc) 3413(water), 1694, 1631, 1405, 1196 MS(ES+) 516.3:518.3 (3:1) ie M^+-3 with expected copper isotope pattern. Also 599.7(+Br^-), 633.9(+Br^-+$2H_2O$), peaks every 120 mass units, corresponding to a clustering of KBr, 8 & 11 KBr units more intense than neighbouring multiples

7-[4-((4-amidobutyl)-4-maleimidobutyl)carboxyethyl) carbamoyl-1,4,7-triazacyclononane-1,4-diyldiactic acid **92**

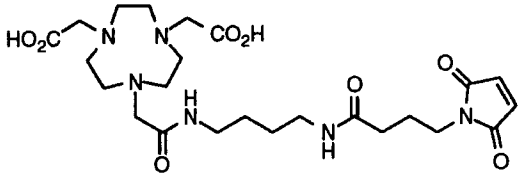

To the HBr salt of **58** (100mg, 0.22mmol) in PIPES buffer (0.75ml) was added N-succinimidyl-4-maleimidobutyric acid (250mg, 0.88mmol) in 1,4-dioxane (0.75ml). A suspension formed, but the majority of material remained in solution. After 4 hours, with periodic vortex mixing, the supernatant was subjected to preparative HPLC. The ligand was collected as an offwhite solid (9.8mg, 8.3%)

HPLC: Dynamax 60A (10ml min^{-1}); elution A=MeCN/TFA; B=H_2O/TFA from 10% A, 90% B to 25% A, 75% B over 20 minutes; observed λ=302nm; R_t=11.6 minutes. ^1H NMR (D_2O) 1.29(4H, m, CH_2), 1.69(2H, p, CH_2), 2.04(2H, t, CH_2CO), 2.8-3.1(12H, m (maxima at 2.86, 3.02, 3.05), CH_2N (sidechain), CH_2N (ring γ, δ to amide carbonyl)), 3.13(4H, s, CH_2N (ring, opposite unique nitogen)), 3.27(2H, t, CH_2N (maleimide)), 3.46(2H, s, NCH_2CO), 3.69(4H, s, NCH_2CO), 6.64(2H, s, CH) ^{13}C NMR(D_2O) 26.6, 28.8, 28.9, 35.9(CH_2), 40.0, 42.1, 52.3, 52.5, 52.6, 53.5, 59.4, 61.7(CH_2N), 137.3(CH, maleimide), 174.5(CO), 175.3 (2C, CO, maleimide), 176.1, 178.3(CO) IR(film) 3200-3600, 2942, 2872, 1705 (with shoulder to low frequency),

1553, 1411, 1200, 1135 MS(ES+) 539.41 (100%, M + 1) 561.35 (93%, M + Na)
$C_{24}H_{38}N_6O_8Na$ requires 561.35

7-(1-carboxylic acid-4-amidobutyl)-4-nitrophenyl)carboxyethyl) -1,4,7-triazacyclononane-1,4-diyldiactic acid[12] **29**

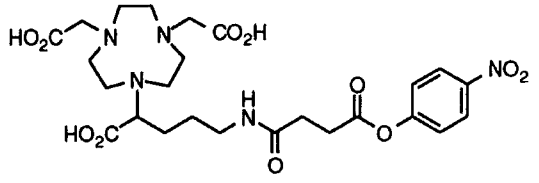

To crude **52** (42mg, 0.106mmol) in DMSO (1ml) was added solid bisnitrophenyl-1,4-butanoate **87** (115mg, 0.318mmol) and triethylamine (75mg, 103µl, 0.742mmol) with vigorous mixing. The reaction was followed by HPLC, and terminated by cooling the solution to -78°C after 40 minutes at room temperature. The title compound was isolated by preparative HPLC, to give a lemon solid. (15mg, 23%)

HPLC: Dynamax 60A (10ml min^{-1}); elution A=MeCN/TFA; B=H_2O/TFA from 10% A, 90% B to 25% A, 75% B over 20 minutes; observed λ=278nm; R_t=15.5 minutes. ^1H NMR (D_2O) 1.5-1.9(4H, br m, CH_2), 2.53(2H, t, $C\underline{H}_2CO_2Ar$), 2.79(2H, t, $C\underline{H}_2CONH$), 2.8-3.2(10H, m (maxima at 2.84, 2.91, 3.02), CH_2N), 3.42(2H, m, CH_2N), 3.53(2H, m, CH_2N), 3.65(4H, s, $NC\underline{H}_2CO_2H$), 3.83(1H, s, $NC\underline{H}CO_2H$), 7.22 & 8.19(2H, 2x d, Ar)

7-[4-((4-amidobutyl)-4-nitrophenyl)carboxyethyl) carbamoyl-1,4,7-triazacyclononane-1,4-diyldiactic acid **93**

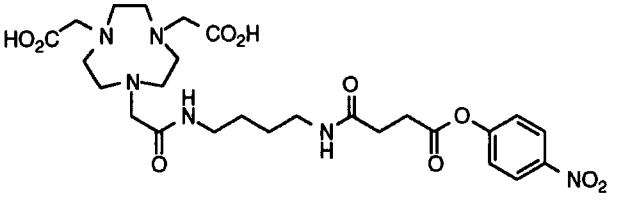

To **58** (40mg, 0.088mmol) in PIPES buffer (1ml) was added bis-4-nitrophenyl-1,4-butanoate **87** (95mg, 0.264mmol) in 1,4-dioxane (1ml). The reaction was heated to 60°C with periodic vortex mixing. The reaction was stopped after 4 hours. Preparative HPLC afforded a minute sample of a pale yellow solid (<1mg), which slowly decomposed in deuterium oxide, liberating 4-nitrophenol.

HPLC: Dynamax 60A (10ml min^{-1}); elution A=MeCN/TFA; B=H_2O/TFA from 10% A, 90% B to 25% A, 75% B over 20 minutes; observed λ=278nm; R_t=14.2 minutes. ^1H NMR (D_2O) 1.35(4H, m, CH_2), 2.5(2H, t, CH_2CO), 2.6-3.8(24H, m (maxima at 2.9(t like), 3.0(t like), 3.1, 3.6)), 7.15(2H, d, ArH), 8.1(2H, d, ArH) MS(ES-) 593.40 (M^+-1)

9-Acridine carbamoylethyl-2-(2-aminoethyl)-2-methyl amine **94**

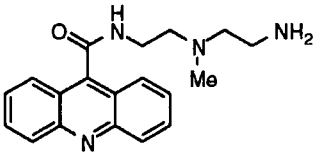

The amino amide was prepared by a similar method to Fiona Smith,[13] but, in the absence of DMAP. To an ice cold stirred solution of N-methyldiethylenetriamine **96** (590mg, 5mmol) in CH_2Cl_2 (1ml) was added 9-acridine carboxylic acid chloride (prepared by dissolving the carboxylic acid (200mg, 0.9mmol) in thioyl chloride (1.5ml), and removing the excess *in vacuo*, followed by reconstituting the acid chloride in CH_2Cl_2 (5ml)). A white precipitate formed immediately. The reaction was allowed to rise to room temperature, whilst stirring continued for a further 15 hours. Aqueous potassium hydroxide (1.0mol dm^{-3}, 10ml) was then added, followed by extraction with $CHCl_3$. The compound was purified by HPLC to give the required amine, a viscous yellow glass, as the trifluoroacetate salt. (391mg, 80%)

HPLC: Dynamax 60A (10ml min^{-1}); elution A=MeCN/TFA; B=H_2O/TFA from 10% A, 90% B to 90% A, 10% B over 20 minutes; observed λ=320nm; R_t=10.4 minutes. ^1H NMR(D_2O, pD ~3) 2.90(3H, s, NCH_3), 3.36(2H, m, $C\underline{H}_2NH_2$), 3.49(4H, m, CH_2N), 3.91(2H, t, $CONHC\underline{H}_2$), 7.66(2H, m, ArH), 7.97(6H, m, ArH) MS(ES+) 323.11 (M^++1) ($C_{19}H_{22}N_4O$ requires 323.18)

9-Acridine carbamoylethyl-2-(2-(4-nitrophenyl carboxyethyl) amidoethyl-N-methylamine **95**

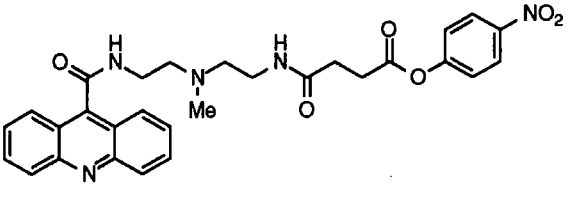

Following a procedure adapted from Fiona Smith,[12] to a vortex mixed solution of the previously prepared acridine amine **94** (60mg, 0.11mmol) in DMSO (0.5ml) was added

the bis ester (120mg, 0.33mmol), which was only partially soluble. Triethylamine (22.4mg, 31μL, 0.22mmol) was added with violent mixing. After 5 minutes mixing, the reaction was quenched by the addition of TFA (1 drop). Purification by HPLC afforded the acridine active ester (14mg, 20%) as a TFA salt.

HPLC: Dynamax 60A (10ml min^{-1}); elution A=MeCN/TFA; B=H_2O/TFA from 10% A, 90% B to 75% A, 25% B over 20 minutes then 100% A; observed λ=353nm; R_t=14.6 minutes. ^1H NMR(D_2O) 2.25(4H, m, CH_2CO), 2.94(3H, s, NCH_3), 3.35(2H, m, $C\underline{H}_2NHCO$), 3.54(4H, m, CH_2N), 3.88(2H, t, $CONHC\underline{H}_2$), 6.82(2H, d, ArH), 7.8(2H, m, ArH (acridine)), 7.77(2H, m, ArH), 7.97(6H, m, ArH (Acridine) MS(ES+) 544.29 (M^++1) ($C_{29}H_{30}N_5O_6$ requires 544.22) A sharp decomposition point was not observed for this compound.

9-Acridine carbamoylethyl-2-(bis(2-aminoethyl)) amine **97**

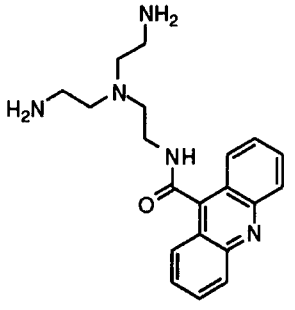

Acridine-9-carboxylic acid (250mg, 1.12mmol) was refluxed for 3 hours in thionyl chloride (5ml). The excess thionyl chloride was removed *in vacuo*, followed by the four times repeated cycle of addition of CH_2Cl_2 and evaporation to dryness. The acid chloride was taken up in CH_2Cl_2 (5ml), and slowly added to a stirred ice cold solution of tris(aminoethyl) amine (1.2g, 8.22mmol) in CH_2Cl_2 (5ml), immediately forming a precipitate of the hydrochloride salt. The temperature of the reaction was then allowed to rise to room temperature over 30 minutes, when KOH solution was added to attain a pH = 13. Extraction into $CHCl_3$ (3 x 20ml) gave a sample which, on concentration, was amenable to HPLC purification, to give a yellow oil, the TFA salt. (415mg, 54% yield)

HPLC: Dynamax 60A (10ml min^{-1}); elution A=MeCN/TFA; B=H_2O/TFA from 10% A, 90% B to 75% A, 25% B over 20 minutes then 100% A; observed λ=302nm; R_t=8.0 minutes. ^1H NMR(D_2O) 3.04(10H, symmetric m, CH_2N), 3.72(2H, t, $CONHC\underline{H}_2$), 7.75(2H, m, ArH (acridine)), 8.05(6H, m, ArH (Acridine) MS(ES+) 176.8 $(M+1)^{2+}$

Acridine maleimide amines **98** and **99**

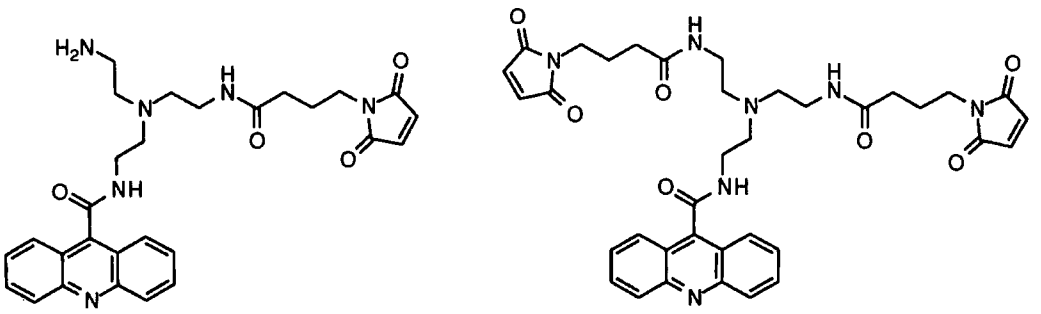

To the triamine **97** prepared above (54mg, 0.155mmol), dissolved in PIPES buffer (0.5ml), was added a solution of N-hydroxysuccinimide-4-maleimidobutanoate (43.4mg, 0.155mmol) in 1,4-dioxane (0.5ml). The reaction went turbid on addition, as the buffer came out of solution. The pH remained at 6.8. The reaction at room temperature was followed by reverse phase HPLC, and was terminated by the addition of acid after 4 hours. The PIPES was filtered off, and the filtrate purified by HPLC, to give **98** as the TFA salt, a bright yellow solid (14mg, 13%)

HPLC: Dynamax 60A (10ml min^{-1}); elution A=MeCN/TFA; B=H_2O/TFA from 10% A, 90% B to 75% A, 25% B over 40 minutes; observed λ=302nm; R_t=14.4 minutes. ^1H NMR(D_2O, pD ~4) 1.50(2H, p, CH_2), 2.03(2H, t, CH_2CO), 3.16(2H, t, CH_2N(maleimide)), 3.2-3.5(10H, m, CH_2N+CONHC$\underline{H}_2$), 3.94(2H, br t, ArCONHC$\underline{H}_2$), 6.57(2H, s, CH), 7.87(2H, m, ArH), 8.22(8H, m, ArH) ^{13}C NMR(D_2O) 23.2(CH_2), 32.0, 34.3, 35.3, 35.8, 36.5, 49.8, 51.8, 52.7, 54.0(CH_2N), 120.1, 122.2, 125. 9, 129.3, 134.1, 137.7, 141.1, 149.5, 166.8(Ar+maleimide), 172.7, 176.6(CO) IR(film) 3400 (br), 1676, 1551, 1432, 1202, 1133 MS(ES+) 517.42 (M^++1)

The acridine bismaleimide compound **99** was identified as well, also a yellow solid (20mg, 33%).

HPLC: R_t=17.9 minutes ^1H NMR(D_2O, pD ~4) 1.41(4H, p, CH_2), 2.03(4H, t, CH_2CO), 3.12(4H, t, CH_2N(maleimide)), 3.51(8H, m, CH_2N+CONHC$\underline{H}_2$), 3.68(2H, br t, C$\underline{H}_2$N), 3.98(2H, br t, ArCONHC$\underline{H}_2$), 6.59(4H, s, CH), 7.87(2H, m, ArH), 8.21(8H, m, ArH) ^{13}C NMR(D_2O) 23.1(CH_2), 32.1, 34.6, 35.6, 36.4, 38.4, 53.2, 54.6(CH_2N), 120.2, 122.1, 126.0, 129.2, 134.0, 137.6, 140.1, 153.8, 166.8(Ar+maleimide), 172.6, 176.6(CO) IR (film) 3423(br), 1704, 1553, 1414, 1203, 1138 MS(ES+) 683.10 (M^++2)

5.3. References

1. W. DeW. Horrocks, Jr. and D.R. Sudnick, *Science* 1979, **206**, 1194

2. J.P.L. Cox, *PhD Thesis*, University of Durham, 1989
3. H. Stetter and W. Frank, *Angew. Chem., Int. Ed. Engl.*, 1976, **15**, 686
4. S. Aime, A.S. Batsanov, M. Botta, J.A.K. Howard, D. Parker, K. Senanayake and G.Williams, *Inorg. Chem.*, 1994, **33**, 4696
5. J.R. Morphy, D. Parker, R. Kataky, M.A.W. Eaton, A.T. Millican, R. Alexander, A.Harrison and C. Walker, *J. Chem. Soc., Perkin Trans. 2*, 1990, 573
6. R.K. Garlick, R.W. Giese, *J. Biol. Chem.*, 1988, **263**, 210
7. K. Wieghardt, U. Bossek, P. Chaudhuri, W. Herrmann, B.C. Menke and J. Weiss, Inorg. Chem., 1982, **21**, 4308
8. K.P. Pulukkody, T.J. Norman, D. Parker, L. Royle and C.J. Broan, *J.Chem. Soc., Perkin Trans. 2*, 1993, 605
9. S. Yoshitake, Y. Yamada, E. Ishikawa and R. Masseyeff, *Eur. J. Biochem.*, 1979, **101**, 395
10. O. Keller and J. Rudinger, *Helv. Chim. Acta.*, 1975, **58**, 531
11. T. J. Norman, *PhD Thesis*, University of Durham, 1994
12. T.J. Norman, F.C.Smith, D. Parker, A. Harrison, L. Royle and C.A. Walker, *Supramolecular Chemistry*, 1995, **4**, 308
13. T.J. Norman, D. Parker, F.C. Smith and D.J. King, *Chem. Commun.*, 1995, 1879

Appendix

The author attended the following lecture courses:

NMR Spectroscopy, by Dr. A.M. Kenwright, Dr. P.G. Steel and Prof. D. Parker
Organometallic Chemistry, by Prof. V.C. Gibson and Prof. D. Parker
Diffraction Techniques, by Prof. J.A.K. Howard
Amino Acids, Peptides and Proteins by Dr. M. Richardson

The author attended the following colloquia between October 1993 and September 1996:

1993

October 14 Dr. P. Hubberstey, University of Nottingham
Alkali Metals: Alchemist's Nightmare, Biochemist's Puzzle and Technologist's Dream

October 20 Dr. P. Quayle†, University of Manchester
Aspects of Aqueous ROMP Chemistry

October 27 Dr. R.A.L. Jones†, Cavendish Laboratory, Cambridge
Perambulating Polymers

November 25 Dr. R.P. Wayne, University of Oxford
The Origin and Evolution of the Atmosphere

December 1 Prof. M.A. McKervey†, Queen's University, Belfast
Synthesis and Applications of Chemically Modified Calixarenes

December 8 Prof. O. Meth-Cohn†, University of Sunderland
Friedel's Folly Revisited - A Super Way to Fused Pyridines

1994

February 9 Prof. D. Young†, University of Sussex
Chemical and Biological Studies on the Coenzyme Tetrahydrofolic Acid

March 2 Dr. C. Hunter†, University of Sheffield
Noncovalent Interactions between Aromatic Molecules

March 10 Prof. S.V. Ley, University of Cambridge
New Methods for Organic Synthesis

March 25 Dr. J. Dilworth, University of Essex
Technetium and Rhenium Compounds with Applications as Imaging Agents

April 28 Prof. R. J. Gillespie, McMaster University, Canada
The Molecular Structure of some Metal Fluorides and Oxofluorides: Apparent Exceptions to the VSEPR Model.

November 16 Prof. M. Page, University of Huddersfield
Four-membered Rings and β-Lactamase

November 23 Dr J. M. J. Williams, University of Loughborough
New Approaches to Asymmetric Catalysis

1995

January 11 Prof. P. Parsons, University of Reading
Applications of Tandem Reactions in Organic Synthesis

January 18 Dr G. Rumbles, Imperial College, London
Real or Imaginary Third Order Non-linear Optical Materials

January 25 Dr D. A. Roberts, Zeneca Pharmaceuticals
The Design and Synthesis of Inhibitors of the Renin-angiotensin System

February 8 Dr D. O'Hare, Oxford University
Synthesis and Solid-state Properties of Poly-, Oligo- and Multidecker Metallocenes

March 1 Dr M. Rosseinsky, Oxford University
Fullerene Intercalation Chemistry

April 26 Dr M. Schroder, University of Edinburgh
Redox-active Macrocyclic Complexes : Rings, Stacks and Liquid Crystals

May 4 Prof. A. J. Kresge, University of Toronto
The Ingold Lecture Reactive Intermediates : Carboxylic-acid Enols and Other Unstable Species

October 13 Prof. R. Schmultzer, Univ Braunschweig, FRG.
Calixarene-Phosphorus Chemistry: A New Dimension in Phosphorus Chemistry

October 18 Prof. A. Alexakis, Univ. Pierre et Marie Curie, Paris,
Synthetic and Analytical Uses of Chiral Diamines

November 1 Prof. W. Motherwell, UCL London
New Reactions for Organic Synthesis

November 8 Dr. D. Craig, Imperial College, London
New Stategies for the Assembly of Heterocyclic Systems

December 8 Professor M.T. Reetz, Max Planck Institut, Mulheim
Perkin Regional Meeting

1996

January 10 Dr Bill Henderson, Waikato University, NZ
Electrospray Mass Spectrometry - a new sporting technique

January 17 Prof. J. W. Emsley , Southampton University
Liquid Crystals: More than Meets the Eye

January 24 Dr Alan Armstrong, Nottingham Univesity
Alkene Oxidation and Natural Product Synthesis

February 12 Dr Paul Pringle, University of Bristol
Catalytic Self-Replication of Phosphines on Platinum(O)

February 28 Prof. E. W. Randall, Queen Mary & Westfield College
New Perspectives in NMR Imaging

March 6 Dr Richard Whitby, Univ of Southampton
New approaches to chiral catalysts: Induction of planar and metal centred asymmetry

March 7 Dr D.S. Wright, University of Cambridge
Synthetic Applications of Me_2N-p-Block Metal Reagents

March 12 RSC Endowed Lecture - Prof. V. Balzani, Univ of Bologna
Supramolecular Photochemistry

† Invited specially for the graduate training programme.

Conferences

The author attended the following meetings:

1. North of England Cancer Research Campaign Meeting,* University of Newcastle, 26th July 1994
2. Stereochemistry at Sheffield, University of Sheffield, 14th December 1994
3. RSC UK Macrocycles Group, University of Newcastle, 4-5th January 1995
4. International Isotope Society, UK Group Meeting, Fison's Pharmaceuticals, Loughborough, 22nd May 1995
5. International Symposium on Radiopharmaceutical Chemistry,* Vancouver, Canada, 13-17th August 1995
6. Workshop on Targetry and Target Chemistry, Vancouver, Canada, 17-19th August 1995
7. Stereochemistry at Sheffield, University of Sheffield, 19th December 1995
8. Easter School in Radiopharmaceutics,* King's College, London, 24-29th March 1996

* Indicates a poster presentation by the author.